UNIVERSITY OF LEEDS

Intelligent 5G Network Slicing for Vehicular Networks

Alican Topcu

Submitted in accordance with the requirements for the degree of PhD. Electrical and Electronic Engineering

The University of Leeds

Faculty of Engineering and Physical Sciences

School of Electronic and Electrical Engineering

May 2023

Intellectual Property

The candidate confirms that the work submitted is his own, except where work which has formed part of jointly-authored publications has been included. The contribution of the candidate and the other authors to this work has been explicitly indicated below. The candidate confirms that appropriate credit has been given within the thesis where reference has been made to the work of others.

Chapter 3 is based on the work from: A.Topcu, S.A.R. Zaidi, A. Q. Lawey, "Joint Optimization of Multi-Numerology Bandwidth Part Partitioning, Routing, and Resource Allocation for 5G Vehicular Networks", IEEE Transactions on Network and Service Management, 2023

This paper has been submitted jointly with my PhD supervisors, Dr. Ahmed Lawey, Dr Syed Zaidi.

Signed 

Dedication

This thesis is humbly dedicated to the visionary leader who founded the modern Turkish Republic, Mustafa Kemal Ataturk. His impact on society, exemplified by initiatives like this scholarship program he established, serves as a powerful testament to his enduring vision and ideals, even 85 years after his passing. Ataturk's extraordinary foresight and tireless commitment to progress opened the world of higher education to countless aspiring students like myself, enabling us to pursue our dreams and make meaningful contributions to society. I am deeply grateful to him for the opportunity to pursue a PhD degree in the UK.

I would like to express my deepest gratitude to Mevlüde, Soner and Erkan, my mother, father, and brother, whose substantial support and encouragement have been a constant source of strength throughout my academic journey. Their trust in me has been influential in helping me overcome the many challenges I've faced along the way.

And, of course, I would also like to extend my heartfelt thanks to Melek, my dearest wife, whose unwavering love and support have been the foundation of my success. Her inexhaustible patience, understanding, and constant encouragement have been the driving force of my achievements. I am immensely grateful to have such an extraordinary partner by my side, and I attribute much of my accomplishments to her incredible presence. I am also profoundly grateful to İpek, my beautiful daughter, whose infectious laughter and boundless energy have brought immeasurable joy, inspiration, and strength into my life.

I am deeply indebted to all of them for their love, support, encouragement, and guidance, and I dedicate this thesis to them with all my heart.

Acknowledgements

First, I would like to express my utmost gratitude to Dr Ahmed Lawey. His constant guidance, insightful feedback, and encouragement have consistently steered me in the right direction throughout my academic journey. His mentorship and generous investment of time have played a vital role in shaping my academic growth and enabling me to accomplish my research objectives. I am genuinely grateful for his dedication, support, and inspiration, which have motivated me to overcome challenges and strive for excellence.

I would like to express my appreciation to Dr Syed Ali Raza Zaidi, my co-supervisor, for his valuable guidance, recommendations, and collaboration during my PhD study.

I would also like to extend my gratitude to Prof. Mohsen Razavi, my Postgraduate Research Tutor, for his invaluable advice and timely recommendations that helped me navigate challenges and overcome obstacles during my academic journey.

Finally, I want to extend my most profound appreciation to my colleagues and the exceptional academic staff at the School of Electronic and Electrical Engineering, University of Leeds.

Abstract

5G and beyond is envisioned as a flexible and heterogeneous network that supports use cases with a wide range of requirements. This thesis focuses on the optimisation of physical RB and power allocation among users, bandwidth allocation among bandwidth part (BWP)s, and data routing and user association in vehicular networks in a wireless network, considering the concept of network slicing. All the above-given elements involve solving a complex joint optimisation problem with multiple objectives and constraints, including minimising power consumption, maximising bandwidth and energy efficiency, ensuring the quality of service, and maintaining network slicing requirements. This thesis addresses the challenges of solving joint optimisation problems by proposing novel algorithms and techniques that enable efficient and effective optimisation for the above-given objectives. This thesis, therefore, employs three optimisation tools, namely, Mixed-Integer Linear Programming (MILP), heuristics and machine learning.

The study considers a city environment with multiple cells that support radio slicing and multi-numerology techniques. Randomly located users generate traffic demands characterised by data rate and delay requirements. Additionally, the vehicles in the network serve as mobile Integrated Access and Backhaul (IAB) nodes, referred to as vehicular base station (VBS). In this work, the backhaul network utilises mmWave frequency bands, while the access links operate in sub-6 GHz frequency bands. The developed model can be flexibly adapted to support other frequency distributions between backhaul and access networks. The VBSs establish communication links with nearby BSs and users, facilitating the exchange of data. This combination of mmWave and sub-6 GHz frequency bands allows for efficient and reliable communication between the VBSs and users, enabling the seamless operation of the IAB network for

vehicular-based backhaul and access communication.

In the MILP optimisation, we consider the weighted objectives of minimising the total transmit power in the downlink direction and co-channel interference (CCI) while maximising the number of simultaneously served users. MILP efficiently allocates RBs and power to the users, bandwidths among BWPs, and makes data routing and user association for the proposed optimisation framework while considering CCI and the many required constraints. MILP allows the simultaneous optimisation of multiple objectives, resulting in an effective and efficient optimisation strategy in the vehicular-based mmWave backhaul network.

A multi-objective problem involving multiple dimensions causes an exponentially increasing number of parameters and variables, therefore, prolonged computation times and the need for extensive verification of obtained outputs. Hence, we propose a hybrid optimisation framework designed to address the complex problem of resource allocation and routing in multi-numerology systems with multiple users and sources. By combining heuristic and meta-heuristic approaches, specifically genetic algorithms, we overcome the performance limitations of MILP and provide an efficient, effective, reliable and alternative solution. Furthermore, the same scenario with a low number of users is employed in MILP and heuristic algorithms, and the outputs are compared for verification purposes.

In addition to the heuristic algorithms, we also incorporated an Reinforcement Learning (RL) algorithm to further reduce decision time for the optimisation problem. We utilised various techniques to optimise power and numerology allocation among users in a pre-allocated BWP environment. With these techniques, we aimed to achieve optimal resource utilisation while meeting the various requirements of users in a 5G and beyond RAN.

Contents

List of Figures

List of Tables

Acronyms

3GPP The 3rd Generation Partnership Project

5G-NR Fifth Generation New Radio

AI Artificial Intelligence

ANN Artificial Neural Network

AR/VR augmented and virtual reality

AWGN additive white Gaussian noise

BS base station

BWP bandwidth part

C-V2X Cellular-V2X

CAM cooperative awareness messages

CapEx Capital Expenditure

CCI co-channel interference

CN Core Network

CP cyclic prefix

CU Central Unit

D2D Device-to-Device

DENM decentralized environmental notification messages

DNN deep neural networks

DP demand point

DQN deep Q-Network

DRL deep reinforcement learning

DU Distributed Unit

EA Evolutionary algorithm

eMBB enhanced Mobile Broadband

ETSI The European Telecommunications Standards Institute

FR1 Frequency Range 1

FR2 Frequency Range 2

FSPL free-space path loss

GA Genetic Algorithms

HetNets Heterogeneous Networks

IAB Integrated Access and Backhaul

IMT International Mobile Telecommunications

INI inter-numerology interference

IoT Internet of Things

IoV Internet of Vehicles

ITS Intelligent Transportation Systems

LOS line-of-sight

LSF large scale fading

LTE Long Term Evolution

MDP Markov decision process

MILP Mixed-Integer Linear Programming

MINLP Mixed-Integer Non Linear Programming

ML Machine Learning

mMTC massive Machine-Type Communication

mmWave Millimeter Wave

MT Mobile-Termination

NFV Network Functions Virtualization

NSGA the Nearest Source Genetic Algorithm

OpEx Operating Expenses

QoS quality of service

RAN Radio Access Network

RB resource block

ReLU Rectified Linear Unit

RL Reinforcement Learning

RSU the roadside unit

RU Radio Unit

SCS sub-carrier spacing

SDN Software Defined Networking

SINR Signal to Interference-plus-Noise Ratio

SNR Signal to Noise Ratio

SSF small scale fading

TRGA the Total Random Genetic Algorithm

UEs user equipments

URLLC Ultra-Reliable and Low-Latency Communication

V2I Vehicle-to-Infrastructure

V2N Vehicle-to-Network

V2P Vehicle-to-Pedestrian

V2V Vehicle-to-Vehicle

V2X Vehicle-to-Everything

VBS vehicular base station

Chapter 1

Introduction

1.1 Background

The concept of economics, which deals with allocating limited resources to satisfy unlimited human desires, applies to various fields. The resources are always limited and must be shared efficiently among those who want a share. These resources could range from government grants for researchers to food for the family dinner table or a toy shared by two siblings over time.

In the context of mobile networks, specifically Radio Access Network (RAN), the resources are physical resource blocks that must be efficiently allocated to satisfy multiple objectives, including user requirements, fairness, and efficiency, while also adhering to various constraints such as limited bandwidth, limited transmission power, and interference limitations. Fifth Generation New Radio (5G-NR) networks provide a flexible and service-oriented structure to meet diverse user needs. In this thesis, we optimise resource allocation and routing for 5G-NR RAN, considering the flexible nature of 5G-NR networks and the aforementioned requirements and constraints.

With the emergence of 5G-NR networks, there is a need to optimise resource allocation and routing to meet the diverse needs of users while ensuring efficiency. The approach presented in this thesis considers multiple objectives, including user requirements, and leverages the flexible nature of 5G-NR networks to achieve efficient resource allocation and routing. This work contributes to the ongoing efforts to improve the performance of 5G-NR networks and provides a foundation for future research.

1.2 5G-NR Overview

5G-NR networks offer multi-Gbps peak data speeds, ultra-low latency, high reliability, and enhanced network capacity to the users [1]. However, more than these improvements are needed to call 5G-NR a new generation of mobile networks. The previous generations of mobile networks utilised the one size fits all architecture; however, 5G-NR provides a service-oriented architecture and flexibility to the vertical industries [2]. Thus, 5G-NR supports multiple services on a virtually separated single physical network [3]. Therefore, network slicing is one of the critical elements of 5G-NR technology; it allows to operate logically separated services with different requirements in the same architecture [3].

A network slice refers to a collection of Core Network (CN) and RAN functions, where these functions' settings are configured to satisfy the various requirements of given use cases regarding functionalities (e.g. security, mobility, support) and delivery performance (e.g. latency, reliability, capacity) [4]. Network slices are the mechanism that allows the coexistence of a wide variety of services with various requirements [5]. For example, the International Mobile Telecommunications (IMT) Vision document defines 5G-NR in terms of eight parameters regarding; latency, connection density, network energy efficiency, peak and user-experienced data rate, spectrum efficiency, traffic capacity, and mobility [6]. These parameters are illustrated in Fig. 1.1 with the comparison with the previous generation [6].

1.2.1 Virtualisation of the Network

5G-NR differs by allowing logically separated and isolated flexible networks from existing one-type-fits-all networks [7]. Software Defined Networking (SDN) and Network Functions Virtualization (NFV) can be simultaneously utilised to virtually separate the single physical network [8]. In 5G-NR, SDN and NFV are employed at the higher communication layers. SDN decouples the control and forwarding planes where the former is logically centralised in a software entity and the latter consists of high-performance switches [9]. NFV virtualises all the network functions to create end-to-end isolation among network slices ([10]). Providing isolation among network slices and efficiently utilising radio resources is essential. SDN creates large and complex networks and manages these networks effectively while abstracting the infrastructure from hardware

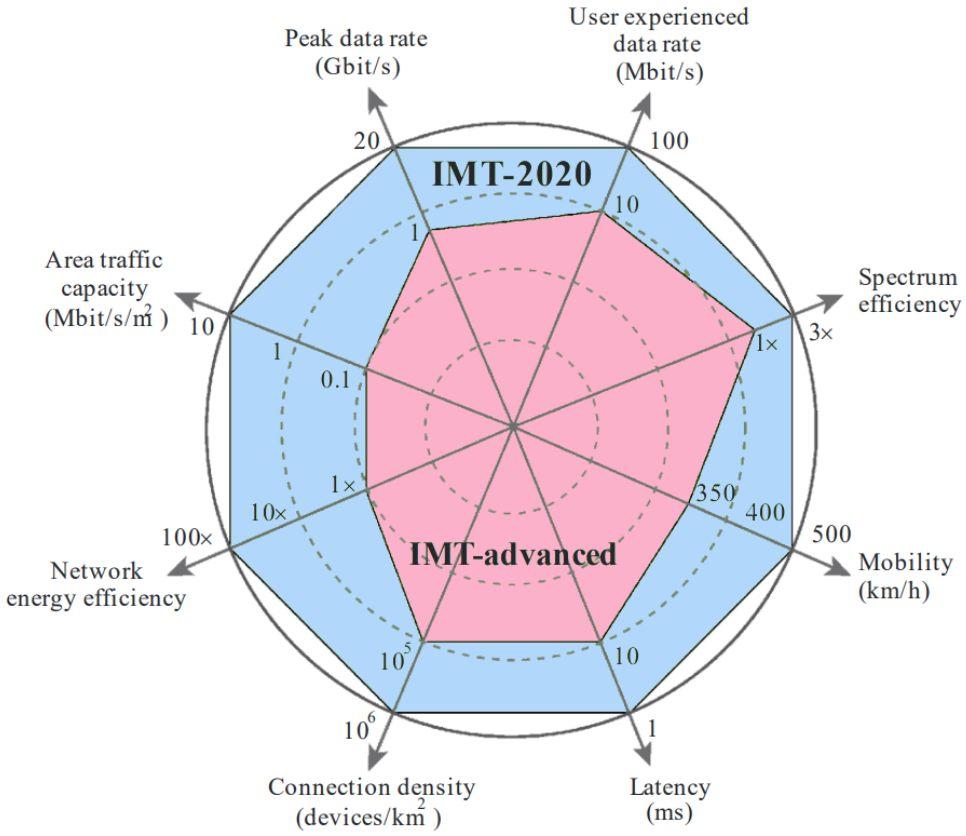

Figure 1.1: Enhancement of key capabilities from IMT-Advanced to IMT-2020[6]

for virtual networks [11].

Utilising dedicated hardware increases the Capital Expenditure (CapEx) and Operating Expenses (OpEx) of network operators and causes ossification [12]. SDN and NFV decouple network functions from dedicated hardware in the mobile network [12]. Therefore, SDN and NFV reduce the dependency on application-specific integrated circuits.

1.2.2 5G-NR Use Cases

5G-NR provides the flexibility to support services with diverse requirements in the same network. Three major network service classes are defined for 5G-NR; enhanced Mobile Broadband (eMBB), Ultra-Reliable and Low-Latency Communication (URLLC), and massive Machine-Type Communication (mMTC) [13]. eMBB is the successor of the classic mobile broadband connectivity scenario where high data-rate requirements are provided to support multimedia and data services [14]. URLLC has strict constraints for latency and reliability, where the former shall be less than 1 ms for end-to-end latency, and the latter is expected to provide 99.99% reliability [15]. Internet

of Things (IoT) refers to the concept of connecting physical objects (i.e. household appliances, vehicular sensors or probes, healthcare equipment) to the existing internet infrastructure [16]. mMTC slice supports the massive connectivity demands for IoT devices [17]. The emphasis of the above-given parameters differs for each major service. Fig. 1.2 shows the importance of key performance indicators for each service [6].

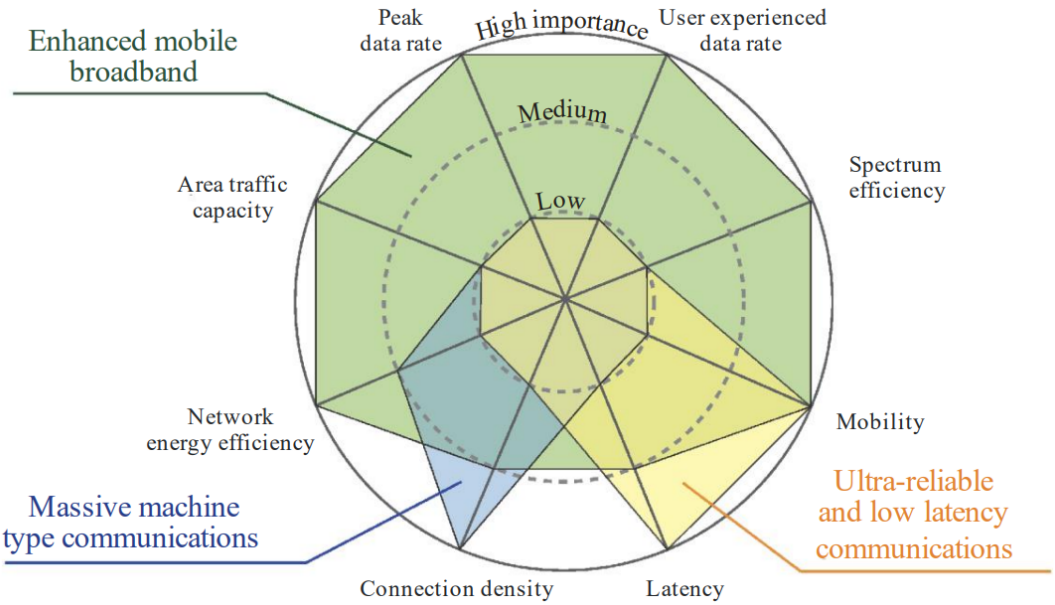

Figure 1.2: The importance of key performance indicators in different usage scenarios [6]

1.2.3 Multi-Numerology Concept

The 5G-NR flexibility is enabled with multiple deployment options provided by multiple numerologies. In 5G-NR systems, the numerology term identifies the specifications of the radio frame where these specifications indicate the sub-carrier spacing (SCS). For example, LTE has a fixed SCS with 15 kHz, whilst 5G-NR has various types of SCSs and distinct subframe times [18]. The numerology accepts 15 kHz SCS as a base frequency and simply multiplies it by a factor of 2^{μ} where $\mu \in N$ and $0 \leq \mu \leq 4$. One resource block (RB) includes 12 of those subcarriers; therefore, the bandwidth of one RB of the numerologies can be calculated by multiplying with 12 with their SCS frequency (i.e. the bandwidth of each RB of the first numerology can be calculated as $12 \times 15kHz = 180$ kHz [19]). Figure 1.3 shows the SCS size of each numerology in time and frequency domains.

Each time slot includes 14 symbols (excluding 60 kHz extended, it has 12 symbols); in

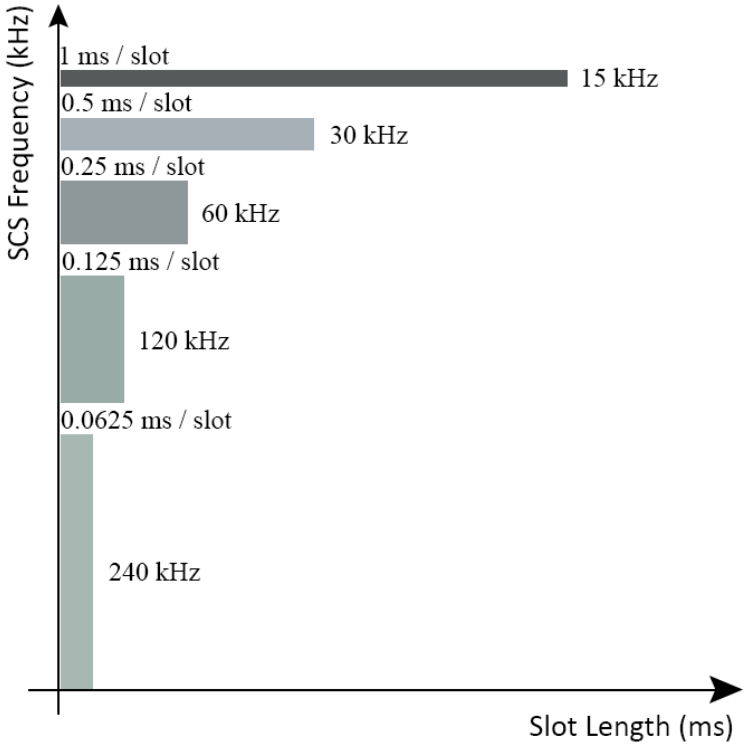

Figure 1.3: Slot length and frequency occupation for the given numerologies

other words, the symbol duration changes for each numerology [20]. Since one radio frame equals 10 ms and consists of ten sub-frames, each sub-frame has a different number of slots given in Table 1.1 [20].

Table 1.1: Numerology parameters [20]

μ	0	1	2	2	3	4
SCS = $15x2^{\mu}$ (kHz)	15	30	60	60	120	240
Slot duration $1/2^{\mu}$ (ms)	1	0.5	0.25	0.25	0.125	0.0625
OFDM Symbol Duration (us)	66.67	33.33	16.67	16.67	8.33	4.17
Number of Slots in one Sub-Frame	1	2	4	4	8	16
Number of Sub-Frames in one Frame	10	20	40	40	80	160
Cyclic prefix (CP)	Normal	Normal	Normal	Extended	Normal	Normal

The slot length of the first three numerologies for one sub-frame is given in Fig. 1.4 [21].

5G-NR services utilise the numerologies to provide differing user requirements. For example, mMTC is delay-tolerant, therefore, prefers small SCS with large symbol duration, whilst eMMB employs both small and large SCSs according to the channel (e.g. fast fading, Doppler spread, etc.) to provide high throughput demands [22]. Likewise, URLLC requires reliability and low end-to-end delay, as the name implies;

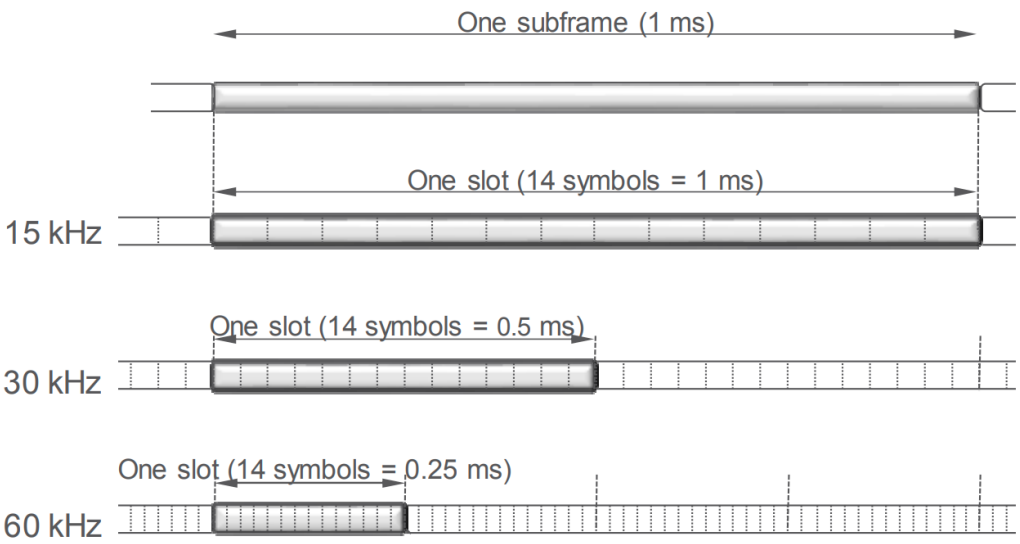

Figure 1.4: 5G-NR time domain structure [21]

hence, it requires large SCS to afford these requirements [23].

1.2.4 Bandwidth Part

The multi-numerology deployment in the same radio resources causes an additional interference, known as inter-numerology interference (INI) [24]. Resource elements in the same numerology are orthogonal to each other; however, utilising different numerologies disrupts orthogonality and creates INI [22]. Therefore, the correlative services that use the same numerology are grouped to provide BWP that helps to decrease the INI and the necessary guard bands [25]. In order to provide BWP, the carrier bandwidth is isolated to narrower parts that include contiguous RBs that belong to the same numerology, taking into account the service requirements [18]. In other words, the physical resources are divided into several BWPs with different numerologies that consider the data rate and latency requirements of the user equipments (UEs). Furthermore, the standard strictly describes the activation of BWPs; according to [18], an UE can be designed with a single active downlink BWP whilst up to four BWPs can be configured to a single UE. On the other hand, single carrier bandwidth supports multiple BWPs [26].

1.2.5 5G-NR Frequency Range and Spectrum

5G-NR is designed to operate in both the lower frequency ranges, up to 100 MHz bandwidth for Frequency Range 1 (FR1) and up to 400 MHz bandwidth for Frequency

Range 2 (FR2) which are also known as sub-6 GHz and Millimeter Wave (mmWave) frequency, respectively [20]. FR2 is globally identified between 24.25 GHz to 71 GHz; this frequency band is also known as mmWave due to the wavelength of the frequency [27]. The logic behind employing higher carrier frequencies is to satisfy the continuously boosting traffic, higher consumer data rates and the related need for more spectrum; therefore, wider transmission bandwidths [28]. mmWave frequency bands have the larger available bandwidth for very high throughput [29].

In urban scenarios, including crowded areas and hotspots with pervasive smartphone users, eMBB leverages from high network capacity of mmWave [30]. Moreover, video streaming/broadcasts everywhere augmented and virtual reality (AR/VR) for enhanced online gaming experiences, and the evolution of the 5G-NR smart factory applications enjoy the low latency characteristics of 5G-NR mmWave [30].

On the other hand, mmWave frequency bands have some significant disadvantages. With the increasing frequency, mmWave signals suffer from high path loss and penetration loss [31]. Also, decreased RF hardware performance and the existence of auxiliary systems for mmWave are other disadvantages [14]. One of the pioneer studies in [32] proved that beamforming is a solution to achieve high-performance communication at mmWave frequencies. In 5G-NR, IAB improve the performance of mmWave frequencies without requiring fibre backhaul connection with the core network [33].

1.2.6 Integrated Access and Backhaul

The global data traffic demand for mobile broadband systems doubles each year because of the boost of multimedia streaming [34]; hence, network densification increases in parallel. Also, 5G-NR wireless network links are anticipated to be economical and feasible to provide flexibility even in dense network deployments. Hence, instead of employing fibre backhaul everywhere, wireless backhaul communications gain importance to increase the network capacity.

Although the wireless backhaul was considered in the past, it was based on non-standardised solutions that relied on line-of-sight (LOS) or point-to-point connections [35]. IAB enables backhaul connectivity without fibre deployment for 5G-NR services; therefore, IAB enables flexibility in dense networks without densifying the transport network [36]. Thanks to IAB, proportionally increasing the wired transport network is

avoidable when the wireless network deployment for 5G-NR is utilised [29]. IAB supports access and backhaul in mmWave and sub-6GHz carrier frequency bands; 3GPP defines in-band operation where access and backhaul links partially or fully overlap in frequency and out-band operation where access and backhaul links use different frequency resources [36]. Moreover, the out-band operation can utilise different frequency ranges simultaneously (e.g. mmWave for backhaul and sub-6 GHz for access) [37]. IAB nodes support multi-hop deployment utilising the same or different frequency bands for access and backhaul [27].

IAB can be utilised to serve users that are far from mmWave base stations and require high data rates, and low latency demands [27]. Users recognise and connect to IAB nodes as regular base station (BS); moreover, IAB nodes create their own cells, which can be used in special events or emergencies as temporary deployments of small cells [28].

1.3 Vehicular Networks

Intelligent Transportation Systems (ITS) need digital applications to realise the vision for the roads, which desires to eliminate road accidents and reduce congestion and emissions [38]. Autonomous vehicles should exploit the information in their vicinity and exchange messages among themselves to improve road safety [39]. Moreover, network connectivity with reliable coverage is a factor in developing autonomous vehicles. The information must be delivered in real-time, or as quickly as possible, and securely. Increasing reliability and decreasing latency of data packets in 5G-NR help to improve road safety and vehicular communication systems.

The 3rd Generation Partnership Project (3GPP) defines four types of vehicular communications that allow for Vehicle-to-Vehicle (V2V), Vehicle-to-Infrastructure (V2I), Vehicle-to-Pedestrian (V2P), and Vehicle-to-Network (V2N) connections [40]. Vehicular communications are combined under Vehicle-to-Everything (V2X) umbrella in Release 14 [40]. V2Vs are networks in which cars communicate directly without any external infrastructure. This type of Device-to-Device (D2D) communication can be named sidelink communication [41]. The European Telecommunications Standards Institute (ETSI) has defined two types of safety messages, cooperative awareness mes-

sages (CAM) [42] and decentralized environmental notification messages (DENM) [43]. V2V and V2P exchange CAM and DENM messages among vehicles and pedestrians via sidelink [44]. V2N enables to connect to a server supporting vehicular applications, and V2I refers to communications between vehicles and infrastructure such as the roadside unit (RSU)s [4]. Vehicular communications types are illustrated in Fig. 1.5.

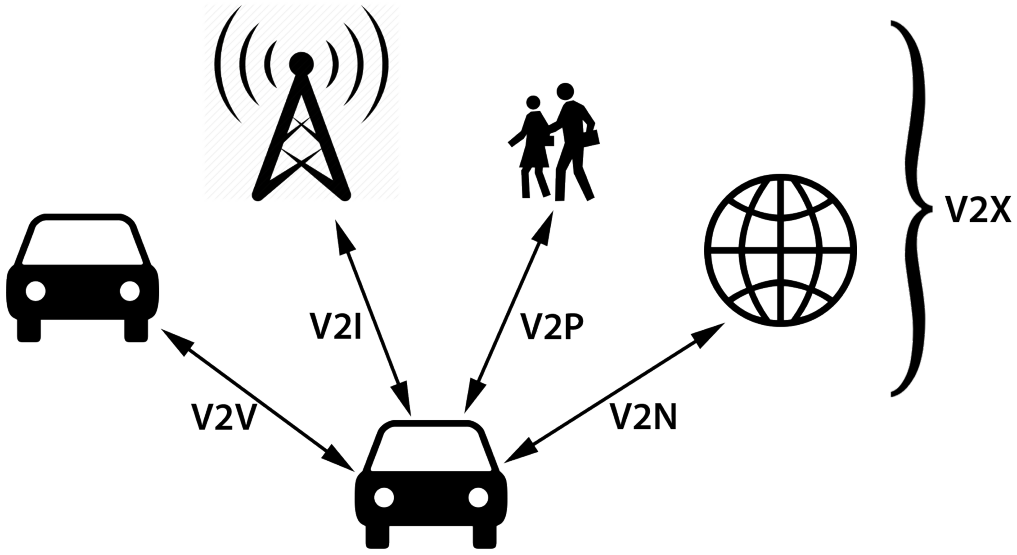

Figure 1.5: Vehicular communication types

V2X applications have limited coverage; in some conditions, V2X may be insufficient; for example, if a vehicle detects some unexpected road condition and there is no vehicle to communicate around it, the vehicle will not be able to send the information to others. Moreover, V2X networks suffer from high mobility, delay, and packet dropping due to their dynamic nature [45]. The high mobility causes non-stationary channel statistics and high Doppler spread [46].

Hence, V2X has evolved into Cellular-V2X (C-V2X) to provide continuous connection using cellular networks. By employing C-V2X, autonomous and connected vehicles' requirements can be satisfied more efficiently, even by utilising the Long Term Evolution (LTE) network [47].

The service-oriented approach of 5G-NR services (eMBB, mMTC and URLLC) leads to various verticals for the vehicular networks such as improved road safety [48], in-vehicle experience and by paving the road to autonomous driving [49]. However, the most distinguished specification of the 5G-NR for the vehicular communication is con-

necting vehicles to everything with lower latency and higher reliability which is highly critical for applications like remote driving, platooning, and advanced driving [50]. Furthermore, 5G-NR enables vehicular communication in real-time with enhanced cryptographic-based security [39]. The service-oriented approach also ameliorates services other than road safety for vehicles. 5G-NR C-V2X applications will harness the power of network slicing as follows:

- To enable more autonomous vehicles on the road, data traffic must flow among vehicles with low latency and high reliability. Therefore URLLC slice is employed for self-driving or autonomous vehicles [51]. Moreover, safety applications such as collision warning, blind spot, lane change warning, and adaptive cruise control [52], platooning applications [53] enjoy the low latency and high reliability of this network slice.
- eMBB slice is employed to serve infotainment services, which generally require high user demands, high data rates, and high bandwidth requirements [41].
- Vehicles are getting smarter and filled with numerous sensors that collect, store and send a massive amount of data. Internet of Vehicles (IoV) is a significant branch of IoT [54] and is utilized in vehicular networks and traffic data. Furthermore, D2D communication can be employed for mMTC applications where mobile devices work as a relay for a group of mMTC sensors [55].

5G-NR is employed in highways (as well as the city centres) due to an increase in the necessity of reliable coverage and low latency of communications. 5G-NR coverage map [56] shows that network connectivity for vehicles is a crucial factor in the development of autonomous vehicles and vehicular communications. Outside the city centres, Fig. 1.6 shows examples of the 5G-NR coverage for the UK, Japan, and France.

In addition to all, high speeds cause higher Doppler spread on highways. Therefore, in order to satisfy vehicular demands, high bandwidth provided by higher numerologies (possibly by URLLC slice) might be essential.

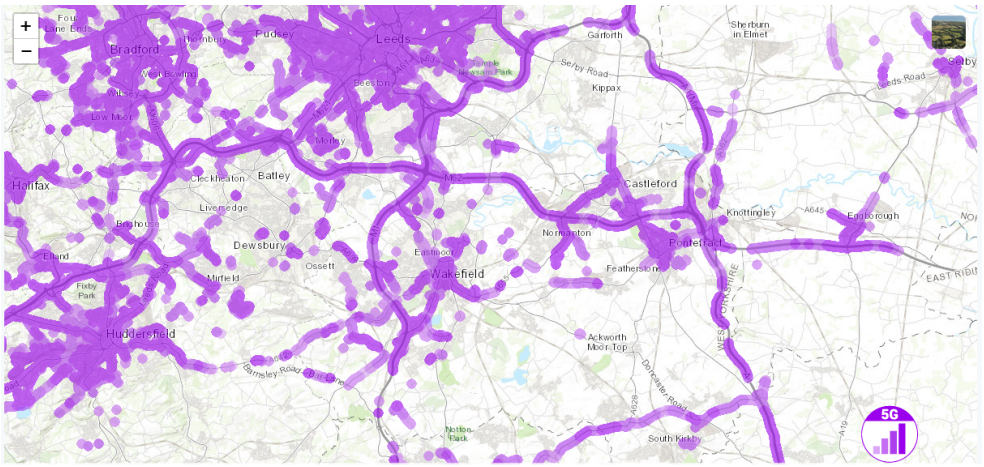

The UK 5G Coverage Map

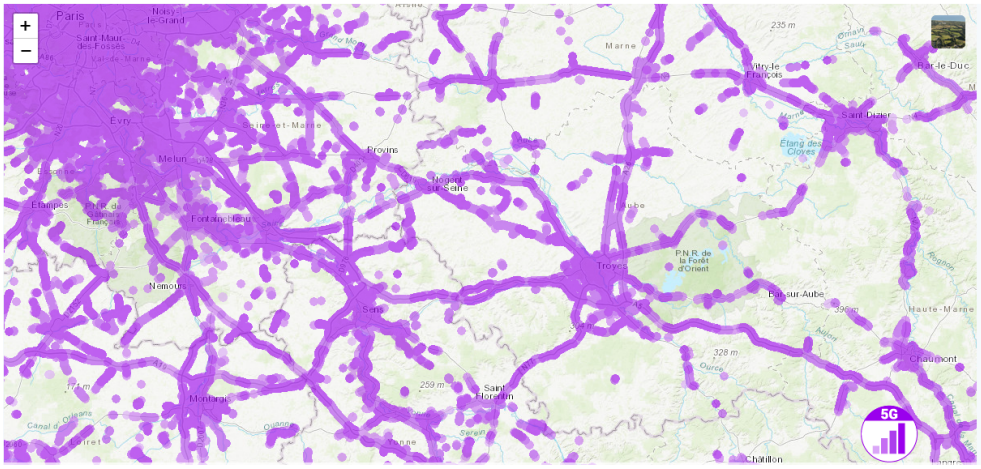

France 5G Coverage Map

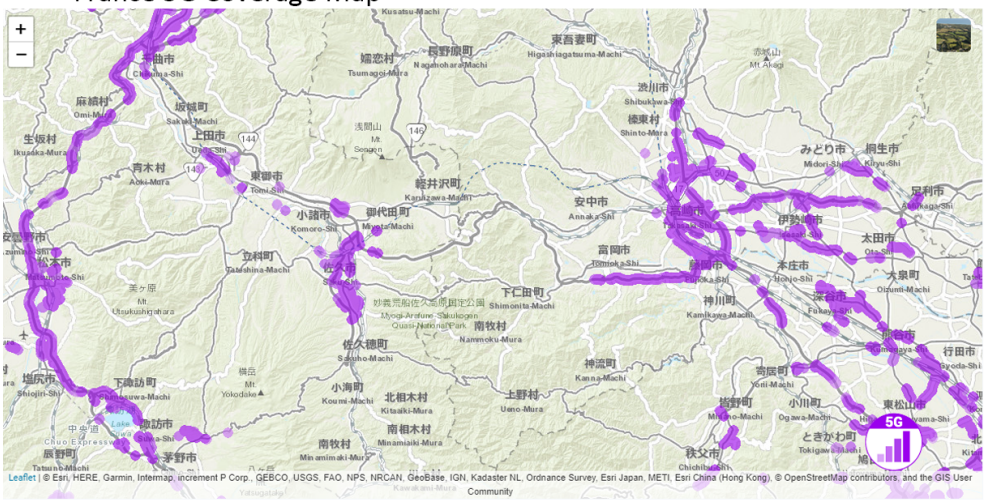

Japan 5G Coverage Map

Figure 1.6: 5G-NR coverage map for three different countries and regions [56]

1.4 Optimisation Tools

Optimisation tools are essential for solving resource allocation and routing problems in mobile networks. These tools help to maximise the use of available resources, minimise costs and energy consumption, and improve the overall performance of the network. In

this section, we provide an overview of some of the most commonly used optimisation tools, including MILP, heuristics, and Machine Learning (ML).

MILP is a powerful mathematical optimisation technique that can solve a wide range of constraints and objectives but can be computationally expensive for large-scale problems. Heuristics, on the other hand, are rule-based or stochastic algorithms that can quickly find good solutions for complex problems. Although they do not guarantee optimality, they are useful for large-scale problems where exact methods like MILP are impractical. ML techniques have gained popularity in recent years for their ability to learn patterns and make predictions based on large amounts of data. In the context of mobile network optimisation, ML can be used to predict network traffic patterns, predict user demand, and even to develop decision-making models for resource allocation and routing. ML techniques are particularly well-suited for applications where data is abundant but analytical models are difficult to construct.

1.4.1 MILP

MILP is a robust optimisation tool that is well-suited for addressing complex optimisation problems, such as resource allocation and routing. Many examples have been provided in the Related Works Chapter to demonstrate its efficiency. MILP models consist of linear constraints and objective functions, where certain variables are constrained to be binary numbers, and real numbers, for example, to show the user association and the power allocation, respectively. The capability to incorporate a diverse set of constraints and objectives renders MILP an appropriate optimisation tool for a wide range of applications, including mobile network optimisation. However, the solution of large-scale MILP problems can be computationally demanding and challenging.

In optimisation models, the first step is to determine an objective, which is a quantitative measure of the system's performance where this objective could be any quantity that can be represented by a single number, such as profit, time, or potential energy [57]. Variables and constraints characterise the model, and the aim is to find values that optimise the objective. For example, MILP models for mobile network optimisation typically include variables representing RBs and users. The constraints ensure that the resources are allocated by taking into account user requirements, while the

objective function aims to maximise the overall performance of the network. For example, the objective function could be to minimise the power consumption of the network while meeting the users' demand for services.

In this thesis, the MILP optimisation model is presented in detail in Chapter 3. It encompasses all constraints, variables, and objectives and is tailored to solve complex resource allocation and routing problems in the context of mobile network optimisation.

1.4.2 Heuristics

Heuristics are algorithms that use rule-based or stochastic approaches to find quickly acceptable solutions to complex problems. Unlike MILP, heuristics do not guarantee optimality but can often find good solutions in a reasonable amount of time. Heuristics are particularly useful for large-scale problems where the computational complexity of exact methods such as MILP becomes prohibitive.

In addition to heuristics, meta-heuristics are also widely used in optimisation problems. Meta-heuristics are higher-level strategies that guide the search for solutions by combining multiple heuristics or modifying existing ones to improve their performance. Meta-heuristics can help overcome some of the limitations of individual heuristics, such as getting trapped in local optima or converging too quickly. Examples of meta-heuristics used in mobile network optimisation include ant colony optimisation [58], particle swarm optimisation [59], and genetic algorithms[60]. We have provided many examples in both Chapter 2 and Chapter 4.

MILP optimisation is computationally intensive and requires significant computational resources to find the optimal solution. In contrast, heuristic algorithms are designed to provide solutions in a much shorter period of time, often at the cost of reduced optimality. Thus, heuristic algorithms can be used as an alternative approach to find sufficient solutions to MILP problems within a reasonable timeframe. Furthermore, heuristic results can be compared with the optimal solution obtained through MILP to evaluate the performance of the heuristic algorithm. By striking a balance between computational resources and solution quality, heuristics can provide practical solutions to large-scale optimisation problems in a timely manner.

Another reason to employ heuristic or ML algorithms is NP-hard problems. In compu-

tational complexity theory, NP stands for "nondeterministic polynomial time," which refers to a set of problems that can be solved in polynomial time by a nondeterministic algorithm [61]. NP-hard, on the other hand, is a term used to describe the complexity class of decision problems that are considered more difficult than those that can be solved by a nondeterministic algorithm in polynomial time [62]. Therefore, solvers may require exponential time to solve NP-hard problems. MILP can solve NP-hard problems, but finding the exact solution for large-scale problems can be computationally infeasible, making heuristic or ML algorithms necessary for finding satisfactory solutions in a reasonable amount of time.

1.4.3 Machine Learning

Next-generation wireless networks are becoming increasingly complex, with diverse service requirements and the need to use available resources efficiently. Traditional approaches and limited data analysis tools might not be adequate for efficient and cost-effective operation and optimisation [63]. ML is an optimisation tool that can be utilised to solve complex resource allocation problems in 5G-NR networks. ML techniques can learn patterns and make predictions based on large amounts of data, making them suitable for predicting traffic patterns, user demand, and other variables that affect resource allocation and routing decisions. Moreover, ML algorithms can be used to predict the traffic demand for different parts of the network and allocate resources accordingly [64].

ML techniques can be employed to optimise the power allocation and user association in a network while ensuring compliance with user requirements, as demonstrated in prior research [65]. The key advantage of utilising ML in this context is its ability to learn from previous data and adapt to dynamic changes in network conditions. This dynamic and flexible approach offers a promising solution to resource allocation problems in the network domain.

However, ML also has some limitations. One of the significant limitations is the need for large amounts of data for training the ML algorithms except reinforcement learning. In addition, ML algorithms may only be able to handle some types of optimisation problems and may require expert knowledge to design and tune the algorithms properly. Finally, ML algorithms may not always provide an interpretable solution,

making it difficult to understand why a particular decision was made. Despite these limitations, ML has shown promise in solving complex resource allocation problems in 5G-NR networks and is an active area of research in mobile network optimisation.

RL is a subfield of ML that has also shown promise in resource allocation problems. RL involves an agent observing an environment, then taking actions to build a policy and receiving feedback as rewards or penalties based on the actions. The agent learns to take actions through these trial-and-error interactions and by observing the environment. RL has been applied to various resource allocation problems, such as power allocation and radio resource management, and has shown to be effective in finding optimal or near-optimal solutions. The examples and the context of ML are elaborated on in Chapter 2 and Chapter 5.

1.5 The Summary of the Thesis

The main focus of our study is to optimise the physical RB and power allocation among users in a wireless network, considering BWP allocation and the concept of network slicing. Additionally, we aim to find the optimum route for data transmission in vehicular networks where vehicles are employed as intermediate nodes. Therefore, user association is another objective of the proposed optimisation framework. All the above-given objectives involve solving a complex optimisation problem that considers multiple objectives and constraints, including minimising power consumption, maximising RB utilisation, ensuring quality of service (QoS), and maintaining network slicing requirements. Our study addresses these challenges by proposing novel algorithms and techniques that enable efficient and effective RB allocation and data routing in wireless networks. The study considers a city environment with multiple cells that support radio slicing and multi-numerology techniques. Randomly located users generate traffic demands characterised by data rate in Mbps and delay requirements in milliseconds (ms). Although there are two distinct requirements, the requirements are related to each other to represent 5G-NR network slices. For instance, in our optimisation framework, we consider three distinct user types: eMBB, which demands low latency and high data rates; URLLC, necessitating both low latency and data rates; and mMTC, characterized by high latency and low data rate requirements.

Additionally, the vehicles in the network serve as mobile IAB nodes, referred to as VBS. In the IAB (Integrated Access and Backhaul) network context, the backhaul network utilises mmWave frequency bands, while the access links operate in sub-6 GHz frequency bands. The VBSs establish communication links with nearby BSs and users, facilitating the exchange of data and information. This combination of mmWave and sub-6 GHz frequency bands allows for efficient and reliable communication between the VBSs and users, enabling the seamless operation of the IAB network for vehicular-based backhaul and access communication.

In the optimisation problem, we consider the weighted objectives of minimising the total transmit power in the downlink direction and CCI while maximising the number of simultaneously served users. The proposed framework utilises MILP to jointly optimise multiple objectives. By employing MILP, the framework aims to efficiently allocate radio resources, such as physical RBs and power, while considering the trade-off between power consumption, interference, and capacity. This approach allows for the simultaneous optimisation of multiple objectives, resulting in an effective and efficient resource allocation strategy in the vehicular-based mmWave backhaul network.

To address the challenges associated with optimisation problems involving multiple dimensions, such as the increased number of parameters and variables, prolonged computation times, and the need for extensive verification of obtained outputs, we employed Genetic Algorithms (GA) as an alternative solution. GA provides a heuristic optimisation approach that can efficiently search for solutions in large search spaces and has been widely used in various optimisation problems. In this thesis, we have developed two distinct GA algorithms that jointly optimise the aforementioned resource allocation problem. These GA algorithms aim to find near-optimal solutions by iteratively evolving a population of candidate solutions based on genetic operators, namely crossover and mutation, to explore the search space and converge towards optimal or near-optimal solutions. By utilising GA as an alternative optimisation approach, we aim to enhance the efficiency and reliability of the resource allocation process and validate the outputs obtained from the MILP optimisation process.

In addition to the Genetic Algorithms, we also incorporated an RL algorithm to further reduce decision time for the optimisation problem. We utilised a variety of techniques to optimise power and numerology allocation among users in a pre-allocated BWP

environment. With these techniques, we aimed to achieve optimal resource utilisation while meeting the various requirements of users in a 5G-NR RAN.

1.6 Main Contributions

In this section, we outline the main contributions of this thesis and highlight the key features that distinguish it from previous works. This thesis makes several key contributions, including the development of a novel optimisation framework to address the comprehensive resource allocation problem. This proposed framework considers both sub-6 GHz (FR1) and mmWave (FR2) channel models and optimises bandwidth allocation for BWPs and RB allocation for users while leveraging vehicles as routing nodes to increase total system capacity.

The main contributions of this thesis can be summarised as follows:

- We propose an optimisation framework that jointly optimises three elements: the bandwidth of multi-numerology BWPs, multi-user RB association and power allocation in the downlink direction, and routing through VBS nodes. The weighted objective function maximises the total number of served users and minimises the total downlink transmit power and CCI to increase the power efficiency and Signal to Interference-plus-Noise Ratio (SINR). Thus, the framework can achieve maximum spectral efficiency for the same bandwidth.

- The network is a heterogeneous and flexible 5G-NR vehicular network that supports radio slicing for the various requirements of the users. The heterogeneity is reflected by diverse user requirements, network slices and VBS nodes that enable the out-band IAB backhauling. The flexibility is reflected by users that can choose any numerology while ensuring their requirements are satisfied and bandwidth allocation between BWPs. Users have data rate requirements that must be fulfilled in a specific unit of time. Accordingly, the minimum numerology requirements are determined according to the data rate and delay demands of users.

- An inter-layer optimisation framework which includes both the physical and network layers, is employed. This terminology derives from its interdependence and interaction between the physical and network layer elements. In this optimisation

framework, users can be served either directly by a BS that uses FR1 frequency or indirectly by a VBS that uses mmWave for backhaul and FR1 for access. To the best of our knowledge, no previous work considers the route selection for the resource allocation optimisation problem. The optimisation framework increases power efficiency by routing data through VBS nodes when necessary.

- Furthermore, we formulate the resource allocation optimisation for the above-given problem as a Mixed-Integer Non Linear Programming (MINLP). The effective piecewise linearisation method resolves the difficulty of linearising a logarithmic function. We demonstrate that the linearisation method works with less than 0.04 % error.

- After the MILP optimisation, we leverage a hybrid optimisation framework that leverages both heuristic and meta-heuristic approaches (genetic algorithm) to concurrently optimise the bandwidth of multi-numerology BWPs, multi-user RB association and power allocation in the downlink direction, and data routing via out-band IAB nodes. The hybrid approach allows us to benefit from the strengths of both methods and achieve a more effective optimisation solution.

- We generate the initial population using two algorithms. The first algorithm assumes that each UE establishes a connection to the nearest source; therefore, this algorithm is called the Nearest Source Genetic Algorithm (NSGA). In the second algorithm, UEs are free to select any source; hence, this algorithm is called the Total Random Genetic Algorithm (TRGA). There are slight differences between these two algorithms in terms of the selection of individuals. To obtain noteworthy results and verification, BSs, VBSs, and UEs are located in identical locations used to obtain the MILP results.

- The MILP optimisation problem is computationally expensive; moreover, with an increasing number of users, the problem becomes NP-hard. We solve the same problem for the increased number of users that could not be solved by MILP optimisation by leveraging hybrid heuristic algorithms.

- Then, we propose a novel downlink power allocation optimisation algorithm utilising Reinforcement Learning (RL), where the RL algorithm utilises a unique reward function. This reward function effectively accomplishes two objectives

at once. Firstly, the RL agent meets the data rate requirements of the user, resulting in a positive reward. Secondly, the agent does not allocate more power than requested to maximise the reward, which leads to an implicit minimisation in the transmit power. The transmit power of the users is not located in the objective function; still, the model minimises the transmit power.

- Additionally, we further enhance the RL algorithm to joint power and numerology allocation in the downlink direction for the users, considering a 5G network that supports multi-numerology, and includes multiple BWPs. A similar reward function is employed to minimise power usage while simultaneously maximising fairness among users.

This thesis aims to provide an in-depth analysis of the above-given critical aspects of 5G-NR networks and their implications for the future of wireless communication. Through a comprehensive review of existing literature, this thesis explores the key challenges and opportunities of network slicing, bandwidth part allocation, and integrated access and backhaul in 5G-NR networks. The thesis also provides insights into the state-of-the-art optimisation techniques such as MILP, genetic algorithms, and deep reinforcement learning (DRL), and their potential to address the challenges and opportunities of network slicing, bandwidth part allocation, and integrated access and backhaul in 5G-NR networks. Finally, the thesis concludes with a discussion of future research directions in this area and the potential impact of these features on the overall wireless communication landscape.

In this thesis, we made some assumptions to mitigate the computational complexity. However, the optimisation framework employed in this study has the capability to scale up the complexity and handle more complex scenarios without compromising its efficiency and effectiveness. For example, our focus is primarily on downlink communications throughout this thesis. Therefore, in the results sections of each chapter, we present the transmit power allocated to each user by the corresponding base station in the downlink direction. However, this approach can easily be extended to encompass uplink communications.

Another assumption employed in this thesis is that the allocated data rate is equal to the Shannon capacity. Since the choice of modulation techniques is not our primary

concern, this assumption allows for the consideration of the maximum achievable data rate. The assumption of the achievable data rate as Shannon capacity is widely used in existing literature, as shown in [65], [66], [67], [68], [69], [70], [71], and [72]. By abstracting the details of modulation schemes and encoding techniques, the focus is directed towards optimising other aspects of the system, such as power allocation, RB allocation, and bandwidth allocation among BWPs. Therefore, it is important to note that while this assumption provides a useful approximation, the real achievable data rate may be lower due to the choice of modulation techniques.

In this chapter, we have provided a brief introduction to the topics mentioned above and presented our contributions. In Chapter 2, we conduct a comprehensive literature review of related works in the field of resource allocation, data routing, ML, and heuristic algorithms in 5G-NR networks. Chapter 3 outlines the channel and MILP optimisation model, including its objectives and constraints, and presents results. Chapter 4 describes the heuristic algorithm, including its objectives and constraints, and presents results by comparing them with optimisation outcomes. Chapter 5 provides a detailed explanation of the ML algorithms and our proposed RL algorithm and compares its results with those of the optimisation and heuristic algorithms. Finally, in Chapter 6, we conclude the thesis and provide suggestions for future research.

Chapter 2

Related Works

This thesis specifically focuses on ***5G-NR RAN resources allocation***, considering various aspects of 5G technologies, such as BWP partitioning, data routing via vehicular nodes by employing out-band IAB for user association, co-channel and inter-numerology interference, and multi-numerology employment. Furthermore, different approaches were explored to solve the optimisation problem, including MILP optimisation, genetic algorithms, and ML algorithms.

Before getting to the heart of the matter, an overview of the relevant literature is provided in this chapter. Previous works and studies related to the research topic are included in this literature review, setting the foundation for the research and highlighting gaps and opportunities for further investigation in the 5G-NR resource allocation and optimisation field.

2.1 Resource Allocation Optimisation

Radio resources refer to the physical resources used by a wireless communication system to transmit and receive data over the air. These resources, including frequency bands, time slots, bandwidths, RBs, and transmit power levels, improve network performance and often require careful adjustments to achieve optimal performance [73]. Therefore, the effective allocation of physical resources to efficiently utilise carrier bandwidth resources in 5G wireless channels is a crucial challenge. Hence, the resource allocation optimisation problem has garnered significant attention from researchers, resulting in a substantial body of literature dedicated to this topic. We provided several examples

from the literature to demonstrate the prevalence of resource allocation optimisation problems in wireless communications.

Heterogeneous Networks (HetNets) refers to a type of wireless communication network consisting of multiple types of cells with varying characteristics, such as different coverage areas, cell sizes, and transmission power levels [73]. HetNets are designed to enhance network capacity, coverage, and performance by integrating different types of cells, such as macrocells, microcells, picocells, and femtocells, in a coordinated manner [74]. These cells may operate on different frequency bands, utilise different access technologies, and serve different types of users. Since the users are covered by multiple cells in HetNets, user association is also frequently seen in resource allocation optimisation problems. 3GPP introduced the HetNets architecture in Release 12 [75]. In the 5G HetNet environment, several smaller and simpler base stations, such as microcell BSs, and relay nodes, are backing the current cellular networks to increase network capacity and coverage area [76]. Previous studies, such as [74], [76], and [77], have surveyed the resource allocation problem in 5G HetNets. The authors in [76] investigated the current HetNets studies in the literature regarding user association, power and resource allocation, and interference management. Similarly, radio resource management for HetNets is surveyed in [77] considering spectrum and power allocation, user association, interference management, and complexity. The authors of [74] present a detailed survey on resource allocation in 5G HetNets, covering the definition of HetNets, various network scenarios, different resource allocation models, and a classification of existing resource allocation algorithms.

In the literature, many authors have conducted studies on resource allocation in HetNets. The authors in [70] aimed to maximise the system energy efficiency in a non-orthogonal multiple access HetNet through subchannel and power allocation. They formulated the problem as a mixed integer nonconvex optimisation problem, considering co-channel and cross-tier interference. To acquire an optimal solution, they proposed a suboptimal algorithm that alternately optimised the resource allocation for macrocells and small cells, using convex relaxation and dual-decomposition techniques. Additionally, they derived optimal closed-form power allocation expressions for small-cell and macrocell user equipment using the Lagrangian approach. [78], the authors proposed energy-efficient resource allocation algorithms for the downlink of femtocell

HetNets. They considered a dense deployment of femtocells in the coverage area of a central macrocell and optimised the energy efficiency of both femtocell and macrocell users. The objective is to maximise the weighted sum of individual energy efficiencies and the network energy efficiency while satisfying minimum throughput and fairness constraints for delay-tolerant users, and some other network-related constraints. The authors employed the subsequent convex approximation approach to address the complex RB and power allocation challenge to transform the original problems into a series of convex subproblems for more tractable optimisation. The authors in [71] proposed a method for joint power and subcarrier allocation in a distributed MIMO system, with the goal of eMBB and URLLC services. Different scheduling schemes, including orthogonal and non-orthogonal schemes, were considered for subcarrier assignment to improve spectral efficiency and meet the reliability requirements of URLLC. To ensure low latency, short packet transmission was adopted for URLLC services. The problem was formulated as a mixed-integer optimisation problem, aiming to maximise the energy efficiency of the system while adhering to QoS constraints. Due to the problem's intractability, a low-complexity algorithm was proposed to find a suboptimal solution. Authors in [69] jointly optimise the user association and power allocation problem for HetNets to maximise energy efficiency while satisfying user requirements in the downlink direction without considering physical RB allocation.

As per the Shannon-Hartley theorem, the capacity of a communication channel can be calculated as the product of the bandwidth and the spectral efficiency, where the spectral efficiency is a logarithmic function of the SINR. Nevertheless, linearising a logarithmic function can be challenging due to its non-linear nature. In [79], the authors addressed this issue by employing the big-M method, which involves establishing upper and lower bounds for the logarithmic function to facilitate linearisation. Furthermore, the authors proposed a dynamic two-stage design for downlink resource allocation and baseband unit-remote radio head assignment in Cloud-RAN. They first modelled the resource and power allocation problem as a MILP for real-time fluctuating traffic and then proposed a Knapsack formulation for the baseband unit-remote radio head assignment problem, aiming to improve QoS, power consumption and interference management in C-RAN.

Numerous research studies have focused on investigating network slicing architectures

primarily from the perspective of bandwidth allocation for BWPs only. Furthermore, the majority of these studies have been limited to network scenarios with a single BS and have yet to consider the effects of CCI or channel models [23] [80] [81]. This highlights the need for further research incorporating these important aspects into the design and optimisation of network slicing architectures for more realistic and comprehensive performance evaluations. In [23], a scenario with a single BS and multiple numerologies for uplink and downlink is considered. The authors utilise the ratio of average traffic load to capacity (i.e., normalised loads) as the optimisation objective. A weighted sum of normalised loads is minimised to efficiently utilise resources for two different services, eMBB and URLLC, each associated with a specific numerology. In [80], an optimisation approach for multi-numerology-based adaptive numerology resource allocation is proposed. The authors aim to increase cell throughput, maintain fairness, and minimise the delay. They define a metric for each numerology in terms of throughput and QoS requirements. Then the highest metric value for a specific RB is assigned to related numerology (by considering BWP) to allocate the bandwidth resources between numerologies. In [81], the authors define latency, data rate, and guaranteed bit rate requirements for services such as VoIP, video conference, and real-time gaming. They then perform two optimisations in their model. First, they identify the most demanding service (e.g., video conferencing) and allocate spectrum by considering fairness among users/services. The model is designed to be flexible, allowing the allocation of any numerology to users/services while meeting their requirements. However, this study does not consider channel models or BWP in the analysis.

The knapsack problem is a combinatorial optimisation problem that includes selecting a subset of items with specific weights and values [61] such that the total weight does not surpass a given capacity while maximising the total value. Due to its wide range of applications and challenging nature, the knapsack problem has been extensively studied in various fields. Researchers often utilise the knapsack problem as a benchmark or a foundational problem in their studies, owing to its complexity and relevance to many real-world optimisation scenarios. In the literature, several authors have focused on addressing the RAN slicing problem by approaching it as a multidimensional knapsack problem, specifically considering resource partitioning in the frequency and time domains. This approach has been studied in-depth in [3], [82], and [83]. In [3],

the authors propose a method to maximise the largest unallocated resources in the time-frequency domain, with the aim of increasing spectral efficiency based on RAN slicing. They consider various factors such as resource type (virtual or physical), resource abstraction type (e.g. fixed position, contiguous, non-contiguous RB groups), and resource structure that includes the relevant radio frame numerologies. However, this work should have taken into account BWP and interference aspects, which may be relevant in practical RAN slicing scenarios. In [82], the authors propose a two-level optimisation approach for spectrum allocation among numerologies and RB allocation among users. They refer to spectrum allocation as the first-level allocation and RB allocation as the second-level scheduling. The optimisation problem is formulated and solved for both time and frequency domains, with a focus on maximising fairness among users belonging to the same numerology. However, this work considers a single-cell scenario where CCI and BWP are unavailable for consideration due to the lack of multiple cells. In [83], the authors propose an optimisation method for resource and numerology allocation in a multi-user single-BS scenario, considering two types of users: low latency and non-low latency. Instead of a calculated channel model, they employ a channel estimation method that takes into account ICI, INI, and Doppler shift. The optimisation model considers the requirements of users in terms of delay, SINR, and packet size to allocate numerologies over available resources. While the low latency users are given priority for resource allocation, there is no guarantee that they will always be served. However, the authors could consider increasing the system capacity using methods such as IAB to address this issue. The authors in [84] explored resource allocation optimisation with flexible numerology in the frequency domain and varying frame structure in the time domain for services with diverse requirements. They proposed a scalable optimisation algorithm based on linear programming and Lagrangian duality. They considered two categories of services: one with strict latency requirements and the other to maximise throughput. They formulated the problem of maximising total throughput subject to latency and demand constraints. They solved a 2D knapsack problem considering different numerologies employed in 5G using MILP.

Several authors have conducted research on the allocation of transmit power and RBs for three key communication services in 5G-NR and beyond networks, namely eMBB, URLLC, and mMTC. In [85], the authors allocated transmit power and RB in the

downlink direction for eMBB, URLLC, and mMTC users. The authors assumed that the BSs have already allocated the BWPs in the carrier bandwidth. However, this approach lacks flexibility for the users, as each user can only use its own pre-allocated BWP, regardless of availability. 5G technology, on the other hand, can offer greater flexibility to users by allowing them to choose numerology based on availability. This approach can provide greater adaptability compared to the method used in the study, which does not allow for such user choice. Additionally, BWPs should be allocated based on user requirements rather than pre-allocated to ensure optimal resource usage. In [86], the authors address the issue of conventional resource allocation methods not being optimal for mission-critical IoT communications with URLLC requirements. They propose a novel approach that considers the finite block length and physical-layer security aspects and formulate two optimisation problems: weighted throughput maximisation and total transmit power minimisation. The authors develop methods to solve these non-convex optimisation problems, enabling resource allocation for secure mission-critical IoT communications with URLLC requirements. One of the studies closely related to our work in the literature is [87], where the authors investigated the joint optimisation problem of network slicing, numerology allocation, and admission control. In their work, URLLC and eMBB users were allowed to select numerologies reserved for their respective services. However, the reserved numerologies were strictly separated, with URLLC users able to select the first four numerologies and eMBB users limited to the last two numerologies. The authors focused on minimising the blocking probability of eMBB users' flow while meeting the service requirements of URLLC users. Furthermore, they did not consider aspects such as data routing or HetNets in their optimisation approach. The authors in [88] proposed a dynamic resource allocation scheme to decrease average scheduling latency in a network that employs multiple numerologies. The goal of the scheme is to achieve flexibility and adaptability for a vast variety of services while addressing the complexity of resource allocation with multiplexed non-orthogonal numerologies. The authors conducted a system-level simulation, instead of user-centring, to analyse different combinations of numerologies and service requests of varying priorities. They observed that by compromising the minimum achievable scheduling latency for high-priority requests, a significant reduction in average scheduling latency could be achieved, considering all

different types of service requests and different priorities.

2.2 Backhaul Routing Optimisation and IAB

As HetNets consist of diverse sources, such as microcell and IAB nodes, which are backhauled by a macro cell or fibre infrastructure, optimising access and backhaul links is crucial. Therefore, in this subsection, we present relevant literature examples that focus on backhaul, with a specific emphasis on IAB studies.

The advancement of mobile telecommunications technology has led to the exponential growth of data traffic and the need for more efficient and cost-effective ways of transporting data. The traditional method of transmitting data from a cell site to a central location, such as a mobile switching centre, was accomplished using dedicated leased lines like T1/E1 circuits [89]. This backhaul method has been used for many years and is still widely used in many parts of the world. IAB, on the other hand, refers to a more modern method of backhaul that integrates the access and backhaul networks into a single wireless network [27].

The main advantage of IAB is that it allows for the deployment of 5G-NR cells in dense areas without the need to densify the transport network proportionally and can be used for various deployment scenarios, such as indoor-outdoor small cell deployments or mobile relays on trains or buses [36]. IAB offers dynamic partitioning of resources between access and backhaul links, which enables cost-effective, flexible, and efficient use of network resources [90]. By dynamically allocating resources in an IAB network, the available bandwidth can be used more effectively, making it an ideal solution for ultra-dense wireless networks that require high spatial reuse and large amounts of bandwidth [91]. Additionally, IAB can help reduce the cost of deploying fibre to mmWave BSs, which suffer the severe path and penetration losses of mmWave signals. IAB-powered wireless backhaul can ensure efficient and flexible network operations while reducing costs [90].

3GPP defined two types of IAB, called in-band and out-band, which are based on the frequency overlap characteristics of the access and backhaul links [36]. In in-band backhauling, the access and backhaul links partially or fully overlap in frequency, which results in half-duplexing or interference constraints, which means that IAB nodes

cannot transmit and receive on both links at the same time [36]. In contrast, out-band backhauling uses different frequency resources for access and backhaul links. Therefore, out-band IAB allows for the simultaneous use of different frequency ranges, such as mmWave for backhaul and sub-6 GHz for access which allows the IAB node's ability to transmit and receive simultaneously on both links [37].

Since the same frequency band can be used for both backhaul and access, in-band IAB offers maximum resource efficiency, but to prevent intra-node interference (also known as self-interference), only half-duplexing can be used [92]. Specifically, it is not possible to simultaneously transmit data from the Distributed Unit (DU) and receive data at the Mobile-Termination (MT) in the downlink direction, nor can data be simultaneously received at the DU and transmitted from the MT in the uplink direction [92]. The MT unit is responsible for the wireless access part of the IAB node. It communicates directly with the UE and provides access to the 5G network through the IAB node. On the other hand, the DU is responsible for the backhaul part of the IAB node. It communicates with the Central Unit (CU) and provides the necessary data to the CU to connect to the core network.

Resource allocation in IAB networks is a critical aspect that has garnered significant attention from researchers. The authors in [93] investigated joint resource allocation and relay selection in a multi-hop IAB network with the objective of maximising the geometric mean of UE data rates. The assumption of time division multiplexing among contiguous links was made, and the focus was on in-band relaying, where the partition between access and backhaul resources can range between BSs. In [94], the configuration of incentive mechanisms and resource allocation in a user-provided network formed by Device-to-Device (D2D) links for 5G IAB networks are investigated. The authors formulated an optimisation problem, considering user utility, battery energy sensitivity, incentive compensation, and network resource limitations. They proposed a centralised algorithm for an optimal solution but also developed a distributed algorithm to address privacy concerns. The distributed algorithm decomposes the problem into subproblems for each user and iteratively executes subproblems to converge to the optimal solution of the centralised algorithm.

Since the best available SINR mostly determines user association in the optimisation problems, power allocation and user association problems can be intertwined.

Therefore, some papers jointly optimise the above-given objectives by employing IAB networks [95]. In their paper [95], the authors propose an optimisation problem that maximises network capacity for bandwidth-intensive IoT services like virtual reality, AR, and tactile Internet, using mmWave-based out-band IAB. The proposed approach utilises dedicated mmWave bands for access and backhaul links while considering both intra-cell and inter-cell interference. The problem is formulated as a joint user and transmit power allocation optimisation problem, and the authors address it by solving two sub-problems: user allocation and transmit power allocation.

The efficient access and backhaul routing and scheduling models increase the performance of the 5G network. IAB is a promising candidate to maximise the spectrum efficiency [96] [97]. The authors in [96] investigate the splitting methodologies of the total carrier bandwidth between access and backhaul for three scenarios named equal partitioning, instant partitioning, and average partitioning. They employ a single macro cell and small cell BSs, where the IAB-donor (i.e., a macro cell) and IAB-nodes (i.e., small cells) share the same infrastructure and wireless channel resources. The small cells are deployed at the centres of user hotspots, and users can be served by either small cells or macro cells. The same bandwidth, which employs only mmWave signals, is shared between access and backhaul. The authors [97] have tested three different IAB deployment scenarios; with only IAB nodes, with only BSs and with a mixed scenario. They have implemented end-to-end system-level simulations for mmWave frequencies to demonstrate that IAB provides a feasible solution for efficient network deployment. The authors in [98] propose a resource allocation optimisation among the backhaul link and UE access link of the IAB network, which allocates sub-channels and power. Although they utilised only the mmWave frequency band, they strictly separated the access and backhaul spectrum and considered out-band operation for the IAB network that supports multi-hop. Additionally, the paper conducts a geometric analysis of the IAB network to provide details of the system design. However, the authors did not take into account numerologies and bandwidth parts in their analysis.

When the multiple BSs transmit the same data to improve the signal strength received by the user by utilising the same frequency bands and time is called joint transmission, which can be implemented through coordinated multipoint [99]. In [99], the

authors employed out-of-band mmWave links using IAB for coordinated multipoint joint transmission. This approach requires distributing identical user data to multiple BSs in a joint transmission cluster, which can be a significant burden on the network backhaul. To alleviate this, the authors cache the data in the base stations and reduce the number of resource units used by each BS in the cluster as the SINR of the user increases. The authors in [100] addressed the challenge of wireless backhauling in mmWave networks, which generally require the dense deployment of mmWave BSs. They proposed an efficient scheduling method called "schedule-oriented optimisation" based on matching theory, which optimises QoS metrics jointly with routing. They demonstrated the optimal solution of maximum throughput fair scheduling as an example of schedule-oriented optimisation, showing that optimal scheduling can be acquired for the networks with a large number of mmWave BSs.

The authors in [101] propose an onboard relaying system that enables multi-Gbps data rate transmissions for train and vehicular applications. The system operates in the mmWave frequency band and provides mobile backhaul connectivity for in-vehicle UEs. To ensure stability against high mobility-related behaviours, such as fast channel variation and unsteady handover, the proposed system employs a relaying network architecture with a backhaul link to a vehicular UE and an in-vehicle access link. Since the proposed system can be implemented in high-speed trains, the authors considered Doppler spread and antenna polarisation. The paper presents essential design elements, such as numerology, frame structure, reference signal, multi-antenna scheme, and handover, for their proposed vehicular communication system. The system is validated through experimental tests conducted in existing subway and urban road environments using a testbed including a baseband modem, RF front end, and array antenna units.

In conclusion, in mmWave communications, sending signals over a long distance needs more transmit power; also mmWave signals can be easily blocked. Therefore, using a multi-hop self-backhauling architecture is a better solution to enable long-distance transmissions in mmWave networks instead of a single-hop approach [102]. However, the use of multi-hop self-backhauling can lead to an increase in delay, which should be taken into account during the design of such networks [102]. Due to these challenges in mmWave networks, we adopted a one-hop approach in our model. This approach

can be easily extended to a multi-hop IAB network, considering the potential impact on delay and ensuring careful design considerations.

2.3 Vehicular Networks

Vehicular communication initially emerged to fulfil safety-related requirements by periodically broadcasting messages (such as CAM/DENM) to nearby vehicles [42],[43]. The early stages of V2X applications were centred around Intelligent Transportation Systems (ITS) telematics and advanced auxiliary driving [103]. However, with the growth of mobile internet applications, there has been an increasing demand for vehicles with internet access capabilities to utilise services such as navigation and infotainment [103]. This evolution in vehicular communication has expanded the scope of potential applications and use cases beyond just safety-related communication to include various other services and functionalities enabled by internet connectivity.

Therefore, prior to the deployment of 5G-NR, V2X applications were primarily focused on safety-related communication, encompassing functionalities such as safety messaging [104], traffic incident monitoring [105], and intersection management [106]. Despite this safety orientation, a significant number of internet-based applications, such as navigation and infotainment applications, can also be found in the literature. For example, [107] presents an optimisation-based approach to model and analyse the performance limits of content downloading in vehicular networks, considering V2V relaying. In addition, the authors [108] proposed a 5G V2X ecosystem for IoV based on SDN and evaluated vehicular Internet-based video services traffic and V2V communications in urban and rural scenarios. Simulations were performed utilising mmWave frequencies, furthermore packet delivery ratio, data rate, and delay were analysed for rural and urban IoV scenarios.

Research conducted in the early stages of 5G-NR also encompassed the investigation of safety applications, as evidenced by the existing literature. For example, the authors [109] proposed workflow involves vehicles sending road condition information with GPS coordinates to other vehicles within a certain range and managing this information in a list. Vehicles approaching the location of the road condition update receive the information and forward it. To prevent exponentially increasing messages, the utilising

network slicing and SDN is suggested to enable efficient broadcast of information to vehicles connected through the same BS. However, the 5G-NR technology has further shifted the focus to a broader spectrum of advanced automotive applications. Recognising this trend, 3GPP has defined enhanced V2X (eV2X) use cases, which include extended sensors, vehicle platooning, remote driving, and advanced driving (autonomous vehicles) [110]. These eV2X use cases reflect the growing need for advanced vehicular communication capabilities to support various emerging applications in the automotive domain and highlight the evolving landscape of V2X technologies in the era of 5G-NR.

The extended sensors use cases group facilitates the transfer of either raw or processed data obtained from various sources such as regional sensors, live video images, RSUs, pedestrian devices, and V2X application servers [111]. This group comprises three specific use cases: sensor and state map sharing, collective perception of the environment, and video data sharing for automated driving [111]. The study conducted in [112] proposed an analytical model to assess the performance of a joint perception-sharing application. The analytical evaluation focused on examining the improvements in environmental perception and detection redundancy for connected vehicles, considering various penetration rates of collective perception service and traffic densities. The results showed that LTE-V based service could remarkably improve the aforementioned metrics, though additional improvements may be necessary to satisfy the latency requirements of vehicular safety applications. Furthermore, the analysis highlighted the necessity of decentralised congestion control in specific scenarios.

In vehicular communication, a platooning system refers to a configuration where multiple vehicles are grouped together to share common mobility modes, and all participants are controlled by the leading vehicle [113]. This configuration allows for coordinated and cooperative driving among the vehicles in the platoon, often resulting in improved traffic efficiency, fuel efficiency, and safety. The authors [113] proposed a spatial framework for mmWave V2X networks for platooning using stochastic geometry. In addition, they derived closed-form expressions for blockage caused by vehicles, analysed path loss, and designed user association techniques. The study showed that a higher density of platooning vehicles and larger antenna scales improved coverage performance.

The remote driving use case group enables remote vehicle control, either by humans or cloud/edge computing [111]. It requires V2X communications to support data rates up to 1 Mbps (downlink), 25 Mbps (uplink) for application-related control and video/sensor data, and ultra-high reliability of 99.999% or higher is necessary to avoid application malfunctions [111]. This recent paper [114] demonstrates a study conducted to validate the feasibility of a remote driving application for V2X over mmWave 5G-NR. The study starts with an overview of how a standard mmWave 5G-NR communication system is structured and its essential components for remote driving applications. Then the study explores the technologies that make reliable communication possible for remote driving, including beam switching, automatic gain control, uplink transmit power control, and hybrid automatic repeat request with soft combining. The study also covers the practical aspects of implementing and deploying testbeds and shares the experimental outcomes acquired from field trials. Finally, the authors executed a comprehensive implementation of the system, starting from theoretical findings on the optimal physical layer design of the network and subsequently integrating the theory into the testbed for a teleoperation scenario. In contrast to the teleoperation scenario at a distance of 470m as studied in [114], the authors in [115] conducted a remote control experiment with a vehicle equipped with sensors and actuators at a distance of 36 km. This remote control experiment enabled the transmission of sensor data and video streams, and vehicle-control commands from a remote operations centre in the uplink and downlink communications, respectively. The main objective of this study is to assess the feasibility of the proposed teleoperated support service by assessing performance metrics such as latency, jitter, throughput, and loss rate. Both Tele-operated Support services studied in [114] and [115] rely solely on human teleoperators for remote control, without the involvement of artificial intelligence.

Advanced driving facilitates a high level of automation in vehicles, enabling fully automated driving while maintaining longer inter-vehicle distances [111]. The advanced driving is achieved through data sharing among vehicles and/or RSUs obtained from local sensors, which allows for coordinated trajectories and manoeuvres [111]. Additionally, vehicles share their driving intentions with nearby vehicles. The key advantages of this use case group include safer travel, collision avoidance, and improved traffic efficiency [111]. The key performance indicators that are required for advanced

driving include an end-to-end latency of less than 3 ms, a throughput of 30 Mbps, and reliability of 99.999%, all to be achieved within the communication range of 500 m [111]. These key performance indicators serve as vital benchmarks for assessing the performance and effectiveness of the communication system under investigation.

The projected growth of autonomous vehicles in the future, driven by urbanisation, improved living standards, and technological advancements, is expected to lead to a significant increase in the demand for communications devices and digital applications to encourage intelligent autonomous vehicles [116]. Furthermore, the emerging services in autonomous vehicles, such as 3-D displays with enhanced depth and viewing experience, free-floating capabilities, holographic control display systems, immersive entertainment, and improved in-car infotainment, are expected to pose new communication challenges to the V2X network [116]. As a result, the development of 6G V2X communications is considering these requirements for autonomous vehicles, which may not be fully met by 5G NR-based V2X networks [116].

As evident from the examples mentioned above, some use cases in 5G-NR vehicular networks require ultra-high reliability, while others demand high data rates, which can be facilitated through network slicing. Hence, network slicing holds significant importance for enabling diverse communication requirements in vehicular networks. Accordingly, several authors have investigated network slicing for vehicular networks, enabling use cases such as remote driving, advanced driving, and platooning. Network slicing allows for the creation of dedicated virtual networks that can provide the specific requirements of these vehicular applications.

Three primary use cases of 5G-NR have been identified and discussed in detail in Chapter I and in this chapter. Here, we provide illustrative examples of how these use cases are applied in the context of vehicular communications. Joint resource allocation for URLLC and eMBB traffics in a one-way highway vehicular network studied in [117]. They assumed full-buffered eMBB traffic with scheduled multimedia transmissions and random arrivals of URLLC traffic during eMBB transmission intervals. To meet URLLC latency constraints, the eMBB time slot was divided into mini-slots and URLLC traffic was scheduled promptly in the next mini-slot by puncturing ongoing eMBB traffics. Guard zones were deployed around vehicle receivers to ensure URLLC reliability by prohibiting eMBB transmissions inside these zones. The authors derived

the transmission probability of RSU nodes, captured association probabilities of vehicle receivers for URLLC and eMBB traffic, and analysed the coverage performance of V2V links and the rate coverage performance of V2I links based on these results. The authors[118] propose a network slicing-based communication solution for vehicular networks, specifically targeting ultra-reliable vehicle-to-everything (V2X) communication. This work modelled a vehicular highway scenario where vehicular nodes have diverse requirements. Two logical slices for safety messages and video streaming are created on the shared infrastructure. A network clustering and slicing algorithm is formulated to splitting the vehicles into different clusters and allocate slice leaders to each cluster. Additionally, RSUs are utilised to provide infotainment services using high-quality V2I links.

Ultra reliability and low latency are critical elements of 5G-NR, and as such, researchers have extensively investigated methods to enhance reliability and reduce latency in vehicular networks within the context of 5G-NR. URLLC slice is designed to fulfil the requirements of latency-sensitive applications. These requirements typically include extremely low end-to-end latency of 1 ms or less, robust security measures, minimal data packet loss of 10^{-5} or lower, and high reliability of 99.999% or above. These stringent performance criteria are crucial for applications that demand ultra-reliable and low-latency communication and form the foundation of URLLC technology for meeting the needs of such applications. The authors in [51] propose a network isolation and slicing solution that expands from resource slicing to service and function slicing to enhance reliability and latency performance in 5G autonomous vehicular networks. Simulation results show that the proposed network slicing method enhances reliability and latency performance, with optimisation depending on vehicle density in 5G autonomous vehicular networks. Furthermore, the authors formulated a stochastic optimisation problem to achieve proactive radio resource allocation in the open-loop uplink of vehicular networks for URLLC [119]. To address computational challenges, the authors proposed a virtual resource slicing algorithm that maps radio resource units to virtual RBs, aiming to reduce computation and improve the efficiency of the Lyapunov optimisation. Link adaptation, which involves adjusting the modulation and coding scheme based on channel state feedback, is essential to achieve reliable outcomes. In [120], a Markov chain-based link adaptation technique is proposed to

support URLLC use cases in vehicular networks. This study proposes a novel Markov Chain model for link adaptation that estimates three key performance indicators: end-to-end link latency, throughput, and block error rate, based on the modulation and coding scheme used.

Regarding resource allocation in vehicular networks, the authors [121] investigate the resource-sharing problem for V2V and V2I communication links. The authors apply graph theory for the first time to solve the resource-sharing problem and propose two interference graph-based schemes: the interference-aware and the interference-classified graph-based resource-sharing schemes. The proposed schemes show an improved network sum rate compared to vehicular networks' traditional orthogonal communication mode. The authors in [122] explain how they consider the connectivity in vehicular networks, assuming interference among multiple links rather than relying solely on signal strength or distance between pairwise vehicles. They propose a connectivity optimisation problem considering resource allocation utilising graph theory. They provide definitions of connectivity metrics affected by interference, analyse the number of resources needed to guarantee network connectivity, and propose a resource allocation algorithm taking into account the minimum spanning tree to enhance network connectivity within the constraints of limited resources. A recent study conducted a survey on resource allocation in vehicular networks, as referenced in [123]. Further studies can be found and explored for more in-depth insights if desired.

In the field of vehicular networks, there is a wide range of studies and examples beyond the papers mentioned above that can be found in the literature. Numerous papers discuss the intersection of ML and vehicular networks; for example, the authors [124] and [125] propose utilising ML and deep learning algorithms to analyse large-scale transportation data with reduced complexity for traffic flow prediction. Additionally, authors [126] demonstrate approaches for handling big data in traffic estimation, while [49] shares simulation assumptions for vehicular urban scenarios. However, it should be noted that in this thesis, our research focuses explicitly on 5G-NR network slicing and involves the use of MILP, heuristics, and RL algorithms for resource allocation and routing. Therefore, papers unrelated to our research topic have not been extensively investigated in our research.

2.4 Heuristics

Heuristics are problem-solving techniques that use practical approaches and shortcuts to find solutions quickly. They are commonly employed in optimisation problems that require finding an acceptable solution within a reasonable time frame. In addition, heuristics are needed in scenarios where mathematical methods are not feasible due to their complexity or the large scale of the problem. In such cases, heuristics can provide a good approximation of the optimal solution, making them useful for practical applications. We provide a review of various heuristic and meta-heuristic approaches used in the literature for solving optimisation problems related to wireless communication networks.

Metaheuristics are higher-level strategies or frameworks for finding solutions to optimisation problems. They are designed to guide and improve the search process of lower-level heuristics, which are methods used to solve specific problems. Metaheuristics are problem-solving methods that can be utilised for diverse optimisation problems rather than being limited to a specific problem. They use an iterative process to explore the search space and attempt to enhance the quality of solutions, often by combining and adapting different heuristics. For example, Evolutionary algorithm (EA)s are a type of metaheuristic that is inspired by the Darwinian theory of evolution, which emphasises the survival of the fittest. EAs are used to evolve a population of solutions towards an excellent adaptation to their environment, with the goal of producing solutions that closely approximate the global optimum. EAs have been widely used to solve problems in diverse fields, such as energy efficiency in cloud computing [127], finance and economics [128], and diesel engine designing [129] since their inception, as demonstrated by multiple successful applications.

Since evolutionary algorithms are able to handle complex and multi-dimensional optimisation problems, they have been widely used in the literature to solve multi-objective optimisation problems. The papers [130], [131] address the Vehicle Routing Problem using an Evolutionary Multitasking approach, which involves the concurrent optimisation of multiple tasks through a shared population of individuals that evolve over generations. This approach has shown promising results in efficiently solving complex optimisation problems with multiple objectives and constraints by evolutionary algo-

rithms. In [132], an evolutionary algorithm that generates sub-populations at each iteration, each devoted to solving a specific task, was introduced for resource allocation. Resources are allocated to each sub-population based on a task's improvement index, with the assistance of the softmax function.

Moreover, in [133], the authors implemented a joint optimisation of radio access network resources (bandwidth) and mobile cloud networks among users by utilising heuristic approaches. The objective is to maximise the total benefit of users and satisfy the latency requirement of the users. To solve the optimisation problem, they utilised and compared three progressive methods: genetic algorithm, ant colony optimisation with genetic algorithm and quantum genetic algorithm.

In many heuristic papers in the literature, a common approach is to employ MILP optimisation techniques to obtain optimal results initially. Subsequently, a heuristic algorithm is implemented to reduce computational expenses while achieving acceptable results. This approach enables a comparison between the optimal and sub-optimal solutions, providing insights into the performance trade-offs and the effectiveness of the heuristic approach. The authors in [134] addressed the resource allocation problem in 5G-NR that supports eMBB and URLLC services. They formulated the resource allocation problem at the RAN as a sum-rate maximisation problem, subject to constraints such as service isolation, latency, minimum rate, and reliability, while incorporating adaptive modulation and coding. They also proposed a low-complexity heuristic scheduling scheme for efficient multiplexing of URLLC and eMBB services to reduce the complexity of the optimisation-based scheduling algorithm. The resulting solution provides a near-optimal solution to the original problem. Finally, they demonstrated the efficiency of their proposed optimisation and heuristic methods via numerical simulations. In [135], the authors focus on the Open-RAN paradigm, which involves cloudification and network function virtualisation for baseband function processing in dis-aggregated Radio Unit (RU), DUs, and CUs. They propose and compare two resource allocation mechanisms, namely minimum-maximum fairness and auction-based, for creating a sustainable multi-tenant Open-RAN ecosystem for small, medium, and large mobile network operators. The minimum-maximum fairness approach minimises the maximum OPEX of RUs via cost-sharing proportional to their requirements. In contrast, the auction-based approach minimises the total OPEX for all resources

utilised while extracting genuine requirements from RUs. In addition to MILP optimisation, the authors propose a heuristics that outperform conventional greedy resource allocation algorithms regarding economic efficiency and network resource utilisation. In [136], the authors focus on the problem of rate and power allocation in a multiuser orthogonal frequency division multiple access (OFDMA) systems. Using directional derivatives, they derive a solution to the power allocation problem for a general category of rate-power functions. They propose a new heuristic approach and compare it to two existing heuristics using a branch-and-bound algorithm. The performance of the algorithms is evaluated by computing the exact optimum, which is also calculated with heuristic methods with a given number of allocated subcarriers per user. In [137], the authors proposed a frame reconfiguration scheme to provide more flexibility in adapting to dynamic traffic. They formulated the inter-BS scheduling problem as a nonlinear integer programming problem instead of MILP, aiming to maximise the number of flows to satisfy the data request. They also presented a heuristic scheduling algorithm with adaptive power allocation for multi-hop relaying, regarding the traffic load at each BS.

In contrast, some heuristic papers in the literature utilise heuristic methods in their approach without providing an optimal solution. As a result, it is challenging to evaluate the effectiveness of their proposed approach since it cannot be compared to an optimal solution. The authors [138] proposed a novel heuristic method to address the challenges associated with mixed numerology-based frame structures in 5G systems. The authors developed a heuristic method that determines the optimum number of mixed numerologies to be employed in the system, with the aim of controlling overheads in multi-numerology systems. The proposed method also includes an analysis of trade-offs and relationships between various services and user requirements. The algorithm designed by the authors incorporates a new flexibility function and performance metric to achieve the desired outcomes. In [139], a solution for data block allocation in a generalised frequency division multiplexing-based virtualised physical layer is proposed. The authors formulate the data block allocation problem as a Knapsack problem, where the QoS demands of the data flows are incorporated using utility theory. The utility functions provide a metric of urgency for flow scheduling and data block allocation. The authors propose a heuristic solution for the resulting

two-dimensional geometric Knapsack problem and evaluate the data rate and queuing delay performance.

In contrast to some existing literature that has employed heuristic approaches without providing evidence of a proven-optimal solution, our work adopts a rigorous mathematical method, namely the MILP optimisation approach, which guarantees finding the optimal solution within the given problem constraints. For further information on heuristic and meta-heuristic methods, please refer to Chapter 4, where we elaborate on the different optimisation techniques used in our study.

Although the GA is computationally less expensive than MILP optimisation, it cannot be employed in real-time or near-real-time due to its high computational complexity in our model. However, the power allocation and user association algorithm must also be computationally efficient for practical, real-world implementation. Therefore, the algorithm should have a reasonable execution time and should be able to handle the constraints and the number of variables in a realistic system. Thus, we considered to employ ML techniques in this thesis.

2.5 Machine Learning

Machine learning is a rapidly growing domain that leverages computational algorithms to create statistical models. ML enables computers can establish connections between inputs and outputs; thus, computers can learn how to make predictions or take actions based on the corresponding input data. ML has witnessed significant advancements in recent years, with applications ranging from object detection [140], speech recognition [141], and video classification [142] to wireless communications [143]. One subfield of ML that has gained traction is RL, which involves training agents in an environment by making observations, taking actions, and receiving feedback as rewards or penalties. DRL, a variant of RL that utilises deep neural networks (DNN)s, has demonstrated impressive performance in various applications, for example, mastering in atari games [144] and the game of Go [145] without human knowledge. Furthermore, RL has been utilised for power allocation [65] and user association [146] in wireless networks. In this chapter, we explore the applications of ML and RL in the context of our research, building upon the advancements made in these areas.

It is worth noting that we specifically focus on the applications of ML in the areas of 5G-NR, network slicing, and vehicular networks. Chapter 5 of this thesis provides detailed definitions and information on the types of ML techniques used in 5G-NR, network slicing, and vehicular networks. Chapter 5 also discusses various ML algorithms, such as supervised, unsupervised, and reinforcement learning, and their applications in these areas.

Machine Learning in Vehicular Networks

Today's vehicles are equipped with many sensors, lidars, cameras, proximity sensors, and motor and tyre control units; traditional data processing techniques cannot process this massive amount of data. Since autonomous vehicles need more sensors than human-controlled vehicles, a huge data processing and storing capacity is required in real-time. The collected, generated, stored, and communicated data (speed and direction of a vehicle, road conditions, traffic flow) by road elements (vehicles, pedestrians, traffic lights) are called mobile big-data [46]. ML algorithms are one of the enablers of mobile big-data and vehicular communications. Moreover, given the high mobility of vehicles, the fast-response requirements of vehicular networks, and the need to optimise resource allocation in high throughput mmWave frequency bands, the application of machine learning is essential.

There are several reasons to consider the use of ML algorithms in vehicular networks. Firstly, ML algorithms can achieve real-time outputs by learning from collected data without explicitly processing each individual data point [147]. Secondly, the availability of accessible programming libraries, such as Python, Matlab, and R, has enabled researchers and industries to develop ML algorithms more easily [148]. Additionally, ML is well-suited for applications in vehicular networks due to the dynamically changing environments and high mobility of vehicles. It can provide low-latency and high-reliability solutions for applications with stringent requirements.

The utilisation of ML techniques in 5G-NR resource allocation has emerged as a prominent and active research area. This utilisation encompasses not only traditional resource allocation challenges in 5G-NR networks but also extends to the unique resource allocation requirements of vehicular networks. The resources in V2V communication can be shared using the RL approach. The authors in [143] propose a decentralised

resource allocation method for V2V communications based on DRL. They develop an innovative technique that can be applied to unicast and broadcast scenarios, allowing independent vehicles or V2V links to make decisions independently without waiting for global information. The paper addresses the challenges of the broadcast storm problem and package collision that can occur when blindly broadcasting messages in V2V communication. The action space, state space, and reward function are carefully developed for unicast and broadcast scenarios to solve the resource allocation problems in V2V communications. The authors [149] address the problem of distributed resource selection in V2V communication, where each vehicle autonomously chooses communication resources from a shared pool to distribute CAMs. Each vehicle must choose a resource, which becomes more challenging in congested scenarios and in dynamic scenarios where the number of vehicles in the vicinity of each other changes dynamically. The authors propose a multi-agent RL algorithm that builds on a unique state representation. The aim is to perform complex joint behaviour in a distributed manner and tackle the challenges of non-stationarity in resource allocation in V2V communication. Further examples of research in resource allocation with ML can be found in the subsequent subsection. [150] focuses on optimising the transmit power allocation in a V2X communication system to maximise the overall system throughput. The authors propose two methods to solve the power allocation problem: the weighted minimum mean square error algorithm and a deep learning-based method. They use the block coordinate descent method in the former algorithm and then employ supervised learning techniques for the DNN-based approach, with the power allocation from the weighted minimum mean square error algorithm as the target output. They employ an efficient implementation of a mini-batch gradient descent algorithm for training the DNN. The authors in [151] formulate a joint spectrum reuse and power allocation problem for hybrid V2V and V2I communications. They want to maximise the weighted sum of capacities and latency requirements, considering intracell interference and the high capacity and low-latency requirements for V2I and V2V links, respectively. They decompose the problem into a classification subproblem and a regression subproblem and develop a convolutional neural network-based approach to acquire real-time decisions on spectrum reuse and power allocation.

Machine Learning in 5G-NR Resource Allocation

Numerous studies in the literature have utilised DRL techniques to address the challenges of power and resource allocation among users and user resource association in various communication systems. In [152], the power allocation problem in cellular networks with multiple cells and shared frequency spectrum has been addressed using a multi-agent RL algorithm. Each BS is controlled by a DRL agent that adapts power based on local observations, such as cell power, received power, interference, and reward. The approach has achieved substantial energy savings and fairness between users by effectively controlling transmit power. Similarly, in [153], the network consists of multiple cells, each with a single BS serving multiple users. All BSs transmit over the same spectrum, resulting in both intra-cell and co-channel interference. An RL agent controls each BS to determine its transmit power to maximise the network's sum throughput.

In [65], the authors developed a dynamic power allocation scheme for wireless networks using model-free DRL. The scheme is distributively executed, where each transmitter collects channel state information and QoS information from neighbours to adapt its transmit power. The objective is to maximise a weighted sum-rate utility function, which can be customised for different performance goals. The proposed algorithm uses deep Q-learning to address random changes and delays in the channel state information. It is designed to make power allocation decisions in real time, even when there are delays in obtaining the channel state information measurements, and it performs near-optimal solutions. The scheme is particularly suitable for scenarios where the system model is inaccurate, and channel state information delay is significant. The same authors in [72] further propose a learning-based method for optimising discrete subband allocations and continuous power allocations in wireless networks, considering time-varying channel and traffic conditions. They use two complementary DRL algorithms to optimise these allocations based on local and nearby channel state information, which may be delayed and inaccurate. The goal is to maximise a joint objective, addressing the challenges of computational complexity and acquiring instantaneous global channel state information associated with standard model-based approaches for network utility maximisation. The authors in [146] propose an RL approach for solving the joint user association and resource allocation problem in the downlink of

heterogeneous cellular networks. They aim to achieve the maximum long-term overall network utility while ensuring the QoS requirements of UEs. The proposed method is based on multi-agent RL and distributed optimisation, where UEs need to choose a BS and transmission channel at each time step in the RL model. To address the computational complexity of the large action space, a multi-agent DRL method is proposed. This method considers the state, action, and reward function for each UE and includes the duelling double deep Q-network (D3QN) strategy to acquire near-optimal outcomes. Each agent employs the message passing technique to reduce the communication overhead in the global state space.

The optimisation of RAN slicing using ML techniques has gained significant attention as a cutting-edge research topic in wireless communications. This area explores novel approaches to dynamically allocate and manage radio resources among different slices in a wireless network using ML algorithms and has emerged as a prominent and active research area in recent years. The authors [41] address the RAN slicing problem in the context of 5G services, specifically eMBB and V2X. The authors formulated the problem of RAN slicing to support eMBB and V2X communication on the same RAN infrastructure as an optimisation problem. The objective is to determine the allocation of radio resources to each slice while improving radio resource utilisation and meeting specific requirements for each slice, considering uplink, downlink, and sidelink communications. They proposed a new strategy based on offline Q-learning and softmax decision-making as an enhanced solution for resource allocation between the eMBB and V2X slices.

None of the previous studies has addressed the issue of a multi-numerology environment. However, with the emergence of 5G-NR networks, numerology selection has become a crucial aspect of user association problems and, therefore, must be considered in power allocation and user association decision problems.

Machine Learning in Other 5G-NR Applications

The utilisation of higher carrier frequencies in communication systems is essential to address the increasing demand for traffic capacity, consumer data rates, and spectrum resources. This utilisation necessitates the use of wider transmission bandwidths to meet these requirements [28]. mmWave frequency bands are particularly attractive

due to their wider transmission bandwidths and higher data rates compared to sub-6 GHz frequency bands [97]. However, it is important to note that mmWave frequency bands also exhibit higher propagation loss than sub-6 GHz frequency bands at the same distance due to the proportional relationship between frequency and propagation loss [32]. Moreover, due to the high mobility of vehicles, vehicular networks have dynamically changing environments. Therefore, the deployment of mmWave frequency bands in the vehicular must be carefully considered.

ML algorithms can be utilised for beamforming in wireless communication systems to overcome the high propagation disadvantage of mmWave. Beamforming, a technique used to focus the transmitted signal in a specific direction, plays a crucial role in improving the performance of wireless communication systems by mitigating interference, increasing signal quality, and enhancing overall system capacity. In their works, the authors in [31] propose a beam selection model for vehicular networks, where connection requests from vehicles are sent via LTE and associated with 5G mmWave base stations. Their model leverages Fast Machine Learning algorithm and contextual multi-armed bandit problem to autonomously learn the relationships between the environment and decisions. The exploration stage allows the system to learn new knowledge, such as identifying permanent and frequent blockages, while the exploitation stage optimises decisions based on contextual information from prior knowledge. Additionally, the same authors propose a similar machine learning-based approach for optimising the use of mmWave frequencies in 5G vehicular networks in [154]. This approach also employs a contextual multi-armed bandit problem and a fast machine learning algorithm to enable mmWave base stations to learn the relationships between contextual information and their decisions and make optimised beamforming decisions based on that learning. The paper also introduces a beam selection system for ensuring connectivity between vehicles and mmWave base stations.

RL can be used to extend cellular network coverage to out-of-coverage areas by optimising resource allocation and scheduling decisions. For example, in [155], the authors propose a novel approach for resource pre-scheduling in V2V communication in areas outside cellular coverage. Their approach utilises the network infrastructure to perform resource scheduling based on readily available information, such as radio resource occupancy and scheduling requests for periodic transmission, while the vehicles

are still connected to the network. The scheduling decisions are then communicated to the vehicles via scheduling assignments before they enter out-of-coverage areas. Furthermore, the authors employ a DRL algorithm, specifically the asynchronous advantage actor-critic (A3C) algorithm, to exploit V2X-specific information for resource pre-allocation. The A3C algorithm is known for its strong convergence properties and is used to optimise resource scheduling decisions based on available information.

The path selection and rate allocation sub-problems are jointly investigated in the IAB subsection. In this subsection, the same joint problem is optimised by [102] by using RL techniques. They optimise the problem of path selection and rate allocation for multi-hop self-backhaul mmWave networks, considering the challenges of severe path loss and unreliable transmission over long distances at higher frequency bands. They proposed a system design that utilises multiple antenna diversity, mmWave bandwidth, and traffic splitting techniques to improve downlink transmission. The authors utilised stochastic optimisation to separate the problem into path selection and rate allocation sub-problems. For path selection, they employed RL, while for rate allocation, they utilised the successive convex approximation method.

The optimisation of routing and dynamic storage allocation of renewable energy in an electric vehicle network is of paramount importance, as the state of charge plays a critical role in the overall performance and efficiency of the network. The authors in [156] conducted a study on a renewable energy-enabled electric vehicle network, which is an implementation of IoT in energy and vehicular networks. They focused on optimising the routing and dynamic storage allocation of renewable energy in electric vehicle networks to maximise plant-to-station energy transfer efficiency. They proposed a time-expanded topology graph-based model and used linear programming for joint energy storage capacity and route planning. They also extended the problem to cases where the traffic pattern of the electric vehicle network is unknown and utilised deep learning techniques such as long short-term memory (LSTM) and RL to predict and improve the accuracy of traffic pattern prediction.

In conclusion, ML concentrates on the development of algorithms and statistical relationships. These algorithms enable computer systems to learn and then either take actions without being explicitly programmed to do so or provide predictions for unseen data. By leveraging the huge quantities of data generated every day, ML has the poten-

tial to revolutionise how we solve problems and provide predictions or decisions. In our specific case, it is crucial that the optimal response be provided promptly to the users. This optimal response can consider power or numerology allocation for users, BWP allocation for the numerologies, user association, data routing among nodes, or the joint optimisations of the combination of given problems. Additionally, the algorithm must exhibit computational efficiency to be feasible for real-world implementation.

Chapter 3

Optimisation Model

In this chapter, the mixed-integer linear formulation for the resource allocation problem in vehicular networks is presented. The proposed formulation considers the user requirements and utilises binary and non-binary variables to optimise multiple objectives. Linearisation methods and constraints are employed to handle nonlinear equations, such as the Shannon capacity formula involving logarithmic functions. Towards the end of this chapter, the outputs of the optimisation framework are demonstrated, showcasing the results obtained from the formulated approach.

We consider a city environment where multiple cells are deployed, supporting radio slicing and multi-numerology techniques. A demand point (DP) can represent either individual or aggregated user demands, as stated in [157]. These DPs are randomly located and generate traffic demands, which are characterised by data rate in Mbps and delay requirements in milliseconds (ms). Additionally, the vehicles in the network also function as mobile IAB nodes, referred to as VBS. These VBSs establish communication links with nearby BSs and DPs, where the former uses the FR2 (mmWave) frequency range for backhaul, and the latter provides access using the FR1 (sub-6 GHz) frequency range. More details on the FR1 and FR2 frequency bands are discussed in Chapter 3.1.2. Our work involves the implementation of three types of optimisation techniques that are interdependent and closely related to each other.

- First, bandwidth allocation amongst BWPs by considering total carrier bandwidth is optimised. The same bandwidth allocation of BWPs is applied to all BSs in the model. Existing studies in the literature consider that inter-numerology

interference (INI) causes in the same BS and maximises when resource elements from different numerologies are physically close to each other [22], [158], [159]. To the best of our knowledge, no previous work in the literature considers specifically the INI caused by neighbour BSs. We assume that INI can occur among BSs that use the same resource elements for different numerologies due to disrupted orthogonality. Therefore, the BWPs with the same numerology are located in the same frequency resources for all the BSs. Thus, INI caused by another BS is minimised.

- Second, RB and power allocation among DPs are optimised by considering their delay and data rate requirements in the downlink direction. We considered a frequency-selective propagation channel and a multi-cell system where co-channel interference (CCI) affects signal-to-interference-plus-noise ratio (SINR) performance.

- The third optimised object is to achieve maximum power efficiency; the model optimises the route of the data packets from BSs to DPs with or without utilising VBS nodes. Since this optimisation framework is a HetNet, user association is also optimised. Therefore, we optimise an inter-layer framework, including the physical and network layers, where DPs can be served by BSs directly, which are connected to the core network via fibre or VBSs, which are backhauled by BSs using mmWave signals.

The network architecture is a heterogeneous and flexible 5G-NR vehicular network that supports radio slicing to cater to the diverse requirements of DPs. The heterogeneity is reflected in varying DP requirements, network slices, and VBS nodes that enable out-band backhauling. The flexibility is reflected in DPs being able to choose any numerology while ensuring their requirements are met and bandwidth allocation between BWPs. In other words, shared network slices are employed instead of dedicated ones. Minimum numerology requirements are determined based on the data rate and delay demands of DPs to fulfil their specific requirements within a given unit of time.

3.1 System and Channel Model

In this section, we introduce the system and channel model of the proposed framework. This framework is utilised in MILP, Heuristics, and Machine Learning chapters. Thus, the outputs of the proposed framework can be compared with each other.

3.1.1 System Model

We consider a 5G multi-cell cellular system with B base stations, V vehicular base stations indicated by the sets $B = \{1, ..., B\}$ and $V = \{1, ..., V\}$, respectively. Then, the Source set S is defined as the union of the sets BS and VBS, where $|S| = |B|+|V|$. Also, the set of DPs, numerologies, and RBs are denoted by $D = \{1, ..., D\}$, $N = \{1, ..., N\}$, and $R = \{1, ..., R\}$, respectively.

Any BS in the model has two functions: they generate data and provide connectivity. We consider three different types of DPs, each designed to meet the specific requirements of three distinct service types in 5G-NR. These DPs are assumed to have two distinct requirements, data rate and delay. Moreover, each DP is served either directly by a BS or indirectly by a VBS, as illustrated in Fig. 3.1. VBSs are used as a tool to meet wireless demand in 5G networks and can provide an intermediate solution to increase network capacity. According to the DP requirements, the model allocates the corresponding network service that is provided by a related RAN slice. The RAN slices share the same carrier bandwidth; accordingly, the total bandwidth is divided into BWPs, where each BWP occupies a certain portion of the available bandwidth, and each BWP is split into RBs with the same numerology. An RB is the smallest unit of frequency resource that can be allocated to a DP. We consider that the DPs can be served by any network slice as long as their requirements are satisfied. Consequently, bandwidth allocation between BWPs is flexible and depends on interference, transmit power and the number of served DPs.

Let t_d denote the delay requirement of each DP, whereas t_n denotes the slot duration of each numerology $n \in N$. To meet the delay requirement of each DP t_d should be greater or equal to t_n.

$$t_d \geq t_n, \quad \forall\, d \in D \tag{3.1}$$

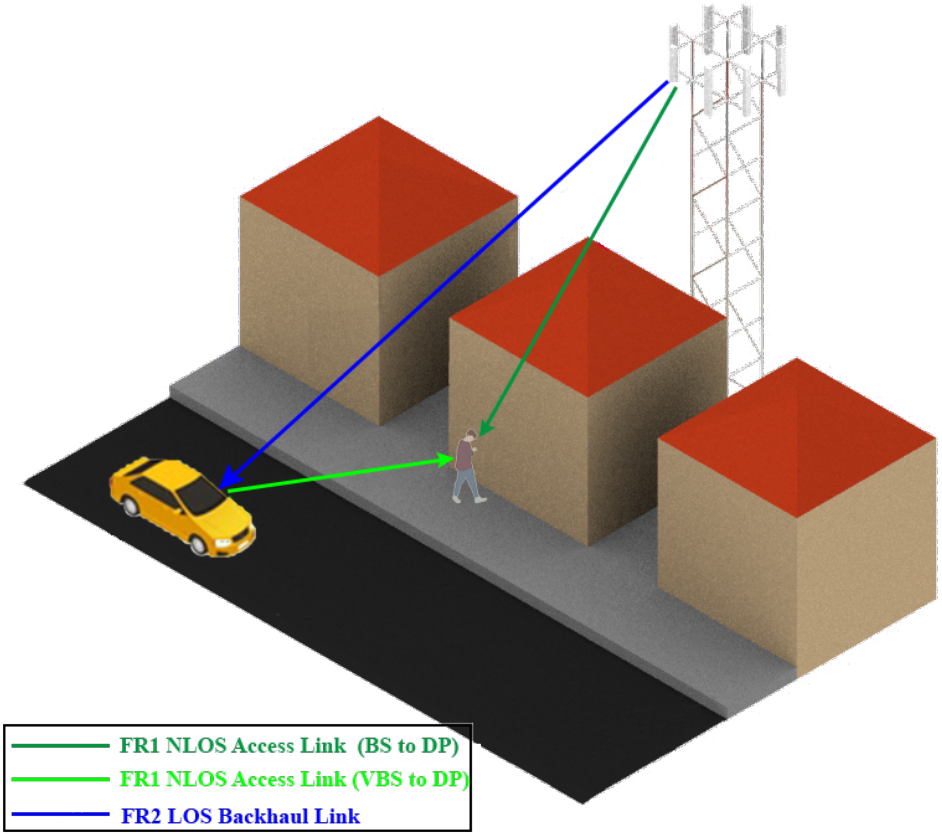

Figure 3.1: Basic system model illustration

DPs have data rate requirements, as well. To ensure that the data rate requirement of each DP, denoted as d_d, is satisfied, it should be less than or equal to the allocated represented by Ω_d.

$$\Omega_d \geq d_d, \quad \forall\ u \in U \tag{3.2}$$

It's important to note that Eq 3.2 exhibits non-linearity because of the data rate calculation. However, due to the MILP nature of our problem, we need to transform it into a linear formulation, which is elaborated in Chapter 3.3.

To reduce the complexity and number of binary decision variables, we have identified all the binary decision variables as 'y' but with different indices. Let us denote y_{sd}^{rn} as the 4-dimensional binary main decision variable that establishes the relation between Sources, DP, RB and numerology. y_{sd}^{rn} gives the information about which source connects to DP with the RB of related numerology, hence:

$$y_{sd}^{rn} = \begin{cases} 1, & \text{If DP } d \text{ is served by source } s \text{ utilizing numerology } n \text{ and RB } r \\ 0, & \text{otherwise} \end{cases} \tag{3.3}$$

It is worth noting that all the binary decision variables are derived from y_{sd}^{rn}. By utilizing following method, any binary decision variable (y_{sd}, y_d^r, y_s^{rn}, etc) can be composed. For example, to get y_{sd} from y_{sd}^{rn}, we utilized the equations Eq (3.4) and Eq (3.5) where K is a large number:

$$\sum_{r \in R} \sum_{n \in N} y_{sd}^{rn} \;\geq\; y_{sd} \tag{3.4}$$

$$\sum_{r \in R} \sum_{n \in N} y_{sd}^{rn} \;\leq\; K\,(y_{sd}) \tag{3.5}$$

Modifying the indices in Eq 3.4 and Eq 3.5 makes it possible to derive the above-mentioned binary decision variables.

The set S represents the set of Sources from which the traffic will be generated or forwarded towards DPs. A DP can be served by only one Source; hence we define the binary decision variable y_{sd} to indicate this as follows:

$$y_{sd} = \begin{cases} 1, & \text{If source } s \text{ establish a connection with DP } d \\ 0, & \text{Otherwise} \end{cases} \tag{3.6}$$

We assume that the total carrier bandwidth W_{total} (MHz) is sliced into three BWPs that serve the above-mentioned services. The RBs that belong to the same numerology are gathered into one BWP, so each BWP includes the same type of RBs. Let W_1, W_2 and W_3 are the bandwidth of three numerologies 0.18, 0.36 or 0.72 MHz, respectively, then

$$W_1 + W_2 + W_3 = \; W_{total} \tag{3.7}$$

Bandwidth allocation among BWPs is flexible; there are no lower or upper boundaries

for the bandwidth of numerologies, but their summation must be equal to the W_{total} in all scenarios.

Fig. 3.2 displays an example of 5 MHz bandwidth frequency resource allocation between RAN slices with guard bands from the number of RB point of view. Increasing the bandwidth of higher numerologies causes a decrease in the number of available RBs. Thus, the total number of RBs changes with the bandwidth allocation between RAN slices. In this example, BWP1, BWP2 and BWP3 have three, five and three RBs that belong to 180, 360 and 720 kHz numerologies, respectively.

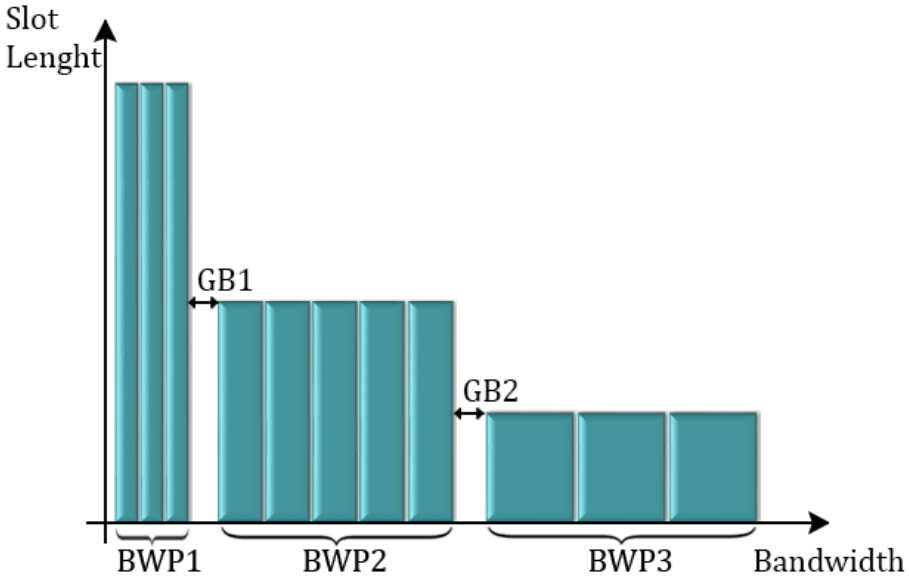

Figure 3.2: Example of bandwidth allocation among BWPs for 5MHz carrier, also, the figure shows the number of RBs for each numerology [20]

Two types of inter-numerology interference INI are assumed in this thesis. The first INI occurs in neighbour RBs that belong to different numerologies in the same BS. The second INI occurs between BSs due to using the same frequency resources for different numerologies.

To minimise former INI, we add guard bands that are at least one RB size among BWPs that employ different numerology. However, this solution can cause a reduction in spectrum efficiency [22], and to minimise this reduction, the RBs that use the same numerology are assigned to one BWP. For example, the RAN that has three BWPs and two required guard bands is illustrated in Fig. 3.2. To minimise the latter INI, we assume that all BSs in the model have the same BWP deployment in the frequency domain. This arrangement ensures that the same bandwidth components

are not used for different numerologies. With these two strategic measures in place, the impact of INI is greatly mitigated, rendering it negligible. Consequently, in order to maintain model simplicity and reduce complexity, the focus is primarily directed towards addressing CCI exclusively. Furthermore, it is worth noting that despite the aforementioned approach, a comprehensive evaluation of INI has been conducted, and the results of this assessment can be found in Chapter 3.4.2.

mmWave signals offer a significant amount of available bandwidth but suffer from high path and penetration loss, as discussed in Chapter 1.2.5. To address this challenge and utilise mmWave signals efficiently, we strategically leverage vehicles as mobile relays as backhaul nodes that use mmWave signals. Within the context of 5G-NR, where mobile relays can be employed as IAB nodes [36], we design VBSs to function as relay nodes in our optimisation framework. We assume vehicles or VBSs have LOS connection with the nearest BS. Thus, VBSs are backhauled by the nearest BS with mmWave signals. BSs and VBSs are serving to DPs with sub-6 GHz frequency bands; by employing VBS nodes, the distance amongst DPs and Sources is shortened. It is important to note that, most of the time, pedestrians (or more general DPs) walk closer to buildings and are vulnerable to obstacles; consequently, connections between Sources and DPs are assumed to be NLOS, as indicated by links 1 and 2 in Figure 3.1. Meanwhile, link 3 illustrates LOS mmWave signal propagation.

Each VBS uses mmWave backhaul links towards BSs and utilises sub-6 GHz access links towards DPs; in other words, out-band IAB operation is considered. As mentioned in [37], out-band IAB operation could be operated alternatively where access and backhaul communication utilise mmWave and sub-6 GHz frequency bands, respectively. BSs connect to the core network with high-speed optical fibre.

VBS nodes work as IAB nodes to reduce total transmit power and CCI and to improve spectrum efficiency. Consequently, the primary purpose of using VBS nodes is to increase the power efficiency; instead of reaching far DPs.

Physical RB allocation among DPs and bandwidth allocation among BWPs are the core of our study as it refers to the design of the 5G multi-numerology RAN slicing including BWP and IAB nodes. A mixed numerology system in which each BWP holds only one type of numerology is designed by considering the physical RB allocation

Table 3.1: Numerology Parameters

μ	0	1	2	2	3	4
SCS = $15x2^{\mu}$ (kHz)	15	30	60	60	120	240
Slot duration $1/2^{\mu}$ (ms)	1	0.5	0.25	0.25	0.125	0.0625
RB size in freq domain (kHz)	180	360	720	720	1440	2880
FR1 Compatibility	✓	✓	✓	X	X	X
FR2 Compatibility	X	X	X	✓	✓	✓
CP	Normal	Normal	Normal	Extended	Normal	Normal

problem for DPs where the serving BSs support multiple numerologies. The model assesses the user requirements to find the network parameters that negotiate among the considered objectives: SINR, latency, data rate and power consumption.

3.1.2 Channel Model

The higher numerologies have shorter OFDM symbol lengths in the time domain; therefore, utilising higher SCS helps decrease latency. Thanks to the shorter slot durations in the time domain, 5G reduces the delay for time-critical applications. FR1 and FR2 are designed by considering such numerologies. FR1 band supports the first three numerologies (15 kHz, 30 kHz, and 60 kHz SCSs) and FR2 supports the last three numerologies (60 kHz, 120 kHz and 240 kHz SCSs) [160] [161] as shown in Table 3.1 with frequency domain compatibility. Different cyclic prefix (CP) for the same SCS causes difference in spectral efficiency and causes a different numerology [138].

The model establishes communication among every element, excluding BS-to-BS and DP-to-DP. We assume that the BS to VBS connection is delivered by mmWave signals, and as mentioned before, this connection is considered as LOS. Any DP can be served by only BS or VBS that is backhauled by a BS. The latter comes with more latency but helps to improve 5G coverage and network capacity. Also, the backhauled communication has less power consumption compared to full mmWave coverage. To achieve the highest system performance with the lowest cost, we employed out-band IAB [27], which has no interference between access and backhaul.

In the propagation model of the access side, channel gain is introduced as multiplication of path loss, small scale fading (SSF) and large scale fading (LSF). For the design of path loss in 5G wireless communication systems, the close-in (CI) free-space reference distance model and an urban micro-street canyon scenario with an NLOS environment

are considered [162]. Pathloss calculation includes free-space path loss (FSPL) and LSF coefficients [162]. The access side communication contains BS to DP and VBS to DP communications; therefore, the access propagation model can be written as follows:

$$PL_{sd}(dB) = FSPL + 10nlog\left(k_{sd}\right) + \sigma^2,\ \forall\ s \in S, \forall\ d \in D \tag{3.8}$$

Equation 3.8 defines the variables used for path loss calculation for access communication. The term PL_{sd} represents the path loss in dB, and $FSPL$ denotes the free space path loss, which can be determined by the carrier frequency (in our case, assumed to be 2 GHz) and is calculated as 38.46 dB. k_{sd} shows the distance between the source and DP, the variable σ^2 is a parameter for close-in shadowing effect (LSF coefficients) and has a value of 7.7 dB in our scenario, while n is the path loss exponent with a value of 3.1. Then we convert the unit of path loss dB to linear scale to use it in the model. Rayleigh distribution is used to calculate the SSF [163] coefficients, which account for the absorbing, diffracting, and scattering effects from the surrounding environment and depend on DP, BS, and RB. Consequently, each RB has different gains even for the same distance, resulting in a more realistic propagation model and accurate results. The SSF function is defined in Eq 3.9 as Rayleigh distribution, where $N\left(0, 1/\sqrt{2}\right)$ represents the zero-mean Gaussian distribution with a standard deviation of $1/\sqrt{2}$.

$$\begin{aligned} SSF^r_{sd} &= \left(\left(N\left(0, 1/\sqrt{2}\right)\right)^2 + N\left(0, 1/\sqrt{2}\right)\right)^2, \\ &\forall\ s \in S, \forall\ d \in D, \forall\ r \in R \end{aligned} \tag{3.9}$$

Then radio access gain between any sources towards DP is calculated as:

$$g^r_{sd} = SSF^r_{sd} \times \left(10^{-(PL_{sd}/10)}\right),\quad \forall\ s \in S, \forall\ d \in D, \forall\ r \in R \tag{3.10}$$

The backhaul communication utilises a 28 GHz carrier frequency and is assumed that it has LOS communication between BS to VBS. The channel propagation model is calculated for the backhaul side as follows [164]:

$$PL_{bv} = \alpha + 10\beta log\left(k_{bv}\right) + \sigma^2 \quad ,\forall\ b \in B, \forall\ v \in V \tag{3.11}$$

PL_{bv} refers to backhaul pathloss between any BS and VBS, and according to [164], for 28 GHz and LOS, $\alpha = 61.4$, $\beta = 2$, and shadowing $\sigma^2 = 5.8$ dB. We allocate bandwidth for the VBSs for the backhaul communication, therefore the linear scale of the PL_{bv} gives the gain between BS and VBS:

$$g_{bv} = 10^{-(PL_{bv}/10)}, \quad \forall\ b \in B, \forall\ v \in V \tag{3.12}$$

Doppler Effect

Since we assume vehicular communication, the Doppler effect must be considered. Doppler effect causes inter-carrier interference [165] and scattering at the receiver [166] and it is calculated as follows:

$$f_d = \frac{v_{max} f_c}{c_0} cos(\alpha) \tag{3.13}$$

f_d refers to the maximum Doppler shift, depending on user velocity v_{max}, carrier frequency f_c, the angle of the moving object $cos(\alpha)$, and speed of light c_0. The maximum speed in urban vehicular scenarios is 50 km/h (or 30 mph). Considering a VBS is moving towards from/to a BS with a perpendicular angle, the maximum Doppler shift can be calculated as follows:

$$f_{backhaul} = \frac{50 \times 28 \times 10^9}{3 \times 10^8} cos(0) = \ 4667\ Hz \tag{3.14}$$

$$f_{access} = \frac{50 \times 2 \times 10^9}{3 \times 10^8} cos(0) = \ 334\ Hz \tag{3.15}$$

The carrier frequencies are 28 GHz and 2 GHz for backhaul and access, respectively, so the calculated maximum Doppler shifts are negligible. Moreover, the angle is likely to be different from zero, which makes the Doppler shift even smaller. Since we assume low-speed urban scenarios and employ SSF that keeps the scattering in mind, we

decided not to add another factor for Doppler shift to our optimisation framework.

3.2 Problem Formulation of the MILP

In this section, the MILP model is introduced that has been developed to maximise the total number of served DPs while minimising the total transmit power (p_t), CCI. First, the problem is formulated as nonlinear, then linearised for MILP formulation in the following section. To do so, we defined the indices, parameters, and variables given in Table 2, Table 3 and Table 4, respectively.

3.2.1 Optimisation Problem

Given the data rate and delay requirements of DPs, the optimisation model responds by selecting the optimum number of RBs and their numerology, as well as the optimum physical RB allocation amongst DPs, so that the number of served DPs is maximised. The optimisation model also minimises the total transmit power for access and backhaul, along with CCI. Accordingly, the optimisation model determines how to serve the demands according to DP requirements to achieve the maximum power efficiency for the limited bandwidth. Moreover, reducing CCI benefits increase the channel capacity. The **objective function** is given as follows:

$$min: \quad -a_1 \left(\sum_{d \in D} y_d \right) + a_2 \left(p_t \right) + a_3 \left(\sum_{d \in D} \sum_{r \in R} IN_d^r \right) \tag{3.16}$$

y_d is a binary decision variable that equals 1 if DP d served and equals 0 otherwise. p_t stands for the total transmit power in the downlink direction, which is the summation of the access and backhaul communication and is calculated in Eq (3.17). IN_d^r shows CCI and noise signal for each DP d allocated to RB r. IN_d^r is calculated at Chapter V, Eq (3.52). The weights are shown as a_1, a_2, and a_3 help to assign priority; for instance, serving all the DPs is more critical than interference. Therefore, the weighted objective function provides better interference management.

$$p_t = \sum_{s \in S} \sum_{d \in D} \sum_{r \in R} p_{sd}^r \; + \sum_{b \in B} \sum_{v \in V} p_{bv} \tag{3.17}$$

Table 3.2: Sets and Indices

Symbol	Description
B	Set of base station nodes
D	Set of demand point nodes
M	set of segments for linearisation method
N_u	Set of neighbourhood nodes
N	Set of numerologies
R	Set of resource blocks
S	set of union of source nodes (BS and VBS)
U	set of union of all nodes (BS,VBS and DP)
V	set of vehicular base station nodes
b, v, d	Indices of BS,VBS and DP nodes, respectively
s, u	Indices of Sources and combination of all nodes, respectively
i, j	Indices of any nodes that data can flow through
n	Indices of numerologies
m	Indices of segments for linearisation method
r	Indices of RBs

Table 3.3: Model Parameters

Symbol	Description
a_1, a_2, a_3	Weights of the objective function
d_d	Data rate requirement for each DP in Mbps
$\bar{E_m}$	m^{th} point of corresponding $\bar{X_m}$ value. $\bar{X_m}$ and $\bar{E_m}$ are used in linearization method section
g^r_{sd}	Channel gain for each Source s to DP d and RB r for access
g_{bv}	Channel gain for each BS b to VBS v for backhaul
k_{bv}	Distance between BS and VBS
k_{sd}	Distance between Source and DP
prb^n	Physical resource block bandwidth
Pt_{bv}	Maximum backhaul transmit power for each link
Pt_{max}	Total maximum transmit power of the BS
Pr_{max}	Maximum transmit power of each RB
t_d	Delay requirement for each DP d in milliseconds (ms)
t_n	Delay for each numerology n given at Table 1
W_{total}	Total carrier bandwidth in MHz
X_{max}	Maximum value of the logarithmic spectral efficiency function
X_{min}	Minimum value of the logarithmic spectral efficiency function
$\bar{X_m}$	m^{th} point of non-linear $log(1 + SINR(m))$ function

Table 3.4: Model Variables (All are Nonnegative Real Numbers)

Symbol	Description
A_d^r	All the received signals by DP d that utilizes RB r (desired signal, interference and additive white Gaussian noise (AWGN)(AWGN))
C_d	Allocated data rate for each DP d in Mbps
C_v	Allocated backhaul data rate for each VBS v in Mbps
D_{sd}	Allocated data rate from each Source s to DP d
E_1 , E_2	Linear outputs of $(log_2(S+I+N))$ and $(log_2(I+N))$ functions
f_{bd}^{ij}	Data traffic flow between bs to dp traversing virtual link i in U to j in N_u
Id_d^r	Ideal/desired signal that includes only multiplication of transmit power and gain, for each DP d allocated to RB r
IN_d^r	CCI plus noise definition for each DP d allocated to RB r
L_d^{rn}	Linear version of spectral efficiency for each DP d, allocated to RB r and numerology n
L_v	Linear version of backhaul spectral efficiency for each VBS v
p_{bd}^r	Transmit power for each BS b to DP d and RB r
p_{bv}	Backhaul transmit power for each BS b to VBS v
p_{sd}^r	Access transmit power for each Source s to DP d and RB r
p_t	Total transmit power, summation of access and backhaul
pl^{rn}	Binary variable that shows which RB belong to which numerology
y_{sd}^{rn}	Binary 4-dimensional main decision variable that gives relation between sources s(either BS or VBS) to DP d, RB r and numerology n
W_1, W_2, W_3	Bandwidth of numerologies in MHz
X_m	Nonlinear input value of linearisation function
xor^{rn}, z^{rn}	Binary variables to provide BWP adaptation for each RB r and numerology n
Z_m	Binary indicator variable that shows which segment is used for linearisation
Λ_{sd}	A binary variable that takes the value of 1 when the Source s is serving the DP d in downlink access. This is the last source along the path from the Source s to the DP d, physical link.
Ψ_{bv}	A binary variable that takes the value of 1 when the BS b is backhauling the VBS v in downlink access, virtual link.
Ω_{sd}	Allocated data rate from each s to d

3.2.2 DP Requirement Constraints

Each DP generates data rate and delay demands that are denoted by d_d and t_d, respectively. Firstly, the model ensures that the requested data rate by a DP is less or equal to the data rate C_d and is formulated as follows:

$$d_d \times y_d \leq C_d, \ \forall \ d \in D \tag{3.18}$$

Ω_{bd} is a variable that shows which source provides how much data rate to which DP. It is important to note that, in this thesis, we assume that the allocated data rate is

equal to the Shannon capacity which is elaborated in Chapter 1.6.

$$\sum_{s \in S} \Omega_{sd} = \ d_d, \quad \forall \ d \in D \tag{3.19}$$

Secondly, numerology is assigned to each DP to satisfy the delay requirement. We formulated this requirement by using binary decision variable y_d^n that equals 1 when DP d utilises numerology n and equals to 0 otherwise, in the following constraint:

$$t_d \geq t_n \left(\sum_{n \in N} y_d^n \right), \quad \forall \ d \in D \tag{3.20}$$

According to [18], DPs must be designed by considering a single active downlink BWP at a time. Therefore, each DP can pick one type of numerology at once given at constraint 3.21, where y_d^n is the binary decision variable equal to 1 when DP d utilises numerology n and equals to 0 otherwise.

$$\sum_{n} y_d^n \leq 1, \ \ \forall \ d \in D \tag{3.21}$$

3.2.3 Flow Conservation Constraints

In order to provide the data rate flow, either directly from BS or indirectly using wireless backhaul network, from BS to DP, flow conservation constraints are used. The set of union of all sets (B, V, and D) is needed and denoted by $\mathcal{U} = \{1, ..., U\}$ where $|\mathcal{U}| = |\mathcal{B}| + |\mathcal{V}| + |\mathcal{D}|$. Then, we defined neighbourhood matrix denoted as N_u, $u \in U$, that shows the possible nodes that can be connected. The flow conservation is formulated as follows

$$\sum_{j \in N_u(i)} f_{sd}^{ij} - \sum_{j \in N_u(i)} f_{sd}^{ji} = \begin{cases} D_{sd} \ i = b \\ -D_{sd} \ \ i = d \\ 0 \ \ otherwise \end{cases}, \qquad \forall \ i \in U, \ j \in \ N_u \tag{3.22}$$

The flow conservation constraint (3.22) ensures that the total incoming traffic is always equal to the total outgoing traffic for VBS nodes, BS nodes are the source of the traffic and DP nodes are the sinks. The most generic flow conservation constraint, with no

limitations, is generated in constraint (3.22). To do so, we assumed that each node can connect to any node at the beginning. This subsection also demonstrates how to achieve the desired flow in the model.

Constraint (3.22) shows that the data can be generated by any source. However, BSs are the only data provider for the DPs; consequently, data rate demand for each DP must be provided by a BS. VBSs can not generate data, they can only provide connectivity among BSs and DPs. Constraint (3.23) prevents VBSs to generate data:

$$\sum_{j \in N_u} f_{sd}^{ij} - \sum_{j \in N_u} f_{sd}^{ji} = 0 \quad \forall\, i \in U,\ j \in\ N_u,\ s \in V,\ d \in D \tag{3.23}$$

It is assumed that DPs receive data only, and BSs generate data only; therefore, we prevent routing among DPs and prevent flow among BSs with constraints (3.24) and (3.25). The flow conservation constraint (3.22) is not minimised in the objective function, so the model supports multiple hops: from Sources to DP, and from VBS to VBS. Instead, the total transmit power is minimised in the objective function.

$$f_{sd}^{ij} = 0, \qquad \forall\, i, j \in D \tag{3.24}$$

$$f_{sd}^{ij} = 0, \qquad \forall\, i, j \in B \tag{3.25}$$

The physical link binary variable is shown as PL^{id}, representing the last hop received by DP d. PL^{id} is employed to restrict the number of sources that serves a DP; that is, each DP can be fed by only one source given at Eq(3.26). PL^{id} is extracted from flow conservation variable. In the original f_{sd}^{ij}, variable j represents the neighbourhood set N_u; however, here, N_u is replaced with the DP. To extract a binary variable from the floating variable, we used the following well-known trick [167] where k is a large number, given at Eq (3.27) and Eq (3.28):

$$\sum_{i \in S} \Lambda^{id} \leq 1, \qquad \forall\, d \in D \tag{3.26}$$

$$\sum_{b \in B} f_{sd}^{id} \geq \Lambda^{id}, \qquad \forall\ i \in S, d \in D \tag{3.27}$$

$$\sum_{b \in B} f_{sd}^{id} \leq k\left(\Lambda^{id}\right), \qquad \forall\ i \in S, d \in D \tag{3.28}$$

3.2.4 RB Allocation Constraints

As noted earlier, each DP can be served by only one BS, even using a VBS condition. y_{bd} is a binary decision variable that equals 1 when DP d utilizes BS b and equals 0 otherwise. Then, the constraint (3.29) indicates that each BS-RB pair can be allocated at most one DP. The constraints (3.30) and (3.31) provide the following conditions: Each BS has its RB resources, and every individual RB can be allocated to one DP. Also, individual RBs, as a resource in a Sources set, can belong to single numerology at once.

$$\sum_{s \in S} y_{sd} \leq 1, \qquad \forall\ d \in D \tag{3.29}$$

$$\sum_{d \in D} y_{sd}^{r} \leq 1, \qquad \forall\ s \in S, r \in R \tag{3.30}$$

$$\sum_{n \in N} y_{s}^{rn} \leq 1, \qquad \forall\ s \in S, r \in\ R \tag{3.31}$$

$$\sum_{d \in D} \sum_{r \in R} p_{sd}^{r} \leq Pt_{max}, \qquad \forall\ s \in S \tag{3.32}$$

$$p_{sd}^{r} \leq y_{sd}^{r} \times Pr_{max}, \qquad \forall\ s \in S,\ d \in D,\ r \in R \tag{3.33}$$

According to [168], the constraint (3.32) shows total transmit power limitations for each Source. Finally, in terms of transmit power fairness between DPs, we limited the allocated power of each RB for all Sources in constraint (3.33).

3.2.5 Bandwidth Allocation Amongst BWPs Constraints

All BSs have the same BWP configuration. Thus, there will be no INI caused by other BS. This is provided by the following three constraints:

$$\sum_{r\in R}\sum_{n\in N} pl^{rn} \times prb^{n} = W_{total} \tag{3.34}$$

$$\sum_{n\in N} pl^{rn} \leq 1,\ \forall\ r \in R \tag{3.35}$$

$$y_{b}^{rn} \leq pl^{rn},\ \forall\ b \in B,\ \forall\ d \in D,\ \forall\ r \in R \tag{3.36}$$

In constraint (3.34), we multiply each RB by its actual bandwidth and force the model to allocate RBs amongst BWPs even if they are not in use. Moreover, in [169], the maximum number of RBs for each transmission bandwidth is defined by considering CP and guard bands, and our model fits into the standard. Constraint (3.35) and (3.36) ensure that each RB can belong to at most one numerology and all RBs that belong to the same numerology are positioned in the same frequency bands in the carrier bandwidth, for all BSs respectively. Constraint (3.36) also highlights that all RBs must belong to one numerology, whereas they do not have to be used by a DP.

$$pl^{rn} + pl^{(r-1)\ n} = 2\,(z^{rn}) + xor^{rn},\quad \forall\ r \in R, \forall\ n \in N \tag{3.37}$$

$$\sum_{r\in R} xor^{rn} \leq 2,\quad \forall\ n \in N \tag{3.38}$$

After bandwidth limitation constraints are satisfied, RBs that are in the same numerology are assembled into groups to provide BWP in constraints (3.37) and (3.38). In constraint (3.37), every two successive RBs are summed, and the result equals two other binary variables called z^{rn} and xor^{rn}. Any numerology shift between two successive RBs causes an output of '1' in xor^{rn} binary variable. This output is summed and limited by '2' for each numerology shown at constraint (3.38).

3.2.6 Backhaul Constraints

Backhaul communication takes place between BS and VBS only; therefore, the binary decision variable y_{bv} is defined as follows:

$$y_{bv} = \begin{cases} 1, & \text{If BS } b \text{ is backhauling the VBS } v \\ 0, & \text{Otherwise} \end{cases} \tag{3.39}$$

Ψ^{ij} variable displays the data flow between BS to VBS and is extracted from the flow variable by considering $i = BS$ and $j = VBS$.

$$\sum_{b \in B} \sum_{d \in D} f_{bd}^{ij} = \Psi^{ij}, \qquad i \in B, j \in V \tag{3.40}$$

VBSs can serve multiple DPs simultaneously. Therefore the bandwidth of backhaul links is assumed that has a 2 RB size of 720 kHz numerology bandwidth:

$$C_{bv} = (2 \times 0.72) \left(log_2 \left(1 + \frac{p_{bv} \times g_{bv}}{\sigma^2} \right) \right) Mbps \tag{3.41}$$

g_{bv} is calculated in Section 3-B for 28 GHz carrier bandwidth, C_{bv} and p_{bv} display data rate between BS to VBS and the transmit power, respectively. Finally, the backhaul data rate must be greater or equal to the flow between BS to VBS:

$$\Psi_{bv} \leq C_{bv}, \quad \forall\, b \in B, v \in V \tag{3.42}$$

The carrier frequency of the backhaul communication is given as 28 GHz in the channel model section. The maximum transmit power of mmWave BS (in our case, it is VBS) per user stream is defined as 25 dBm [170] which makes approximately 316 mW. The maximum backhaul power between each BS and VBS is restricted in constraint 3.43 where Pb_{max} indicates maximum transmit power between BS and VBS:

$$p_{bv} \leq Pb_{max} \times y_{bv}, \quad \forall\, b \in B, v \in V \tag{3.43}$$

The sets and indices used in the model are given in Table 3.2, while the model parameters and variables are presented in Table 3.3, and Table 3.4, respectively. To present the objective function and all the constraints employed in the model in a readable manner, Table 3.5 is utilized.

Table 3.5: Model Constraints

Eq Number	Objective Function
3.16	$min: \quad -a_1\left(\sum_{d\in D} y_d\right) + a_2\left(p_t\right) + a_3\left(\sum_{d\in D}\sum_{r\in R} IN_d^r\right)$
Eq Number	Main Model Constraints
3.1	$t_d \geq t_n, \quad \forall\ d \in D$
3.2	$\Omega_d \geq d_d, \quad \forall\ u \in U$
3.7	$W_1 + W_2 + W_3 = \ W_{total}$
3.4	$\sum_{r\in R}\sum_{n\in N} y_{sd}^{rn} \geq y_{sd}$
3.5	$\sum_{r\in R}\sum_{n\in N} y_{sd}^{rn} \leq K\left(y_{sd}\right)$
3.18	$d_d \times y_d \leq C_d, \forall\ d \in D$
3.19	$\sum_{s\in S} \Omega_{sd} = d_d, \forall\ d \in D$
3.20	$t_d \geq t_n\left(\sum_{n\in N} y_d^n\right), \forall\ d \in D$
3.21	$\sum_{n} y_d^n \leq 1, \forall\ d \in D$
3.22	$\sum_{j\in N_u(i)} f_{sd}^{ij} - \sum_{j\in N_u(i)} f_{sd}^{ji} = \begin{cases} D_{sd} & i = b \\ -D_{sd} & i = d \\ 0 & \text{otherwise} \end{cases}, \forall\ i \in U,\ j \in N_u$
3.23	$\sum_{j\in N_u} f_{sd}^{ij} - \sum_{j\in N_u} f_{sd}^{ji} = 0, \forall\ i \in U,\ j \in N_u,\ s \in V,\ d \in D$
3.24	$f_{sd}^{ij} = 0, \forall\ i, j \in D$
3.25	$f_{sd}^{ij} = 0, \forall\ i, j \in B$
3.26	$\sum_{i\in S} \Lambda^{id} \leq 1, \forall\ d \in D$
3.27	$\sum_{b\in B} f_{sd}^{id} \geq \Lambda^{id}, \forall\ i \in S,\ d \in D$
3.28	$\sum_{b\in B} f_{sd}^{id} \leq k\left(\Lambda^{id}\right), \forall\ i \in S,\ d \in D$
3.29	$\sum_{s\in S} y_{sd} \leq 1, \forall\ d \in D$
3.30	$\sum_{d\in D} y_{sd}^{r} \leq 1, \forall\ s \in S,\ r \in R$
3.31	$\sum_{n\in N} y_{s}^{rn} \leq 1, \forall\ s \in S,\ r \in R$
3.32	$\sum_{d\in D}\sum_{r\in R} p_{sd}^{r} \leq Pt_{max}, \forall\ s \in S$
3.33	$p_{sd}^{r} \leq y_{sd}^{r} \times Pr_{max}, \forall\ s \in S,\ d \in D,\ r \in R$
3.34	$\sum_{r\in R}\sum_{n\in N} pl^{rn} \times prb^{n} = W_{total}$
3.35	$\sum_{n\in N} pl^{rn} \leq 1, \forall\ r \in R$
3.36	$y_b^{rn} \leq pl^{rn}, \forall\ b \in B, \forall\ d \in D, \forall\ r \in R$
3.37	$\sum_{r\in R} pl^{rn} + pl^{(r-1)\ n} = 2\left(z^{rn}\right) + xor^{rn}, \forall\ r \in R, \forall\ n \in N$
3.38	$\sum_{r\in R} xor^{rn} \leq 2, \forall\ n \in N$
3.40	$\sum_{b\in B}\sum_{d\in D} f_{bd}^{ij} = \Psi^{ij}, \forall\ i \in B,\ j \in V$
3.42	$\Psi_{bv} \leq C_{bv}, \forall\ b \in B,\ v \in V$

3.3 Linear Reformulation Methods

The data rate in Section 3.2 is calculated by the Shannon-Hartley formula (Eq (3.44)). The problem is formulated in the previous section as a mixed-integer nonlinear programming (MINLP) and is unsuitable for linear programming. This section demonstrates how to linearise nonlinear constraints, starting from the logarithmic function, and perform this reformulation step.

3.3.1 Linear Reformulation of the Capacity

The constraint described in Eq (3.18) shows the data rate requirement for each DP. C_d refers to the assigned data rate for each DP in Mbps determined by using the Shannon-Hartley formula. We reformulate it with the following method to get a linear form of the Shannon capacity at any given SINR. At the end of this section, we also formulate how to define C_d from the output of the linearisation method in Eq (3.63).

Shannon capacity can be calculated as the multiplication of bandwidth and spectral efficiency given in Eq (3.44) and Eq (3.45)

$$C_d = w\left(log_2\left(1 + SINR\right)\right) \tag{3.44}$$

$$C_d = w\left(log_2\left(1 + \frac{S}{I+N}\right)\right) \tag{3.45}$$

$$C_d = w\left(log_2\left(S + I + N\right) - log_2\left(I + N\right)\right) \tag{3.46}$$

$$C_d = \sum_{r \in R} \sum_{n \in N} prb^n \left(log_2\left(A_d^r\right) - log_2\left(IN_d^r\right)\right), \ \forall\ d \in D \tag{3.47}$$

Eq (3.46) has two logarithmic functions; the first one has all the signals that a DP can receive. The second logarithmic function includes interference and noise. Then, we defined A_d^r variable that equals to desired signal + interference + noise (S+I+N) and IN_d^r variable that equals to interference + noise (I+N), as given in Eq (3.47). The bandwidth of each numerology varies; hence, it is given as follows and utilised in Eq (3.47)

$$W_{total} = \sum_{n \in N} prb^n \tag{3.48}$$

The connection between Sources to DP uses the same propagation model; therefore, we implemented linearisation for the access side data rate at once. A_d^r represents all the signals that received by a specific DP d and a specific RB r, from all sources plus the noise at DP d, as shown at Eq (3.49). Since all the sources are summed in Eq (3.49), A_{dr} variable does not depend on any source. Still, summing all the sources will not lead to multiple connections for a DP; constraint (3.26) ensures that each DP can establish a connection with only one source.

$$A_d^r = \sum_{s \in S} \sum_{d' \in D} (p_{sd'}^r \times g_{sd}^r) + \sigma^2, \quad \forall\ d \in D,\ r \in R \tag{3.49}$$

$$Id_d^r = \sum_{s \in S} (p_{sd}^r \times g_{sd}^r), \quad \forall\ d \in D,\ r \in R \tag{3.50}$$

$$A_d^r = Id_d^r + IN_d^r, \quad \forall\ d \in D,\ r \in R \tag{3.51}$$

$$IN_d^r = A_d^r - Id_d^r, \quad \forall\ d \in D,\ r \in R \tag{3.52}$$

The desired signal that includes only multiplication of power and gain for a specific DP and RB is denoted as Id_d^r and formulated in Eq (3.50). Instead of calculating the denominator of the Shannon-Hartley formula (which is interference and noise, and denoted as IN_d^r), we calculated the desired signal Id_d^r, and subtract it from A_d^r. Thus, IN_d^r can be simply derived, given in Eq (3.51) and Eq (3.52).

A piecewise linearisation method is employed for the linearisation of the logarithmic function, given in [171]. In this method, the argument of the logarithmic function is divided into a set of segments that are denoted as $\mathcal{M} = \{1, ..., M\}$ as shown in Fig (3.3). Then, it is assumed that the curve between two nodes is linear. Also, as can be seen in Fig. (3.3), the linear segments are concave; therefore, the linearisation error is always negative, as shown in Table 3.6.

To begin with the linearisation method, a binary indicator variable Z_m is defined to mark in which segment we are in

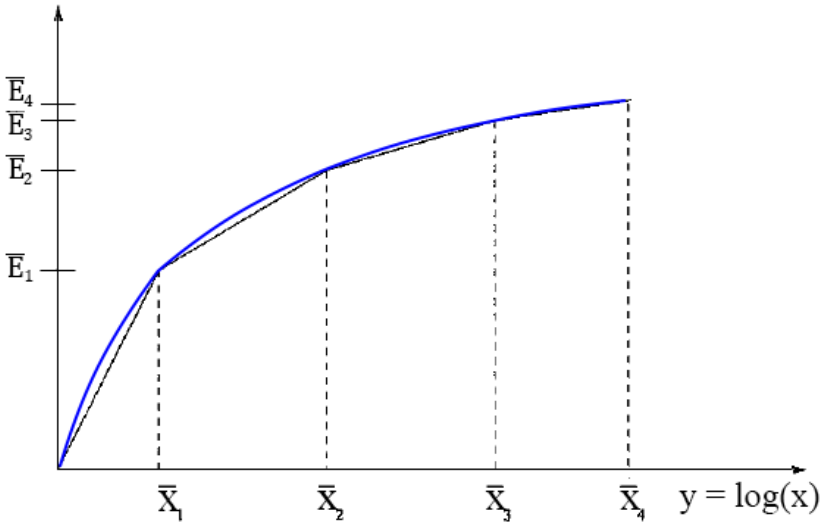

Figure 3.3: Piecewise linearization method

$$Z_m = \begin{cases} 1, & X \in \left[\bar{X_{m-1}},\ \bar{X_m}\right] \\ 0, & \text{Otherwise} \end{cases} \tag{3.53}$$

Then, the following constraints are defined [171];

$$\bar{X_{m-1}} Z_m \leq X_m \leq \bar{X_m} Z_m, \qquad \forall r \tag{3.54}$$

$$\sum_{m \in M} Z_m = 1 \tag{3.55}$$

$$X = \sum_{m \in M} X_m \tag{3.56}$$

Eq (3.54) and Eq (3.55) underline that related X_m point can only be in one segment, and there must be only one positive Z_m that indicates the corresponding segment. Since there is an equality in Eq (3.55), the maximum and the minimum values of the logarithmic function must be defined. If there is no connection, SINR will be equal to zero, and X_{min} equal to zero as well. Maximum data rate demand divided by minimum RB bandwidth that is 180 kHz to calculate the X_{max}.

$$X_{max} = 2^{(\max(d_d))/(\min(prb^n))} \tag{3.57}$$

Therefore, any A_d^r and IN_d^r value must be between X_{min} and X_{max} points

$$X_{min} \leq A_d^r \leq X_{max} \tag{3.58}$$

$$X_{min} \leq IN_d^r \leq X_{max} \tag{3.59}$$

Finally, the linear output of the logarithmic Shannon-Hartley formula can be determined as:

$$E = \sum_{m \in M} \left[\bar{E_{m-1}} Z_m + \left(X_m - \bar{X_{m-1}} Z_m \right) \frac{\bar{E_m} - \bar{E_{m-1}}}{\bar{X_m} - \bar{X_{m-1}}} \right] \tag{3.60}$$

Equation 3.60 is the summation of the two points A and B shown in Fig (3.4) that illustrates the α angle, A, and B points. The former value in equation (point A) displays the lowest value of the previous segment, and the latter gives the remaining part of the value using the slope of the related segment, more specifically $\tan(\alpha)$.

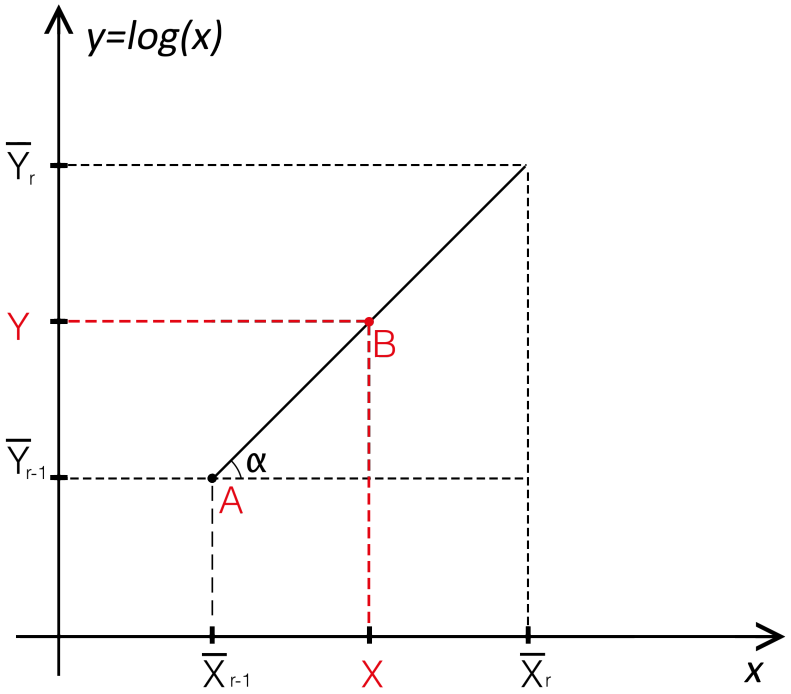

Figure 3.4: Piecewise linearization method

We linearized $log_2(A_d^r)$ and $log_2(IN_d^r)$ separately and the linear outputs are called E_1 and E_2 respectively. E_1 and E_2 variables have the indices of d and r, to reduce the complexity we prefer not to display these indices through linearisation method. Also, E_1 and E_2 variables are calculated with the same method, so we calculate only E variable above. Thus, the linearized version of capacity function (L_d^{rn}) is calculated as:

$$L_d^{rn} = w * (log_2(S + I + N) - log_2(I + N)) \tag{3.61}$$

$$L_d^{rn} = prb^n * (E_1 - E_2) \tag{3.62}$$

Note that the allocated demand to each DP is formulated without including the index of the serving BS. However, Eq (3.29) that is given in Section 4-D, prevents multiple BS connection. The linear version of the assigned data rate is presented above as L_d^{rn} for each DP, RB, and numerology. To test the capability of the linearisation method, we assumed that any DP can utilise multiple RBs from the same BWP. Then, we sum all RBs and numerologies to find the allocated data rate for each DP in Mbps as follows:

$$C_d = \sum_{r \in R} \sum_{n \in N} L_d^{rn}, \ \forall \ d \in D \tag{3.63}$$

The backhaul data rate C_v is also calculated by using the Shannon-Hartley formula, and the same linearisation method is applied to C_{bv}. However, for the backhaul data rate, we assume only SNR, without interference between access and backhaul due to out-band backhauling. Moreover, even in the busiest condition, there is hardly any CCI for backhaul. There are two possible reasons for the low interference; first, the above-mentioned high attenuation for the mmWave signals; CCI is much lower for the FR2 for the same distance when comparing FR1. The second reason is that the mmWave BSs have lower transmit power given in Table 3.7. In addition, TDMA operation (if operated for backhaul) also reduces interference.

Consequently, calculating interference for backhaul transmission brings only complexity and processing time. Hence, interference calculations are removed from the backhaul communications to alleviate the complexity. Moreover, the linearisation was executed without considering any numerology. We assume that backhaul uses only 720 kHz numerology; therefore, the bandwidth of each RB of the numerology is fixed.

L_v, the linear output of the logarithmic spectral efficiency function for the backhaul, is calculated in the same way as L_d^{rn}. Since we assign only the third numerology (720

Table 3.6: Validation of Linearization Method by Comparing A_d^r

	DP1	DP2	DP3	DP4	DP5
Actual Output	5.85901	4.6957	6.72756	5.80606	5.19076
Linear Output	5.85891	4.69419	6.72748	5.80586	5.19076
Difference	1E-04	0.00151	8E-05	0.0002	0
Percent	0.0017	0.0321	0.0012	0.0034	0

kHz bandwidth) for the backhaul data rate, it can be calculated as follows in Mbps:

$$C_v = (0.72)L_v, \ \forall \ v \in V \tag{3.64}$$

The outcomes of the linearisation method are compared to actual values to verify the linearisation method. First, we evaluate the A_d^r and its linear output with actual values. The proposed linearisation method is concave; therefore, all the differences must be less or equal to zero. Table 5 shows the linearised and actual output for each RB. In this linearisation example, all 5 DPs are served by single or multiple RBs. For testing, we pick the RB that carries the largest data rate for each DP. Table 3.6 shows that the maximum error is 0.032% which is disregardable.

3.3.2 Linear Reformulation of the Multiplication of Variables

Multiplying two variables in MILP disrupts linearity. In our optimisation framework, this multiplication happens between a binary variable and a non-negative real number. For example, to eliminate the unnecessary values from A_d^r, it must be multiplied with binary y_d^r variable where:

$$y_d^r = \begin{cases} 1, & \text{If DP } d \text{ utilizes the RB } r \\ 0, & \text{Otherwise} \end{cases} \tag{3.65}$$

A_d^r variable is originally formulated as follows:

$$A_d^r = a_d^r \times y_d^r, \ \ \forall \ d \in D, \ r \in R \tag{3.66}$$

a_d^r shows all the received signals by DP d that utilizes RB r, same as A_d^r. Hence, a_d^r is the version of A_d^r that has not been multiplied with y_d^r yet. In our optimisation framework, we employed A_d^r to prevent any wrong output. Since the multiplication

given at Eq 3.66 is nonlinear, we replaced Eq 3.66 with following four equations by utilising minimum and maximum value of the logarithmic spectral efficiency function [167]:

$$A_d^r \leq X_{max}\,(y_d^r) \tag{3.67}$$

$$A_d^r \leq a_d^r - X_{min}\,(1 - y_d^r) \tag{3.68}$$

$$A_d^r \geq a_d^r - X_{max}\,(1 - y_d^r) \tag{3.69}$$

$$A_d^r \geq X_{min}\,(y_d^r) \tag{3.70}$$

3.4 MILP Model Setup and Results

In this section, we evaluate the performance of the considered RAN resource allocation optimisation model. We used IBM's linear solver CPLEX as well as the modelling program AMPL [172] to develop our model.

First, we investigated the effects of VBS nodes in terms of bandwidth allocation amongst BWPs, transmit power of each RB, total transmit power and CCI. To do so, we run the optimisation model with and without the VBS nodes. In both cases, the objective function and the constraints that are not linked to VBS are kept identical. For the without VBS nodes model, flow conservation constraints do not exist; accordingly, backhaul communication is not considered at all in this case.

Then, to investigate the performance of multi BWP versus single BWP, we assume that the BSs can have only one type of numerology; hence, only one BWP can exist. In other words, only one numerology is available for all BSs at any time. Here, we compare transmit power of each RB, total transmit power consumption and CCI for each RB. In this part, the VBS nodes are always included in all scenarios.

3.4.1 MILP Model Setup

We assume a square 500×500 meters grid. Therefore, the farthest DP can be located 177 meters away from a BS on this grid. This distance is compatible with the signal model proposed in [162]. DPs and VBSs are randomly located in the grid; and illustrated as mobile phones and vehicles, respectively, in Figure 3.5. We split the grid into four equal imaginary squares to locate the BSs at the centre of each square. Any BS can serve any DP on the grid whether the corresponding DP is inside the imaginary square or not. In addition, mmWave backhaul links (FR2) and sub-6 GHz access links (FR1) are demonstrated in Figure 3.5.

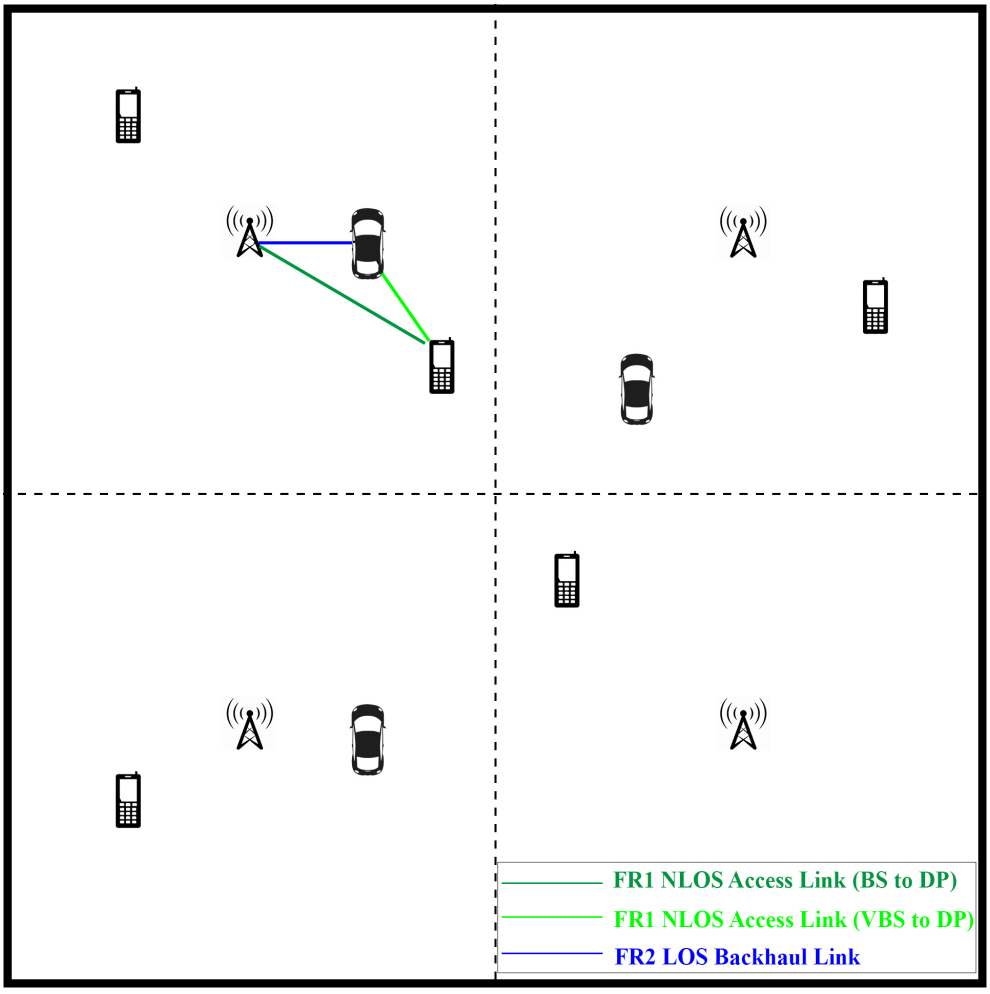

Figure 3.5: System model illustration. Vehicles and cell phones show VBS nodes and DP nodes respectively.

The radio access links (BS and DP, VBS and DP links) utilise FR1 frequency bands. The first three numerologies, $\mu = 0$, $\mu = 1$ and $\mu = 2$, are considered for the access side. On the contrary, backhaul links (BS to VBS) utilise FR2. The backhaul communication is established by using mmWave specifications, and only one numerology

($\mu = 2$) is employed for the backhaul.

The total transmission bandwidth W_{total} is considered as 5 MHz for simplicity and to reduce computational time. The larger transmission bandwidth configurations (up to 100MHz [169]) can be easily adapted to the model. Also, when all the RBs belong to the first numerology (180 kHz RB size), the 5 MHz bandwidth can have a maximum of 25 RBs [169]. As mentioned earlier, we add guard bands between each BWP; hence the total number of the first numerology RB is shrunk to 23. In other words, the total available bandwidth is equal to 23×180kHz.

There are three types of DP requirements in the optimisation model. The first type of DPs require a 5-7 MBPS data rate of 0.8-1.2 ms, the second group of DPs need a 0.2-0.3 MBPS data rate with low latency, in 0.3-0.6 ms, and the last group of DPs require 0.1-0.2 MBPS data rate in 1-2 ms. It is assumed that these groups of DPs reflect the requirements of eMBB, URLLC and mMTC slices, respectively. Data rate requirements of the eMBB DPs are determined considering normalised user throughput for the dense urban scenario [173]. The normalised user throughput is defined in [173] as the received bits in a certain amount of time (e.g. per second), divided by the channel bandwidth and measured as bit/s/Hz. Data rate and delay requirements are similar to those used in [81], [173] and adapted to this model considering aggregated requirements of demand points. In our model, DPs are unrestricted to select any numerology as long as their requirements are satisfied by the related BWP, and the corresponding network slice has available bandwidth.

Although the model supports multi-hop, we confine the maximum number of hops to two. In this thesis, the purpose of employing VBS nodes is not to reach far users from BSs; instead, LOS and NLOS signal propagation scenarios are considered for backhaul and access, respectively. This also means all the DPs and VBSs are inside the coverage area. Moreover, the flow conservation constraint is not minimised in the objective function; therefore, utilising multi-hops in the model brings complexity and unnecessary bandwidth usage. There are two ways to reduce the number of hops to two. First, the flow among VBSs can be prevented:

$$f_{sd}^{ij} = 0, \qquad \forall\ i, j \in V \tag{3.71}$$

When constraints (3.24), (3.25), and (3.71) are employed together, they limit the maximum number of hops to two. The second method is that the neighbourhood matrix N_u can be reshaped by removing the undesirable flows such as BS to BS, VBS to VBS, and DP to DP. This solution comes with fewer constraints and requires less processing time for the solver.

The objective function has weights; providing service to all DPs is the priority; hence the largest weight is (a_1). Some amount of CCI can be affordable in the model; therefore, the smallest weight a_3 is utilised for CCI regulation. These and the rest of the input parameters are displayed in Table 3.7.

Table 3.7: Input Data for the Optimisation Model

Input	Description
Carrier bandwidth for access w	5 MHz
Carrier bandwidth for backhaul w_b	5 MHz
Data demand for each DP d_d	Uniformly distributed 5-7 MBPS for eMBB, 0.2-0.3 MBPS for URLLC, 0.1-0.2 MBPS for mMTC
Delay requirement for each DP t_d	Uniformly distributed 0.8-1.2 ms for eMBB, 0.3-0.6 ms for URLLC, 1-2 ms for mMTC
Delay for each numerology	Given at Table 1
DP locations k_d	Randomly distributed on the grid
VBS locations k_v	Randomly distributed on the grid
Total RB units	23*(180kHz)
Total Number of BSs	4
Utilized numerologies	The numerologies with 15,30,60 kHz SCS
Noise power spectral density	-174 dB/Hz [174]
Weights of the objective function a_1, a_2, a_3	100, 1 and 1 respectively
Pt_{min}	0
Pt_{max}	46 dBm [174]
Pr_{max}	250 mW
Number of segments M	100
Start point of the segments X_{min}	0
End point of the segments X_{max}	$2^{max(demand)/min(PRB)}$

3.4.2 Optimisation Results and Impact of VBSs

optimisation results have been taken with the different numbers of DPs and VBSs. First, we considered eight different scenarios; each scenario possesses a different number of DPs that requires diverse services as shown in Table 3.8. VBS nodes are not included in half of the scenarios; still, the objective function and the rest of the model are identical. It is important to note that scenarios named Sc1 and Sc5, Sc2 and Sc6, Sc3 and Sc7, Sc4 and Sc8 have identical DPs in terms of location on the grid, delay and

Table 3.8: Scenario Parameters

Scenario name	Number of eMBB DPs	Number of URLLC DPs	Number of mMTC DPs	Total number of DPs	Number of VBSs
Sc1	2	2	2	6	5
Sc2	3	3	3	9	5
Sc3	4	4	4	12	5
Sc4	2	1	12	15	5
Sc5	2	2	2	6	0
Sc6	3	3	3	9	0
Sc7	4	4	4	12	0
Sc8	2	1	12	15	0

data rate requirements. The only difference is the existence of VBS nodes.

In what follows, we represent the corresponding optimisation results in terms of transmit power and bandwidth allocation amongst RBs and CCI.

Total transmit power

Optimisation results are obtained for eight scenarios given in Table 3.8. In this subsection, we focus on the total transmit power of Sources (including backhaul and access) in the downlink direction, as well as the average and individual power consumption of each DP.

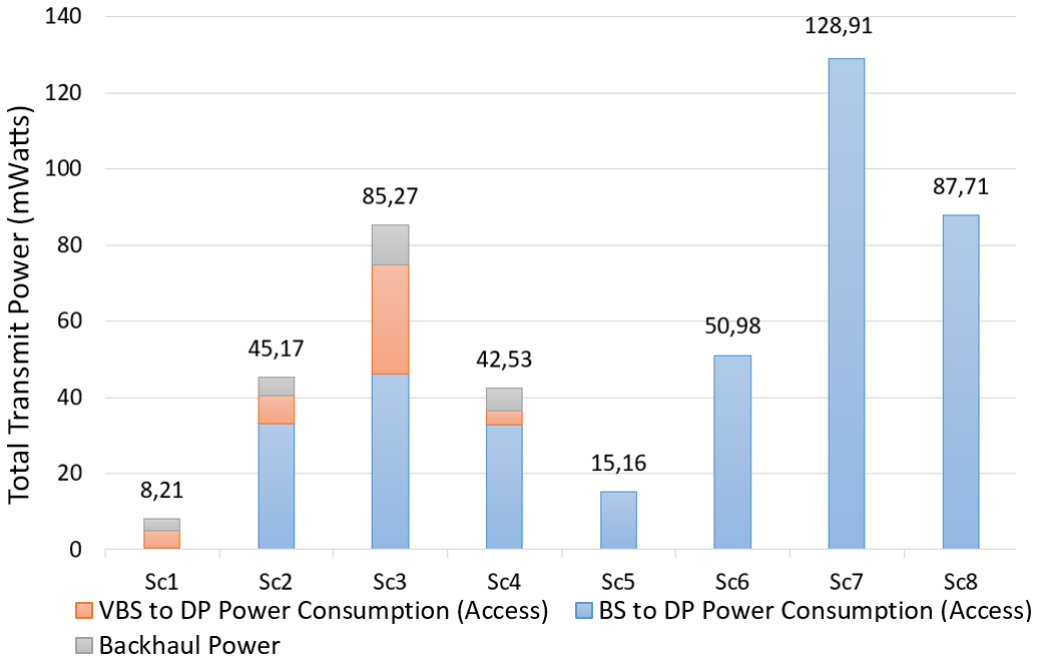

Figure 3.6: Total transmit power for each scenario

Figure 3.6 shows backhaul and each access power separately; the grey colour represents backhaul power consumption, and the orange and blue colours show VBS to DP and BS

to DP access transmit power, respectively, for each scenario. This colour representation is identical for Figures 3.6 to 3.9. BS to DP connection is still in use when VBS nodes are activated. Figure 3.6 shows that the total transmit power is always less when VBS nodes are used. This difference rises when only access power consumption is compared.

The individual power consumption of DPs is investigated to analyse the impact of backhaul communication. To do so, the scenarios that include the same number of DPs are compared. Fig 3.7 illustrates the scenarios with six DPs, Sc1 and Sc5. Sc1 has VBS nodes hence backhaul communication is available. The results demonstrated that the VBS nodes are utilised by high data-requiring DPs, in other words, eMBB DPs. Both eMBB DPs have significant power savings compared to scenario Sc5.

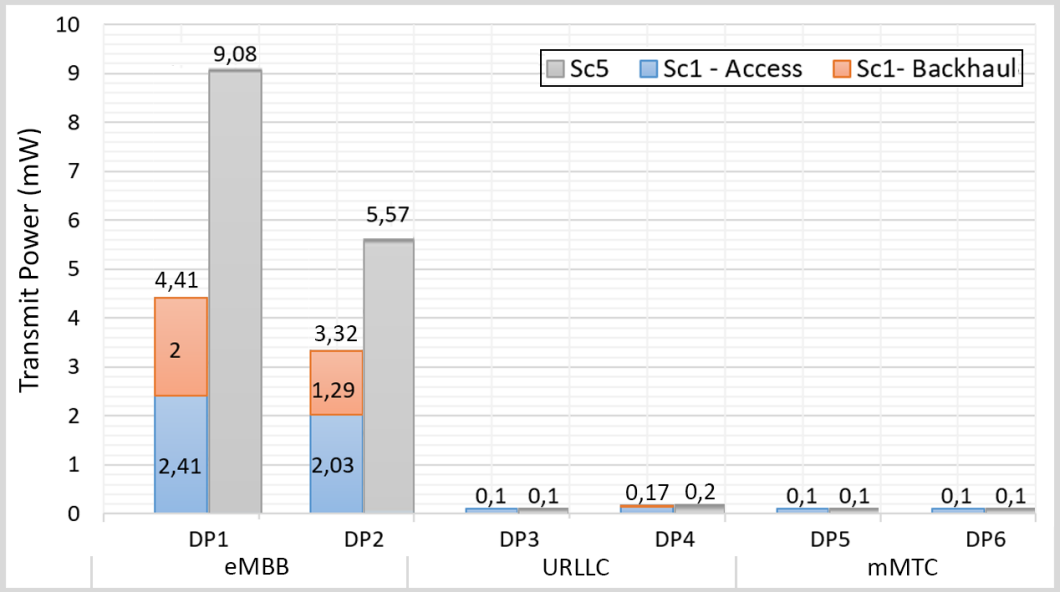

Figure 3.7: Individual transmit power consumption comparison among all DPs for Scenarios Sc1 and Sc5

It is important to note that we employ a frequency-selective channel with SSF coefficients that follow a Rayleigh distribution. SSF refers to the rapid fluctuations in the received signal strength due to multipath propagation, where the signal travels through multiple paths and encounters constructive and destructive interference [175]. The SSF coefficients apply these fluctuations to the channel characteristics. The changes in SSF occur much faster than LSF and FSPL, which change slowly over longer distances. Therefore, channel gain might differ for different frequency bands even for the same distance between a BS and a user. Considering this fact, we utilised two methods to justify the allocated transmit power outputs.

The first method employed to justify the allocated transmit power outputs involves increasing the number of DPs and observing the optimal power allocation across different scenarios. As shown in Fig 3.6, there is a continuous increase in power consumption as the number of DPs is increased. Scenarios Sc1, Sc2, and Sc3 have an equal rate of DPs, with an equal number of eMBB, URLLC, and mMTC DPs, respectively. However, as the total number of DPs increases from 6 to 9 and then to 12, the power allocation steadily increases for these scenarios. Similarly, scenarios Sc5, Sc6, and Sc7 exhibit the same relationship, with a corresponding increase in power observed across these scenarios.

The second method to justify the allocated transmit power outputs is, considering the framework's four BSs and five VBSs, we positioned DPs at equal distances for each Source and observed the corresponding allocated transmit power. Specifically, we employed the two eMBB DPs from the 6-DP scenarios and observed access power only. DP number 1 and DP number 2 are located at distances of 61 meters and 71 meters from their respective Sources. To assess the SSF coefficients, we placed these DPs at the same distance from all BSs and VBSs. For instance, DP number 1 was located 61 meters away from each BSs and VBSs. Subsequently, we calculated the average and standard deviation based on these measurements.

The average access power for DP numbers 1 and 2 are 3.17 mW and 1.9 mW, respectively. As illustrated in Fig 3.7, the allocated access power for the corresponding DPs is 2.41 mW and 2.03 mW, respectively. Thus, DP number 1 experienced a better channel condition than the average, while DP number 2 encountered a worse channel condition than the average. This observation suggests that channel conditions may vary depending on the location or frequency band, but the displayed transmit power tends to align around the average. Table 3.9 shows the optimal power allocation for two eMBB DPs with no CCI or INI.

Table 3.9: Transmit Power for DP1 and DP2 (mW)

Sources	BS1	BS2	BS3	BS4	VBS1	VBS2	VBS3	VBS4	VBS5
DP1	2.35	3.72	4.92	2.30	2.41	2.54	4.14	4.86	3.18
DP2	1.29	1.48	2.58	1.06	1.18	2.05	2.03	2.95	2.16

Figure 3.8 demonstrates the scenarios with nine DPs: Sc2 and Sc6. Only DP1 utilises the VBS nodes in Sc2; hence, the reduction in transmit power. On the other hand,

DP2 and DP3 indicate that power consumption is equal when VBS nodes are available but not active. Up to now, backhaul communication has been employed for the high data-requiring eMBB DPs only.

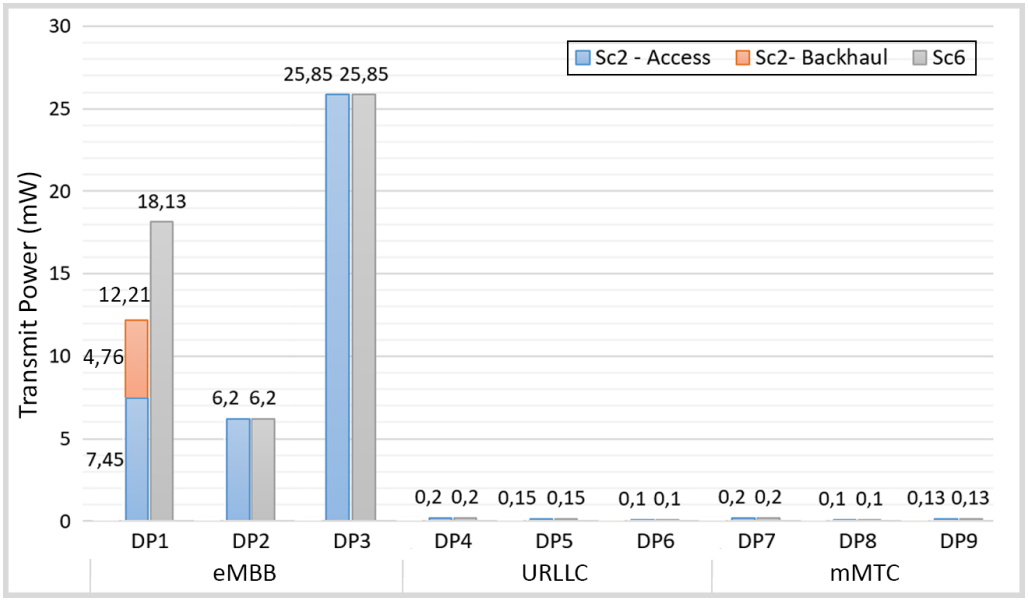

Figure 3.8: Individual transmit power consumption comparison among all DPs for Scenarios Sc2 and Sc6

Sc3 and Sc7 are compared in Figure 3.9. All types of DPs utilise the backhaul communication for the first time; however, the most significant change can be observed in eMBB DPs; for instance, a dramatic reduction in transmit power can be seen in DP4.

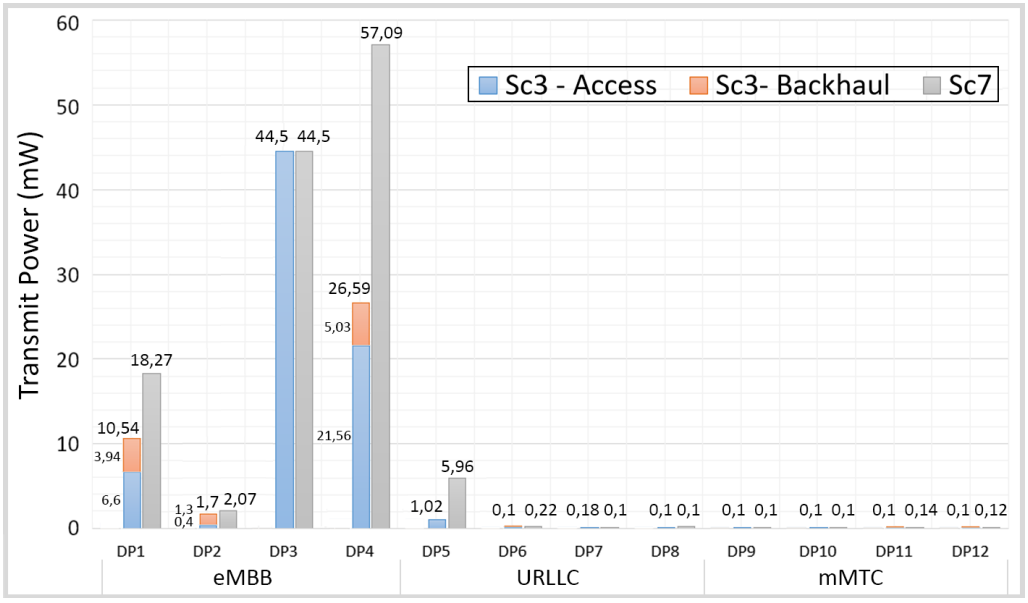

Figure 3.9: Individual transmit power consumption comparison among all DPs for Scenarios Sc3 and Sc7

Since the locations of the VBSs are chosen randomly, the distance between a source and DP might reduce. The closer the distance, the lower the transmit power. Lower transmit power causes lower interference for those DPs that utilise the same RB. Hence, lower transmit powers can satisfy the requirements of the DPs that suffer from high interference. This accumulative transmit power reduction can be observed for DP5 in scenarios Sc3 and Sc7. Although no VBS is activated for the DP5, the transmit power reduces when other DPs utilised VBSs. This situation is investigated further in the 'CCI for DPs' subsection.

The overall results in this subsection demonstrate that the services that require a high data rate, are more likely to use VBS nodes to reduce total power consumption. Moreover, as anticipated, the DPs that have higher data rate demands consume more power than others, and utilising VBS nodes makes significant changes in those DPs. Figure 3.7, 3.8 and 3.9 illustrate that the difference in transmit power can be seen on eMBB DPs mostly. Consequently, the power efficiency for individual DPs is improved; the same DPs are served with lower power consumption. The individual power consumption of DPs is decreased by 48%.

In addition, average power consumption for each scenario and standard deviation are lessened when VBS nodes are employed which is illustrated in Figure 3.10. The fall in average power consumption and standard deviation shows that VBSs alleviate the consumed power and help to maintain fairness in terms of power consumption. The average power consumption for each DP is decreased by 54% also the standard deviation is reduced by 50%.

Just as high data rate and low latency, connection density is a factor in 5G [173]. Therefore, instead of simply increasing the number of DPs proportionally, we use scenarios Sc4 and Sc8 to reflect the nature of mMTC. Hence, scenarios Sc4 and Sc8 have 12 mMTC DPs, 2 eMBB DPs and 1 URLLC DP. Since the focus is on the mMTC DPs in Sc4 and Sc8, it is a good opportunity to discuss the bandwidth allocation among BWPs. Instead of focusing on similar results on the individual transmit power that mostly changes for eMBB DPs, we show the flexibility of the bandwidth in the following subsection.

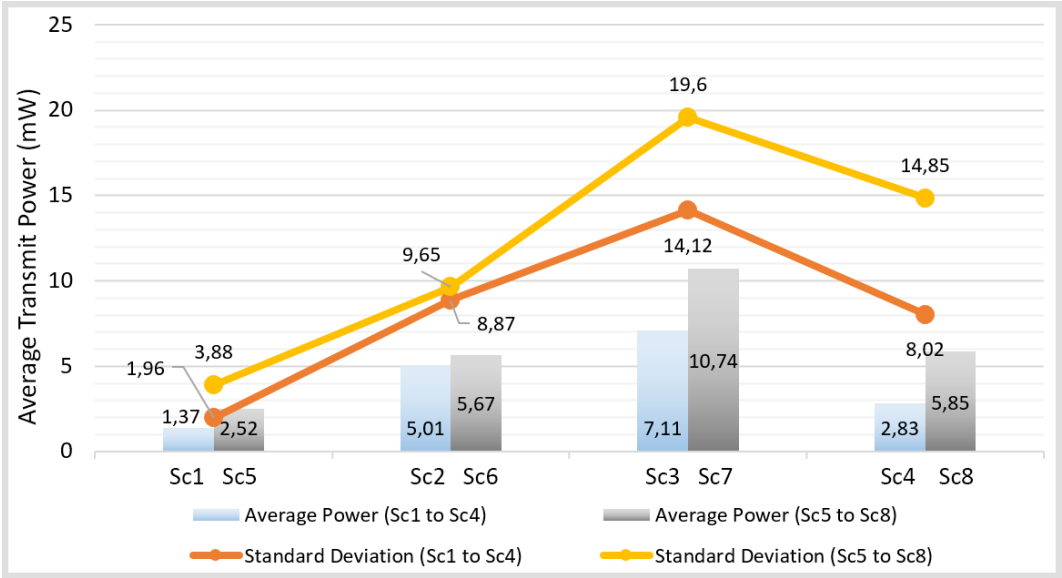

Figure 3.10: Average transmit power and standard deviation comparison among scenarios

Bandwidth allocation amongst BWPs

We investigate the bandwidth allocation amongst BWPs as well as RB allocation among numerologies. Due to the given delay requirements, the first numerology (with 15 kHz SCS, also displayed as BWP1 in Figure 3.11 and Figure 3.12) is not available for URLLC DPs at all. Moreover, the first numerology comes with the lowest SCS bandwidth; according to our constraints and objective function, all DPs tend to use higher numerologies due to the higher bandwidth advantages.

Figure 3.11 shows the bandwidth allocation amongst BWPs for each scenario. The numerologies with 15, 30 and 60 kHz SCSs are shown as BWP1, BWP2 and BWP3, respectively. As stated earlier in this thesis, each BWP includes only one type of numerology, and there is only one BWP for each numerology. Since three numerologies are utilised in this model, there can be at most three separate BWPs.

Maximising the BWP that contains the 3^{rd} numerology comes with the minimum number of RBs; however, this is the optimum bandwidth allocation in this optimisation framework in 6 out of 8 scenarios. Due to the low number of RBs, CCI is inevitable for all scenarios except Sc1 and Sc5. Yet, the optimisation model tolerates the CCI by utilising lower transmit power. However, scenarios Sc4 and Sc8 have a few data and delay critical DPs. The rest of the DPs have lower data and delay requirements; therefore, the optimisation model employs more RBs with lower numerologies.

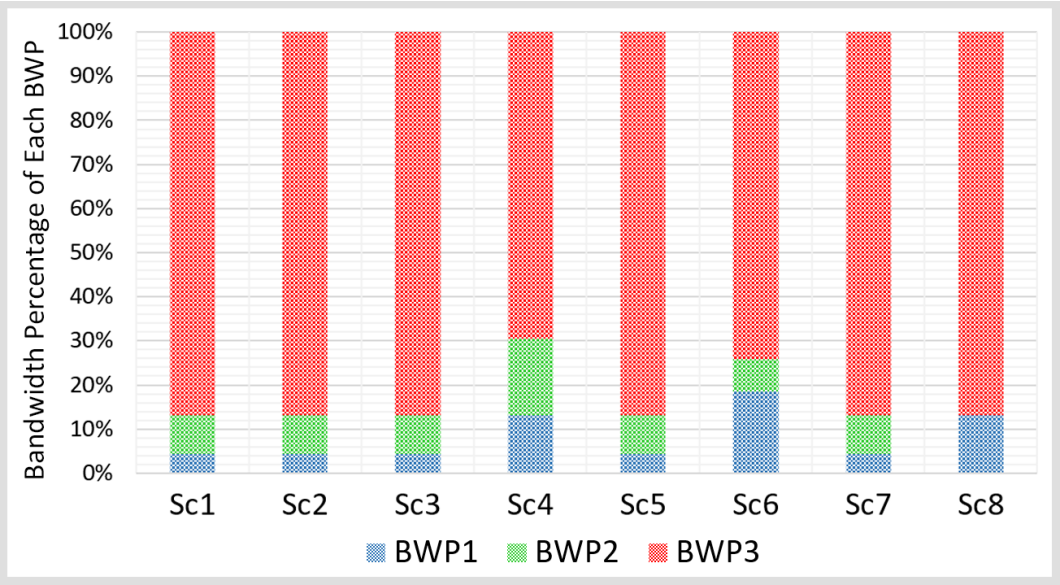

Figure 3.11: Bandwidth allocation between BWPs

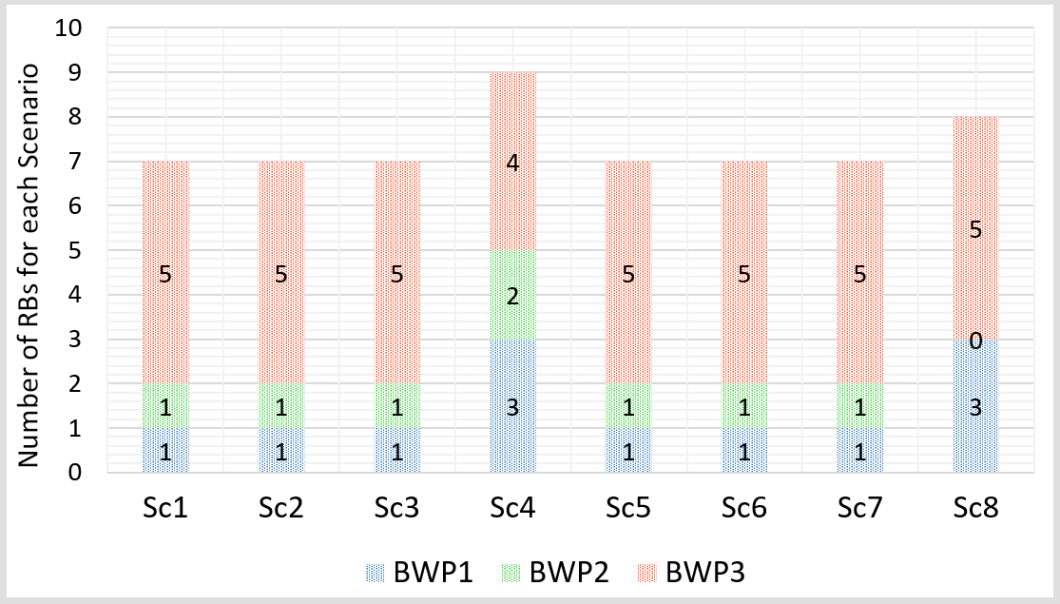

Figure 3.12: Total number of RBs for each scenario

Bandwidth allocation amongst BWPs should be evaluated with the number of RBs for each numerology. The scenarios with a low number of DPs do not need a high number of RBs; however, due to CCI restrictions, as the number of DPs is rising, increasing the number of RBs eases CCI. Figure 3.12 illustrates the number of RBs for corresponding BWP.

Figure 3.13 shows the numerology selection of the DPs for scenarios Sc3 and Sc7. According to their requirements, the DPs are flexible to select any numerology. Thus, the model can offer higher numerologies (consequently higher bandwidth) to the DPs

even when they do not need to. For example, URLLC DPs have to pick 3^{rd} numerology due to delay requirements, and eMBB DPs have high data rate requirements; selecting 3^{rd} numerology helps to reduce the transmit power significantly. However, mMTC DPs do not have strict delay or high data rate requirements. Thanks to the flexibility, it can be seen that DP10 selects 3^{rd} numerology, although it does not have to.

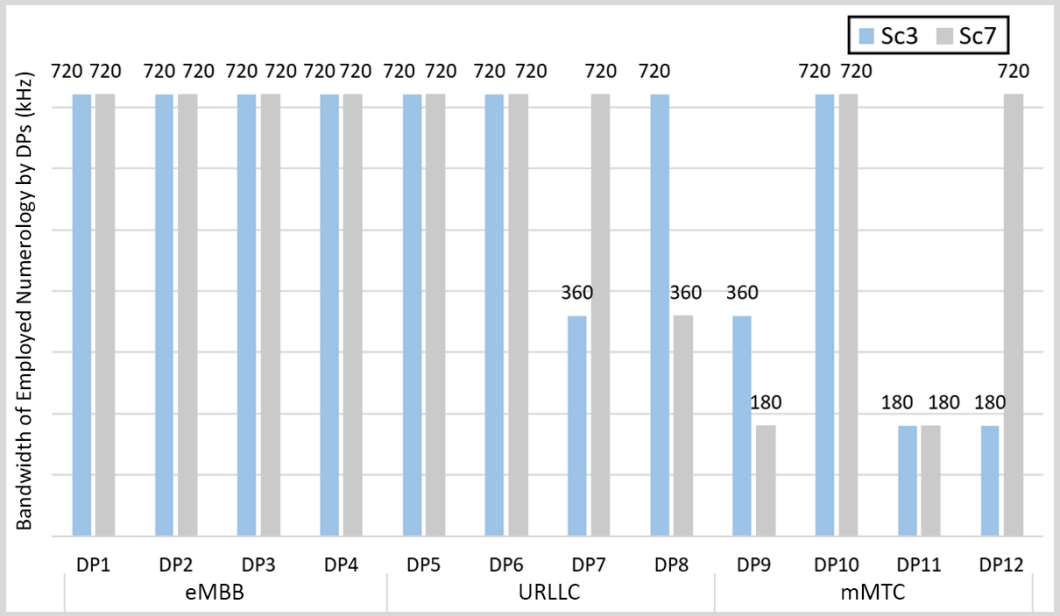

Figure 3.13: Numerology deployment for 12-DP scenarios Sc3 and Sc7

Interference

In this subsection, we investigate the interference focusing on two aspects: co-channel interference and inter-numerology interference.

CCI

The CCI is calculated for each RB that is allocated to a DP. The scenarios with 6-DPs avoid the CCI by selecting unallocated RBs; however, the rest suffers from CCI. Instead of analysing the standalone interference power, CCI is investigated by considering its percentage over all the signals that a DP receives. Since the eMBB DPs consume relatively more power than other DPs, analysing the CCI percentage helps maintain a CCI presentation standard in the model.

Also, we utilise sub-6 GHz for access and mmWave for backhaul; hence, there is no interference between access and backhaul. When a DP selects a VBS as a supplier, the signal comes from a closer source to the corresponding DP and transmit power can be

reduced. Moreover, the distance of the interfering sources can be further when a VBS node is activated. Considering propagation loss, moving away from the interfering sources helps to reduce the CCI.

The 6-DPs scenarios, Sc1 and Sc5, have no CCI, and the 9-DPs scenarios, Sc2 and Sc6, have insignificant CCI percentages. Figure 3.14 shows the percentage of CCI for the 12-DPs scenarios, Sc3 and Sc7, respectively. In Figure 3.14, interfering DPs are shown by the same colour; for instance, DP5 and DP8 use the same RB of different BSs in Sc3, and DP6, DP10, and DP12 interfere with each other in Sc7. As a result, the maximum percentage of interference is reduced by 69% (from 24,47% to 7,35%).

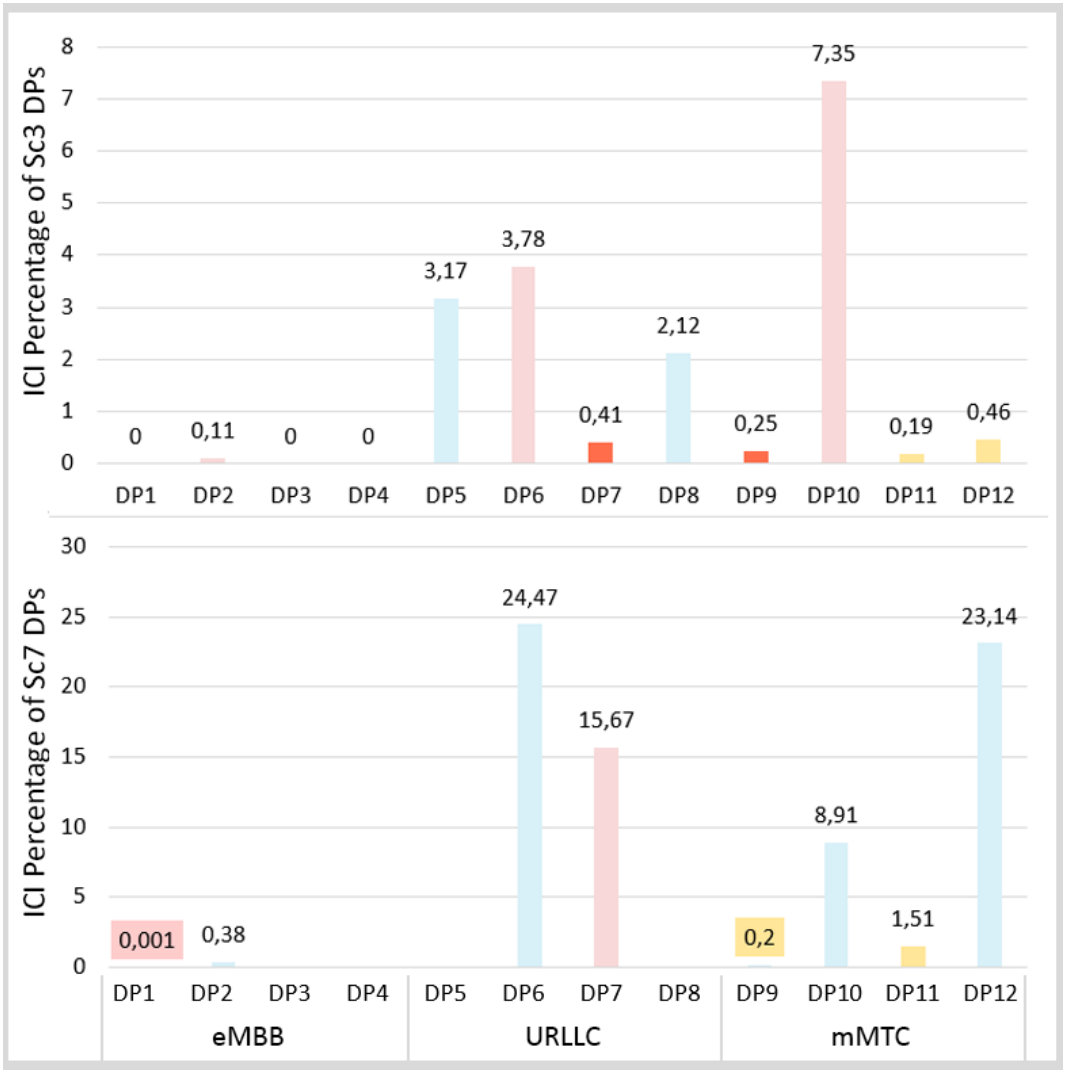

Figure 3.14: CCI percentage of each DP for 12 DP scenarios Sc3 and Sc7. Interfering DPs are shown in the same colour.

It is demonstrated in the previous subsection that utilising VBS nodes decreases the difference among individual transmit power (standard deviation) of DPs. In other

words, fairness is better in the scenarios with VBS nodes; moreover, the percentage of CCI is significantly diminished. Also, it can be seen from Figure 3.14 that eMBB DPs hardly ever interfere with other DPs. Since eMBB DPs consume more power than other DPs, interfering with DPs that use other services would cause a huge percentage of CCI for the URLLC and mMTC DPs. Most of the time, eMBB DPs have no CCI; however, when they have CCI, they either interfere with each other or interfere with other types of DPs that are located far on the grid to compensate huge power differences. Besides, all the scenarios are in a similar trend; the percentage of CCI is significantly diminished when VBS nodes are in use. In addition to that, when a VBS is activated, the location of the interfering source changes. Therefore, there is a chance to increase the distance of the interfering sources; hence, interference reduces.

INI

In Chapter 3.1.1, we previously emphasised that we ignored the INI. This subsection demonstrates the INI and its genuine effect on total interference in our optimisation problem. To investigate the INI, we will begin by exploring the concept of orthogonality. Let $x_1(t)$ and $x_2(t)$ be two scalar waveforms. The inner product of these signals is calculated as follows, where $x_2^*(t)$ shows the complex conjugate of $x_2(t)$ [176]:

$$(x_1, x_2) = \int_{-\infty}^{\infty} x_1(t) \cdot x_2^*(t)\, dt \tag{3.72}$$

When the inner product of two signals is equal to zero, such signals are considered orthogonal to each other, meaning those signals are completely independent and do not interfere with one another [176]. To analyse sinusoidal signals, let us consider two sinusoidal functions with different frequencies: $x_1(t) = \cos[2\pi f_1(t) + \phi(t)]$ and $x_2(t) = \cos[2\pi f_2(t)]$. In order for these signals to be orthogonal to each other, it is necessary that the following equation is satisfied:

$$\int_0^T \cos[2\pi f_1(t) + \phi(t)] \cdot \cos[2\pi f_2(t)]\, dt = 0 \tag{3.73}$$

If $f_1 - f_2 = \frac{L}{T}$, where "L" is a positive integer, the Eq 3.73 is satisfied. Thus, it can be concluded that signals with frequencies being integer multiples of each other are

orthogonal to each other. Fig 3.15 shows orthogonal signals in the frequency domain.

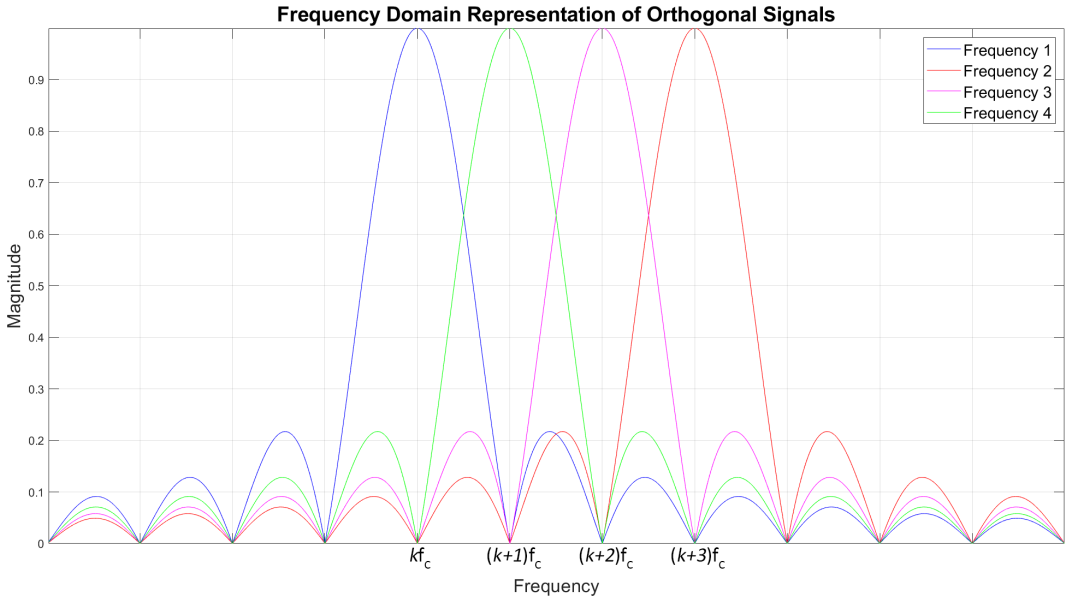

Figure 3.15: Frequency Domain Representation of Orthogonal Signals.

Fig 3.15 demonstrates that the power of orthogonal signals exhibits an inverse relationship where one signal reaches its maximum while the other signal reaches zero, and vice versa. Also, the signals in the Fig 3.15 are normalised.

Using orthogonal signals helps to utilise the bandwidth more efficiently. As mentioned before, employing a multi-numerology system disrupts orthogonality and causes INI. In this subsection, we investigate the allocated RBs, which have been found as optimal and employed by the optimisation framework, to assess the extent of INI. In the optimisation problem, an optimal bandwidth allocation has been determined for different numerologies. However, it is important to emphasise that we initially disregarded INI, rendering it absent from any equations or constraints. In other words, we did not incorporate INI into our model or aim to minimise its effects, among other considerations. This investigation aims to show the INI patterns for the allocated bandwidth.

Fig 3.16 illustrates the optimum RBs employed in the framework, where blue, red and magenta lines show the 1^{st}, 2^{nd} and 3^{rd} numerologies, respectively. In the optimal BWP allocation, there are one, one and six RBs for 1^{st}, 2^{nd} and 3^{rd} numerologies, respectively. The green lines in Fig 3.16 represent the guard bands employed between BWPs. In order to reduce the complexity of the figure, the first three RBs of the 3^{rd} numerology are displayed. Table 3.10 is employed to show the INI among different RBs from different numerologies. The centre frequencies of the RBs and guard bands

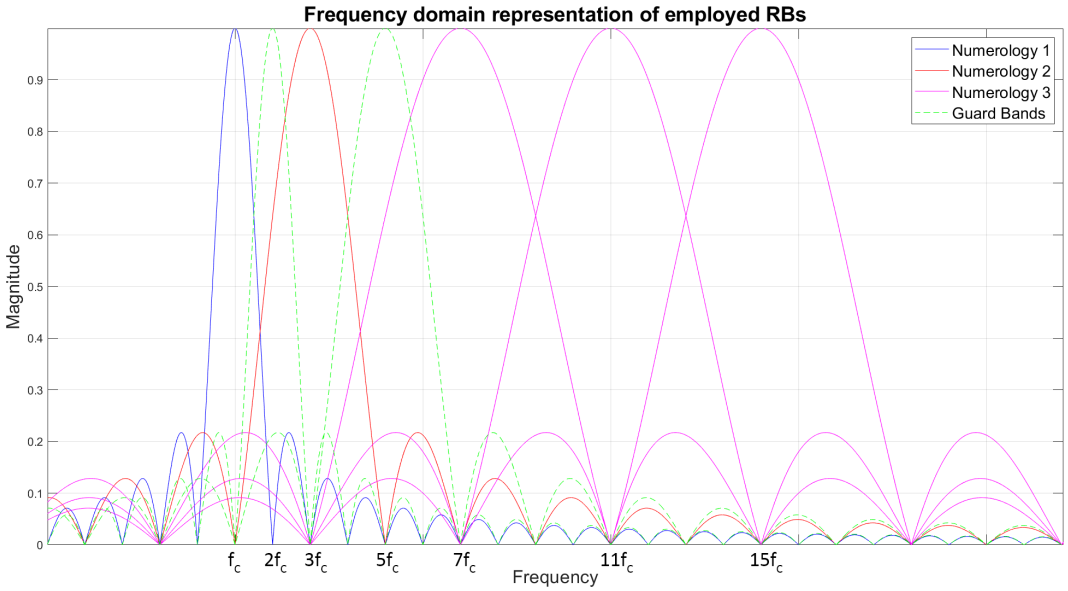

Figure 3.16: Frequency Domain Representation of Employed RBs.

are marked below in the figure.

Table 3.10: INI Among Numerologies

INI caused by \ INI caused to	1^{st} numerology	2^{nd} numerology	3^{rd} numerology
1^{st} numerology	NA	X	X
2^{nd} numerology	X	NA	X
3^{rd} numerology	✓	X	NA

It can be clearly seen from Fig 3.16 that the 1^{st} numerology causes no interference to the higher numerologies because its centre frequency will always be an integer multiple of the higher numerologies' frequencies. Thanks to the first guard band between the first and second numerology RBs, 2^{nd} numerology also causes no interference to the 3^{rd} numerology. This guard band also helps to cancel INI caused by 2^{nd} numerology to the 1^{st} numerology. Considering this specific BWP allocation which is found as optimum and has any INI constraints and calculations, the only INI caused by the 3^{rd} numerology to the 1^{st} numerology Table 3.10 shows the INI relation among numerologies for this BWP allocation.

Given the abundance of available resources in scenarios with 6 DPs, CCI and INI can be avoidable. Consequently, our focus shifts towards investigating INI in scenarios involving 9 DPs. In this subsection, we aim to calculate the actual INI. To achieve this, we utilise frequency domain analysis which is given in Fig 3.16 to calculate the interference power.

The power of side lobes reduces and starts from 21% then 12% 9% 7% to 5% in the 5^{th} side lobe. The nearest 3^{rd} numerology RB causes higher INI than those located further in the carrier frequency. Although the power of the side lobes can be filtered [177] to reduce this interference, in this subsection, we analyse all the side lobes without considering any filter applied.

DP number 9 is served by BS number 1, which is 102 meters away, and utilises only 1^{st} numerology RB. The closest 3^{rd} numerology RB in the carrier bandwidth, which is located at the $7f_c$ in Fig 3.16, is employed by DP number 7, a URLLC DP, which requires 0.21 mW and is served by BS number 4. The distance between DP number 9 and BS number 4 is 453 meters. Since only the 21% of its power causes an INI to DP number 9, the power that causes INI is calculated as 0.04 mW. Table 3.11 shows the same relation for the RBs that cause the INI for DP number 9.

Table 3.11: INI Power That Is Caused by Other DPs

Interfering DPs to DP #9	Power for other DP	Source of other DP	Distance to interfering DP	Side Lobe Power	Interfering Power
URLLC (7)	0.21 mW	BS #4	453 m	21%	0.04 mW
eMBB (1)	7.45 mW	VBS #3	590 m	12%	0.89 mW
eMBB (2)	6.19 mW	BS #3	342 m	9%	0.55 mW
URLLC (5)	0.14 mW	BS #3	342 m	7%	0.01 mW
eMBB (3)	25.85 mW	BS #2	314 m	5%	1.29 mW

The channel gain amongst DP number 9 and interfering Sources is calculated for the channel gain the same as CCI, considering path loss, LSF, and SSF coefficients. The received INI power is given in Table 3.12. This table shows the interfering power, channel gain, and their multiplication; hence, the received INI power can be calculated.

Table 3.12: INI Power Calculation

Interfering DPs to DP #9	Interfering Power	Channel Gain	Received INI Power
URLLC (7)	0.04 mW	8.27×10^{-14}	0.03×10^{-13} mW
eMBB (1)	0.89 mW	1.11×10^{-14}	0.09×10^{-13} mW
eMBB (2)	0.55 mW	3.97×10^{-13}	2.18×10^{-13} mW
URLLC (5)	0.01 mW	4.21×10^{-13}	0.004×10^{-13} mW
eMBB (3)	1.29 mW	3.59×10^{-13}	4.63×10^{-13} mW

The summation of the received INI power to the DP number 9 becomes 6.94×10^{-13} mW. The received noise power of the 1^{st} numerology RB is calculated as 7.16×10^{-13} mW. The transmit power, which is generated for DP number 9 by BS number 1, is 0.13 mW, and the employed channel gain is 5.54×10^{-11}. Thus, the received transmit power

is calculated as 72.02×10^{-13} mW. Just like CCI, INI is also investigated by considering its percentage over all the signals that a DP receives; therefore, the percentage of the actual INI is calculated as 8.04%.

The only INI observed in our framework is caused by the 3^{rd} numerology RBs to the DP number 9. Remarkably, the percentage of INI in this scenario is lower than that caused by CCI without VBS scenarios. Furthermore, it is important to note that we did not apply any filters to mitigate the effects of the sidelobes. Therefore, actual values should be less than the calculated. Additionally, the optimisation framework did not include any specific constraints or calculations for INI. Consequently, we can confirm that the locations of BWPs in the carrier bandwidth are meticulously designed, effectively minimizing the impact of INI. In conclusion, considering all these facts, the decision to ignore INI in our analysis is justified, as it would otherwise introduce further complexity to the system.

Another crucial aspect to consider is that we aim to achieve maximum bandwidth efficiency. As a consequence, the RBs from different numerologies are located closely in our optimisation framework. However, even lower levels of INI can be achieved by making some specific trade-offs, such as increasing the guard bands or allocating more bandwidth to the guard bands. For instance, if we were to allocate a guard band equivalent to the size of 3^{rd} numerology RBs, the result would be a zero-INI among different numerologies for this optimum BWP allocation, as illustrated in Fig 3.17.

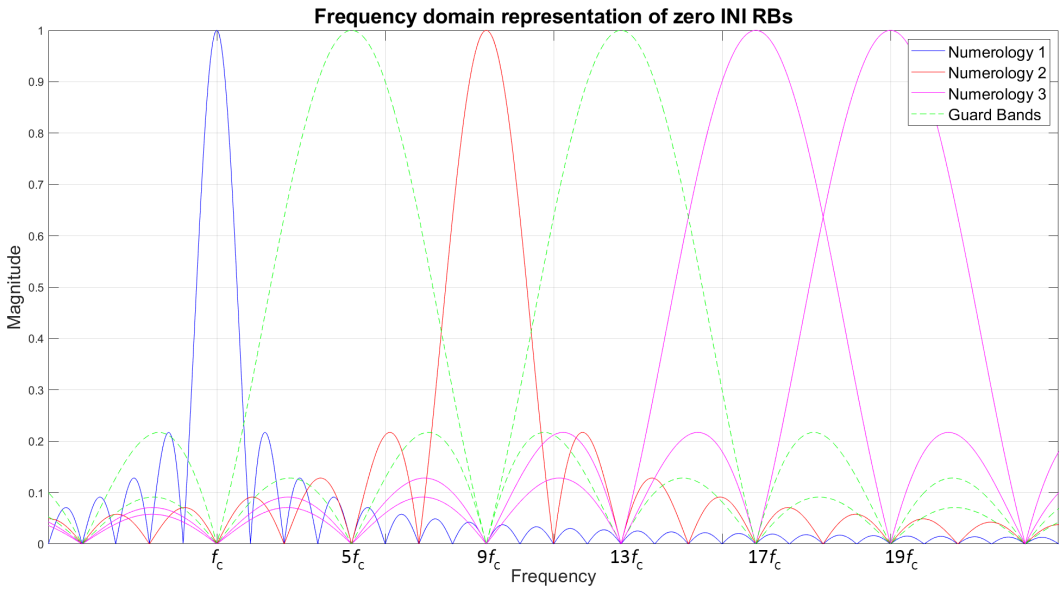

Figure 3.17: Frequency Domain Representation of Zero-INI RBs.

Moreover, since we actively minimise the CCI in the optimisation framework, in the case that INI coefficients are identified in the model, the interfering DPs would be far from each other. This distance helps to reduce the interference among DPs. Further, the distance among interfering DPs is elaborated in the next subsection.

Interfering DP locations

A lower interference is expected to acquire the minimum transmit power and maximum SINR. However, in our optimisation framework, we deliberately minimised CCI in the objective function. Hence, we concentrated on and investigated the interfering DP locations on the map. Fig 3.18 shows the interfering DPs for scenario Sc 3. It can be seen from Fig 3.18 that the interfering DPs are located on the opposite corners of the map to minimise the CCI.

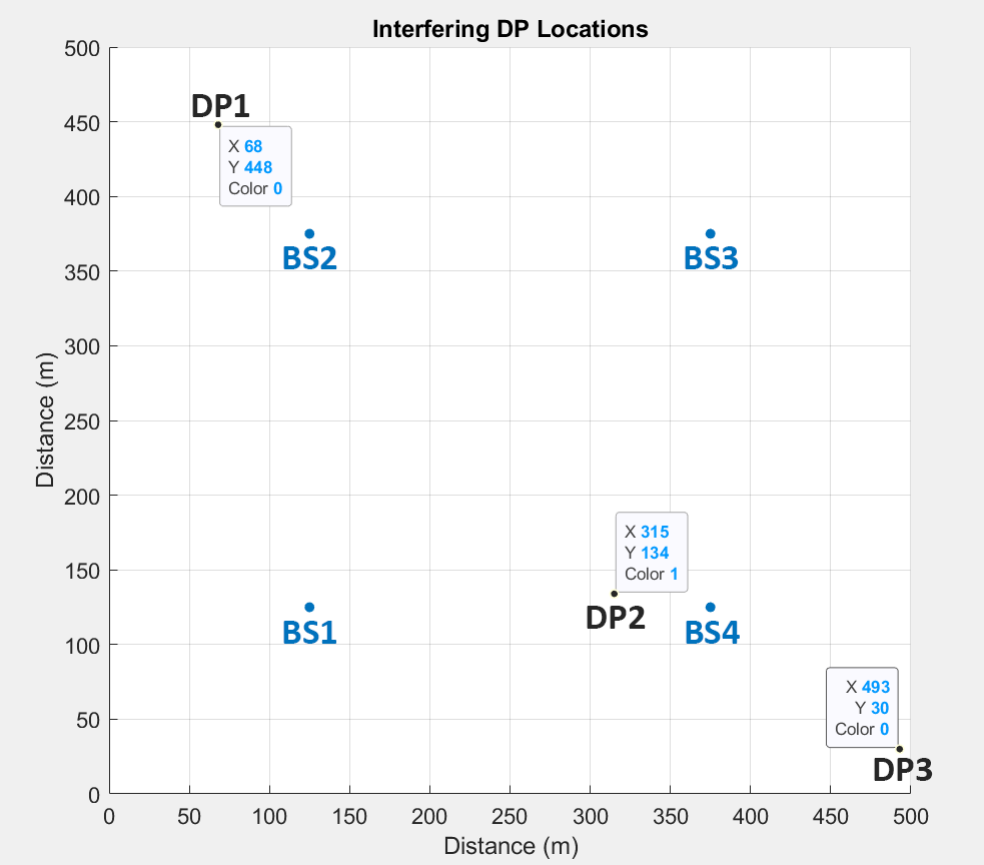

Figure 3.18: Interfering DP locations for the Scenario Sc3. Blue dots show the BSs and the precise locations of interfering DPs are shown.

3.4.3 Impact of a Flexible BWP Compared to Non-Flexible BWP

In this subsection, we withdraw the flexibility of the numerology selection for the DPs. Each type of DP can utilise only pre-defined numerology. Considering the delay requirements, the URLLC DPs can only use 3^{rd} numerology. eMBB DPs require a high data rate, consequently, high bandwidth; therefore, we allocated the 2^{nd} numerology for the eMBB DPs. Since the mMTC DPs have no strict data rate and delay requirements, we assume that the 1^{st} numerology is appropriate for them.

When DPs are flexible in selecting numerology, all the eMBB DPs enjoy a high data rate advantage of the 3^{rd} numerology that is shown in Figure 3.13. However, when the flexibility is prevented, the eMBB DPs are forced to utilise 2^{nd} numerology. The greater numerology utilises the DP, the larger bandwidth the DP gets. Reducing the bandwidth to half causes a significant increase in the transmit power for those DPs. For example, for Sc1, the transmit power increases 66 times (from 4,4 mW to 293 mW) and 26 times (from 3,3mW to 86 mW) for DP1 and DP2, respectively.

Since all eMBB DPs used to employ 3^{rd} numerology in previous sections, we decided to reduce the data rate requirements of eMBB DPs to alleviate this clear effect of reducing bandwidth. The data rate requirements of eMBB DPs, therefore, are reduced to 1-1.5 Mbps from 5-7 MBPS in this subsection. The rest of the DP requirements and locations are identical. The lower data rate requirements enable investigation of the BWP allocation among BWPs and CCI percentage for the scenarios with reduced data rate requirements by ignoring the obvious transmit power increase of high data rate-requiring scenarios. The scenarios with VBS nodes (Sc1 to Sc4) are employed to analyse the flexible and non-flexible scenarios.

Figure 3.19 provides a comparison between flexible and non-flexible numerology selection in terms of bandwidth allocation among BWPs for scenarios from Sc1 to Sc4. Non-flexible scenarios increase the 2^{nd} numerology utilised by the eMBB DPs, leading to an increase in the probability of finding RBs with higher gains and a reduction in interference among eMBB DPs. However, flexible scenarios maximise the 3^{rd} numerology as expected, which leads to a lower number of RBs, but more manageable CCI in lower transmit power. Considering the objective function, the optimisation model can compromise some power against interference, and selecting the larger band-

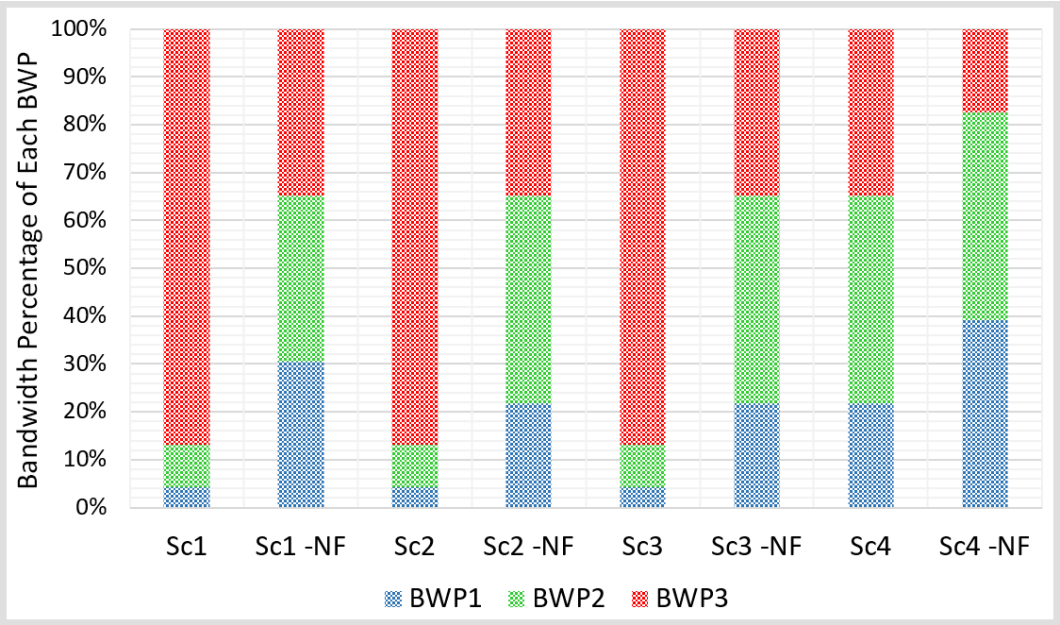

Figure 3.19: Bandwidth allocation comparison between flexible and non-flexible BWP allocation scenarios

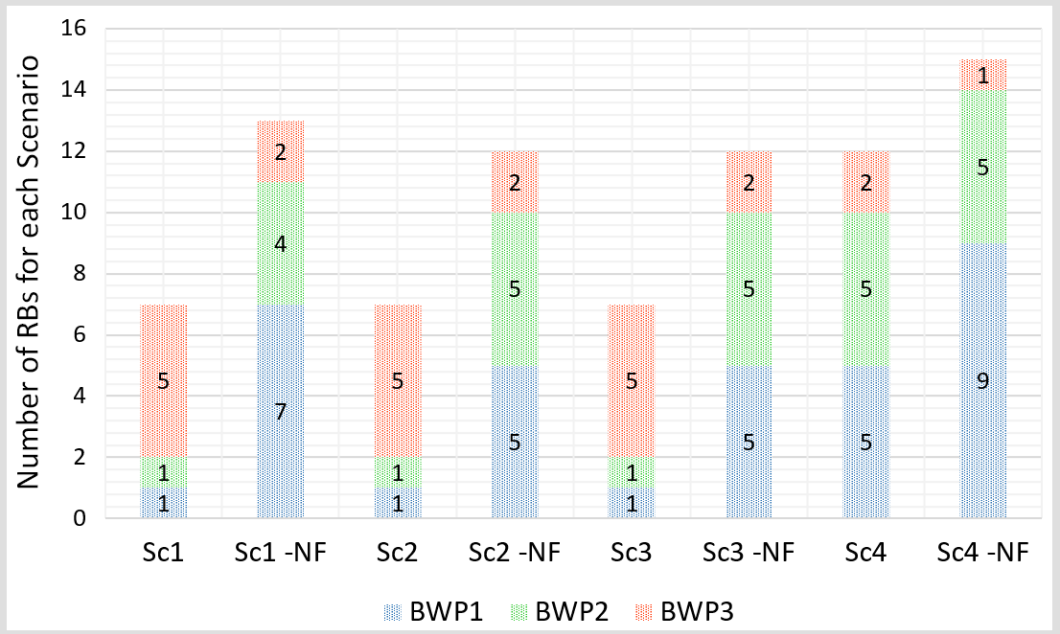

Figure 3.20: Total number of RBs for comparison between flexible and non-flexible BWP allocation scenarios

width counterpoises this compromise. Figure 3.20 shows the number of RBs for each corresponding scenario.

In order to further evaluate the performance of the proposed optimisation model, we compared the total transmit power consumption of flexible and non-flexible scenarios. Figure 3.21 shows the power consumption for each scenario. As the optimisation model consistently selects the 3^{rd} numerology for almost all DPs, it is expected that the non-

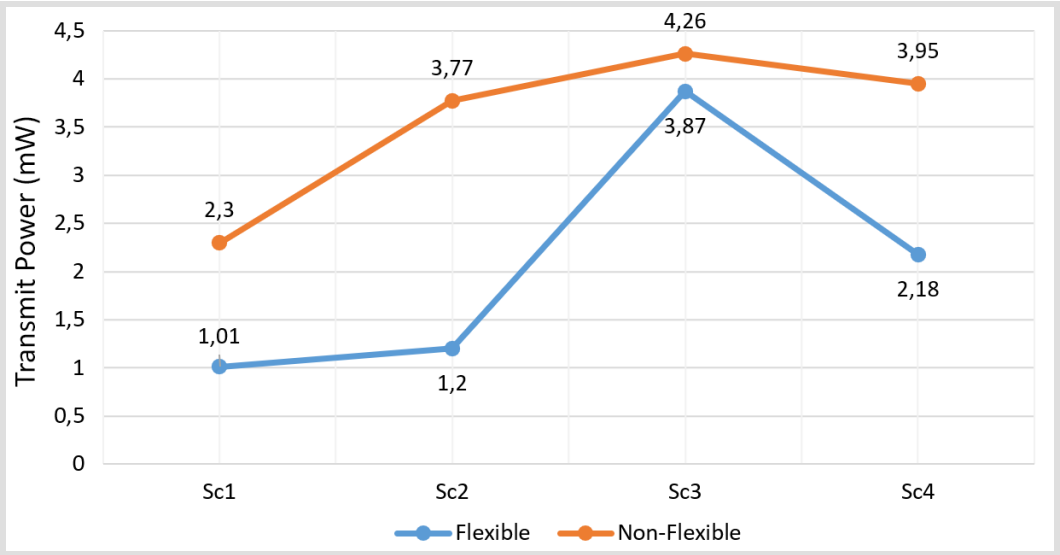

Figure 3.21: Total transmit power comparison of flexible and non-flexible scenarios.

flexible scenarios consume more power due to the utilisation of higher numerologies for eMBB DPs. The results demonstrate that the flexible BWP allocation model reduces the total transmit power consumption, which aligns with the objective of reducing energy consumption in communication networks.

In the impact of non-flexible BWP results, we examined the scenarios for CCI, where Sc1 had no interfering DPs, Sc2 and Sc4 had considerably less CCI; therefore, Sc3 is investigated for CCI. Due to RB shortage in the flexible scenario, it is anticipated to have a higher number of interfering DPs; however, Figure 3.22 illustrates that the percentage of CCI is consistently lower when flexible scenarios are employed. These results demonstrate that using higher numerologies with interfering RBs can maintain the advantage of higher bandwidth for DPs, allowing them to achieve the desired SINR with lower power and less CCI.

In addition to comparing flexible and non-flexible scenarios, it is also essential to consider a single BWP scenario. In such a scenario, only 3^{rd} numerology can be employed to meet the delay and data rate requirements, regardless of the scenario. However, if a 5 MHz carrier bandwidth frequency is employed with only 3^{rd} numerology, the total number of available RBs becomes six. As a result, scenarios with more than six DPs are guaranteed to experience interference. Conversely, in a hypothetical no delay requirement scenario, the single BWP can employ 1^{st} or 2^{nd} numerology. However, given our parameters, the total transmit power would increase exponentially due to

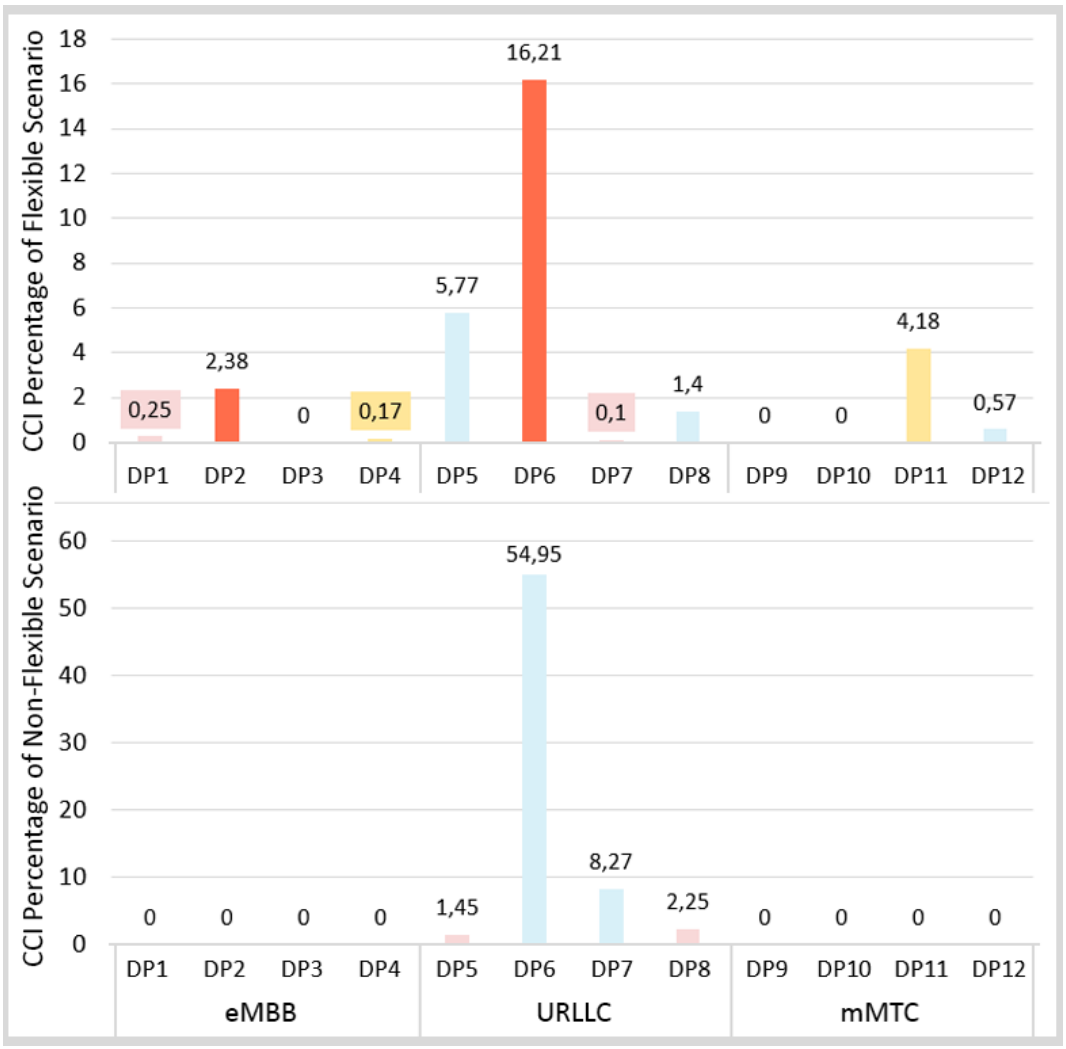

Figure 3.22: CCI percentage of each DP for Flexible and Non-Flexible scenarios. 12-DP Scenario Sc3 is utilised. Interfering DPs are shown in the same colour.

the lower bandwidth of lower numerologies. This exponential increase highlights the advantage of flexible BWP allocation.

3.5 Conclusions

In this chapter, we proposed a joint optimisation framework that optimises the downlink RAN power allocation, user association, bandwidth allocation among BWPs and data routing through vehicular networks. The proposed optimisation framework aims to improve network efficiency and reduce the total transmit power while considering CCI. To achieve this, a MILP model was developed that jointly optimises the above-given objects by taking into account the total carrier bandwidth, routing data through VBS nodes when necessary, and RB allocation among DPs by considering their delay and data rate requirements. The proposed optimisation model is designed to increase

the flexibility of the network by incorporating VBS nodes, which allows DPs to receive their demand from other sources, supported by the out-band IAB network. Access and backhaul communications are achieved through the FR1 and FR2 frequency bands, respectively. The objective function of the model aims to maximise the number of served users while minimising the weighted sum of the total transmit power and the CCI. To achieve this, the model optimises the distribution of resources per DP, considering their specific data rate and delay requirements.

In determining the data rate requirements of the DPs, a minimum requirement of 0.225 (bit/s/Hz) as specified in [173] was considered. However, our user requirements are much higher than this value. For instance, if a 720 kHz BW numerology is used, each RB must carry at least 0.162 Mbps; on the other hand, our mMTC DPs require data rates between 5-7 Mbps.

The proposed optimisation approach effectively reduces transmit power and CCI, indicating the benefits of properly configured numerologies, which could support the implementation of RAN slicing. Additionally, we present a logarithmic function linearization method based on piecewise linearization. Overall, the proposed model can significantly enhance network efficiency, reduce power consumption and CCI, and effectively implement RAN slicing. Moreover, the proposed optimisation framework can be extended to address new problems by incorporating additional constraints. For instance, in-band IAB optimisation can be considered for similar scenarios, or the parameters can be increased to tackle more complex and realistic problems.

Chapter 4

Heuristic Model

In the previous chapter, we utilised MILP to obtain optimal solutions. However, some MILP problems may be excessively complex, NP-hard, or require considerable time to solve. Additionally, each variable included in the optimisation problem exponentially increases the total number of variables, leading to a significant increase in computational load and time. For instance, as the number of DPs, VBSs, the total carrier bandwidth, and numerologies increases, computational time increases exponentially. This phenomenon is known as the curse of dimensionality, which arises due to the vast amount of data or parameters required for data analysis [178].

For example, in our MILP optimisation model, we observed that the computational time required to obtain an optimal solution increases significantly as the problem size grows larger. Specifically, for the scenario with the highest number of DPs and VBSs, which includes 15 DPs and 5 VBSs (denoted as Sc8), the optimisation problem took over 36 hours to solve on a computer with an Intel Core i7 10750H 2.59 GHz processor and 32 GB RAM. Furthermore, as the number of DPs increases, the problem becomes increasingly complex and can become NP-hard, meaning that finding an integer solution becomes infeasible.

Due to challenges such as the curse of dimensionality and the difficulty of solving some optimisation problems, researchers have turned to alternative algorithms that can offer near-optimal solutions in less time. One such approach is to use heuristic algorithms, which trade off maximum accuracy and optimality for reduced computational time. In addition, heuristic algorithms may be particularly useful for addressing problems with

unknown features.

The heuristic algorithms can be written by making some observations or assumptions; for example, in our problem, we can say that the nearest source must serve each DP. On the other hand, the meta-heuristic algorithms are significantly inspired by nature; for example, the Ant System (or ant colony) optimisation model is derived from the study of actual ant colonies [58]. The shortest path leaves more intense traces and scents for the ants, and after some iterations, the ant colony starts to follow the shortest route. Particle Swarm Optimisation is derived from a bird flock or fish school; each agent (either a bird or a fish) keeps its distance to its surrounding agents the same all the time [59]. The velocity of the nearest agent is assigned to the corresponding agent, and after some iteration, a random velocity value is assigned to the agent to increase 'craziness.' The expected behaviour is that agents maintain an optimum velocity for themselves and the distance between themselves and their neighbours. Moreover, the Bees algorithm and Bacterial Foraging Optimization are examples of nature-inspired optimisation algorithms in the literature. [60].

The Genetic Algorithm (GA) draws inspiration from the principles of evolution, whereby species adapt to environmental changes over generations [60]. These principles are based on natural selection and sexual reproduction [179]. In nature, fitness tests are used to select individuals in many ways; for instance, organisms that fail the fight or flight test perish [179]. Humans, on the other hand, use another selection method by choosing the best offspring to improve the quality of crops, horses, and dogs across generations [179]. However, those tests are not enough for mating. Individuals must also dominate weaker ones in a species-specific competition known as "survival of the fittest" [180]. Those who pass their genes to the next generation are regarded as successful individuals. During mating, two individuals swap genetic material if their chromosomes match, with the smallest unit determining an organism's traits known as a gene [180].

The GA is a computational method that relies on a population of individuals to exchange genetic material for obtaining optimal solutions. The GA is an iterative process, and the fitness of each chromosome is evaluated in each iteration. Each generation brings more individuals into the population. Since the GA is an iterative process, the population size must be constant to hinder exponential population growth [181]. As

part of the iterative process, the GA employs a selection (or elitism) process to identify and retain the best individuals while eliminating the rest. In this thesis, the terms "chromosome" and "individual" are used interchangeably to represent a solution for our optimisation problem.

The GA is a search algorithm that aims to find the optimal solution from a vast set of possible outcomes by following steps, including selection, crossover, and mutation. An essential component of the GA is the evaluation method used to select the best chromosomes and regulate population growth. In each generation, the chromosomes are evaluated based on their fitness, and the fittest are chosen for reproduction [182]. The initial population can be generated randomly, using heuristics, or through fully valid chromosomes [181]. Two common selection techniques are used: roulette and tournament [183]. The roulette method selects the best chromosome based on its fitness, while the tournament method uses the roulette method several times to obtain a subset of chromosomes [183].

After evaluating and selecting the chromosomes, the GA proceeds with the crossover and mutation process, which boosts genetic diversity and evolution. Occasionally, genes are modified through mutation [179]. The crossover process involves the exchange of genetic material between parent chromosomes to generate new generations. However, not all parent chromosomes participate in the crossover process; instead, a certain number of parent chromosomes are selected with a probability of crossover rate p_c [183]. Two types of crossover methods, single-point and two-point crossover, are commonly used [183]. In this thesis, we used the single-point crossover method, which combines the top part of one chromosome with the bottom part of the other chromosome.

To avoid being trapped in local optima and premature convergence, the GA utilises mutation to explore the genetic material within the population [182]. By introducing new genetic material, mutation can help the population escape local optima and increase its diversity [182]. Therefore, the role of mutation in GA is to promote the exploration of the search space. Compared to crossover, the mutation rate p_m is typically set to a relatively low-value [183].

We have generated the initial population by considering two algorithms. The first algo-

rithm assumes that each DP establishes a connection to the nearest source; therefore, this algorithm is called the Nearest Source Genetic Algorithm (NSGA). In the second algorithm, DPs are free to select any source; hence, this algorithm is called the Total Random Genetic Algorithm (TRGA). To get noteworthy results, BSs, VBSs and DPs are located in the identical locations used to obtain the MILP results.

In this study, both NSGA and TRGA algorithms generate a population of 1 million chromosomes, which are divided into 100 groups of 10000 chromosomes each. Each group represents a set of chromosomes produced in order of their generation. The term "group" refers to these sets of populations that include 10000 chromosomes. The chromosomes generated by the algorithms are evaluated to determine if they meet the constraints of the problem. Invalid chromosomes are removed, and the initial generation comprises the first valid chromosomes. Therefore, the number of chromosomes in the initial generation may vary depending on the number of valid chromosomes in each group. After obtaining the initial generation composed of valid chromosomes, the algorithms proceed to selection, mutation, and crossover operations on each group separately to generate new generations. It should be noted that the groups are designed assuming they do not share any chromosomes or genes with each other. Therefore, the algorithms produce 100 different outputs obtained from the 1 million generated chromosomes.

In our study, we conducted multiple iterations of evaluation, selection, mutation, and crossover in each group. Specifically, the algorithm evaluated the chromosomes in each group, eliminated any faulty ones, selected the best chromosomes, and implemented mutation and crossover operators.

To obtain statistically significant results, we analysed the average, standard deviation, and best outputs of each group in the results section. These numerical analyses were performed using 10,000 chromosomes, and as a result, we can expect to observe an average output with some standard deviation.

4.1 The Nearest Source GA (NSGA)

The primary decision variable of the MILP optimisation model consisted of four dimensions, denoted by y_{sd}^{rn}, representing whether user equipment 'd' is served by source'

s' using numerology' n' and RB 'r'. Heuristically, the nearest source can provide the requested data rate to consume minimum transmit power. In the NSGA, we consider this postulate, the dimension of the sources is removed, and the resource allocation problem becomes three-dimensional. Assuming that the algorithm has four BSs and five VBSs, removing sources dimension from y_{sd}^{rn} reduces the size of the chromosome by 89%.

Furthermore, to further reduce the dimensionality of the problem, we incorporated numerology information into the RBs. The relationship between the RBs and numerology is encoded at the beginning of the chromosome; hence, we obtain a two-dimensional problem that considers RB and power allocation among users. Thus, the primary decision variable in the NSGA becomes y_d^r, indicating whether user equipment 'd' is allocated RB' r'. Throughout this thesis, it is essential to note that we employ the terms "DP" and "user" interchangeably.

The MILP optimisation model also considers the BWP allocation among carrier bandwidth, resulting in the need to include BWP allocation in the chromosomes. As a result, each chromosome is split into two segments: the initial binary portion indicating the BWP allocation among the carrier bandwidth (and hence the numerologies of the RBs), and the second part consisting of non-negative real numbers indicating the RB and corresponding transmit power allocation among users. The chromosome representation for each user allocated an RB includes a non-negative real number indicating the transmit power in milliwatts, as well as the specific RB of a given numerology being utilised. Conversely, if a user is not using the corresponding RB, the value in the chromosome is set to zero. In other words, to simplify the problem, we used a single variable that combines RB-user association, power allocation, and numerology-user association instead of using separate variables for each. This approach reduces the complexity of the problem and makes it easier to optimise.

$$p_d^r = \begin{cases} > 0, & \text{If DP } d \text{ utilizes RB } r \text{ with corresponding transmit power} \\ 0, & \text{otherwise} \end{cases} \tag{4.1}$$

RB numerology association determines the bandwidth allocation among BWPs. Bandwidth allocation among numerologies that alters the total number of RBs is carried out

randomly. For example, the maximum available number of the RBs can be achieved when all RBs belong to the first numerology. To accommodate all possible outcomes and keep the chromosome size constant, we allocate sufficient space in the chromosome for BWP allocation among carrier bandwidth. The total transmission bandwidth W_{total} is considered as 5 MHz that can have a maximum of 25 RBs [169]. Considering an RB size guard band between BWPs, the maximum available number of the first numerology RB is reduced to 23. Thus, the first 23 genes of any chromosome indicate the number of RBs for each BWP. These genes are binary, and they ensure that each RB can belong to at most one numerology, as follows:

$$\sum_{n \in N} y^{rn} \leq 1, \ \forall \ r \in R \tag{4.2}$$

In the NSGA, the second part of the chromosome consists of a total of ($number\ of\ UEs$) x ($maximum\ available\ number\ of\ the\ RBs$) genes. For a carrier bandwidth of 5 MHz and 6 UEs, the second part of the chromosome consists of 138 genes, resulting in a total of 161 genes in a single chromosome when BWP allocation is included. It is necessary to repeat that the total number of RBs in each generation may vary and is typically less than 23, except for very rare scenarios. Therefore, although the chromosome reserves space for 23 RBs, not all RBs may be present in most cases. The first 23 genes in the chromosome represent the RB allocation among BWPs, and the corresponding numerology of the allocated RB can be found within these genes. Each RB can be allocated to one of the six users.

To illustrate how numerology-RB allocation is incorporated into a chromosome, we consider a straightforward example depicted in Figure 4.1. The chromosome consists of two parts. The first part, which is common for all UEs, represents the allocation of RBs among BWPs using a binary code. The second part consists of $N_r \times N_u$ genes, where N_r is the maximum possible number of RBs and N_u is the number of UEs. Each UE is represented with N_r genes, and only one gene can have a value greater than zero, indicating the transmit power of the corresponding UE-RB pair as a real number. Thus, the chromosome size becomes $(N_r \times N_u) + N_r$.

In the example, the maximum number of RBs is seven, and there are three UEs. The first seven genes in both chromosomes are binary and represent the bandwidth

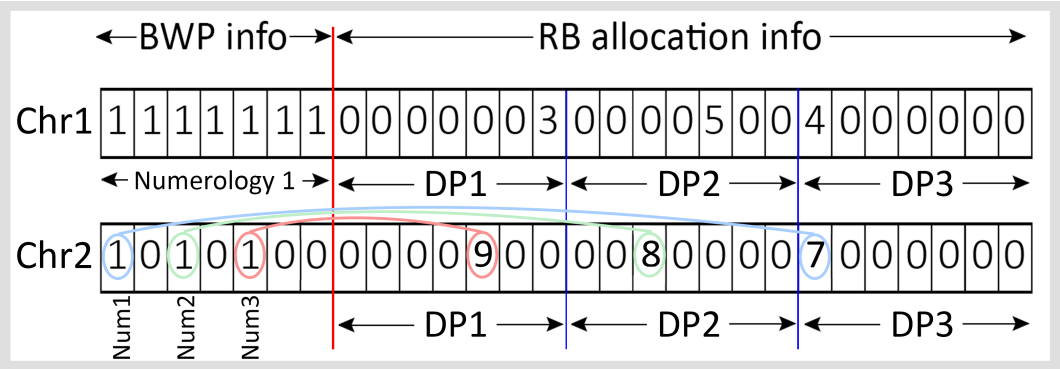

Figure 4.1: Numerology DP RB allocation example for the Nearest Source Genetic Algorithm (NSGA)

allocation among BWPs. Each UE can select one of the seven RBs; hence, only one RB-UE pair can have a non-zero value. Figure 4.1 illustrates two chromosomes, each with a different BWP allocation. The first chromosome has one BWP that belongs to the 1^{st} numerology, which achieves the maximum number RBs. UE1, UE2, and UE3 utilise RB numbers 7, 5, and 1, respectively, and consume 3, 5, and 4 milliwatts, respectively. The second chromosome has three RBs and BWPs, one of each. The zeros before the ones that are given in the BWP info domain separate the BWPs. UE1 uses the only RB that belongs to the 3^{rd} numerology and consumes 9 milliwatts. UE2 and UE3 employ the 2^{nd} and 1^{st} numerologies, respectively, and consume 8 and 7 milliwatts, respectively. Figure 4.1 also shows that the total number of RBs in each generation may vary and be less than N_r. Thus, some of the allocated spaces for RBs may remain empty in some scenarios.

4.1.1 Initialization

The initial population of chromosomes is generated by randomly selecting a numerology and assigning random transmit power to the users. In our MILP optimisation problem, we observed that all URLLC and mMTC UEs require less than 0.3 mW of power to meet their requirements. Therefore, the NSGA algorithm allocates a default power of 0.3 mW to all URLLC and mMTC UEs. For eMBB UEs, power is randomly allocated between 0.1 to 50 mW. Each chromosome in the initial population is produced by considering the following constraints:

$$\sum_{d \in D} y_d^r \leq 1, \quad \forall\, r \in R \tag{4.3}$$

$$\sum_{r \in R} y_d^r \leq 1, \quad \forall\, d \in D \tag{4.4}$$

The constraint (4.3) indicates that each RB can be allocated at most one DP, however since the allocation occurs among the DP and the nearest source, Eq (4.3) implicitly means that each RB in each source can be allocated at most one DP. The constraint (4.4) demonstrates that each DP can utilise a maximum of one RB. Since RB-numerology relation is given in the beginning of the chromosome, there is no need to write a constraint to explicitly indicate that each RB can belong to one numerology. The constraints (4.3) and (4.4) are not necessary to create initial chromosomes, yet, they help to increase the number of valid chromosomes that will be evaluated in the following subsection.

In the next step of our GA, we apply termination criteria to exclude any chromosomes that do not satisfy the user requirements. Only the remaining chromosomes are then used to initiate the first generation of the population, ensuring that the initial population is composed of solutions that meet the minimum requirements of the problem. This approach helps to improve the efficiency of the GA by preventing the generation of invalid solutions and focusing on feasible solutions that can converge towards the optimal solution more effectively.

4.1.2 Evaluation

The evaluation operator is a crucial step in the GA that eliminates the invalid chromosomes to create the initial generation. Two requirements, data rate and delay, are evaluated in this step. First, since the GA randomly generates the transmit power, the allocated data rate must be compared to the requested for each DP. To do so, SINR is calculated using transmit power, and according to the bandwidth of the corresponding RB, the allocated data rate is determined. The data rate and delay requirements are denoted by d_d and t_d, respectively. The data rate requirements of the DPs must be less than or equal to the data rate allocated, and this constraint is formulated as follows, where C_d shows allocated data rate:

$$d_d \leq C_d, \ \forall\, d \in D \tag{4.5}$$

The second requirement is the delay requirement that is satisfied with the assigned numerology. We formulated this requirement by using binary decision variable y_d^n that equals 1 when DP 'd' utilises numerology 'n' and equals 0 otherwise, in the following constraint:

$$t_d \geq t_n \left(\sum_{n \in N} y_d^n \right), \quad \forall\ d \in D \tag{4.6}$$

DPs are flexible in selecting a numerology as long as their requirements are satisfied. Therefore, in our heuristic algorithms, the GA only checks the DPs that require higher numerologies. Finally, the evaluation operator eliminates the chromosomes that do not satisfy the DP requirements, leaving only the valid ones to constitute the first generation.

After generating the initial generation using valid chromosomes, the NSGA algorithm identifies the DPs connected to a VBS as their source. If the nearest source is a VBS, the algorithm finds the closest BS to the corresponding VBS. The same system parameters used in the optimisation chapter for the Heuristics model, such as the locations of BSs, VBSs, and DPs, as well as the data rate and latency requirements, are maintained. Since we employed the same channel model, parameters and variables in this Chapter, discussing the signal propagation model or identifying the parameters and variables would be unnecessary.

Since different bandwidths are employed for access and backhaul communication, which was emphasised in the MILP optimisation chapter, there is no interference between the backhaul and access links. The backhaul links utilise mmWave frequency bands, which employ numerologies higher than the third numerology. Since we assume the optimisation framework employs the first three numerologies, the only available numerology for backhaul becomes the third numerology with 720 kHz SCS. Therefore, the backhaul data rate formula is given as follows:

$$d_d = \ (0.72) \left(log_2 \left(1 + \frac{p_{bv} \times g_{bv}}{\sigma^2} \right) \right) \tag{4.7}$$

The parameters d_d, g_{bv} and σ^2 represent the data rate requirement in Mbps, channel gain between VBSs and BSs and noise power, respectively. The noise power spectral

density was also given as -174 dB/Hz [174]. The only variable in Eq. 4.7 is the transmit power p_{bv}. To calculate the transmit power between BS and VBS p_{bv}, we use the following equation, which is derived from Eq. 4.7:

$$p_{bv} = \frac{\sigma^2}{g_{bv}} \times 2^{(1.38 \times d_d) - 1} \quad \forall\ d \in D \tag{4.8}$$

At this algorithm stage, we have two main motivations to calculate the exact transmit power between the corresponding BS and VBS. Firstly, since the transmit power equation (Eq (4.8)) includes parameters that are already known to the algorithm, computing the exact transmit power only when necessary does not affect the computational overhead. Moreover, assigning a random transmit power and evaluating the backhaul SINR requirement would require more computational resources. Secondly, assigning a random transmit power from a random BS could cause a decrease in the percentage of valid chromosomes in the first generation, as a valid chromosome could become invalid due to randomly allocated unsatisfactory backhaul power. Additionally, when the nearest BS-VBS pair is not selected, the required transmit power to meet the data rate requirement may exceed the limits. Given that the percentage of valid chromosomes is already low, assigning random transmit power would further decrease the number of valid chromosomes in the first generation, and 1 million chromosomes would not be sufficient to obtain satisfactory results.

4.1.3 Sorting

A maximum number of chromosomes limit is set for each generation in the GA to minimize the computational time. Before applying crossover and mutation operators, the valid chromosomes are sorted based on their total transmit power in ascending order. If the number of chromosomes exceeds the set limit, the GA eliminates inefficient chromosomes with higher power consumption. If the population size is still within the limit, the population is sorted only, and no further chromosomes are removed.

4.1.4 Selection

The output of the crossover and mutation operators extends the number of total individuals in the population. For crossover, two chromosomes must be selected to

reproduce two new individuals. The selection operator ensures to pick the chromosomes that have the same BWP deployment for the crossover. Selecting two chromosomes with the same BWP deployment has two main advantages. Firstly, it prevents the creation of invalid chromosomes. When the selected chromosomes have different BWP deployments, the selected RBs can belong to another numerology, causing the crossover operator to fail. Alternatively, due to the change in the total number of RBs, the selected RB might not exist in the pairing chromosome.

Secondly, it also alleviates the burden of the evaluation operator. Since all the chromosomes and genes are valid, there is no need to check the data rate and latency requirements once more. Therefore, after the crossover and mutation, the evaluation operator only checks the number of non-zero genes in a chromosome. If a random selection operation were employed, the data rate and delay requirements of the users would also have to be checked, significantly increasing the computational cost.

In the NSGA algorithm, the first step is to sort the chromosomes according to their total transmit power. Afterwards, a binary selection matrix is utilized to determine which chromosomes can be selected for crossover. The matrix elements are set to 1 if chromosomes a_1 and a_2 have the same BWP deployment and 0 otherwise. The matrix size is $a \times a$, where a denotes the total number of chromosomes in the population. It is necessary to select chromosomes for crossover in a manner that maintains diversity among the population. Therefore, the GA does not apply crossover to all chromosomes, nor are chromosomes selected randomly. Instead, the binary selection matrix is employed to select pairs of chromosomes with similar BWP deployment, ensuring that the crossover operator can be applied without creating invalid chromosomes. This approach promotes the diversity of the population while minimizing computational costs.

Figure 4.2 illustrates the binary selection matrix employed in the NSGA, which only marks half of the chromosome matches as 1 in the matrix. For instance, the first and second chromosomes share the same BWP deployment, but this is only indicated by a 1 on the right side of the matrix. The algorithm checks the binary selection matrix vertically, as indicated by the red dashed lines in Fig 4.2. This approach increases the interaction among the best chromosomes. In this example, if the algorithm checked the matrix horizontally and followed the blue line, the crossover operator would utilize the

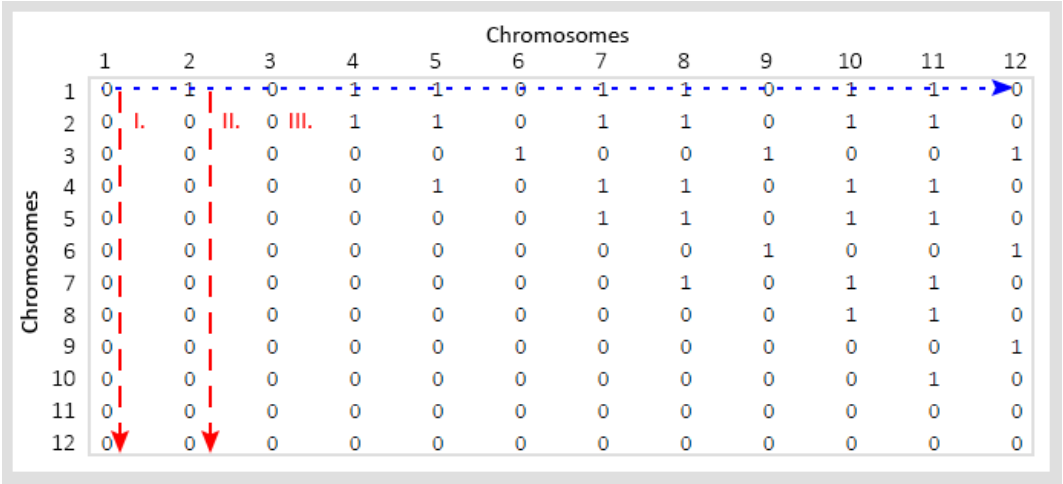

Figure 4.2: A binary selection matrix. The selection operator follows the dotted red line.

first-best chromosome. However, the last chromosomes have the worst performance, so the advantage of using the first-best chromosome would fade. The power efficiency performance of the last chromosomes is likely to be low. Considering the algorithm has hundreds of chromosomes, using the second and third-best chromosomes would be more effective in obtaining better new generations.

4.1.5 Crossover

The crossover operation used in our approach consists of two types. Firstly, we employ classic single-point crossover between two chromosomes to generate a new generation. Then, to increase the genetic diversity, we expose one-third of the chromosomes to bit flipping on top of the single-point crossover.

In the single-point crossover, as shown in Fig 4.3, the position of the single-point is determined by following rules. First, the chromosomes to be crossed over must have the same BWP deployment, and therefore, the first part of the chromosome that contains the BWP deployment information is excluded from the crossover operation. As a result of the first rule, the single point must be selected to the right side of the red line illustrated in Fig 4.3. Second, the DP-RB sets must be preserved during the crossover operation to prevent the division of a chromosome in a way that causes a DP to have two RBs while another DP has zero RBs. In other words, the crossover point should be an integer multiple of the number of possible RBs in the first part of the chromosome.

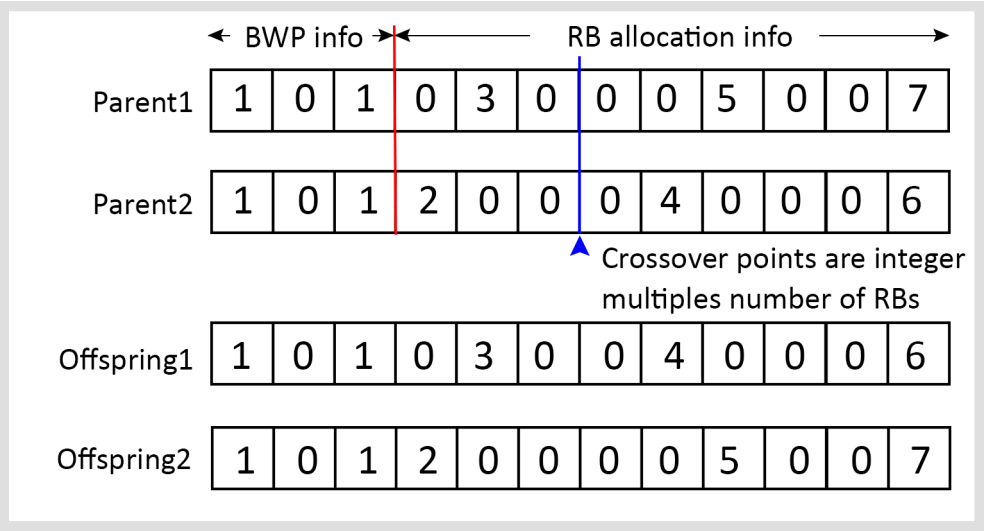

Figure 4.3: Crossover operation for the 12 gene chromosomes.

$$scp = k \times |R| \tag{4.9}$$

In Eq 4.9, scp, k, and $|R|$ show the single crossover point, an integer, and the total number of possible RBs for the given carrier bandwidth, respectively.

Figure 4.3 illustrates the single point selection of the crossover operation and the resulting two reproduced chromosomes. The crossover operator selects a point on the chromosome that is an integer multiple of the number of possible RBs, located on the right-hand side of the red line in the figure. By using this method, two new individuals are produced for the population, increasing its genetic diversity.

The second crossover operator, which involves bit flipping, is applied to the chromosomes that have already undergone the single-point crossover operation. Since the chromosomes have been filtered according to their BWP deployment in the first crossover operation, there is no need to check the BWP allocation among the chromosomes in the second crossover. The bit-flipping operation also excludes the initial bits that represent the BWP allocation of the chromosome. During the bit-flipping operation, the NSGA randomly selects a DP number, and the corresponding DPs swap their transmit power with each other. This operation is carried out for one-third of the chromosomes that are already involved single point crossover to increase genetic diversity and improve the overall performance of the algorithm.

4.1.6 Mutation

In the MILP optimisation, p^r_{sd} denotes the downlink transmit power; it equals a real number between p_{min} and p_{max} when the DP 'd' is served by the source 's' utilising the RB 'r', otherwise, it is equal to zero. Since the NSGA removes the source dimension, the power matrix p^r_{sd} is transformed into p^r_d.

The mutation operation is performed on a randomly selected non-zero element of the p^r_d matrix for a selected DP. The mutation only changes the value of r in p^r_d. The selected element is set to zero, and the same power is assigned to another RB. Each RB has a different channel gain due to the SSF coefficients; thus, there is a chance to make the chromosome valid. However, implementing this mutation to valid chromosomes may cause them to become invalid. Furthermore, since the aim is to minimise total transmit power, the output of this method may not have a significant impact on the optimisation problem. For these reasons, the chromosomes to be mutated are selected from the set of invalid chromosomes to increase the number of valid chromosomes.

After the mutation, the NSGA evaluates the chromosome. Thus, the NSGA ensures that the output chromosomes of the mutation operation are valid. It is worth noting that the predetermined mutation rate is relatively lower than the crossover rate.

In the proposed NSGA for the optimisation problem, the crossover and mutation operations may produce chromosomes with zero or multiple RBs for DPs, which render the chromosomes invalid. Such chromosomes are detected and removed from the population. After performing the crossover and mutation operations, the current population is formed by combining both the parent and offspring populations. The combined population is then sorted based on their fitness values. If the number of chromosomes in the population exceeds the maximum allowed limit, the worst-performing chromosomes are removed. This removal ensures that the most promising chromosomes with the best genes are preserved for the next generations, thus increasing the likelihood of obtaining an optimal solution to the problem.

Algorithm 1 outlines the steps involved in the NSGA. The algorithm begins by evaluating the groups that contain 10000 chromosomes, and only valid chromosomes are selected to generate the initial generation. From there, the NSGA expands the generations using crossover and mutation operators with different rates indicated by 'c'

and 'm', respectively. The algorithm keeps track of the best-performing chromosomes based on their total transmit power in each iteration that occurs 'j' times.

Algorithm 1 The Nearest Source Genetic Algorithm

Input: W_{total}, DP requirements, min/max transmit power, initial generation size (i), crossover rate (c), mutation rate (m), number of GA iterations (j)
Output: BWP allocation (y^{rn}), RB (y_d^r) and power allocation among DPs (p_d^r) which is provided by the nearest Source

```
Initialize (i) chromosomes randomly
[Constraint Handling]
for each chromosome do
    Calculate data rates and numerology allocations
    if valid data rates and numerology for all DPs then
        Mark chromosome as valid
    else
        Remove the chromosome
    for j ≥ 0 do
        Select parent chromosomes for crossover and mutation according to the method
        Perform crossover
        Apply mutation to the selected chromosomes
        Remove duplicate chromosomes
        Sort chromosomes based on transmit power
        Eliminate excess chromosomes if needed
        j = j − 1
```

4.1.7 The NSGA Results

The NSGA is conducted for 100 cycles, producing distinct outcomes for each cycle. Table 4.1 outlines all the input parameters needed for the NSGA. The NSGA initiates the first 'parent' generation, denoted as 'Generation 1' in the figures. The first reproduced generation, which is created by applying crossover and mutation operators, is 'Generation 2'. The term "iterations" refers to instances where the mutation and crossover operators are executed on the previous generation to yield new generations. In the NSGA, the number of iterations is set to 7, leading to a total of 8 generations, including the parent generation.

Table 4.1: The NSGA input parameters

Description	Input
Number of chromosomes in each group	10000
Total number of groups (i)	100
Maximum # of chromosomes that have been kept in each generation	75
Crossover rate (c)	75
Mutation rate (m)	25
Number of new generations (j)	7

The NSGA results are demonstrated in Figure (4.4) shows the average and standard deviation calculated from the 100 groups. In Fig (4.4), the red line indicates the best-performing generation in terms of the difference between the first and last generation, the best output shows the minimum power-consuming generation and the blue line indicates the average performance across all 100 groups. As shown in the Figure, after the third iteration, the performance does not exhibit significant improvement, suggesting that increasing the number of iterations beyond seven would not provide substantial benefits in terms of performance improvement, especially considering the computational load.

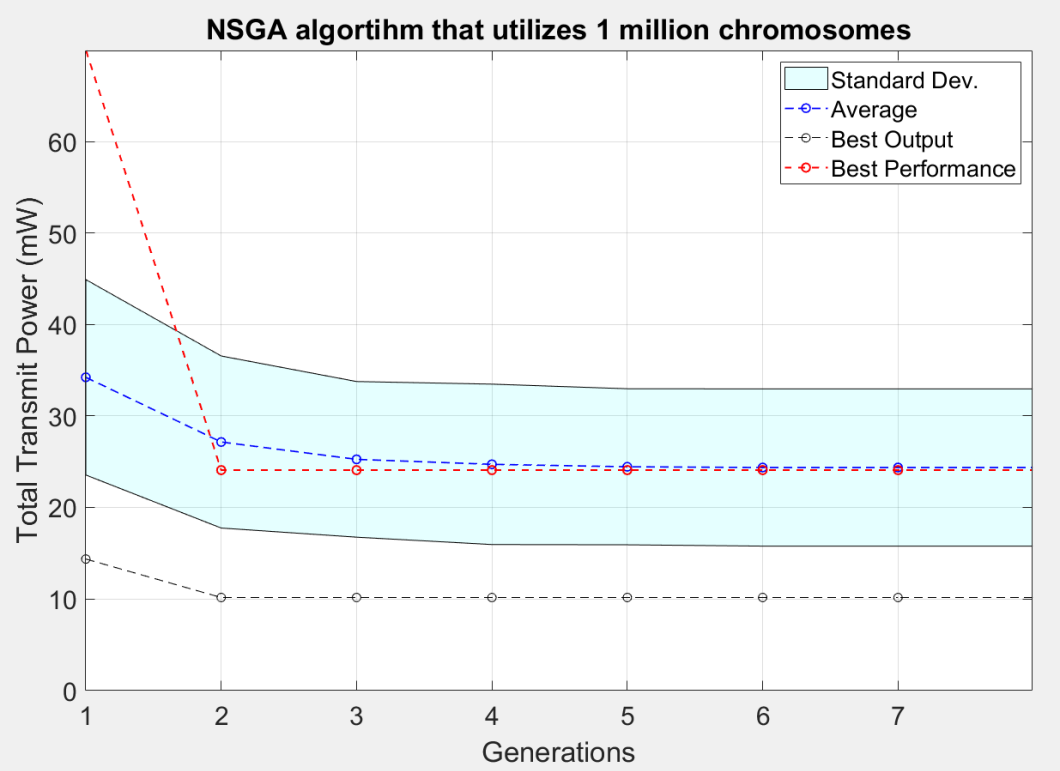

Figure 4.4: The NSGA output utilises 100 groups.

To validate the results of the algorithm, identical DPs with their requirements and locations must be employed. Specifically, the validation is carried out on Sc1, a scenario already subjected to MILP optimisation, encompassing 6 DPs and 5 VBSs. This validation process is elaborated in Chapter 4.2.8, where we compare the algorithm's outputs and the optimal outputs found by MILP optimisation.

In the results of the NSGA, the average total transmit power of 100 groups is found to be 24.35 mW, which is slightly higher than the optimal solution found in the MILP optimisation model, which is 8.21 mW. However, the best result obtained by the

NSGA (shown as a black line) with a minimum output of 10.14 mW is still acceptable, considering the significant reduction in solver time compared to the MILP model. It should be noted that it is possible to obtain even better outputs by combining all successful chromosomes from all groups. However, this approach would require a significant increase in computational resources, which makes it impractical. Therefore, if the optimization process requires significant computational time, it might be more feasible to use the MILP optimization approach.

The NSGA is also capable of optimizing the allocation of bandwidth among the BWPs. In order to analyze the bandwidth allocation results, we followed a similar approach to that of the power allocation problem. The average and standard deviation of the number of RBs in each BWP are calculated using the final generation of the groups. The number of RBs, or the allocated bandwidth for BWPs, differs from that obtained in the MILP optimization. While the number of RBs in the 3^{rd} numerology is higher than the others, our findings suggest that the 1^{st} and 2^{nd} numerologies have a higher number of RBs compared to the previous MILP optimisation results.

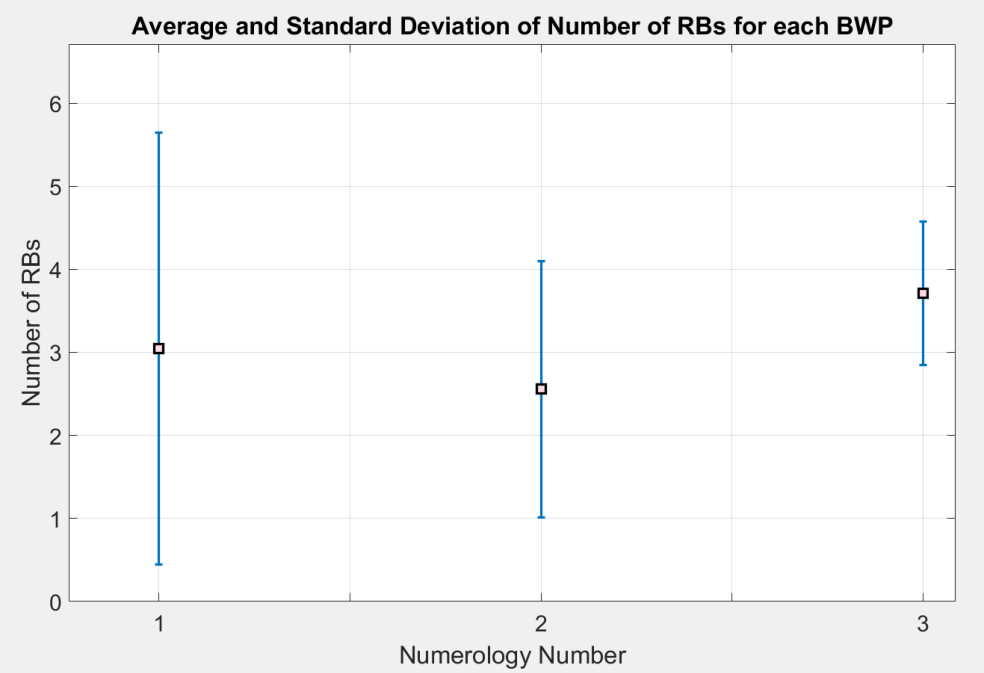

Figure 4.5: Average and standard deviation of the number of RBs for each numerology

Figure 4.5 displays the average and standard deviation of the number of RBs for each numerology. The average number of RBs allocated to 1^{st}, 2^{nd}, and 3^{rd} numerologies are 3.04, 2.55, and 3.71, respectively. The standard deviations for 1^{st}, 2^{nd}, and 3^{rd} numerologies are 2.6, 1.54, and 0.86, respectively. The standard deviations imply that

the number of RBs assigned to 3^{rd} numerology varies less than the other numerologies. It should be noted that the optimum number of RBs allocated to 1^{st}, 2^{nd}, and 3^{rd} numerologies were found as 1, 1, and 6, respectively, in the previous Chapter. Given that the maximum carrier bandwidth allows for a maximum of 23 RBs of 1^{st} numerology, the average summation of RBs in the example scenario is calculated as 22.98.

The locations of VBSs and DPs are generated randomly by AMPL at the beginning, while the locations of BSs remain fixed. In the NSGA algorithm, the locations of BSs, VBSs, and DPs remain the same for all scenarios. Therefore, it is necessary to investigate the distances among BS, VBS, and DP on a map. Figure (4.6) displays the locations of BSs, VBSs, and DPs, represented by blue, red, and green dots, respectively. It is worth noting that the algorithm finds the nearest source to a DP and the nearest BS to a VBS.

In this section, we discuss the results obtained from the NSGA algorithm, which indicate that the nearest source is only sometimes optimal in a network that employs VBSs as out-band IAB nodes. As can be observed in Figure (4.6), some DPs are closer to a VBS than a BS. However, the close VBSs are far from the BSs, which can lead

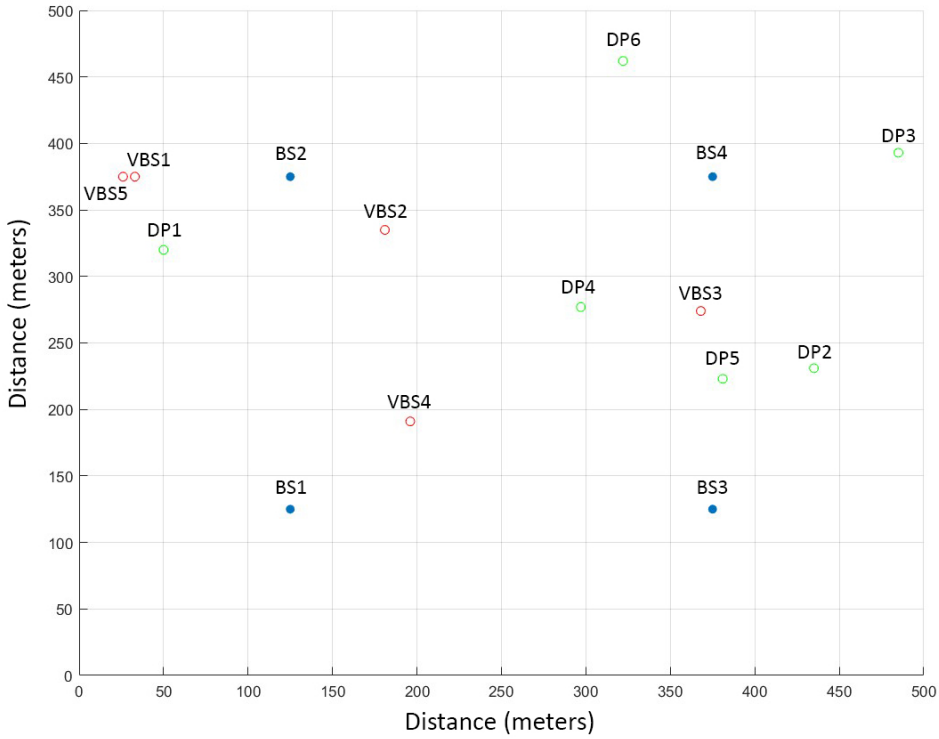

Figure 4.6: BS, VBS, and DP locations that are utilised in the MILP optimisation and the NSGA

to suboptimal results. This situation can be worse in cases where the DP is located between a BS and a VBS, but it is far from the BS by δ, where δ represents the minimum possible distance. Figure (4.7) illustrates one of the worst-case scenarios where the BS is the data provider, and the VBS is closer to the DP. In such cases, the data must flow from the BS to the VBS and then from the VBS to the DP, leading to a waste of resources.

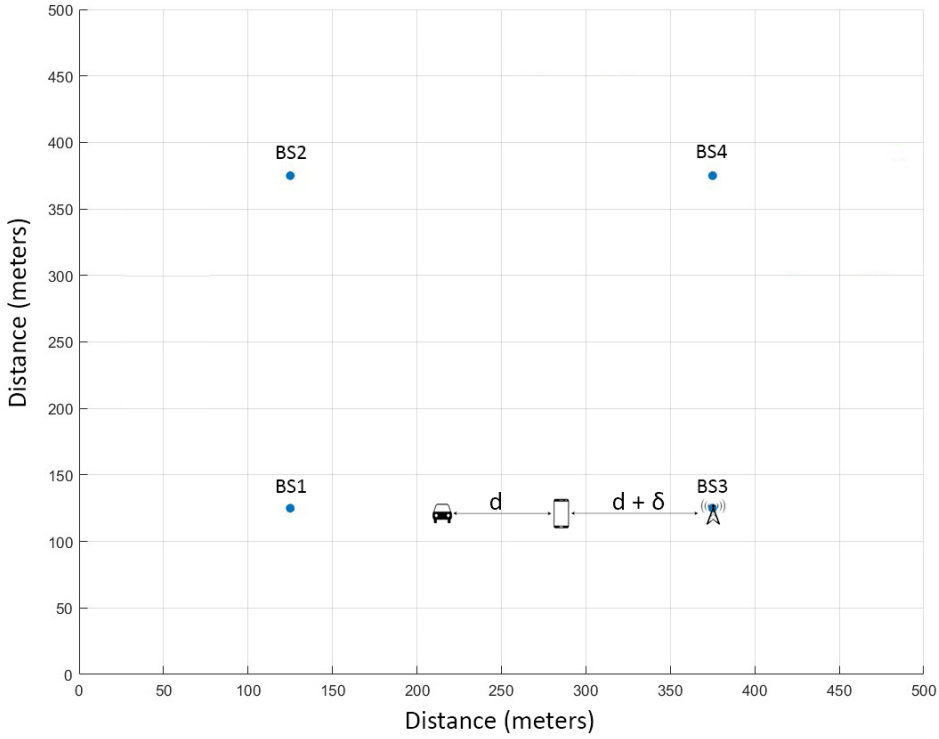

Figure 4.7: One of the possible worst-case scenarios for the NSGA

The NSGA generated the 1 million chromosomes in slightly more than 75 minutes; that means each group provided a result in an average of 45 seconds. However, despite its speed and performance, it is evident that a new algorithm is necessary to improve the results in terms of transmit power consumption. Therefore, we developed the Total Random GA (TRGA).

4.2 Total Random GA (TRGA)

The NSGA has two main advantages for the optimization problem at hand. Firstly, it enables a shortened chromosome size by not including the Source-DP pairing information as a variable. As a result, the dimensionality of the main association variable

is reduced, leading to a significant reduction in the total number of possible outcomes, thus avoiding the curse of dimensionality. Secondly, the NSGA increases the number of valid initial chromosomes by pairing DPs with their nearest source. This approach ensures that even a small amount of transmit power is sufficient for a DP to establish a connection, resulting in more valid initial chromosomes. In contrast, the TRGA algorithm yields an average of only 0.13% valid chromosomes, compared to 0.36% with a maximum of 0.52% in a group with NSGA. The power allocation remains the same for both algorithms, where URLLC and mMTC DPs have a default power of 0.3 mW, and eMBB DPs have randomly allocated power between 0.1 to 50 mW.

Although the NSGA algorithm works fast, the trade-off between speed and accuracy must be considered to obtain results closer to the optimum. Therefore, we developed the TRGA algorithm, which balances speed and accuracy while achieving comparable results to the NSGA.

Just like the NSGA, we embedded the numerology information into the RBs; thus, this information is given at the beginning of the chromosome. Hence, the main optimisation variable is three-dimensional in the TRGA; y^r_{sd}=1, if DP 'd' is served by source 's' using and RB 'r'. The TRGA randomly creates a 3-dimensional power matrix from a source to each DP by utilizing an RB that is shown in the p^r_{sd} matrix. Each RB that uses different numerology has different bandwidth, and the numerology information of the RBs is demonstrated in the BWP allocation information.

Like the NSGA, the TRGA also incorporates the numerology information into the RBs, provided at the beginning of the chromosome. It is worth noting that each RB using a different numerology has different bandwidth, and the BWP allocation information represents the numerology information of the RBs. Since we consider user association as well, the primary optimisation variable in the TRGA becomes three-dimensional, where ysd^r equals 1 if the DP 'd' is served by the source 's' using RB 'r'. Therefore, the TRGA generates a 3-dimensional power matrix randomly p^r_{sd}, which denotes the downlink transmit power; it equals a real number between p_{min} and p_{max} when the DP 'd' is served by the source 's' utilising the RB 'r', otherwise, it is equal to zero.

4.2.1 Initialization

This algorithm generates the first generation of chromosomes using a similar method as presented in the NSGA. The first 23 genes of the chromosomes are reserved for binary BWP allocation information. However, the second part of the chromosome presents the power allocation as a three-dimensional matrix. The second part includes a number of genes equal to the product of the total number of sources, the number of DPs, and the maximum available number of RBs. For example, if the algorithm has 4 BSs, 5 VBSs, 6 DPs, and 23 maximum available RBs, the number of genes in the second part would be $((4+5)\times 6\times 23) = 1242$. Thus, including the BWP information, the total number of genes in one chromosome becomes 1265.

$$\sum_{s\in S}\sum_{r\in R} y_{sd}^{r} \leq 1, \quad \forall\ d \in D \tag{4.10}$$

$$\sum_{r\in R} y_{d}^{r} \leq 1, \quad \forall\ d \in D \tag{4.11}$$

The constraints (4.10) and (4.11) indicate that each DP can select at most one RB from one source, and each DP can utilise a maximum of one RB. In both the NSGA and TRGA algorithms, the relationship between RBs and numerology is included at the beginning of the chromosome. This means that there is no need to explicitly state a constraint that each RB can only belong to one numerology, as this is already accounted for in the chromosome. The constraints (4.10) and (4.11) are used to increase the overall number of valid chromosomes in the TRGA algorithm.

4.2.2 Evaluation

The TRGA evaluates the initial chromosomes for each DP and removes any chromosomes that do not satisfy their data rate or delay requirements. The allocated data rate is calculated using the transmit power p_{sd}^{r}, and BWP allocation information (RB-numerology association) are used to calculate SINR and data rate for each DP. It is worth noting that each DP is unrestricted to select any numerology as long as their requirements are satisfied. Therefore, in both heuristic algorithms, the GA only checks the DPs that require higher numerologies. Once the invalid chromosomes are

removed, the remaining chromosomes form the initial generation. The data rate and delay constraints are satisfied for all DPs in a valid generation acquired from the initial chromosomes.

The backhaul power is also calculated when a DP uses a VBS as a source, and a distance matrix is employed to establish communication with the nearest BS-VBS pair. Since the total number of BSs is set to 4, this action only requires a little computational power. Moreover, implementing a random process for BS-VBS pairing would cause more invalid chromosomes due to power allocation constraints. The same formula is used to calculate backhaul power in the TRGA, as given in Eq (4.8).

4.2.3 Sorting

The TRGA tends to keep the best-performing chromosomes and eliminates the worst-performing chromosomes to reproduce better chromosomes in each generation. First, the chromosomes are sorted considering their total transmit power to identify the worst and best-performing ones. Then, the algorithm scraps the worst-performing chromosomes by considering a pre-determined maximum number of chromosomes limit. The identical limit is employed in the NSGA, as well. This limit is consistently applied in both TRGA and NSGA to ensure statistical consistency of the results.

4.2.4 Selection

At this stage of the algorithm, a random selection process, instead of selecting the best chromosomes, is implemented for crossover and mutation. A pair of chromosomes are selected randomly for the crossover, and a chromosome is selected randomly for the mutation. However, parallel to NSGA, the TRGA can utilize crossover when the paired chromosomes have the same BWP deployment.

4.2.5 Crossover

The TRGA also employs two crossover methods, single-point and bit-flipping, similar to the NSGA. However, the difference lies in the selection process, which aims to randomly select the best-performing genes from poor-performing chromosomes to improve the overall performance of the algorithm. This random selection process requires more generations to reach the optimal solution optimisation.

The crossover rate determines the number of randomly selected and paired chromosomes for the crossover operation in each generation. However, this rate only indicates the total attempts of the crossover operation, not the number of successful crossovers. A generation can be generated without any chromosomes undergoing a crossover operation. Specifically, in the TRGA, this can occur when paired chromosomes have different BWP deployments, rendering the crossover operation infeasible. In such cases, the initial and extended generations would be identical.

4.2.6 Mutation

The same mutation operator is employed to randomly selected invalid chromosomes. The mutation rate also defines the total number of attempts to implement mutation operation. Algorithm 2 outlines the steps involved in the TRGA.

Algorithm 2 The Total Random Genetic Algorithm

Input: W_{total}, DP requirements, min/max transmit power, initial generation size (i), crossover rate (c), mutation rate (m), number of GA iterations (j)

Output: BWP allocation (y^{rn}), RB (y^r_{sd}) and power allocation among DPs (p^r_{sd}) which can be provided by any Source

```
Initialize (i) chromosomes randomly
[Constraint Handling]
for each chromosome do
    Calculate data rates and numerology allocations
    if valid data rates and numerology for all DPs then
        Mark chromosome as valid
    else
        Remove the chromosome
    for j ≥ 0 do
        Select parent chromosomes for crossover and mutation randomly
        Perform crossover
        Apply mutation to a pair of chromosomes if BWP allocations match
        Remove duplicate chromosomes
        Sort chromosomes based on transmit power
        Eliminate excess chromosomes if needed
        j = j − 1
```

4.2.7 Results

The TRGA aims to randomly select the best-performing genes from poorly-performing chromosomes, resulting in a selection process that requires more generations to reach an optimal solution. However, this is a worthwhile trade-off as the best genes will eventually emerge, as is observed in nature. The input parameters for the TRGA are presented in Table (4.2).

Table 4.2: The TRGA input parameters

Description	Input
Number of chromosomes in each group	10000
Total number of groups (i)	100
Maximum # of chromosomes that have been kept in each generation	75
Crossover rate (c)	75
Mutation rate (m)	25
Number of new generations (j)	15

The TRGA and NSGA utilize the same number of chromosomes for each group, which is set to 10000 chromosomes grouped according to their numerical production order. The TRGA's average percentage of successful chromosomes is 0.13%, with a maximum of 0.23% in a group, after 100 iterations. This average is lower than the NSGA, which is expected due to the TRGA's random source-DP pairing process. The random pairing of distant sources in the TRGA results in a larger amount of transmit power needed to ensure a valid chromosome than the NSGA's utilization of the nearest source. As a result, the average successful chromosomes of the TRGA decreased by a factor of 2.7 compared to the NSGA.

The TRGA algorithm employs a larger number of genes in each chromosome, which increases the time required for evaluating each chromosome. Additionally, the TRGA also requires more iterations than the NSGA. The TRGA generated one million chromosomes in approximately 7 hours and 50 minutes, resulting in an average processing time of 4 minutes and 42 seconds per group. This computational time of the TRGA is 6.2 times longer than that of the NSGA.

The results obtained from TRGA are presented in Figure (4.8), which demonstrates the average, standard deviation, best performing, and minimum total transmit power. Similar to Figure (4.4) presented earlier, the average and standard deviation are calculated from 100 runs. Furthermore, Figure (4.8) also illustrates the best result that attains the minimum total transmit power and the best-performing result that achieves the highest difference between the first and last generations. The evaluation is carried out on Sc1, which consists of 6 DPs and 5 VBSs.

Despite its drawbacks, the TRGA exhibits superior downlink transmit power performance and produces better results in terms of total transmit power, standard deviation, and the best output that yields the minimum total transmit power. The average total

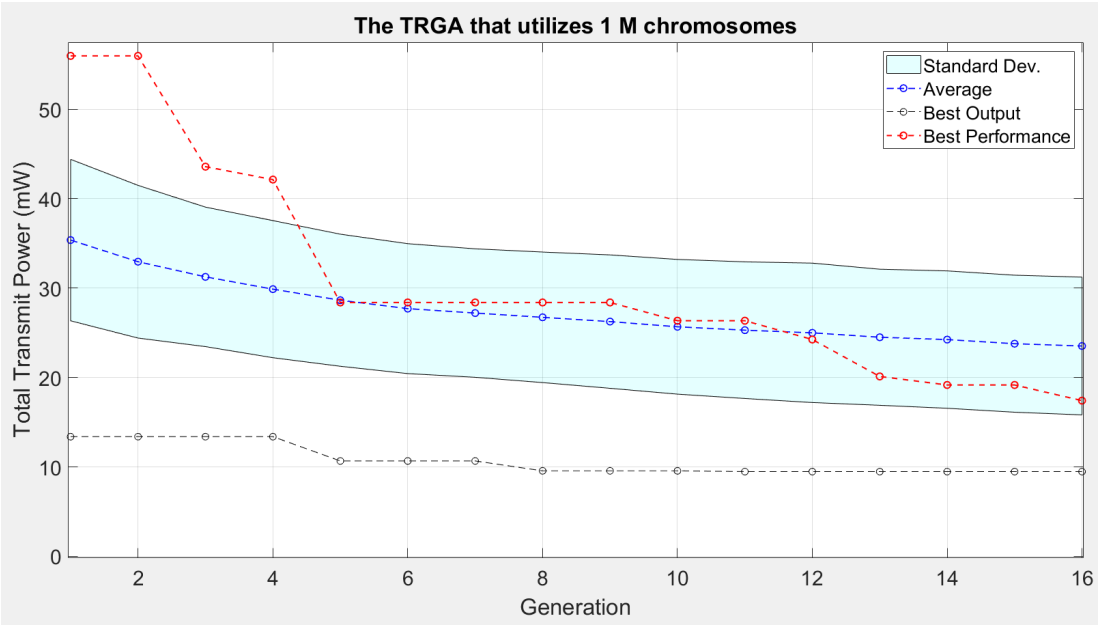

Figure 4.8: The TRGA output that utilizes 100 groups.

transmit power is reduced from 24.35mW to 23.52mW in the TRGA, representing a 3.4% improvement. The standard deviation is also improved by 11%; since the standard deviation is a quantity that shows how much differs the individuals from the arithmetic mean of the group, reducing the standard deviation means getting better results in our problem. The best output of 100 iterations is 9.46mW, which is closer to the optimal result of 8.21mW.

Despite the TRGA's ability to produce superior results, the NSGA remains the preferred algorithm for our optimization problem due to its shorter computational time. As the number of users, RBs, or sources increases, the use of TRGA becomes impractical. Therefore, NSGA is a more suitable option for practical implementation in scenarios with large-scale networks.

4.2.8 Comparison of Optimisation Algorithms

In this subsection, we compare the output of the three above-given optimisation algorithms to assess their performance in addressing the joint optimisation problem. The presented analysis offers insights into the effectiveness of each algorithm and its respective outcomes, as illustrated in Fig 4.9 and Fig 4.10. In both figures, the red line represents the optimal solution obtained from the MILP optimisation. The output of the MILP optimisation yields precise and optimal results, serving as a benchmark for comparison.

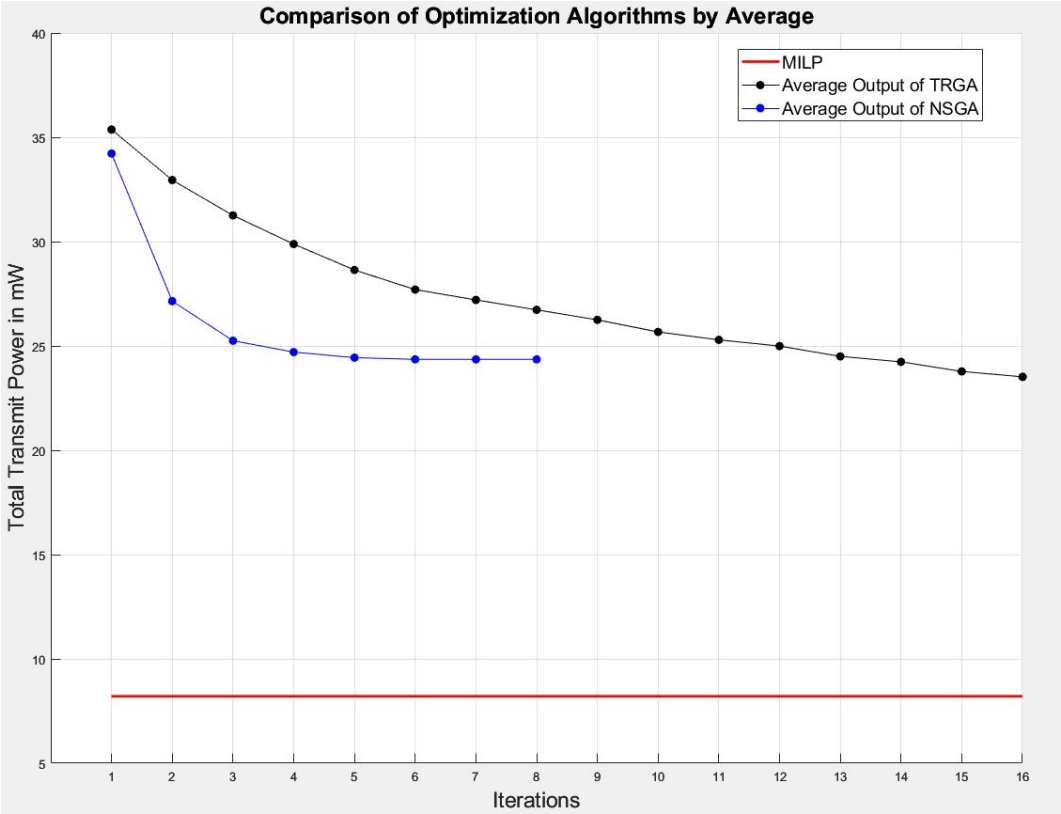

Figure 4.9: Comparison of Optimisation Algorithms by Average

In Fig 4.9, the black curve illustrates the results obtained from the TRGA. It's worth noting that both algorithms' outputs are presented in terms of averages before. Therefore, Fig 4.9 displays the average outcome across these 100 generations conducted over sixteen iterations. This approach provides a basis for evaluating the algorithm's convergence and performance. Also, the blue curve corresponds to the outcomes generated by the NSGA. Despite its comparatively lower iteration count of seven, the NSGA demonstrates a noteworthy trend toward optimal results, highlighting its efficiency in yielding high-quality solutions.

The next figure, labelled as Fig 4.10, shows the optimal outcomes achieved through 100 iterations of the optimisation process. In this representation, "best output" refers to the most favourable results obtained from these 100 iterations. The figure provides a clear visualisation of the performances achieved by the optimisation algorithms when considering their best-performing outputs throughout these iterations.

The choice of utilising the NSGA over the TRGA is strategic. While the TRGA may exhibit slightly improved outcomes, this advantage comes at the cost of significantly increased computational time. In contrast, the NSGA, with its faster execution, strikes

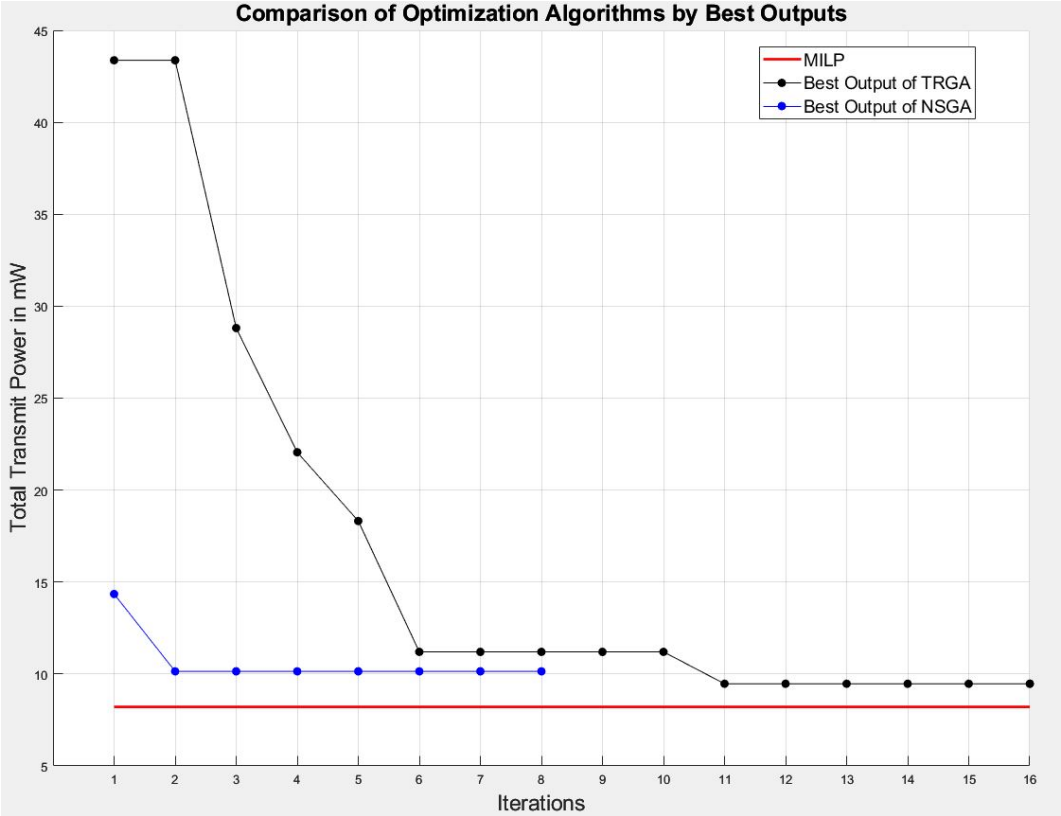

Figure 4.10: Comparison of Optimisation Algorithms by Best Outputs

a balance by delivering slightly worse solutions than TRGA in exchange for a significantly reduced runtime. Given the optimisation problems' constraints, this strategic trade-off makes the NSGA a more efficient choice. The presented results provide valuable insights for selecting an appropriate optimisation approach based on desired trade-offs between solution quality and computational effort.

4.3 NP-Hard Problems

In the heuristics chapter of this thesis, we have conducted experiments using six DPs to validate the outputs of our proposed optimisation algorithms. We compared the outputs of heuristics algorithms with MILP optimisation. After validating the results, instead of increasing the number of DPs proportionally or utilising the same scenarios as in the MILP optimisation problem, we aimed to tackle an NP-hard problem that MILP could not solve. This approach allowed us to test the scalability and effectiveness of our proposed algorithms in solving more complex problems that require significant computational power and time.

This section considers a scenario consisting of 20 DPs, comprising 2 eMBB DPs, 2

URLLC DPs, and 16 mMTC DPs. The data rate requirements of eMBB DPs are set to a range of 1-1.5 Mbps, as previously described in Chapter 3.4.3, while the requirements of the remaining DPs remain unchanged. Despite reducing the data rate requirements of the eMBB DPs, the MILP solver fails to solve the problem, regardless of how low the user requirements are.

In order to determine the appropriate algorithm for NP-hard problems, the total probabilities of the algorithms must be evaluated. For instance, consider a scenario where each user can have one RB and the corresponding power value of that RB can be only 1 mW. If there are 20 DPs located in this scenario, the number of possible outcomes is estimated to be approximately $\approx 9.5 \times 10^{26}$ when the NSGA is employed. On the other hand, the TRGA would have $\approx 8.5 \times 10^{45}$ possible outcomes when a fixed 1mW transmit power is considered for the 20 DPs scenario. It is important to note that the actual outcome of the algorithms is practically infinite, considering the transmit power is a real number. However, these examples provide an indication of the computational expenses of the algorithms. Consequently, we chose to employ the NSGA algorithm for NP-hard problems, which results in an increased number of valid chromosomes at the cost of sacrificing optimality in terms of transmit power.

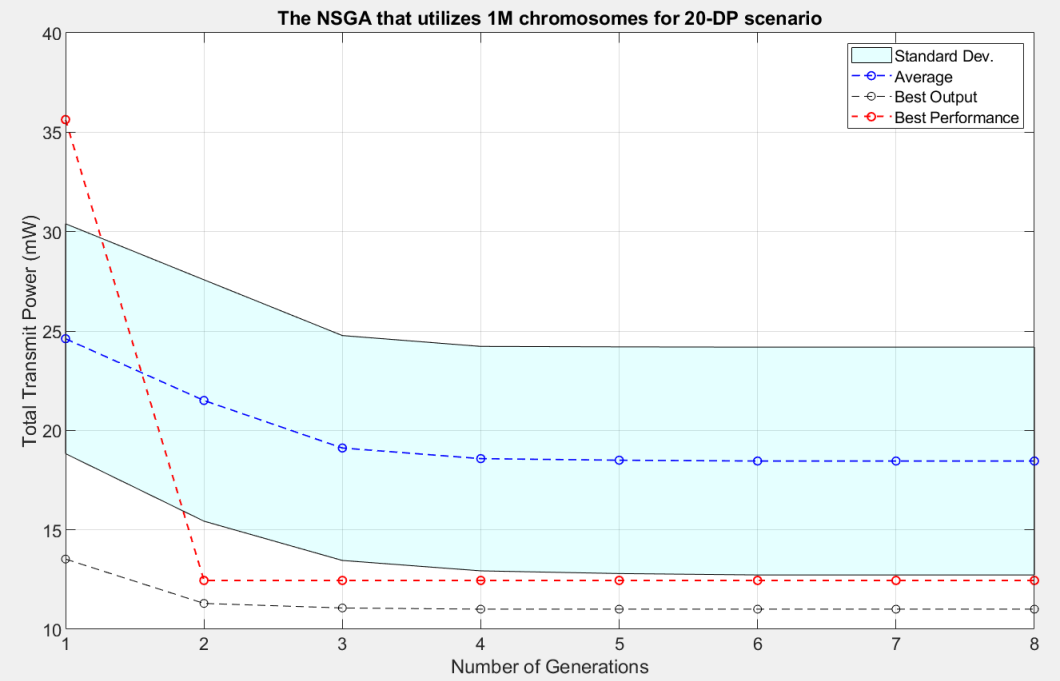

Figure 4.11: The NSGA that utilizes 1M chromosomes for the 20-DP scenario.

In this specific example, the NSGA produced acceptable outputs given in Fig. 4.11. The presentation of the figure is the same as before; the red line shows the generation

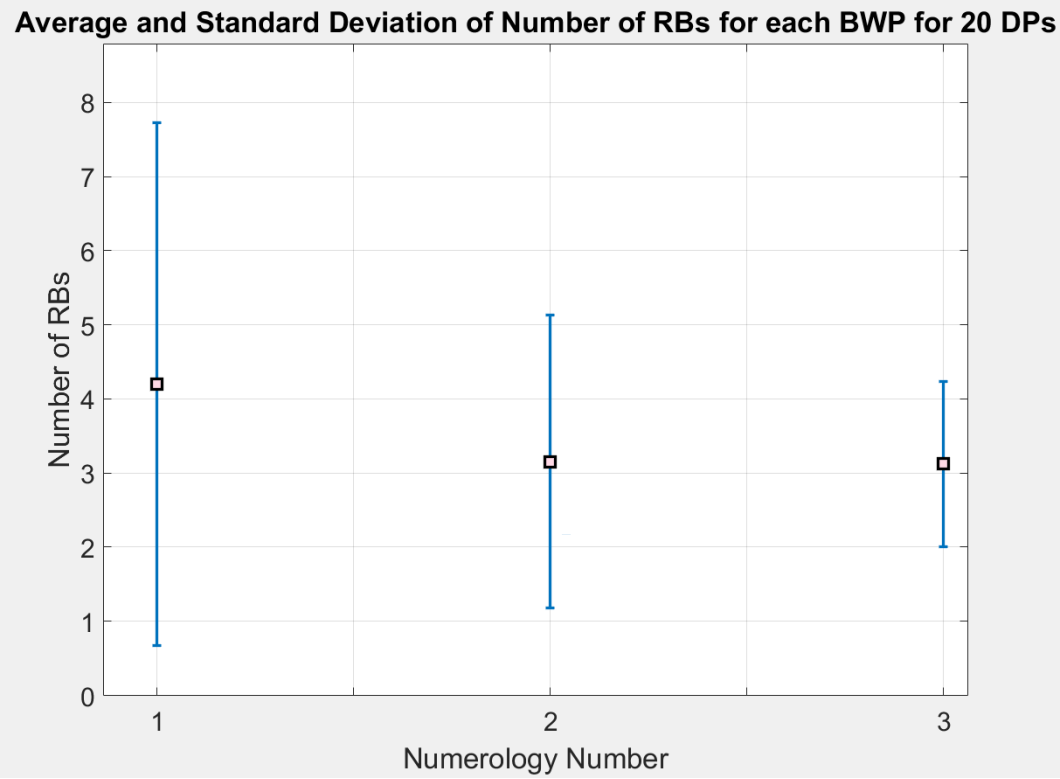

Figure 4.12: Average and standard deviation of the number of RBs for each numerology for 20-DP scenario.

that delivers the best performance considering its first and last generation. The blue line shows the average of the 100 results. The NSGA generally reaches the optimum output after two iterations, so the outputs do not significantly improve after the third generation. Thus, the number of generations could be reduced to achieve even faster results. The average total transmit power of 100 groups is 18.45 mW, with a 5.72 standard deviation, and the best result is 11 mW.

The results of the bandwidth allocation among BWPs are presented in Fig 4.12. The average number of RBs allocated to the 1^{st}, 2^{nd}, and 3^{rd} numerologies are 4.19, 3.15, and 3.12, respectively. The standard deviations for the 1^{st}, 2^{nd}, and 3^{rd} numerologies are 3.53, 1.97, and 1.11, respectively, indicating a relatively high level of variability in the allocation. The increase in the allocation of RBs for the 1^{st} numerology and decrease for the 3^{rd} numerology can be observed. It should be noted that the optimal number of RBs could not be found in the previous chapter for the 20-DP scenario. Since the validation is done with 6-DP scenarios, the solution presented in Fig. 4.12 can be considered a suboptimal solution for the resource allocation and routing problem.

To assess the algorithm's performance in challenging scenarios, we consider a problem

consisting of 25 DPs, including 3 eMBB DPs, 3 URLLC DPs, and 19 mMTC DPs. We use the NSGA algorithm to solve this problem and obtain an average successful chromosome rate of 2.04% over 100 iterations. The results for the 25-DP scenario are presented in Fig. 4.13. The average total transmit power of 100 solutions is 29.41 mW, with a standard deviation of 11.07 mW, and the best solution has a total transmit power of 13.21 mW. These results show the algorithm's effectiveness in tackling complex and challenging optimisation problems involving a large number of DPs.

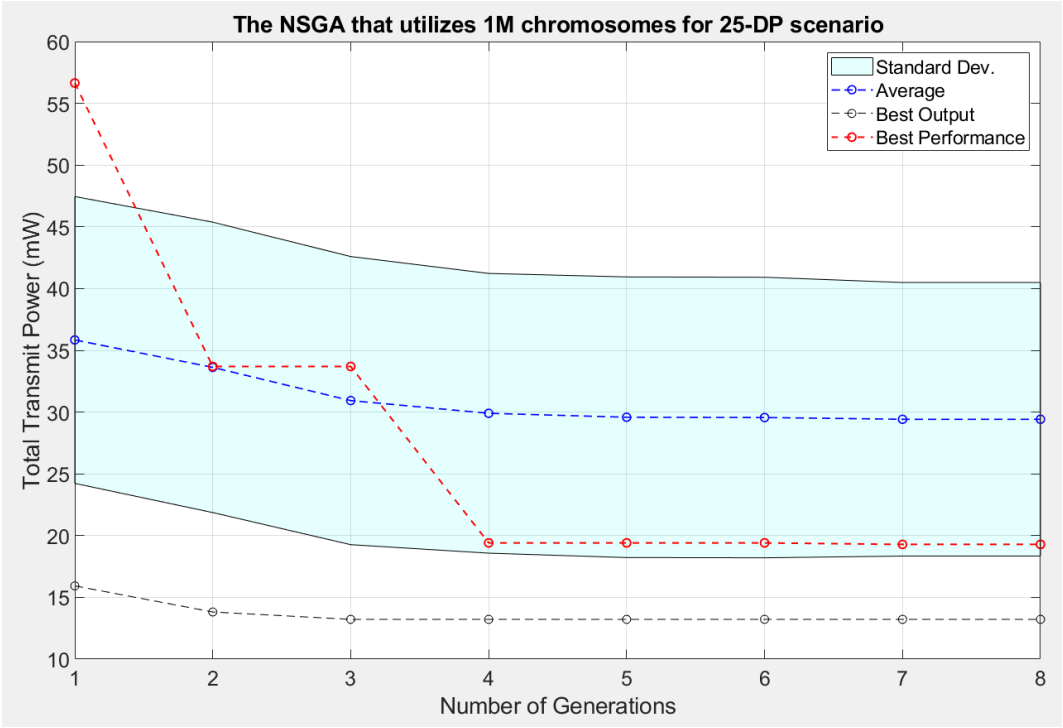

Figure 4.13: The NSGA that utilizes 1M chromosomes for the 25-DP scenario.

The results of the bandwidth allocation among BWPs are presented in Fig 4.14 for 25-DP optimisation problem. The average number of RBs allocated to the 1^{st}, 2^{nd}, and 3^{rd} numerologies are 4.22, 3.15, and 3.04, respectively. The standard deviations for the 1^{st}, 2^{nd}, and 3^{rd} numerologies are 3.78, 2.1, and 1.25, respectively, indicating a slightly high level of variability in the allocation compared to 20-DP scenario. The slight increase in the allocation of RBs for the 1^{st} numerology is observed. The optimal number of RBs is not available in the previous chapter for the 25-DP scenario, as well. Therefore, solution presented in Fig. 4.14 can be considered a suboptimal solution for the resource allocation and routing problem for 25 DPs.

The results of the bandwidth allocation among BWPs for the 25-DP optimisation problem are illustrated in Fig. 4.14. The average number of RBs allocated to the 1^{st},

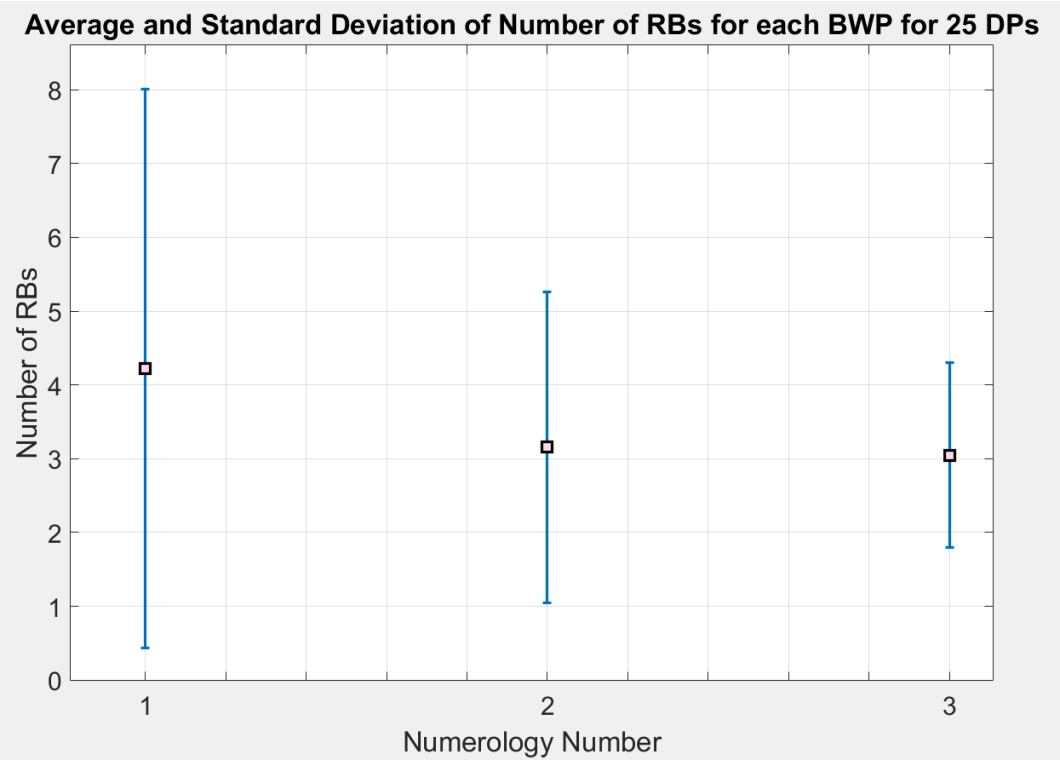

Figure 4.14: Average and standard deviation of the number of RBs for each numerology for 25-DP scenario.

2^{nd}, and 3^{rd} numerologies are 4.22, 3.15, and 3.04, respectively, indicating a slightly higher level of allocation for the 1^{st} numerology compared to the 20-DP scenario. The standard deviations for the 1^{st}, 2^{nd}, and 3^{rd} numerologies are 3.78, 2.1, and 1.25, respectively, which suggests narrowly high variability in the allocation of RBs. It should be noted that the optimal number of RBs is not available in the previous chapter for the 25-DP scenario. Therefore, the solution presented in Fig. 4.14 can be considered a suboptimal solution for the resource allocation and routing problem for 25 DPs.

4.4 Conclusions

Based on the findings of this chapter, it appears that selecting the nearest source may not always lead to optimal results in the given problem due to the location of DPs. Furthermore, the results obtained from the TRGA demonstrate that introducing more randomness into the algorithm can lead to the identification of individual high-performing genes within a chromosome, even if the overall transmit power of that chromosome is high. Therefore, increasing the level of randomness in the TRGA may

lead to improved outcomes. However, both the mutation and crossover operators in both algorithms are effective at identifying individual high-performing genes.

For example, the outputs generated by our proposed hybrid heuristic algorithm and those produced by the MILP approach, which provides optimal results are compared. This comparison allowed us to assess the proximity of the hybrid heuristic algorithm's outputs to the optimal ones. Our analysis demonstrated that the hybrid heuristic algorithm could achieve a total transmit power as close as 87% to the optimal solution.

Although its proximity to the optimum, the TRGA is not practical to use due to its computational expense. As demonstrated in the binary example presented earlier, the number of possible outcomes for the TRGA is approximately $\approx 9 \times 10^{18}$ times higher than that of the NSGA for the 20-DP problem. Furthermore, the total number of possible outcomes for the problem is infinite since a real number is assigned for the transmit power. Therefore, although the TRGA can achieve near-optimal results, given the enormous number of possible outcomes, it is more reasonable to use the NSGA to achieve acceptable results.

On the other hand, considering an infinite number of possibilities, both GA can produce near-optimal solutions by producing 1 million chromosomes. These outcomes indicate the effectiveness of the algorithms.

Considering the advantages and disadvantages of the algorithms discussed in this chapter, the NSGA was chosen for solving the NP-hard problems. As mentioned earlier in this chapter, speed is prioritised over maximum accuracy and optimality.

After carefully weighing the advantages and disadvantages of the algorithms discussed in this chapter, the NSGA was chosen as the primary algorithm for solving NP-hard problems. The decision is based on the need for speed, which was prioritised over maximum accuracy and optimality. The NSGA is able to provide acceptable results in a reasonable amount of time, making it a practical choice for the resource allocation and routing problem.

Genetic algorithms have proven to be effective in solving complex optimisation problems, but there is a need for faster algorithms that can provide better approximations of the optimum solution. Machine Learning (ML) can be employed to address this issue by leveraging the data generated by GAs and heuristics. Even without using the

data, ML can learn by itself how to behave in a specified environment. By training an ML model, we can predict the optimal solution for a given set of input parameters, resulting in quicker and more accurate problem-solving. Furthermore, ML can help discover patterns and relationships in the data, which can be used to develop new and improved algorithms for solving the problem. In conclusion, integrating ML into the optimisation problem helps to achieve results in a shorter amount of time and better near-optimal results, making it a valuable tool for solving complex optimisation problems.

Chapter 5

Machine Learning Model

Artificial Intelligence (AI) which covers ML, is defined in [184] as "all techniques that enable machines to mimic human intelligence". The human learning system inspires AI; both have neurons, and the employed neurons develop stronger connections. An artificial neuron consists of four mathematical elements; incoming connections, outgoing connections, an activation value assigned to each neuron, and a weight value showing connection strength between neurons where a combination of the artificial neurons creates the Artificial Neural Network (ANN) [185].

ML can handle many optimisation problems; for example, it can overcome the curse of dimensionality, which is a significant challenge in optimization problems [186]. ML algorithms have been extensively employed in diverse areas such as speech recognition, robotic tasks, and radio resource allocation, as illustrated in Chapter 2 and further exemplified in this current chapter. Furthermore, ML is becoming increasingly popular and accessible to more people and industries with the increasing available data, computing power and storage. ML is a powerful tool that enables computer systems to learn with different methods, which will be elaborated on in this section, and then either take actions without being explicitly programmed to do so or provide predictions.

In the context of the thesis, it is crucial to thoroughly understand the applications of ML algorithms in 5G-NR and vehicular networks. Therefore, we begin by explaining the concept of ML and its fundamentals. For example, ML has recently been employed to enhance performance and efficiency in 5G-NR networks [65], [72]. Specifically,

RL has emerged as a promising technique to optimize resource allocation in 5G-NR networks. Subsequently, in this chapter, our focus will be on our proposed DRL-based method for optimizing user and power association, considering pre-allocated BWPs for different numerologies. Finally, we will provide detailed explanations of the problem formulation, the design of the DRL algorithm, and the performance evaluation of our proposed method.

5.1 An Overview of Machine Learning

The learning of a machine process involves several steps, including data collection, pre-processing, model selection, model training, model evaluation, and model deployment [187]. Data collection involves gathering data from diverse sources such as databases, sensors, and online sources. Data pre-processing involves cleaning and preparing the data for analysis, which may include data normalization, feature selection, and handling missing values.

ML can be broadly categorized into two main types based on the characteristics of neurons and the type of learning: (1) connection type of neurons, which refers to the architecture and connectivity of neural networks, and (2) learning type, which encompasses the algorithms and techniques used for learning from data. In the literature, three main types of ML are commonly recognized: supervised, unsupervised, and reinforcement learning [188]. However, there are more than 30 connection types available, such as recurrent neural networks, feedforward neural networks, generative adversarial networks, and LSTM, as documented in [185]. During the model selection process, the most suitable ML algorithm or model is chosen to address a given problem effectively. In the field of ML, the four main types of learning paradigms are as follows:

- Supervised learning employs labelled data to train a model to predict an output variable based on one or more input variables [147]. Common supervised learning algorithms include but are not limited to linear and logistic regression, random forests, and artificial neural networks. However, in this type of ML, finding labelled data might be challenging.
- Unsupervised learning employs unlabeled data to find patterns or relations in the raw data where the aim is to find hidden patterns or clusters in the data without

any prior knowledge of the output variable [189]. Some unsupervised learning algorithms are called Naive Bayes classifiers, and K-means clustering [190].

- Reinforcement Learning involves learning by trial and error to find the optimal action or sequence of actions to take in a given environment to maximize a reward as a consequence of the corresponding action [191]. RL is often used in robotics, game-playing, and control systems.

5.1.1 Supervised Learning

The process of building a supervised learning algorithm involves collecting a labelled dataset which will be used for training the classification and regression models. During training, the algorithm is demonstrated labelled input data and produces output scores as a vector for each category [192]. The desired category typically does not have the highest score initially, as the algorithm's weights, which are adjustable parameters that define its input-output function, are randomly initialized [140]. Then the supervised learning algorithm calculates the error between the output and the desired or expected output. Then it adjusts the weights to minimize this error. The algorithm calculates and adjusts each weight, indicating how the error would change if a small amount adjusted the weight. Finally, the weight vector is updated with corresponding adjustments of weights to reduce the error. This process is repeated until the algorithm's performance converges to an acceptable level.

Supervised learning algorithms, such as convolutional neural networks (CNNs), are commonly used in computer vision studies like image classification (GoogLeNet)[193], (Inception) [194], speech recognition [141], and video classification [142].

5.1.2 Unsupervised Learning

Supervision with labelled data is commonly used in many visual recognition and classification tasks. However, generating or acquiring labels for large datasets that can be useful can be hard and costly. In unsupervised learning, where the algorithm receives inputs but lacks supervised target outputs or rewards from the environment, the absence of feedback may seem puzzling regarding what the algorithm could learn [195]. An unsupervised learning algorithm is developed to build meaningful representations of the data, decision-making or estimating future outcomes. Unsupervised

learning can be seen as identifying patterns in the data beyond pure unstructured noise, such as clustering and dimensionality reduction, which are traditional examples of unsupervised learning [195].

In such cases, unsupervised learning methods provide significant success. This success can be attributed to various factors, including the availability of abundant unlabeled data, advancements in modelling techniques, diverse choices of optimization algorithms, and, notably, the integration of domain-specific knowledge into structured models [196]. Unsupervised methods have been utilized in diverse domains, including but not limited to speech processing, tumour characterization [197], and depth estimation [198]. Moreover, unsupervised learning methods have demonstrated notable success in recent natural language processing research [196].

In some scenarios, a combination of supervised and unsupervised learning techniques can be employed as a hybrid approach, known as semi-supervised learning. Semi-supervised machine learning represents a synergistic combination of supervised and unsupervised machine learning approaches, making it a potentially valuable tool in domains where obtaining labeled data is laborious or impractical, and where a significant portion of data remains unlabeled [190]. Semi-supervised learning is also utilized in the fields of speech recognition [141], and image classification [199]. For example, the authors [141] present results from using large-scale pre-trained automatic speech recognition models, trained on diverse unlabelled datasets with millions of hours of audio, and show that fine-tuning such models significantly increases data efficiency and achieves state-of-the-art performance on automatic speech recognition tasks even with limited labelled data.

5.1.3 Reinforcement Learning

As the utilization of RL constitutes a fundamental aspect of this thesis, we provide a more comprehensive and detailed explanation of RL to facilitate a better understanding of its principles and concepts. RL is a ML technique used for control problems, where the objective is to select actions to achieve a desired goal. The goal of RL is to develop an intelligent controller that can make optimal decisions in different situations based on learned experiences, rather than being explicitly programmed by a human designer as in traditional control methods [148]. RL is well-suited for scenarios

where extensive experimentation can be conducted quickly and inexpensively, often through simulations, as it deals with complex systems and overall goal-oriented behaviors rather than individual component tasks [148]. Unlike other common ML tasks such as clustering or classification, RL is unique in that it aims to achieve a measurable goal without explicit labeling or scoring of individual actions [148]. This necessitates an iterative process of trial and error, where different actions are tried in various situations, and the learning occurs from these experiences to determine the optimal action in any given situation.

An RL agent interacts with the environment and learns to modify its behavior based on the observed consequences of its actions and the rewards it receives. In RL, the state is considered a sufficient statistic of the environment, containing all the necessary information for the agent to make optimal decisions, which may include parts of the agent itself [186]. Let S and A represent a discrete set of states and a discrete set of actions, respectively. The agent, controlled by an RL algorithm, observes the state of the environment $s(t)$ at a given time step t. The agent selects an action $a(t)$ based on a policy π, and this action impacts the environment by transitioning it from the current state $s(t)$ to the next state $s(t+1)$. Fig. 5.1 illustrates agent-environment interaction in RL [148].

In RL, the policy serves as a rule for determining the action to be taken in a given situation. The primary objective of RL is to discover an optimal policy. The quality of a policy is determined by the actions taken by the agent and the rewards received in return [148]. The policy $\pi(s, a)$ represents the probability of taking action a for the corresponding state s, where the policy function must meet the following [65]:

$$\sum_{a \in A} \pi(s, a) = 1 \tag{5.1}$$

The objective of the agent is maximising the summation of the reward that is received over time. The agent learns to select actions that lead to maximum reward through trial and error, utilizing a training algorithm that updates the policy based on expected rewards [148]. A training algorithm is utilized to develop an understanding of which actions are effective in different situations and to make better decisions based on experience [148]. The training algorithm updates the policy based on actions that are

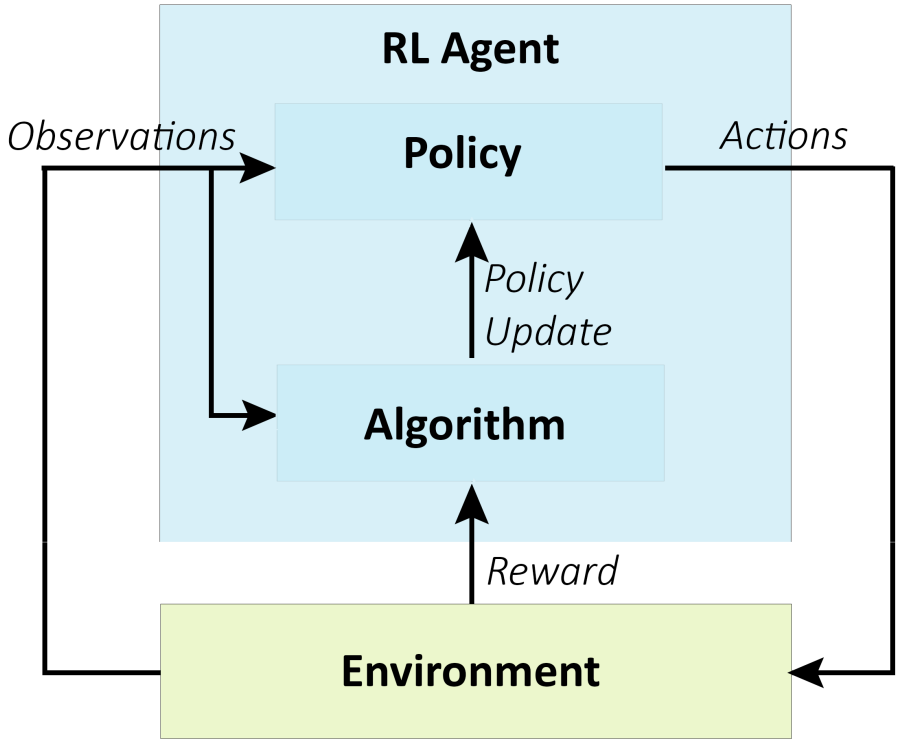

Figure 5.1: Agent-environment interaction in RL [148]

expected to yield higher rewards. Each iteration of the training algorithm, aimed at finding the most efficient approach, is referred to as an episode. During training, the algorithm executes multiple episodes, continually evaluating and improving the policy.

The Q-learning algorithm

The Q-learning algorithm, a widely utilised approach in the field of RL, focuses on learning a state-action function, known as the Quality function, or Q-function [148]. This function estimates the expected reward associated with taking a specific action a in a given state s and following a policy π subsequently [152]. The Q-function for a policy π and a state-action pair (s, a) considering the discounting factor $\gamma \in [0, 1)$ is defined as follows [152]:

$$Q_\pi(s, a) = \mathbb{E}\left[\sum_{t=0}^{\infty} \gamma^t r(s_t, \pi(s_t)) \mid s_0 = s,\ a_0 = a\right] \tag{5.2}$$

In the Q-learning algorithm, the agent begins with no prior knowledge, and the Q matrix is initialized with zeros. In each episode, the algorithm randomly selects an initial state and chooses one action among all possible actions for the current state. The

selected action is then used to transition to the next state. The algorithm calculates the maximum Q value for the next state using the Bellman equation, considering all possible state-action pairs [152]:

$$Q(s_t, a_t) = r_{t+1} + \gamma \max_{a_{t+1}} Q(s_{t+1}, a_{t+1}), \quad \forall s_t, a_t. \tag{5.3}$$

where, $Q(s_t, a_t)$ is the Q-function for state s_t and action a_t, r_{t+1} is the reward that received at time step $t+1$, γ is the discount factor of the future rewards, and $\max_{a_{t+1}}$ denotes the maximum value of all actions a_{t+1} in the next state s_{t+1}.

Q-learning is an effective process when the action-state spaces are relatively small, and a look-up table can be used to update the Q-values [148]. However, it becomes impractical when the state-action space is large, as many states might not be visited, resulting in infrequent updates to the Q-values and slower convergence [148].deep Q-Network (DQN) addresses this issue by combining Q-learning with deep neural networks to approximate the Q-function, enabling more efficient and scalable learning in large state-action spaces.

Markov decision processes

RL can be mathematically described as a Markov decision process (MDP), where the optimal Q-function can be derived using the Bellman equality given in Eq 5.3 [152]. The MDP comprises several crucial components in determining the optimal Q-function. These components include a set of states, an initial state, a set of actions, transition dynamics, which map a state-action pair at time t to the distribution of states at the time $(t + 1)$, a reward function, a discount factor ($\gamma \in [0, 1]$) that determines the weight of given to immediate rewards [186]. In order to obtain discounted future rewards, the lower values of γ, which increase the significance of immediate rewards, can be employed and vice versa.

The ε is a parameter that is responsible for the exploration and exploitation rates of the agent. The ε decay shows the craziness of the agent; at the beginning of the training, the agent does not know the environment; therefore, it takes random actions. However, the more it learns about the environment, it takes actions according to a policy. Hence, the rate of random actions reduces. The policy (π) maps states to a

probability distribution over actions [186]:

$$\pi : \ \mathcal{S} \rightarrow p(\mathcal{A} = a \mid \mathcal{S}) \tag{5.4}$$

When an episode comes to an end, the state is reset, and the sum of rewards accumulated over an episode compose the return, which is shown as summation in Eq 5.5. The aim of RL is to discover an optimal policy, denoted as π^*, that achieves the maximum expected long-term accumulated rewards from all states when the state is reset after each episode of length T [186],[200]:

$$\pi^* = \arg\max_{\pi} \mathbb{E}\left[\sum_{t=0}^{T-1} \gamma^t r_{t+1} | \pi\right] \tag{5.5}$$

Note that the Bellman equation defined in Eq 5.3 is the recursive form of Eq 5.5.

In conclusion, the modeling of the environment as a MDP in RL [46] results in the actions and rewards becoming Markov processes. Each action is associated with a reward, and the agent's objective is to maximize the cumulative reward throughout the RL process.

5.1.4 Deep Learning

Due to its unique characteristics and significant impact on various applications, deep learning merits a dedicated chapter in this context. In the formal parlance of ML, a network with more than three hidden layers is often referred to as a "deep" network [188]. This terminology is applicable to various learning paradigms, such as supervised learning, unsupervised learning, and RL, where the addition of multiple hidden layers in the network architecture is commonly referred to as "deep" variants of these respective paradigms. For instance, in the case of RL, the usage of deep neural network is called as "deep reinforcement learning" [143].

In the classification of ML algorithms, a distinction is made between shallow and deep architectures. Deep learning utilizes artificial neural network that is inspired by the structure and process of the human brain [201]. The utilization of multiple layers in the neural network architecture allows for the learning of hierarchical representations of the input data. This utilization leads to state-of-the-art performance in various fields,

such as Atari2600 games [144], improving visuomotor skills of robots (i.e., sorting cubes according to their shapes, and opening a bottle cap) [202], and wireless communication [143]. For example, in [202] the authors generate four robotic tasks, including coat hanger at three different distances, inserting the claw of a toy hammer underneath a toy plastic nail, screwing on a bottle cap, and placing a shaped block in the correct hole. Their study demonstrated that DNNs can be trained end-to-end, directly from raw camera inputs, to learn visuomotor policies, thereby proving the possibility of using this approach for learning visual control.

More impressively, deep learning models have shown remarkable capabilities in generating responses that are comparable to human-like responses. ChatGPT, a language model developed using OpenAI's GPT-3.5 and GPT-4 LLMs, has been fine-tuned through supervised and reinforcement learning methods [203]. As such, ChatGPT can be effectively utilized to tackle complex issues such as global warming [204], and public health [205]. However, the use of ChatGPT in educational settings must be approached with caution, as it raises concerns about plagiarism in academia [206]. Since ChatGPT can generate human-like responses, it may be difficult to distinguish between original work and responses generated by the model.

Expanding the size of DNNs, either by increasing their depth or width, is a common approach to enhance their performance. However, this approach has drawbacks including increased risk of overfitting and increased computational resources required [193]. Larger networks with more parameters are more susceptible to overfitting, especially with limited labeled training data, and increasing the size of network filters in convolutional layers can lead to a quadratic increase in computation, adding to the computational cost [193]. Balancing the width and depth of the network is crucial to achieve optimal performance. By increasing both the width (number of filters per stage) and depth (number of network levels) of the network in parallel, higher quality networks can be obtained while maintaining a balanced distribution of the computational budget [194]. This ensures that the improvement in performance is maximized for a given amount of computation, resulting in an efficient and effective network design [194].

In a DNN, the input layer receives raw data, which is then passed through to the hidden layers. The deep term refers to the use of multiple layers in the neural network

architecture, which enables the network to learn hierarchical relations of the input data [188]. Each hidden layer contains multiple nodes, also known as neurons, and the links between neurons have weights that are acquired by utilising mathematical functions [185]. The input of the next hidden layer is the output of the previous hidden layer, which leads to an increased learning rate that can be useful in finding the complex relations of the data. In other words, the hidden layers are cascades of modules that include trainable parameters at all levels [207]. A DNN is illustrated in Fig. 5.2.

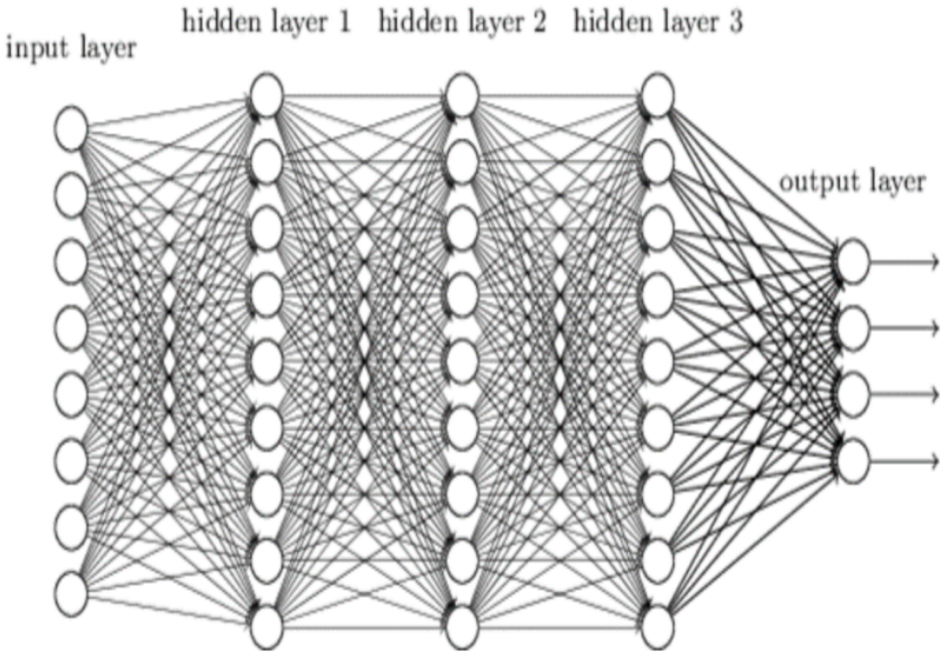

Figure 5.2: DNN illustration [178]. In this example, the input to the neural network is fed into three fully connected layers, with each valid action having a single output.

Deep learning can be used with supervised learning, unsupervised learning, and reinforcement learning [208]. With the help of deep learning, better results can be obtained; however, deeper layers bring new challenges, like requiring more training data.

While there has been extensive research on vehicular networks, 5G-NR, and wireless communication, our focus in this thesis is on RAN resource allocation. Specifically, we aim to develop a novel approach to optimize user and power association in RANs, considering a network that supports radio slicing and multi-numerology. By addressing this problem, we hope to contribute to the ongoing efforts to increase the performance and efficiency of 5G-NR networks. Based on the comprehensive literature review of ML in vehicular networks and ML employment in 5G-NR conducted in Chapter 2, we proceed with the system model in this chapter.

5.2 Power Allocation Problem

In this section, we aim to address the classical power allocation problem in a network with multiple links, focusing on a single frequency band with flat fading for simplicity, similar to the approach taken by the authors in [65]. We randomly distributed users within a field of a maximum size of 177m, which is similar to the approach employed in Chapters 3 and 4. The data rate requirements of each user were also randomly allocated for the training process. The downlink transmit power is determined based on their corresponding data rate requirements and the channel model. To evaluate the performance of our proposed RL model, we compare it with the calculated optimum outputs. The set of users is denoted by $U = \{1, ..., U\}$, and the BS is displayed as b. For the RL algorithm, the set of states, actions, and rewards are denoted by $S = \{1, ..., S\}$, $A = \{1, ..., A\}$, and $R = \{1, ..., R\}$, respectively.

The primary objective of this problem is to achieve a near-optimal power allocation solution that is faster than the provided MILP and GA algorithms. Specifically, the aim is to obtain near-real-time results where the trained RL agent can provide an optimal solution within a few steps. We utilise the deep reinforcement learning (DRL) approach to tackle this optimisation problem. By utilising a "deep" approach, which includes training a neural network with multiple layers, we aim to train an agent that can recognise patterns in the environment. To be more specific, we employ DQN agents for our proposed optimisation models. This pattern recognition enables the DQN agent to learn better power allocation strategies to approximate the optimum result utilising the state, action and reward function. Moreover, the deep approach in the Q-Networks can improve the speed and efficiency of the power allocation process in large-scale environments [148]. The DQN agent can handle the increased complexity of large-scale environments by employing deep neural networks [148].

Last but not least, we adopt a similar approach as in Chapters 3 and 4, where we consider a system in which each user has only one RB, and evaluate the system performance concerning the single BS scenario.

5.2.1 Channel Model

We use the channel model employed in Chapter 3 and Chapter 4 to illustrate the radio access gain between BS and users. This model is used to evaluate the performance of the DRL algorithm for the single BS scenario. We also assume that the users are static; hence the channel gain is not changing over time. The gain is calculated using Eq 5.6, where g_{bu} represents the gain between the BS and user, PL_{bu} denotes the path loss in dB calculated using Eq 5.7, and the SSF coefficient calculated using Eq 5.8.

$$g_{bu} = SSF_{bu} \times \left(10^{-(PL_{bu}/10)}\right), \quad \forall\ u \in U \tag{5.6}$$

$$PL_{bu}(dB) = FSPL + 10nlog\left(k_{bu}\right) + \sigma,\ \forall\ u \in U \tag{5.7}$$

$$SSF = \left(\left(N\left(0, 1/\sqrt{2}\right)\right)^2 + N\left(0, 1/\sqrt{2}\right)\right)^2 \tag{5.8}$$

Eq 5.7 defines the variables used for path loss calculation. The term PL_{bu} represents the path loss in dB, and $FSPL$ denotes the free space path loss, which can be determined by the carrier frequency and is calculated as 38.46 dB. The parameter σ shows LSF coefficients and has a value of 7.7 dB in our scenario, while n and d show the path loss exponent with a value of 3.1 and distance between BS and user, respectively. Since the gain calculation uses a linear scale, the path loss is converted from dB to the linear scale in Eq 5.6. Finally, Rayleigh distribution is used to calculate the SSF [163] coefficients, accounting for the absorbing, diffracting, and scattering effects of the surrounding environment.

5.2.2 System Model

Our proposed DRL algorithm for power allocation does not directly minimise the downlink transmit power in the objective function. Instead, we utilise the following objective function and constraint to ensure satisfactory performance. The constraint requires the allocated data rate to be greater than or equal to the requested data rate. Thanks to the constraint in Eq 5.10, the DRL algorithm ensures that all users

receive at least their minimum required data rate. Meanwhile, the objective function maximises the ratio of the requested data rate to the allocated data rate, denoted as Ω_u and d_u, respectively, for each user. By maximising the objective function and satisfying the constraint, we can achieve satisfactory performance and handle greedy users without over-allocating resources beyond their requests.

$$maximise: \quad \sum_{u \in U} \frac{d_u}{\Omega_u} \tag{5.9}$$

$$subject\ to: \quad \Omega_u \geq d_u, \quad \forall\ u \in U \tag{5.10}$$

The objective function and the constraint also ensure fairness among users. Eq 5.10 also leads to a power allocation that maintains fairness among users and prevents any single user from monopolising the system resources. Since we assume a single BS scenario for the power allocation problem, co-channel interference is not considered. Therefore, the allocated data rate for each user is calculated using the Signal to Noise Ratio (SNR) as follows:

$$C_u = w\left(log_2\left(1 + \frac{p_u \times g_{bu}}{\sigma^2}\right)\right) \tag{5.11}$$

The variable C_u, and parameters w, and σ^2 in Eq 5.11 represent the allocated data rate to the corresponding user, the bandwidth of the RB, and the additive white Gaussian noise (AWGN), respectively.

In communication systems, Shannon capacity and data rate are measured with bits-per-second; hence, they describe the amount of transmitted data over a communication channel. The Shannon capacity is the theoretical upper limit of data that can be transmitted without any data loss in a given amount of time. On the other hand, when the data rate term is utilised, errors and employed modulations are also considered; thus, it can be far from the maximum transmitted data. Since the choice of modulation techniques is not our primary concern, we assume that the allocated data rate is equal to the Shannon capacity, shown in Eq 5.12. This assumption allows us to evaluate the system's performance based on the theoretical maximum limit of the channel.

$$C_u = \Omega_u \tag{5.12}$$

As described before, the DRL approach utilises three elements: state, action, and reward. By utilising these elements, an agent can learn to navigate the environment by observing states, taking actions, and then optimising its behaviour, considering a policy to receive the highest reward. The environment is represented by the cellular network that includes single BS, a flat fading channel and users. The following subsection outlines the state, action, and reward function utilised in the proposed DRL algorithm.

States

The allocated transmit power for each user is represented as a vector, which shows the state where the agent observes, modifies and gets a reward from it. Note that in this section, we can use the terms 'state' and 'transmit power' interchangeably to refer to the power level allocated to each user in the system. Although we optimise the allocated data rate for the users, the only variable in the environment is the transmit power that is allocated separately for each user. Moreover, we assume integer numbers for the state instead of real numbers to reduce complexity and computational load. Consequently, the state space becomes discrete and finite, which simplifies the problem and makes it more tractable. Hence, the deep Q-learning algorithm that operates in discrete state and action spaces can be used.

Choosing how to divide the state space into smaller pieces is essential because it affects how accurate and fast the algorithm can find the best solution. If the pieces are too small, the algorithm might take a long time to find the solution, while if they are too big, the solution might not be accurate. Therefore, to find a balance between accuracy and speed, we decide to divide the state space as a set of integers. This approach can provide a reasonable accuracy level while reducing the computational complexity of the algorithm.

In addition to defining the state space and the system dynamics, the DRL algorithm also requires an initial state. The initial state can be set arbitrarily, but a better approach is to use a state that is representative of the operating conditions of the system. Therefore, instead of defining the initial system state randomly, we define the

initial system for each user as follows:

$$s_u(1) = \frac{p_{max} + p_{min}}{2} \tag{5.13}$$

Equation 5.13 demonstrates the initial state $s_u(t)$ for each user at the time step 1, as the average of the maximum and minimum allowed transmit power, denoted as p_{max} and p_{min}, respectively. Beginning from the average power for each user minimises the error and reduces the number of steps required to reach the optimum.

In our proposed DRL algorithm, the state is represented as a vector where the dimensions of the vector depends on the number of users in the system, denoted by u, resulting in a state vector of size $[1 \times u]$. In each iteration, the agent selects an action, and this action changes the state vector (i.e. transmit power), resulting in an updated state representation for the next iteration of the algorithm. Also note that the reward function employs two states, current and next, to provide a scalar reward value.

Actions

The proposed DRL algorithm performs transmit power allocation for each user in the downlink direction. Also, the set of actions available to each user is defined by considering all possible combinations of increasing, decreasing, or maintaining the transmit power. To ensure that the action space is finite, we restrict the increase and decrease in transmit power to integer values. Specifically, for a user with an initial transmit power of p_u, the available actions are to increase the transmit power by a positive integer a, decrease the transmit power by a positive integer a, or maintain the transmit power level at p_u. By doing so, we obtain a finite set of actions for each user. For instance, in the case of six users with three different actions for each user, the total number of possible actions in the action space is 729, which can be calculated as follows:

$$a_{total} = |a|^{|u|} \tag{5.14}$$

In Eq 5.14, the number of actions available is calculated where $|a|$ is the total number of possible actions for each user and $|u|$ is the total number of users in the model.

If the action space were a real number between [-a, a], the number of actions would be infinite. A continuous range of actions would give a more precise output as the system can take any possible action value. However, this approach would significantly increase the computational load and training time. Training and implementing the system in real-time scenarios may not be feasible as the output is getting closer to the optimum. Moreover, the system's complexity would also increase, making it harder to interpret the results and understand the algorithm's behaviour. Therefore, although increasing the action space might lead to better performance, it is essential to balance performance with computational complexity for practical implementation. To provide that balance, we limit the number of possible transmit power levels for each user to ensure that the action space is finite. Despite this limitation, the number of possible actions is still large enough to enable the system to reach a reasonable optimum.

The initial state starts from the average of the maximum and minimum power in our DRL algorithm for each user. However, after taking some actions, the transmit power allocated to each user must remain within the allowable limits. To ensure that the actions are feasible, we employed the following constraint to control the transmit power for each user:

$$s_u(t+1) = min\left(max\left((s_u(t) + a_u(t)), p_{min}\right), p_{max}\right); \tag{5.15}$$

The summation of the current state $s_u(t)$ and action $a_u(t)$ gives the next state, represented as $s_u(t+1)$ in the Eq 5.15. The DRL algorithm must check the new state to see if it is within the allowable limits. The Eq 5.15 represents a constraint to control the power allocated to each user. The value of $s_u(t+1)$ is obtained by taking the maximum between the next state value for that user, denoted by $(s_u(t) + a_u(t))$, and the minimum power limit for that user, denoted by p_{min}, and taking the minimum between this value and the maximum power limit for that user, denoted by p_{max}. This constraint ensures that the transmit power for each user remains within the allowable range specified by p_{min} and p_{max}, thus preventing any violation of power limits during the training process.

Then, the DQN agent compares the initial state $s_u(t)$ and the next state $s_u(t+1)$ to determine the action that resulted in the state transition. Based on this comparison,

the agent receives a reward $r(t)$ that displays the effectiveness of the selected action.

Reward Function

The conventional reward functions are based on metrics such as SINR, log(1+SINR) [65], or Shannon capacity for power allocation optimisation in wireless communication problems. However, our research proposes a new approach where a novel reward function is employed compared to traditional approaches. The reward calculation involves several steps, which are outlined below.

First, the RAN gain for each user is computed based on the current state. Since the user locations remain identical between the current and next states, the calculation of radio access gain is performed only once, avoiding unnecessary computation during training. After that, the allocated data rate for all users is calculated using the current state at time t. Then, the ratio between the requested and allocated data rate is calculated for each user. If the allocated data rate is less than the requested, the individual reward is assigned as -1. Otherwise, the requested and allocated data rate ratio is assigned as the individual reward. The individual reward at time t is denoted as $r_u(t)$ and is represented by the following equation:

$$r_u(t) = \begin{cases} \dfrac{d_u}{\Omega_u}, & \text{if } (\Omega_u \geq d_u) \\ -1, & \text{otherwise} \end{cases} \tag{5.16}$$

Subsequently, the overall reward for the current state at time t is calculated by summing the individual rewards for each user, where the reward at time t is represented as $R(t)$ as follows:

$$R(t) = \sum_{u \in U} r_u(t) \tag{5.17}$$

It is crucial to say that the system is a time-invariant system where the next state is represented as $(t + 1)$, the allocated data rate for each user in the next state is represented as $\Omega_u(t + 1)$, and the sum of allocated data rate for all users in next state denoted as $R(t + 1)$. In this case, Eq 5.18 provides the sum of the allocated data rate for all users in the next state:

$$R(t+1) = \sum_{u \in U} r_u(t+1) \tag{5.18}$$

Finally, to calculate the episode reward which is the agent gets, we compare the state rewards $R(t)$ and $R(t+1)$. If the overall ratio at the next state is greater or equal to the current state and the data requirement is satisfied, the reward is set to the sum of the allocated data rate for all users in the next state multiplied by 2, $(R(t+1) \times 2)$, to indicate a good action. On the other hand, if any user receives less data rate than requested, the reward is set to -1 to indicate an invalid action. Otherwise, the reward is set to $R(t+1)$ to indicate a suboptimal but valid action when only the data rate requirement is satisfied. Thus, the reward function effectively encourages the DRL algorithm to allocate resources in a way that satisfies user requirements while avoiding actions that result in a reduced data rate. The Eq 5.19 shows the episode reward function. The aim is to maximise the ratio between the requested and allocated data rates.

The state rewards $R(t)$ and $R(t+1)$ are compared to calculate the episode reward $R_e(t)$ obtained by the agent. The aim is to maximise the ratio between the requested and allocated data rates. Eq 5.19 presents the episode reward function, which considers three cases:

$$R_e(t) = \begin{cases} R(t+1) \times 2, & \text{if } (R(t+1) \geq R(t)) \ \ \& \ \ (\Omega_u \geq d_u) \\ R(t+1), & \text{if } \Omega_u \geq d_u \\ -1, & \text{if } \Omega_u < d_u \end{cases} \tag{5.19}$$

The ratio between the requested and allocated data rate explicitly tells to the DRL algorithm that it should not allocate more resources than the users' data rate request. Moreover, this reward function implicitly indicates to the DRL algorithm that it should minimise the transmit power. This approach encourages the algorithm to allocate resources efficiently while meeting the requested data rate. It also enhances fairness by preventing the allocation of excessive resources to one user while allocating insufficient resources to another. By minimising the transmit power implicitly while meeting the users' data rate requirements, this novel reward function provides a new

perspective for optimising resource allocation in wireless communication systems using DRL techniques. It is important to note that this reward function can solve the power allocation problem with a single constraint. Having a single constraint simplifies the problem and makes it more tractable, which is often desirable in practical applications.

5.2.3 Simulation Setup and Results

We evaluate the performance of the proposed power allocation optimisation model. We utilize the Matlab RL environment class to create the environment, and for the training, we use Matlab Reinforcement Learning Designer Toolbox.

Simulation Setup

We consider a single BS model, where the farthest user is assumed to be located at a distance of 177 meters away from the BS, similar to the scenarios discussed in Chapter 3 and Chapter 4. The users are located randomly on this grid. Since the lowest (180 kHz) bandwidth for an RB is considered, the user requirements are similar to those employed in Chapter 4. The data rate requirements of the users vary randomly between 0.3 Mbps to 2.5 Mbps.

To determine the optimal step size for the power allocation problem, we conducted a trade-off analysis between the resolution of the power levels and the number of steps required to reach near-optimal solutions. We found that increasing the step size to 3 mW decreased the number of steps to reach optimum but at the cost of reduced optimality. After conducting a series of tests using Matlab, we determined that a step size of 1 mW is an appropriate balance between resolution and the number of steps required to reach near-optimal solutions. Therefore, we selected a step size of 1 mW for our power allocation optimisation model.

We utilise the standard framework of RL, where an agent interacts with an environment throughout a series of discrete actions in discrete time steps. The agent observes a state $s(t)$ and takes an action $a(t)$ based on its policy π in each time step t. Then, the agent receives a scalar reward $R(t)$ by comparing the corresponding states. During this process, the agent explores the environment with a reducing rate, ε, which changes between [0, 1]. Since the agent learns to optimise its actions based on its experience, ε determines the balance between exploration and exploitation. At the beginning of the

training, the epsilon value is high; thus, the agent is encouraged with a high exploration rate to explore the environment and discover the actions that lead to higher rewards. As the agent gets experience, the exploration rate is gradually reduced to the favour of exploitation of the acquired knowledge. In this work, we employ an exponential decay function for the ε parameter, which starts from 1 and reaches its minimum value of 0.01 after 1000 time steps. The ε decay function is illustrated in Fig 5.3.

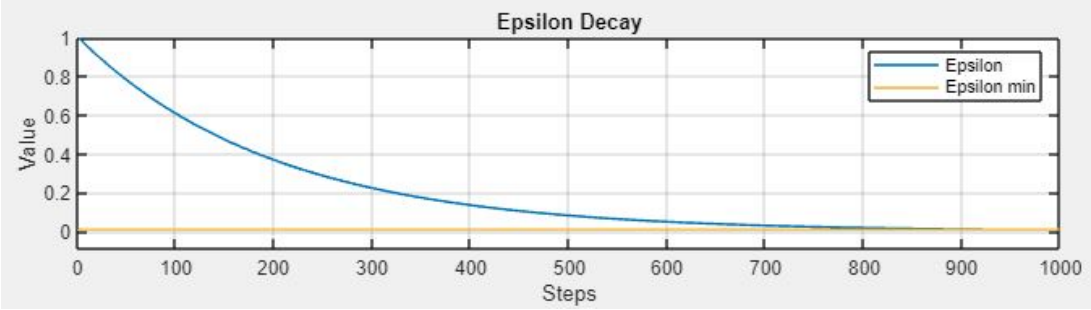

Figure 5.3: Epsilon decay of the employed agent.

In RL, the discount factor γ is a parameter that determines the significance of immediate and future rewards [148]. It also changes between (0, 1); a high discount factor aims to increase future rewards, while a low discount factor aims to increase immediate rewards. Mathematically, the discounted cumulative reward can be represented as:

$$G_t = R_{t+1} + \gamma R_{t+2} + \gamma^2 R_{t+3} + \ldots = \sum_{k=0}^{\infty} \gamma^k R_{t+k+1} \tag{5.20}$$

where R_t is the reward received at time step t, and γ is the discount factor. In this RL algorithm, we employ a high discount factor, γ, to increase the future rewards, which is set to 0.99.

The DQN agent has a neural network that consists of an input layer, a fully connected layer, a Rectified Linear Unit (ReLU), another fully connected layer, another ReLU and an output layer. In neural networks, the neurons are connected to each other with different weights, demonstrating the connection strength between neurons [185]. After a fully connected layer, some weights might have negative values, and the ReLU activation function sets the output value to zero for any negative input while leaving positive values unchanged [209]. In our problem, the input layer of the neural network consists of a number of neurons equal to the number of users. The fully connected layers include 256 neurons, and finally, the output layer consists of a number of neurons

equal to the number of actions.

Training

In this study, we set the maximum number of episodes to 2000, which provides enough training for the agent. Additionally, we define the episode length as 50, meaning that the agent takes 50 actions in each episode and receives a summation of those actions as the reward for the corresponding episode.

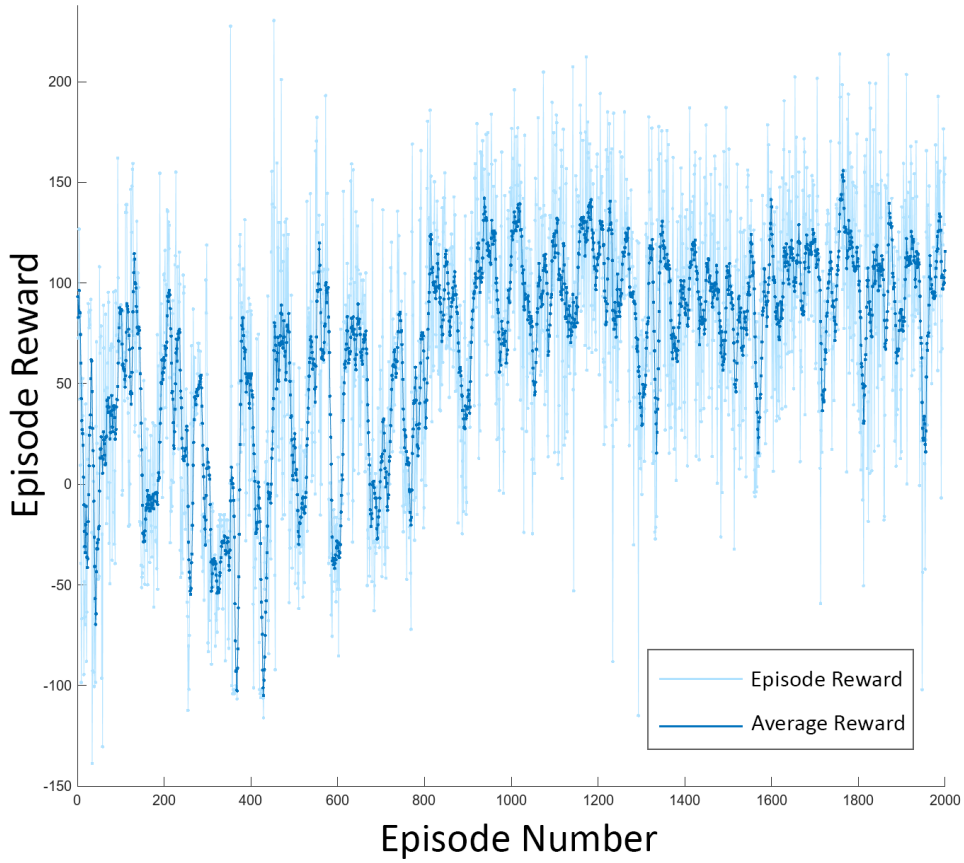

Figure 5.4: The episode reward through the training phase.

Figure 5.4 shows the episode reward achieved during training, where the dark blue line represents the average reward over 10 episodes, and the light blue line represents the reward obtained in each individual episode. The presence of spikes in the reward function indicates that the agent is still actively exploring the environment. Fig 5.4 also shows that the reward steadily increases over time, indicating that the agent is learning to optimise its actions and make better decisions. The final reward value is close to the optimal value, indicating that the agent has learned an effective policy for the given task.

Results

One of the primary constraints of our DRL algorithm is that all allocated data rates must be greater than or equal to the requested data rates. Given that the RL model is not designed to minimise transmit power explicitly, it is reasonable to observe a slightly higher transmit power than the optimal solution. However, the optimal solution typically produces the desired output almost instantaneously, as desired. Therefore, Fig 5.5 illustrates the requested and allocated data rates for a six-user scenario.

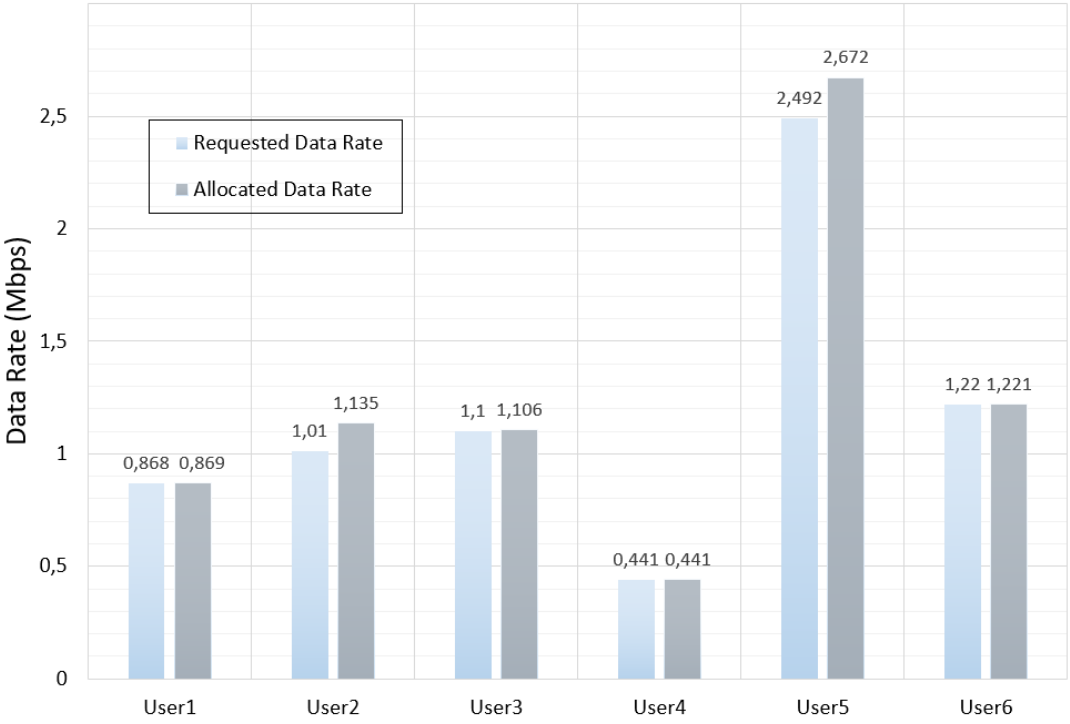

Figure 5.5: The requested and allocated data rates for a six-user scenario

The performance evaluation of the DRL algorithm in Fig 5.5 reveals that all users' minimum data rate requirements are met, which also indicates the high accuracy and advantage of the proposed algorithm. Specifically, four out of six users exceed the requested data rate by less than 0.5% while User2 and User4 exceed by 12.3% and 7.2%, respectively.

Another crucial aspect in evaluating the performance of our proposed DRL algorithm is its speed in reaching the optimal solution. To evaluate this aspect, we illustrate the steps that are required for the algorithm to achieve near-optimal power allocation in Fig 5.6. Our aim is to achieve near-real-time results where the trained DQN agent could provide an optimal solution within a few steps. The figure shows that after the

37^{th} step, the agent no longer takes significant actions, indicating that the optimal solution has been achieved. The results indicate that the DRL algorithm can reach near-optimal solutions within a few steps, demonstrating its efficiency and effectiveness in solving the power allocation problem.

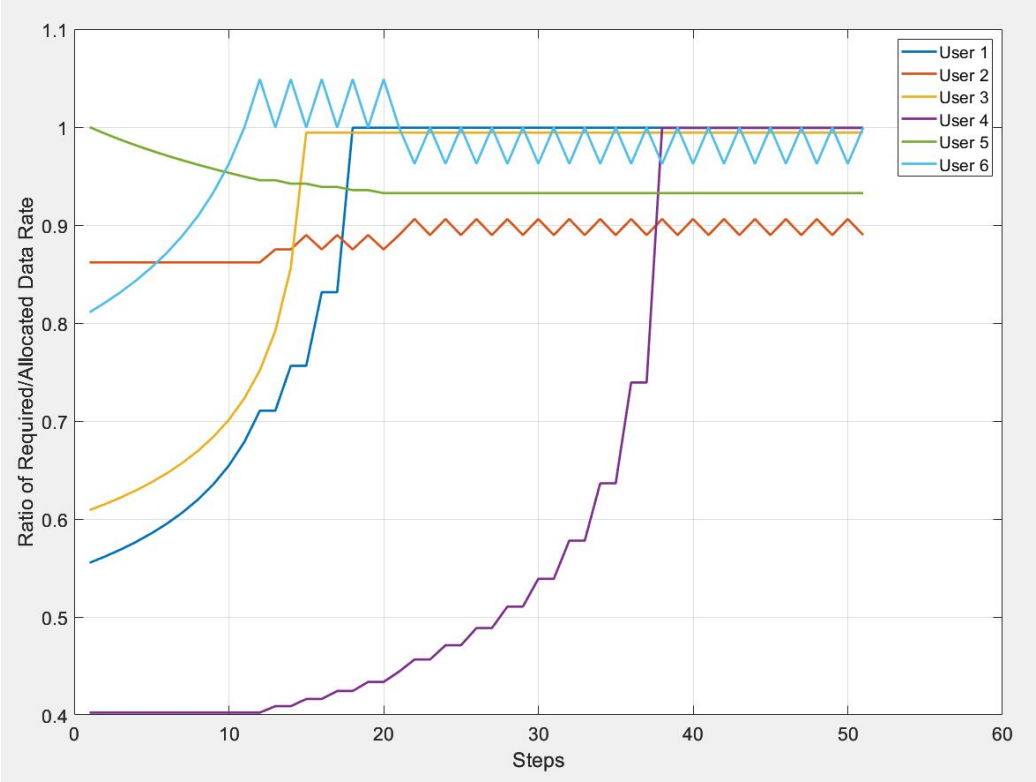

Figure 5.6: The individual rewards for each episode.

In the proposed DRL algorithm, when the ratio of the required data rate to the allocated data rate for a user is greater than 1, it indicates that the user's data rate requirement is not satisfied. Therefore, in such cases, the individual reward for that user is set to -1. Furthermore, since we compare the current state with the next state to calculate the reward, the RL agent adjusts the power value in order to obtain a higher reward. This need for change to get a higher reward explains the observed ripple effect in the performance of users number 2 and 6.

We compared the performance of our DRL algorithm with the calculated optimal results for validation purposes. In the following section, we consider network slicing and implement joint power and numerology allocation optimisation.

5.3 Joint Power and Numerology Allocation

In this section, we extend the power allocation problem presented in Chapter 5.2 by incorporating the selection of numerology by users. Since this is an extension of the power allocation problem, the channel model and most constraints remain the same. Similar to Chapters 3 and 4, users are allowed to select any numerology as long as their data rate requirements are met.

The optimal BWP allocation is found in Chapter 3; therefore, we decide to utilise the optimal bandwidth allocation here. In this pre-allocated 5 MHz bandwidth, 1 RB, 1 RB, and 6 RBs are allocated for numerology 1, 2, and 3, respectively, resulting in a total of 8 RBs that are available for selection by any user.

In order to demonstrate the feasibility of joint power and numerology allocation using DRL, we assume higher data rate requirements which can be provided by using higher numerologies with higher bandwidths. For example, the data rate requirements of the users are expanded to those utilised in Chapter 3. Moreover, URLLC users have strict delay requirements that can be satisfied by higher numerologies.

Nonetheless, most of the problem remains the same except for the exponentially increasing action space. For instance, we maintain the integer power values for the users to prevent further expansion of the action space. Using integer power values allows us to tackle the problem while keeping most aspects consistent with the previous approach.

5.3.1 System Model

The proposed DRL algorithm for joint power and numerology allocation employs a similar objective function provided in Eq 5.21. The objective function 5.21 has two elements with the same weight. First, the required and allocated data rate ratio is multiplied with the maximum allowed power level is maximised. Since the maximum allowed power level is a fixed parameter, the maximum positive outcome can be achieved when the required data rate equals allocated. Conversely, the total transmit power is minimised to encourage the agent to choose the higher numerologies; hence, the objective function can be maximised.

$$maximise: \quad \left(\left(\sum_{u \in U} \frac{d_u}{\Omega_u}\right) \times p_{max}\right) - \sum_{u \in U} p_u \tag{5.21}$$

$$subject\ to: \quad \Omega_u \geq d_u, \quad \forall\ u \in U \tag{5.22}$$

$$subject\ to: \quad t_u \geq t_n, \quad \forall\ u \in U \tag{5.23}$$

The constraint in Eq 5.22, which ensures that the allocated data rate is greater than or equal to the requested data rate, is also the same. With Eq 5.22, we ensure that the value of the objective function is negative when the required data rate is more than the allocated. This constraint prevents the model from receiving false positive objectives. Furthermore, the constraint stated in Eq 5.23 guarantees that the allocated numerologies' delay is less than or equal to the delay requirement, thereby satisfying the users' delay constraints. In Eq 5.23, t_u and t_n represent the delay requirement of the users and slot length of the corresponding numerology, respectively. By including this constraint, we ensure that the selected numerology for each user satisfies their delay requirements.

Since each numerology employs different RB bandwidth, the allocated data rate is calculated as follows:

$$\Omega_u = n_u \left(log_2 \left(1 + \frac{p_u \times g_{bu}}{\sigma^2}\right)\right) \tag{5.24}$$

In Eq 5.24, n_u represents the bandwidth of the allocated numerology for the corresponding user. Since we assume that the allocated data rate is equal to the Shannon capacity, we expressed this assumption using Eq 5.12.

In the context of our proposed DRL algorithm, the environment represents a cellular network that consists of a single BS containing multiple numerologies, a flat fading channel, and multiple users. The following subsection outlines the state representation, action space, and reward function components of the proposed DRL algorithm for the joint power and numerology allocation problem.

States

In order to enable joint optimisation of power and numerology allocation, the state must represent both power and numerology for each user. To achieve this state, we construct a single state vector that is logically divided into two parts. The first half of the state vector represents the transmit power allocation, same as before. The transmit power is allocated separately for each user as an integer number. The second half, on the other hand, shows the allocated numerology for each user. As a result, the entire state consists of integer values for the state instead of real numbers. Any state vector is represented as follows, where $p_u(t)$ and $n_u(t)$ represent vectors of size $[1 \times u]$:

$$s_u(t) = [p_u(t) \;\; n_u(t)] \tag{5.25}$$

To ensure that the initial system state is representative of the operating conditions of the joint optimisation problem, we adopt the following approach. We must consider both the power allocation and numerology allocation aspects to determine the initial state. The initial transmit power for each user is determined as the average of the maximum and minimum permitted transmit power, as done previously. Then, we allocate the maximum numerology to each user for numerology allocation, hoping to achieve a positive reward at the beginning. Therefore, rather than randomly assigning the initial system state, we adopt the following approach to define the initial system state for each user:

$$p_u(1) = \frac{p_{max} + p_{min}}{2} \tag{5.26}$$

$$n_u(1) = n_{max} \tag{5.27}$$

$$s_u(1) = [p_u(1) \;\; n_u(1)] \tag{5.28}$$

$p_u(1)$ and $n_u(1)$ represent power and numerology allocation for the initial state, respectively. $p_u(1)$, and $n_u(1)$ together form the initial state denoted as $s_u(1)$.

The size of the state vector depends on the number of users, and there are two states for each user. Hence, the size of the state vector becomes $[1 \times (2 \times u)]$. In each iteration, the agent selects an action, and this action changes the transmit power and numerology for each user, and the next state is obtained.

Actions

The proposed DRL algorithm performs transmit power and numerology allocation for each user simultaneously. The set of actions available to each user is the combination of the set of power and numerology actions. The set of power actions remains identical; it includes all possible combinations of increasing, decreasing, or maintaining the transmit power by using integer numbers. On the other hand, the set of numerology actions is independent of the previous state, allowing users to switch directly from the 3^{rd} numerology to the 1^{st} numerology and vice versa.

When the numerology selection is introduced to the action space as an additional dimension, the number of elements in the set of actions increases exponentially. For example, in the previous section, with six users, the total number of possible actions in the action space was 729. However, considering the scenario with three available numerologies for the same six users, the action space expands to 531.441 possible actions. This exponential growth highlights how the additional dimension significantly increases the complexity of the problem.

$$a_{total} = |a_p|^{|u|} \times |a_n|^{|u|} \tag{5.29}$$

The number of available actions is calculated in Eq 5.29. Here, $|a_p|$ represents the total number of power actions, $|a_n|$ represents the total number of numerology actions for each user, and $|u|$ represents the total number of users in the model. This equation provides the overall size of the action space, considering the different power and numerology options available to each user.

We employ a constraint that verifies the updated transmit power after applying a power action to maintain the transmit power within the allowed limits. This constraint ensures that the transmit power remains within the predefined limits for each user. By using this constraint, we ensure that the power actions taken by the RL algorithm

are valid and do not exceed the specified boundaries. The constraint is formulated as follows:

$$s_u(t+1) = min(max((s_u(t) + a_u(t)), p_{min}), p_{max}); \tag{5.30}$$

The numerology allocation operation directly modifies the states without any arithmetic operations such as addition or subtraction. Consequently, there is no need to employ a constraint to check if the new state exceeds the limits for numerology allocation. Thus, the numerology allocation automatically ensures that the selected numerology remains within the allowed limits without additional constraints.

Reward

In this section, we employ a similar reward function as before. However, we adopt a simplified approach where the reward is based solely on the comparison between the output and the user requirements without considering the performance of the next state compared to the current state. The allocated data rate for each user is determined based on the RAN gain, power allocation, and numerology allocation. The reward calculation considers two main constraints: the delay and data rate requirements. If any user requirement constraints are not satisfied, the individual reward is set to a negative value of the maximum allowed transmit power. On the other hand, if both constraints are satisfied, the individual reward is computed using the same approach as the objective function. The reward equals the requested and allocated data rate ratio multiplied by the maximum allowed transmit power, and the employed transmit power is subtracted from the multiplication. The individual reward at time t is denoted as $r_u(t)$ and is given by the following equation:

$$r_u(t) = \begin{cases} \left(\left(\frac{d_u}{\Omega_u}\right) \times p_{max}\right) - p_u, & \text{if } (\Omega_u \geq d_u) \ \& \ (t_u \leq t_n)\,, \ \forall \ u \in U \\ -\left(p_{max}\right), & \text{if } (\Omega_u < d_u) \, or \, (t_u > t_n)\,, \ \forall \ u \in U \end{cases} \tag{5.31}$$

When both constraints are satisfied, the reward function has two elements. First, the ratio between the requested and allocated data rates is multiplied by the maximum

allowed power level to obtain a positive reward. The highest positive reward is achieved when the allocated data rate is equal to the requested data rate. Conversely, the reward decreases as the transmit power consumption increases. This negative value is intended to encourage the agent to select higher numerologies, thereby reducing the impact of the negative reward.

Next, the episode reward for the current state at time t is calculated by summing the individual rewards for each user. The episode reward at time t is denoted as $R(t)$ and is computed as follows:

$$R(t) = \sum_{u \in U} r_u(t) \tag{5.32}$$

The episode reward for the next state at time $t+1$, denoted as $R(t+1)$, is calculated as the sum of the individual rewards for each user. A positive reward signifies a favourable action, which can be provided when all the constraints are satisfied, and the ratio is close to 1. On the other hand, any negative reward indicates an invalid action. The agent can increase the positive reward by minimizing the allocated data rate to meet the requirements or increasing the numerology, both of which result in power reduction. Consequently, in this section, the reward function implicitly guides the DRL algorithm towards minimizing the transmit power.

5.3.2 Simulation Setup and Results

We evaluate the performance of the considered joint power and numerology allocation optimisation model. Just like before, we utilize Matlab RL environment class to create the environment, and for the training, we use Matlab Reinforcement Learning Designer Toolbox.

Simulation Setup

In this scenario, we consider a carrier bandwidth of 5 MHz and three numerologies with bandwidths of 180 kHz, 360 kHz, and 720 kHz. The slot lengths associated with these numerologies are 1 ms, 0.5 ms, and 0.25 ms, respectively. Based on the optimum bandwidth allocation determined in Chapter 3, the carrier bandwidth includes 1 RB, 1 RB, and 6 RBs for the 1^{st}, 2^{ns} and 3^{rd} numerologies, respectively.

Also, we assume a single BS model, and the users can be located around the BS at distances ranging from 1 to 177 meters. Since higher numerology provides higher bandwidth, hence, higher data rate, the data rate requirements of the users are increased, similar to those in Chapters 3 and 4. Moreover, the delay requirement of the URLLC users is included in this section.

The algorithm takes two actions at once in the step function. The step of the power action is maintained in the algorithm; the size of each step is 1 mW, which also ensures that the minimum power level is 1 mW. The second action is that the agent can modify the employed numerology by the users, independent of their previous numerology at each step. In other words, the step function allows for a 1 mW transmit power change compared to the previous time step, and the numerology can change regardless of the previous state.

In this study, we employ a single agent that is responsible for both power and numerology allocation for all users. Immediately after a new dimension is introduced or when the number of variables, such as users, RBs, and numerologies, is increased, the curse of dimensionality arises. Therefore, to prove the feasibility of joint power and numerology allocation using DRL is possible with a single-agent DRL algorithm, we employed five users and three available numerologies in our scenario.

In the joint power and numerology allocation optimisation problem, we employ the same rate of exploration rate (ε) decay and the minimum ε value to those employed in the power allocation optimisation problem. However, the total number of actions in the environment is increased 81 times. Moreover, according to the Matlab Reinforcement Learning Designer Toolbox, the total learnables, which indicates the variables that agent explores, are increased almost 60 times (from 254.9k to 15.2M). Consequently, keeping the rate of ε decay and the minimum ε value the same means that exploration ends relatively sooner than the previous problem. The following exponential decay function for the ε parameter is employed, which starts from 1 and with a minimum value of 0.01 after 1000 time steps illustrated in Fig 5.7.

Since the exploration fades relatively quickly, the agent is expected to find the optimal policy faster and improve it with the agent's acquired knowledge. However, the agent can still explore the environment with the minimum ε parameter.

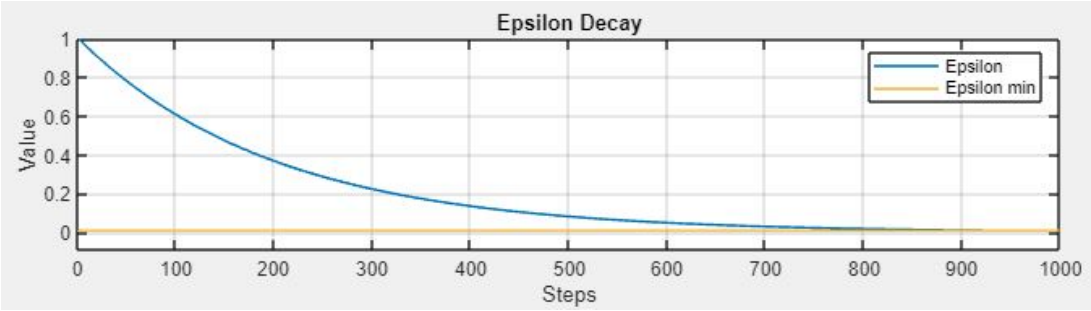

Figure 5.7: Epsilon decay of the multi-objective problem's agent.

To solve this joint problem, a different discount factor γ, which equals 0.75, is employed. The utilised γ decreases the importance of future rewards and increases the importance of immediate rewards. Thus, the agent prioritises more accurate actions at the beginning, and to maximise the episode reward, it selects the actions that yield higher immediate rewards.

Finally, we employ the same neural network to train the DQN agent. This neural network also includes an input layer, a fully connected layer, a ReLU, another fully connected layer, another ReLU and an output layer, which is illustrated in Fig 5.8. The number of neurons is also the same, where the fully connected layers include 256 neurons, and the number of neurons for input and output layers are equal to the number of users and the number of actions, respectively.

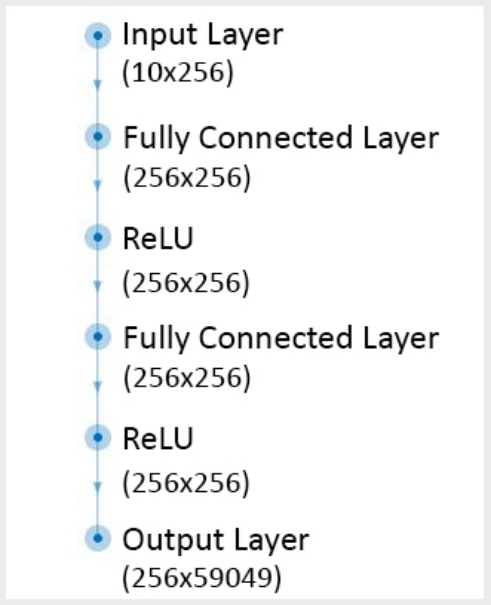

Figure 5.8: The neural network that is employed in the joint optimization problem.

Training

In this study, we set the maximum number of episodes to 2400, which provides enough training for the agent. Additionally, long episode lengths might be challenging for the agent due to the difficulty of determination of the action-reward relationship in long episodes. To address this issue, more clarity than the previous problem is provided for the agent. Hence, the agent can more easily identify which actions lead to better or worse outcomes in achieving the desired results. The episode length is maintained despite the exponentially increased problem size, which can be observed from the action and observation vectors, the number of possible actions, and action space. In other words, instead of increasing the episode length proportionally with the total number of actions, we define the episode length as 50, meaning that the agent takes 50 actions in each episode and receives a summation of those actions as the reward for the corresponding episode. Considering the maximum number of episodes, the total number of steps in the training is equal to 120000.

Figure 5.9 shows the episode reward achieved during training, where the dark blue line represents the average reward over 10 episodes, and the light blue line represents the reward obtained in each individual episode.

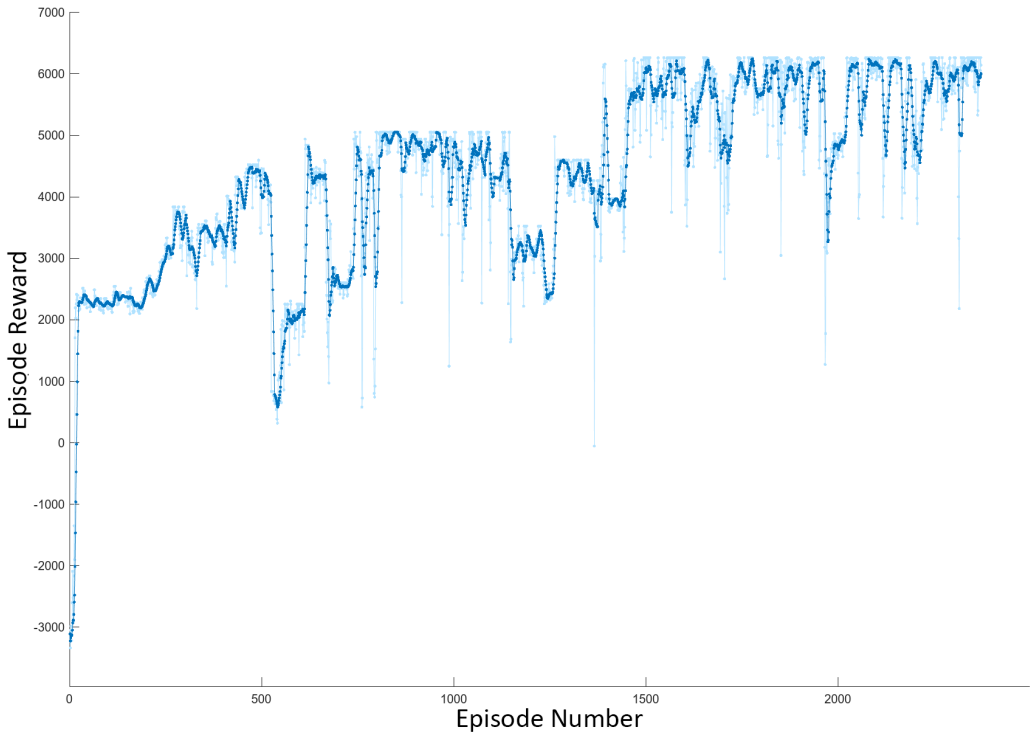

Figure 5.9: The episode reward through the training phase.

Compared to the previous power allocation optimisation problem, the increasing trend of the episode reward can be seen more clearly in Fig 5.9. This trend is mainly caused by the ε and γ parameters employed in this problem formulation. The ε fades in the first 1000 steps to its minimum; nonetheless, the presence of spikes in the reward function indicates that the agent is still actively exploring the environment till the end of the training. The length of the spikes, on the other hand, is reduced due to a relative reduction in ε and a reduction in the discount factor γ. Because of the decreased γ, the future rewards have less importance; thus, the agent focuses more on immediate rewards. This reduction mitigates the impact of large reward fluctuations throughout the episodes. The steadily increasing reward over time also shows that the agent is learning to optimise its actions and make better decisions.

By setting a high ε and maintaining it until the end of the training, with a higher minimum ε, the DQN agent can provide satisfactory optimisation results in small environments, such as our power allocation optimisation problem. However, when another dimension is introduced, the number of variables increases exponentially, and the agent no longer has the same luxury. Instead, the agent must stick with acceptable outcomes and carefully explore the surroundings to find better solutions. In other words, the exploration rate is reduced to increase exploitation and generate a more greedy DQN agent. Otherwise, the agent may become lost in the environment and struggle to reach the optimal outcome.

Results

There are two primary constraints in the joint power and numerology allocation optimisation problem. The first constraint dictates that the allocated data rate must be greater than or equal to the requested, like the previous power allocation optimisation problem. Fig 5.10 illustrates the requested and allocated data rates for the joint power and numerology allocation optimisation problem with a five-user scenario.

The second constraint is the delay requirement, which is also satisfied for all users. Only User3 has a critical delay requirement which must select the 3^{rd} numerology. The other users are free to select any numerology. Table 5.1 shows the delay requirements and numerology allocations for all users. Moreover, the allocated power for each user is also demonstrated in Table 5.1.

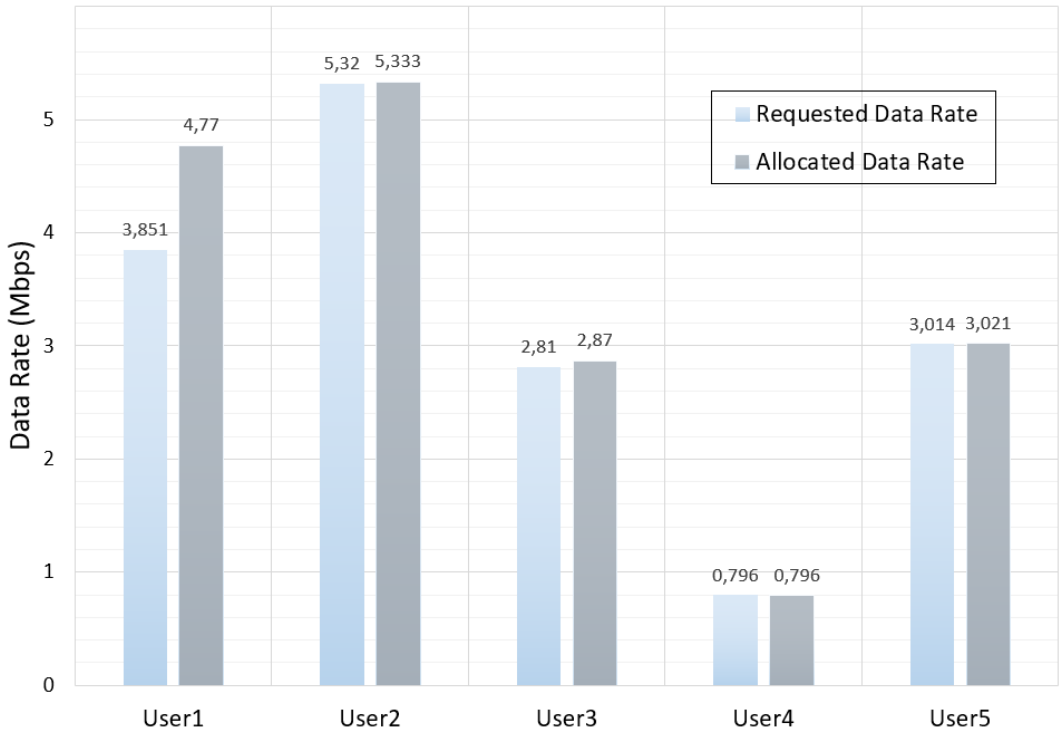

Figure 5.10: The requested and allocated data rates for the joint optimisation problem

Table 5.1: Delay requirements and numerology allocation of the Users

	User1	User2	User3	User4	User5
Delay requirement	> 1 ms	> 1 ms	0.45 ms	> 1 ms	> 1 ms
Allocated numerology	4^{th}	4^{th}	4^{th}	1^{st}	2^{nd}
Allocated power	$1mW$	$5mW$	$1mW$	$1mW$	$1mW$

The behaviour of the agent and the corresponding allocated data rate to each user can be only described using Fig 5.10 and Table 5.1 together. For example, it can be observed from the figure that the most significant difference is in User1, where the allocated data rate exceeds the requested by 23.8%. Considering the reward function, the ratio between the requested and allocated data rate for User1 is 0.8073, and the utilised transmit power is 1mW; hence the reward equals $30 \times 0.8073 - 1 = 23.219$. On the other hand, if User1 selected the 2^{nd} numerology, the ratio would be almost equal to 1 with a power consumption of 17 mW. In this case, the reward would be $30 \times 1 - 17 = 13$. This reward calculation proves that despite the lower requested and allocated data rate ratio, the agent selects the larger reward, which is also optimal for User1.

Although there is no strict delay requirement for User2, it cannot select any other numerology to satisfy its data rate requirement without exceeding the maximum transmit

power limit. User2 would need 665 mW for the 2^{nd} numerology selection.

User3 also could reach a higher ratio if the 2^{nd} numerology would be employed. However, the transmit power would be 15 mW, and the reward would be less. Regardless, the 2^{nd} numerology would not satisfy User3's delay requirement.

The allocated data rate meets exactly the requested data rate for User4, which selects the only 1^{st} numerology RB in the carrier bandwidth. Having 1^{st} numerology and 1 mW, User4 receives approximately 29 as a reward. User5 also voluntarily selects the only RB that belongs to the 2^{nd} numerology; hence it can maximise its reward. If User5 selected the 3^{rd} numerology, and the ratio would be approximately 0.5.

Before evaluating the speed requirement of the proposed algorithm, it is essential to state that all data and delay requirements are successfully met for all users. The outputs demonstrate that the agent shows an excellent performance in selecting the most appropriate numerology and power level for each user for the given reward function. By considering these achievements, we can conclude that the proposed algorithm effectively addresses the objectives of the joint optimisation problem with a sufficient decision-making process, and a single-agent DRL algorithm can optimise the users' individual performances.

We also evaluate the proposed DRL algorithm's speed in reaching the optimal solution. To evaluate the speed of the algorithm, we demonstrate the steps that are required for the algorithm to achieve the optimal solution in Fig 5.11. The total number of steps is limited to 60, and the optimal solution is achieved at the 40^{th} step for the first time, and the data rate allocation of this step is illustrated in Fig 5.10. All the users are settled in the 39^{th} step, except User2. The actions of User2 change in a pattern; therefore, the optimum output is achieved more than once in 60 iterations. The obtained results demonstrate that the proposed DRL algorithm shows promising performance in terms of reaching optimal solutions within a few steps. These findings highlight the efficiency and effectiveness of the proposed RL algorithm.

Although the complexity of the problem significantly increases, the joint power and numerology allocation problem has been successfully solved using a single DQN agent. However, it must be noted that the training process requires careful parameter tuning for the optimal performance. Parameters such as ε (exploration rate), γ (discount

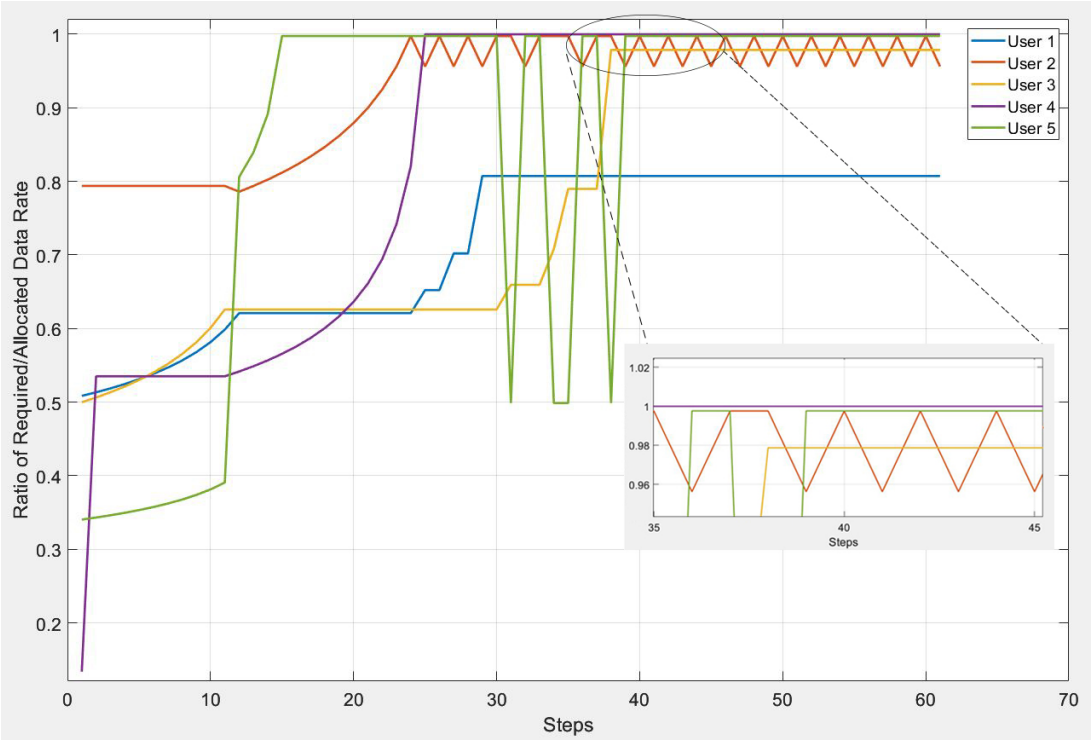

Figure 5.11: The requested and allocated data rates for a four-user scenario

factor), and the number of steps in each episode must be assessed for each particular problem. Furthermore, the problem can be extended to user association or data routing; the DQN agent can achieve the desired convergence of the DRL algorithm by conducting detailed parameter tuning.

5.4 Conclusions

This section starts with providing a brief overview of Machine Learning, focusing on Reinforcement Learning. Then we propose a novel reward function specifically designed for power allocation optimisation problems. We leverage the deep Q-Network agents and deep reinforcement learning algorithms to solve these optimisation problems. Next, we introduce two algorithms that employ the novel reward function in a single-cell scenario. The first algorithm allocates the downlink transmit power among users efficiently. The second developed algorithm extends the downlink transmit power allocation optimisation by including numerology allocation in a cellular network that employs multi-numerology. This enhancement in the algorithm enables placing 5G constraints in the utilised cellular network.

The changes in the user requirements or the distance between BS and the user can

be tolerated by the agent. In other words, the trained DQN agent can solve similar problems in some cases. To do so, instead of the fixed parameters (e.g. fixed locations and requirements), varying parameters can be employed during the training. In this changing environment, the learning rate of the agent decreases dramatically; hence, the number of episodes, ε rate, and minimum ε must be increased in training. Alternatively, the agent would be more flexible for the changes with a reduced amount of training when the fixed parameters are employed, which leads to a decrease in the ability to find the optimal solution of the agent. On the other hand, when the same parameters are utilised, and the number of episodes in the training is increased, the agent will be a problem-specific solver. This approach reduces the generalisation ability to solve similar problems.

Moreover, this study can easily be extended by adding user association and data routing dimension. In order to deal with exponentially increasing complexity, the number of episodes, ε rate, and minimum ε must be increased in training. Furthermore, a multi-agent approach can be employed to solve the multi-objective problem. For example, each agent might be assigned to a specific user, allocating a power level and numerology, and selecting the optimal path for that user. Alternatively, each agent might be assigned to a specific action for all users. For example, one agent allocates power, and another allocates numerology while another selects the optimal path for all users simultaneously.

However, in both cases, the agents must interact with each other to share some information. This provided information can be useful and required, or sometimes using this information might affect the agent in the opposite way expected. For example, considering a multi-cell scenario, when two separate agents select the same RB from different sources, the CCI must be calculated. In this case, the communication is required and necessary. On the other hand, this communication might be unnecessary and harmful to the learning process. For example, the agents can share their experiences via their rewards which are obtained by selecting an RB, numerology and source. However, this information sharing might be confusing for another agent. Firstly, from the user-source pairing point of view, each user has a different location on the grid; therefore, the user-source pairing is unique. Secondly, when SSF coefficients are introduced, the gain of the RBs changes with the smallest changes in the location. Therefore, even

close users might experience different RB gains due to SSF coefficients. Consequently, sharing this information might be misleading to other users; the results can confuse the other agents and result in not finding a relation between location and connected sources.

Chapter 6

Conclusions & Future Works

This thesis has investigated various aspects of resource allocation and data routing optimisation in 5G-NR networks, with a particular focus on network slicing and its implications for the efficient utilisation of network resources. Throughout this thesis, we have explored a wide range of topics related to the 5G-NR wireless communication networks. In the second chapter, we conducted a comprehensive literature review that covered various areas of interest, including but not limited to 5G-NR network slicing, resource allocation optimisation, bandwidth partitioning, vehicular networks, heuristics, genetic algorithms, and machine learning. This review served as a foundation for our subsequent research, allowing us to build upon existing knowledge and identify gaps in the literature that we could address through our research.

In Chapter 3, the downlink RAN resource allocation optimisation framework is proposed for vehicular communications to enhance the network efficiency and reduce the total transmit power while considering CCI for demand points. A MILP model was developed to jointly optimise BWP allocation by considering total carrier bandwidth, routing data through VBS nodes when necessary, hence user association, and RB and power allocation among DPs by considering their delay and data rate requirements. VBS nodes increase the flexibility in the model; the DPs can receive their demand from another source, which is supported by the out-band IAB network. FR1 and FR2 frequency bands are utilised for access and backhaul communications, respectively. The objection function maximises the number of served users and minimises the weighted sum of the total transmit power as well as the weighted sum of the CCI, for which the

optimal distribution of the resources per DP is obtained. The proposed optimisation approach effectively reduces transmit power and CCI, indicating the benefits of properly configured numerologies, which could support the implementation of RAN slicing. Additionally, we present a logarithmic function linearisation method based on piecewise linearisation. Overall, the proposed model can significantly enhances network efficiency, reduces power consumption and CCI, and enables effective implementation of RAN slicing.

As a future direction, optimisation remains an area of active research. In the context of this thesis, one potential extension is to optimise in-band IAB networks, where access and backhaul links share the same resource elements. Furthermore, currently, we assume all BSs have the same BWP allocation in our environment, but this approach may not be practical for larger networks. Therefore, considering INI, an optimisation framework can be built for the scenario that BSs have different BWP allocations. Our optimisation framework can easily be extended into these scenarios. Moreover, joint power allocation and beamforming for mmWave networks optimisation is an open research area. Considering an urban or highway scenario, our optimisation framework also can be extended into this field. Furthermore, new technologies with the developing technology will require new requirements. Some applications, such as Augmented Reality/Virtual Reality (AR/VR), already require high throughput and low latency. Considering these user requirements, there is a need for a novel resource allocation optimisation approach that can effectively provide the specific demands of these emerging technologies.

Chapter 4 introduces a hybrid optimisation framework that combines heuristic and meta-heuristic approaches, specifically the genetic algorithm, to optimise the bandwidth allocation of multi-numerology BWPs, multi-user RB allocation, and data routing through out-band IAB nodes. This approach leverages the strengths of both methods to achieve a more effective and comprehensive optimisation solution. In our study, we evaluated the performance of NSGA and TRGA algorithms to achieve the optimum solution and observed their impact on the overall system performance. Our results revealed that while TRGA can improve power efficiency, it comes at a higher computational cost compared to NSGA. On the other hand, NSGA may be slightly further from the optimum solution, but it is faster in terms of computational time

compared to TRGA. In this chapter, we also presented a near-optimum solution for the allocation of BWPs among the total carrier bandwidth by calculating the average of all valid outputs. Additionally, we are able to solve NP-hard problems that were previously unsolvable by MILP optimisation methods. In other words, the proposed hybrid GA approach allowed us to solve NP-hard problems that could not be solved in our MILP optimisation problem. By leveraging the strengths of both heuristic and meta-heuristic methods, we were able to effectively optimise the bandwidth of multi-numerology BWPs, multi-user RB allocation, and data routing via out-band IAB nodes.

As a future work, the effectiveness of the GA is already proven by many papers. We can implement the GA algorithm into many optimisation problems to achieve near-optimum results faster or solve NP-hard problems, or both. More realistic outcomes can be achieved with the increased number of parameters in the optimisation problems; however, using a MILP optimisation becomes harder due to the curse of dimensionality. GAs can help to solve such problems in less amount time with a little sacrifice of optimality. Therefore, all the mentioned optimisation problems can be solved using heuristic approaches.

Chapter 5 starts with exploring the basics of machine learning; then, it simply shows that the resource and numerology allocation problem can be solved by reinforcement learning. First, the power allocation problem is solved by employing a novel reward function. This reward function can achieve two objectives at once; first, the RL agent satisfies the data rate requirements of the user to get a positive reward. Second, the agent does not allocate more than requested to maximise the reward; hence, it implicitly minimises the transmit power. Then Chapter 5 presents joint power and numerology allocation for a single BS environment. For the numerology allocation among bandwidth, pre-allocated BWP for 5 MHz bandwidth and a fixed number of RBs are employed. The users select the optimum resources in a few steps with the well-trained agent.

A newly introduced dimension exponentially increases the number of variables and parameters in any optimisation problem. Introducing the data routing or bandwidth allocation among BWPs dimension to our problem would have the same effect on our problem. Therefore, multi-agent RL can be employed when further dimensions are

introduced. Considering our problem, each individual objective, such as user association, power allocation, and data routing, can be optimised by a different agent. Alternatively, a user-agent assignment can be employed where each agent is dedicated to optimising all the objectives for that user. To the best of our knowledge, this multi-objective problem has not been addressed in the existing literature. As a concluding remark, real-time heuristics or machine learning algorithms should be developed to obtain real-time results. Moreover, future system states can be predicted using machine learning for a better resource allocation model.

References

[1] Qualcomm, *Everything you need to know about 5G.* online, accessed 20/12/22, https://www.qualcomm.com/5g/what-is-5g, 2022.

[2] C.-Y. Chang and N. Nikaein, "Ran runtime slicing system for flexible and dynamic service execution environment," *IEEE Access*, vol. 6, pp. 34 018–34 042, 2018.

[3] C.-Y. Chang, N. Nikaein, and T. Spyropoulos, "Radio access network resource slicing for flexible service execution," in *IEEE INFOCOM 2018-IEEE Conference on Computer Communications Workshops (INFOCOM WKSHPS)*, IEEE, 2018, pp. 668–673.

[4] C. Campolo, A. Molinaro, A. Iera, and F. Menichella, "5g network slicing for vehicle-to-everything services," *IEEE Wireless Communications*, vol. 24, no. 6, pp. 38–45, 2017.

[5] ETSI, *What Are The Main Usage Scenarios Of 5G?* online, accessed 08/18/21, https://www.etsi.org/technologies/mobile/5g, 2021.

[6] IMT, "Imt vision framework and overall objectives of the future development of imt for 2020 and beyond," *Recommendation ITU*, 2015.

[7] C. Campolo, A. Molinaro, A. Iera, R. R. Fontes, and C. E. Rothenberg, "Towards 5g network slicing for the v2x ecosystem," in *2018 4th IEEE conference on network softwarization and workshops (NetSoft)*, IEEE, 2018, pp. 400–405.

[8] X. Foukas, G. Patounas, A. Elmokashfi, and M. K. Marina, "Network slicing in 5g: Survey and challenges," *IEEE communications magazine*, vol. 55, no. 5, pp. 94–100, 2017.

[9] G. Faraci and G. Schembra, "An analytical model to design and manage a green sdn/nfv cpe node," *IEEE Transactions on Network and Service Management*, vol. 12, no. 3, pp. 435–450, 2015.

[10] M. Vaezi, Z. Ding, and H. V. Poor, *Multiple access techniques for 5G wireless networks and beyond*. Springer, 2019, vol. 159.

[11] I. Yaqoob, I. Ahmad, E. Ahmed, A. Gani, M. Imran, and N. Guizani, "Overcoming the key challenges to establishing vehicular communication: Is sdn the answer?" *IEEE Communications Magazine*, vol. 55, no. 7, pp. 128–134, 2017.

[12] L. Ma, X. Wen, L. Wang, Z. Lu, and R. Knopp, "An sdn/nfv based framework for management and deployment of service based 5g core network," *China Communications*, vol. 15, no. 10, pp. 86–98, 2018.

[13] 3GPP, "Study on scenarios and requirements for next generation access technologies; (release 14)," 3GPP, Tech. Rep. document 38.913, ver 14.3.0, 2017.

[14] A. Zaidi, F. Athley, J. Medbo, U. Gustavsson, G. Durisi, and X. Chen, *5G Physical Layer: principles, models and technology components*. Academic Press, 2018.

[15] R. Ali, Y. B. Zikria, A. K. Bashir, S. Garg, and H. S. Kim, "Urllc for 5g and beyond: Requirements, enabling incumbent technologies and network intelligence," *IEEE Access*, vol. 9, pp. 67 064–67 095, 2021.

[16] J. Wahlström, I. Skog, and P. Händel, "Smartphone-based vehicle telematics: A ten-year anniversary," *IEEE Transactions on Intelligent Transportation Systems*, vol. 18, no. 10, pp. 2802–2825, 2017.

[17] S. Han, X. Xu, S. Fang, *et al.*, "Energy efficient secure computation offloading in noma-based mmtc networks for iot," *IEEE Internet of Things Journal*, vol. 6, no. 3, pp. 5674–5690, 2019.

[18] 3. G. P. Project, "Technical specification group radio access network; nr; physical channels and modulation (release 15), v1.2.0, document ts 38.211," 3GPP, Tech. Rep. document TS 38.211, 2017.

[19] A. N. Al-Quzweeni, A. Q. Lawey, T. E. Elgorashi, and J. M. Elmirghani, "Optimized energy aware 5g network function virtualization," *IEEE Access*, vol. 7, pp. 44 939–44 958, 2019.

[20] sharetechnote, *5G/NR - Frame Structure*, online, accessed 08/18/21, https://www.sharetechnote.com/html/5G/5G-FrameStructure.html, 2021.

[21] E. Dahlman and S. Parkvall, "Nr-the new 5g radio-access technology," in *2018 IEEE 87th Vehicular Technology Conference (VTC Spring)*, IEEE, 2018, pp. 1–6.

[22] X. Zhang, L. Zhang, P. Xiao, D. Ma, J. Wei, and Y. Xin, "Mixed numerologies interference analysis and inter-numerology interference cancellation for windowed ofdm systems," *IEEE Transactions on Vehicular Technology*, vol. 67, no. 8, pp. 7047–7061, 2018.

[23] S. Lagen, B. Bojovic, S. Goyal, L. Giupponi, and J. Mangues-Bafalluy, "Subband configuration optimization for multiplexing of numerologies in 5g tdd new radio," in *2018 IEEE 29th Annual International Symposium on Personal, Indoor and Mobile Radio Communications (PIMRC)*, IEEE, 2018, pp. 1–7.

[24] A. B. Kihero, M. S. J. Solaija, A. Yazar, and H. Arslan, "Inter-numerology interference analysis for 5g and beyond," in *2018 IEEE Globecom Workshops (GC Wkshps)*, IEEE, 2018, pp. 1–6.

[25] A. Yazar, B. Peköz, and H. Arslan, "Fundamentals of multi-numerology 5g new radio," *preprint: arXiv: 1805.02842*, 2019.

[26] F. Abinader, A. Marcano, K. Schober, *et al.*, "Impact of bandwidth part (bwp) switching on 5g nr system performance," in *2019 IEEE 2nd 5G World Forum (5GWF)*, IEEE, 2019, pp. 161–166.

[27] H. Ronkainen, J. Edstam, C. Östberg, and A. Ericsson, "Integrated access and backhaul: A new type of wireless backhaul in 5g," *Frontiers in Communications and Networks*, vol. 2, p. 4, 2021.

[28] J. Peisa, P. Persson, S. Parkvall, *et al.*, "5g evolution: 3gpp releases 16 & 17 overview," *Ericsson Technology Review*, vol. 6, pp. 2–13, 2020.

[29] T. Inoue, "5g nr release 16 and millimeter wave integrated access and backhaul," in *2020 IEEE radio and wireless symposium (RWS)*, IEEE, 2020, pp. 56–59.

[30] Ericsson, *Leveraging the potential of 5G millimeter wave.* online, accessed 20/12/22, https://www.ericsson.com/490025/assets/local/reports-papers/further-insights/doc/leveraging-the-potential-of-5g-millimeter-wave.pdf, 2022.

[31] G. H. Sim, S. Klos, A. Asadi, A. Klein, and M. Hollick, "An online context-aware machine learning algorithm for 5g mmwave vehicular communications," *IEEE/ACM Transactions on Networking*, vol. 26, no. 6, pp. 2487–2500, 2018.

[32] W. Roh, J.-Y. Seol, J. Park, *et al.*, "Millimeter-wave beamforming as an enabling technology for 5g cellular communications: Theoretical feasibility and prototype results," *IEEE communications magazine*, vol. 52, no. 2, pp. 106–113, 2014.

[33] A. Bishnu, M. Holm, and T. Ratnarajah, "Performance evaluation of full-duplex iab multi-cell and multi-user network for fr2 band," *IEEE Access*, vol. 9, pp. 72 269–72 283, 2021.

[34] A. Yastrebova, R. Kirichek, Y. Koucheryavy, A. Borodin, and A. Koucheryavy, "Future networks 2030: Architecture & requirements," in *2018 10th International Congress on Ultra Modern Telecommunications and Control Systems and Workshops (ICUMT)*, IEEE, 2018, pp. 1–8.

[35] V. F. Monteiro, F. R. M. Lima, D. C. Moreira, *et al.*, "Paving the way towards mobile iab: Problems, solutions and challenges," *IEEE Open Journal of the Communications Society*, 2022.

[36] 3. G. P. Project, "Technical specification group radio access network;nr;study on integrated access and backhaul; (release 16) 2018-12," 3GPP, Tech. Rep. document TS 38.874, 2018.

[37] P. Fabian, G. Z. Papadopoulos, P. Savelli, and B. Cousin, "Performance evaluation of integrated access and backhaul in 5g networks," in *2021 IEEE Conference on Standards for Communications and Networking (CSCN)*, IEEE, 2021, pp. 88–93.

[38] Nokia, *Make highways safer, less congested and more sustainable*, online, accessed 20/12/22, https://www.nokia.com/networks/industries/highways/, 2022.

[39] GSMA, *How 5G can make roads safer*, online, accessed 27/12/22, https://www.gsma.com/5GHub/images/How$_5G_Can_Make_Roads_Safer_Screen.pdf$, 2022.

[40] 3. G. P. Project, "Lte; service requirements for v2x services (3gpp ts 22.185 version 14.3.0 release 14," 3GPP, Tech. Rep. document TS 22.185, 2017.

[41] H. D. R. Albonda and J. Pérez-Romero, "An efficient ran slicing strategy for a heterogeneous network with embb and v2x services," *IEEE access*, vol. 7, pp. 44 771–44 782, 2019.

[42] ETSI, "Intelligent transport systems (its); vehicular communications; basic set of applications; part 2: Specification of cooperative awareness basic service," ETSI, Tech. Rep., 2014.

[43] ——, "Intelligent transport systems (its); vehicular communications; basic set of applications; part 3: Specifications of decentralized environmental notification basic service," ETSI, Tech. Rep., 2014.

[44] F. Eckermann, M. Kahlert, and C. Wietfeld, "Performance analysis of c-v2x mode 4 communication introducing an open-source c-v2x simulator," in *2019 IEEE 90th Vehicular Technology Conference (VTC2019-Fall)*, IEEE, 2019, pp. 1–5.

[45] K. N. Qureshi, F. Bashir, and S. Iqbal, "Cloud computing model for vehicular ad hoc networks," in *2018 IEEE 7th International Conference on Cloud Networking (CloudNet)*, IEEE, 2018, pp. 1–3.

[46] L. Liang, H. Ye, and G. Y. Li, "Toward intelligent vehicular networks: A machine learning framework," *IEEE Internet of Things Journal*, vol. 6, no. 1, pp. 124–135, 2018.

[47] H. Chen, R. Zhang, W. Zhai, X. Liang, and G. Song, "Interference-free pilot design and channel estimation using zcz sequences for mimo-ofdm-based c-v2x communications," *China Communications*, vol. 15, no. 7, pp. 47–54, 2018.

[48] G. Noh, J. Kim, S. Choi, N. Lee, H. Chung, and I. Kim, "Feasibility validation of a 5g-enabled mmwave vehicular communication system on a highway," *IEEE Access*, vol. 9, pp. 36 535–36 546, 2021.

[49] Qualcomm, *Accelerating C-V2X commercialization*, online, accessed 27/12/22, https://www.qualcomm.com, 2022.

[50] K. Sehla, T. M. T. Nguyen, G. Pujolle, and P. B. Velloso, "Resource allocation modes in c-v2x: From lte-v2x to 5g-v2x," *IEEE Internet of Things Journal*, 2022.

[51] X. Ge, "Ultra-reliable low-latency communications in autonomous vehicular networks," *IEEE Transactions on Vehicular Technology*, vol. 68, no. 5, pp. 5005–5016, 2019.

[52] M. K. Abdel-Aziz, C.-F. Liu, S. Samarakoon, M. Bennis, and W. Saad, "Ultra-reliable low-latency vehicular networks: Taming the age of information tail," in

2018 IEEE Global Communications Conference (GLOBECOM), IEEE, 2018, pp. 1–7.

[53] S. Samarakoon, M. Bennis, W. Saad, and M. Debbah, "Federated learning for ultra-reliable low-latency v2v communications," in *2018 IEEE Global Communications Conference (GLOBECOM)*, IEEE, 2018, pp. 1–7.

[54] J. Cheng, J. Cheng, M. Zhou, F. Liu, S. Gao, and C. Liu, "Routing in internet of vehicles: A review," *IEEE Transactions on Intelligent Transportation Systems*, vol. 16, no. 5, pp. 2339–2352, 2015.

[55] J. Lianghai, B. Han, M. Liu, and H. D. Schotten, "Applying device-to-device communication to enhance iot services," *IEEE Communications Standards Magazine*, vol. 1, no. 2, pp. 85–91, 2017.

[56] nPerf, *5G coverage map worldwide*, online, accessed 27/12/22, https://www.nperf.com/en/map/5g, 2022.

[57] S. Wright, J. Nocedal, *et al.*, "Numerical optimization," *Springer Science*, vol. 35, no. 67-68, p. 7, 1999.

[58] M. Dorigo, V. Maniezzo, and A. Colorni, "Ant system: Optimization by a colony of cooperating agents," *IEEE Transactions on Systems, Man, and Cybernetics, Part B (Cybernetics)*, vol. 26, no. 1, pp. 29–41, 1996.

[59] J. Kennedy and R. Eberhart, "Particle swarm optimization," in *Proceedings of ICNN'95-international conference on neural networks*, IEEE, vol. 4, 1995, pp. 1942–1948.

[60] S. Das and P. N. Suganthan, "Differential evolution: A survey of the state-of-the-art," *IEEE transactions on evolutionary computation*, vol. 15, no. 1, pp. 4–31, 2010.

[61] A. E. Eiben and J. E. Smith, *Introduction to evolutionary computing*. Springer, 2015.

[62] National Institute of Standards and Technology, *NP-hard*, online, accessed 12/04/23, https://xlinux.nist.gov/dads/HTML/nphard.html, 2021.

[63] M. G. Kibria, K. Nguyen, G. P. Villardi, O. Zhao, K. Ishizu, and F. Kojima, "Big data analytics, machine learning, and artificial intelligence in next-generation wireless networks," *IEEE access*, vol. 6, pp. 32 328–32 338, 2018.

[64] G. Jain and R. R. Prasad, "Machine learning, prophet and xgboost algorithm: Analysis of traffic forecasting in telecom networks with time series data," in *2020 8th International Conference on Reliability, Infocom Technologies and Optimization (Trends and Future Directions)(ICRITO)*, IEEE, 2020, pp. 893–897.

[65] Y. S. Nasir and D. Guo, "Multi-agent deep reinforcement learning for dynamic power allocation in wireless networks," *IEEE Journal on Selected Areas in Communications*, vol. 37, no. 10, pp. 2239–2250, 2019.

[66] C. Kai, H. Li, L. Xu, Y. Li, and T. Jiang, "Joint subcarrier assignment with power allocation for sum rate maximization of d2d communications in wireless cellular networks," *IEEE Transactions on Vehicular Technology*, vol. 68, no. 5, pp. 4748–4759, 2019.

[67] J. Zhu, Q. Li, Z. Liu, H. Chen, and H. V. Poor, "Enhanced user grouping and power allocation for hybrid mmwave mimo-noma systems," *IEEE Transactions on Wireless Communications*, vol. 21, no. 3, pp. 2034–2050, 2021.

[68] D. Hu, Q. Zhang, Q. Li, and J. Qin, "Joint position, decoding order, and power allocation optimization in uav-based noma downlink communications," *IEEE Systems Journal*, vol. 14, no. 2, pp. 2949–2960, 2019.

[69] G. Ye, H. Zhang, H. Liu, J. Cheng, and V. C. Leung, "Energy efficient joint user association and power allocation in a two-tier heterogeneous network," in *2016 IEEE Global Communications Conference (GLOBECOM)*, IEEE, 2016, pp. 1–5.

[70] F. Fang, J. Cheng, and Z. Ding, "Joint energy efficient subchannel and power optimization for a downlink noma heterogeneous network," *IEEE Transactions on Vehicular Technology*, vol. 68, no. 2, pp. 1351–1364, 2018.

[71] B. Liu, P. Zhu, J. Li, D. Wang, and Y. Wang, "Energy-efficient optimization via joint power and subcarrier allocation for embb and urllc services," *IEEE Wireless Communications Letters*, vol. 11, no. 11, pp. 2340–2344, 2022.

[72] Y. S. Nasir and D. Guo, "Deep reinforcement learning for joint spectrum and power allocation in cellular networks," in *2021 IEEE Globecom Workshops (GC Wkshps)*, IEEE, 2021, pp. 1–6.

[73] B. Tezergil and E. Onur, "Wireless backhaul in 5g and beyond: Issues, challenges and opportunities," *IEEE Communications Surveys & Tutorials*, 2022.

[74] Y. Xu, G. Gui, H. Gacanin, and F. Adachi, "A survey on resource allocation for 5g heterogeneous networks: Current research, future trends, and challenges," *IEEE Communications Surveys & Tutorials*, vol. 23, no. 2, pp. 668–695, 2021.

[75] 3. G. P. Project, "Scenarios and requirements for small cell enhancements for e-utra and e-utran (3gpp tr 36.932 version 12.1.0 release 12)," 3GPP, Tech. Rep. document TS 36.932, 2012.

[76] B. Agarwal, M. A. Togou, M. Ruffini, and G.-M. Muntean, "A comprehensive survey on radio resource management in 5g hetnets: Current solutions, future trends and open issues," *IEEE Communications Surveys & Tutorials*, 2022.

[77] S. Manap, K. Dimyati, M. N. Hindia, M. S. A. Talip, and R. Tafazolli, "Survey of radio resource management in 5g heterogeneous networks," *IEEE Access*, vol. 8, pp. 131 202–131 223, 2020.

[78] N.-T. Le, L.-N. Tran, Q.-D. Vu, and D. Jayalath, "Energy-efficient resource allocation for ofdma heterogeneous networks," *IEEE Transactions on Communications*, vol. 67, no. 10, pp. 7043–7057, 2019.

[79] M. Y. Lyazidi, N. Aitsaadi, and R. Langar, "Dynamic resource allocation for cloud-ran in lte with real-time bbu/rrh assignment," in *2016 IEEE international conference on communications (ICC)*, IEEE, 2016, pp. 1–6.

[80] A. Akhtar and H. Arslan, "Downlink resource allocation and packet scheduling in multi-numerology wireless systems," in *2018 IEEE wireless communications and networking conference workshops (WCNCW)*, IEEE, 2018, pp. 362–367.

[81] N. Correia, F. Al-Tam, and J. Rodriguez, "Optimization of mixed numerology profiles for 5g wireless communication scenarios," *Sensors*, vol. 21, no. 4, p. 1494, 2021.

[82] L. Miuccio, D. Panno, P. Pisacane, and S. Riolo, "Channel-aware and qos-aware downlink resource allocation for multi-numerology based 5g nr systems," in *2021 19th Mediterranean Communication and Computer Networking Conference (MedComNet)*, IEEE, 2021, pp. 1–8.

[83] L. Marijanovic, S. Schwarz, and M. Rupp, "Multi-user resource allocation for low latency communications based on mixed numerology," in *2019 IEEE 90th Vehicular Technology Conference (VTC2019-Fall)*, IEEE, 2019, pp. 1–7.

[84] L. You, Q. Liao, N. Pappas, and D. Yuan, "Resource optimization with flexible numerology and frame structure for heterogeneous services," *IEEE Communications Letters*, vol. 22, no. 12, pp. 2579–2582, 2018.

[85] P. K. Korrai, E. Lagunas, A. Bandi, S. K. Sharma, and S. Chatzinotas, "Joint power and resource block allocation for mixed-numerology-based 5g downlink under imperfect csi," *IEEE Open Journal of the Communications Society*, vol. 1, pp. 1583–1601, 2020.

[86] H. Ren, C. Pan, Y. Deng, M. Elkashlan, and A. Nallanathan, "Resource allocation for secure urllc in mission-critical iot scenarios," *IEEE Transactions on Communications*, vol. 68, no. 9, pp. 5793–5807, 2020.

[87] V. N. Ha, T. T. Nguyen, L. B. Le, and J.-F. Frigon, "Admission control and network slicing for multi-numerology 5g wireless networks," *IEEE Networking Letters*, vol. 2, no. 1, pp. 5–9, 2019.

[88] T. Bag, S. Garg, Z. Shaik, and A. Mitschele-Thiel, "Multi-numerology based resource allocation for reducing average scheduling latencies for 5g nr wireless networks," in *2019 European Conference on Networks and Communications (EuCNC)*, IEEE, 2019, pp. 597–602.

[89] O. Tipmongkolsilp, S. Zaghloul, and A. Jukan, "The evolution of cellular backhaul technologies: Current issues and future trends," *IEEE communications surveys & tutorials*, vol. 13, no. 1, pp. 97–113, 2010.

[90] M. N. Islam, S. Subramanian, and A. Sampath, "Integrated access backhaul in millimeter wave networks," in *2017 IEEE Wireless Communications and Networking Conference (WCNC)*, IEEE, 2017, pp. 1–6.

[91] M. Polese, M. Giordani, T. Zugno, *et al.*, "Integrated access and backhaul in 5g mmwave networks: Potential and challenges," *IEEE Communications Magazine*, vol. 58, no. 3, pp. 62–68, 2020.

[92] J. Kim, I. Kim, and H. Chung, "Resource multiplexing enhancements for integrated access and backhaul in 5g new radio release 17," in *2020 International Conference on Information and Communication Technology Convergence (ICTC)*, IEEE, 2020, pp. 936–938.

[93] M. N. Islam, N. Abedini, G. Hampel, S. Subramanian, and J. Li, "Investigation of performance in integrated access and backhaul networks," in *IEEE*

INFOCOM 2018-IEEE Conference on Computer Communications Workshops (INFOCOM WKSHPS), IEEE, 2018, pp. 597–602.

[94] Y. Liu, A. Tang, and X. Wang, "Joint incentive and resource allocation design for user provided network under 5g integrated access and backhaul networks," *IEEE Transactions on Network Science and Engineering*, vol. 7, no. 2, pp. 673–685, 2019.

[95] Q. Zhang, W. Ma, Z. Feng, and Z. Han, "Backhaul-capacity-aware interference mitigation framework in 6g cellular internet of things," *IEEE Internet of Things Journal*, vol. 8, no. 12, pp. 10 071–10 084, 2021.

[96] C. Saha, M. Afshang, and H. S. Dhillon, "Bandwidth partitioning and downlink analysis in millimeter wave integrated access and backhaul for 5g," *IEEE Transactions on Wireless Communications*, vol. 17, no. 12, pp. 8195–8210, 2018.

[97] M. Polese, M. Giordani, T. Zugno, *et al.*, "Integrated access and backhaul in 5g mmwave networks: Potential and challenges," *IEEE Communications Magazine*, vol. 58, no. 3, pp. 62–68, 2020.

[98] J.-H. Kwon, B. Lim, and Y.-C. Ko, "Resource allocation and system design of out-band based integrated access and backhaul network at mmwave band," *IEEE Transactions on Vehicular Technology*, 2022.

[99] Y.-J. Yu, T.-Y. Hsieh, and A.-C. Pang, "Millimeter-wave backhaul traffic minimization for comp over 5g cellular networks," *IEEE Transactions on Vehicular Technology*, vol. 68, no. 4, pp. 4003–4015, 2019.

[100] D. Yuan, H.-Y. Lin, J. Widmer, and M. Hollick, "Optimal joint routing and scheduling in millimeter-wave cellular networks," in *IEEE INFOCOM 2018-IEEE Conference on Computer Communications*, IEEE, 2018, pp. 1205–1213.

[101] G. Noh, J. Kim, H. Chung, and I. Kim, "Realizing multi-gbps vehicular communication: Design, implementation, and validation," *IEEE Access*, vol. 7, pp. 19 435–19 446, 2019.

[102] T. K. Vu, M. Bennis, M. Debbah, and M. Latva-Aho, "Joint path selection and rate allocation framework for 5g self-backhauled mm-wave networks," *IEEE Transactions on Wireless Communications*, vol. 18, no. 4, pp. 2431–2445, 2019.

[103] H. Zhou, W. Xu, J. Chen, and W. Wang, "Evolutionary v2x technologies toward the internet of vehicles: Challenges and opportunities," *Proceedings of the IEEE*, vol. 108, no. 2, pp. 308–323, 2020.

[104] X. Ma, J. Zhang, X. Yin, and K. S. Trivedi, "Design and analysis of a robust broadcast scheme for vanet safety-related services," *IEEE Transactions on Vehicular Technology*, vol. 61, no. 1, pp. 46–61, 2011.

[105] M. De Felice, A. Baiocchi, F. Cuomo, G. Fusco, and C. Colombaroni, "Traffic monitoring and incident detection through vanets," in *2014 11th Annual Conference on Wireless On-demand Network Systems and Services (WONS)*, IEEE, 2014, pp. 122–129.

[106] L. Chen and C. Englund, "Cooperative intersection management: A survey," *IEEE transactions on intelligent transportation systems*, vol. 17, no. 2, pp. 570–586, 2015.

[107] F. Malandrino, C. Casetti, C.-F. Chiasserini, and M. Fiore, "Optimal content downloading in vehicular networks," *IEEE Transactions on Mobile Computing*, vol. 12, no. 7, pp. 1377–1391, 2012.

[108] C. R. Storck and F. Duarte-Figueiredo, "A 5g v2x ecosystem providing internet of vehicles," *Sensors*, vol. 19, no. 3, p. 550, 2019.

[109] T. Soenen, R. Banerjee, W. Tavernier, D. Colle, and M. Pickavet, "Demystifying network slicing: From theory to practice," in *2017 ifip/ieee symposium on integrated network and service management (im)*, IEEE, 2017, pp. 1115–1120.

[110] 3. G. P. Project, "Service requirements for enhanced v2x scenarios (3gpp ts 22.186 version 16.2.0 release 16)," 3GPP, Tech. Rep. document TS 22.186, 2020.

[111] A. Alalewi, I. Dayoub, and S. Cherkaoui, "On 5g-v2x use cases and enabling technologies: A comprehensive survey," *Ieee Access*, vol. 9, pp. 107 710–107 737, 2021.

[112] F. A. Schiegg, N. Brahmi, and I. Llatser, "Analytical performance evaluation of the collective perception service in c-v2x mode 4 networks," in *2019 IEEE Intelligent Transportation Systems Conference (ITSC)*, IEEE, 2019, pp. 181–188.

[113] W. Yi, Y. Liu, Y. Deng, A. Nallanathan, and R. W. Heath, "Modeling and analysis of mmwave v2x networks with vehicular platoon systems," *IEEE Journal on Selected Areas in Communications*, vol. 37, no. 12, pp. 2851–2866, 2019.

[114] J. Kim, Y.-J. Choi, G. Noh, and H. Chung, "On the feasibility of remote driving applications over mmwave 5 g vehicular communications: Implementation and demonstration," *IEEE Transactions on Vehicular Technology*, 2022.

[115] G. Kakkavas, M. Diamanti, K. N. Nyarko, *et al.*, "Realistic field trial evaluation of a tele-operated support service for remote driving over 5g," in *2022 IEEE Conference on Standards for Communications and Networking (CSCN)*, IEEE, 2022, pp. 58–63.

[116] M. Noor-A-Rahim, Z. Liu, H. Lee, *et al.*, "6g for vehicle-to-everything (v2x) communications: Enabling technologies, challenges, and opportunities," *Proceedings of the IEEE*, vol. 110, no. 6, pp. 712–734, 2022.

[117] X. Song and M. Yuan, "Performance analysis of one-way highway vehicular networks with dynamic multiplexing of embb and urllc traffics," *IEEE Access*, vol. 7, pp. 118 020–118 029, 2019.

[118] H. Khan, P. Luoto, S. Samarakoon, M. Bennis, and M. Latva-Aho, "Network slicing for vehicular communication," *Transactions on Emerging Telecommunications Technologies*, vol. 32, no. 1, e3652, 2021.

[119] Y. Zhang, L. Zhao, G. Zheng, X. Chu, Z. Ding, and K.-C. Chen, "Resource allocation for open-loop ultra-reliable and low-latency uplink communications in vehicular networks," *IEEE Transactions on Vehicular Technology*, vol. 70, no. 3, pp. 2590–2604, 2021.

[120] S. Nayak and S. Roy, "Novel markov chain based urllc link adaptation method for 5g vehicular networking," *IEEE Transactions on Vehicular Technology*, vol. 70, no. 12, pp. 12 302–12 311, 2021.

[121] R. Zhang, X. Cheng, Q. Yao, C.-X. Wang, Y. Yang, and B. Jiao, "Interference graph-based resource-sharing schemes for vehicular networks," *IEEE transactions on vehicular technology*, vol. 62, no. 8, pp. 4028–4039, 2013.

[122] Y. Meng, Y. Dong, X. Liu, and Y. Zhao, "An interference-aware resource allocation scheme for connectivity improvement in vehicular networks," *IEEE Access*, vol. 6, pp. 51 319–51 328, 2018.

[123] M. Noor-A-Rahim, Z. Liu, H. Lee, G. M. N. Ali, D. Pesch, and P. Xiao, "A survey on resource allocation in vehicular networks," *IEEE transactions on intelligent transportation systems*, vol. 23, no. 2, pp. 701–721, 2020.

[124] G. Meena, D. Sharma, and M. Mahrishi, "Traffic prediction for intelligent transportation system using machine learning," in *2020 3rd International Conference on Emerging Technologies in Computer Engineering: Machine Learning and Internet of Things (ICETCE)*, IEEE, 2020, pp. 145–148.

[125] J. Zheng and M. Huang, "Traffic flow forecast through time series analysis based on deep learning," *IEEE Access*, vol. 8, pp. 82 562–82 570, 2020.

[126] J. Xue, T. Zhang, W. Wu, H. Zhou, and X. Shen, "Sparse big data for vehicular network traffic flow estimation: A machine learning approach," in *GLOBECOM 2022-2022 IEEE Global Communications Conference*, IEEE, 2022, pp. 4959–4963.

[127] X.-F. Liu, Z.-H. Zhan, J. D. Deng, Y. Li, T. Gu, and J. Zhang, "An energy efficient ant colony system for virtual machine placement in cloud computing," *IEEE transactions on evolutionary computation*, vol. 22, no. 1, pp. 113–128, 2016.

[128] A. Ponsich, A. L. Jaimes, and C. A. C. Coello, "A survey on multiobjective evolutionary algorithms for the solution of the portfolio optimization problem and other finance and economics applications," *IEEE Transactions on evolutionary computation*, vol. 17, no. 3, pp. 321–344, 2012.

[129] T. Hiroyasu, S. Nakayama, and M. Miki, "Comparison study of spea2+, spea2, and nsga-ii in diesel engine emissions and fuel economy problem," in *2005 IEEE congress on evolutionary computation*, IEEE, vol. 1, 2005, pp. 236–242.

[130] L. Zhou, L. Feng, J. Zhong, Y.-S. Ong, Z. Zhu, and E. Sha, "Evolutionary multitasking in combinatorial search spaces: A case study in capacitated vehicle routing problem," in *2016 IEEE Symposium Series on Computational Intelligence (SSCI)*, IEEE, 2016, pp. 1–8.

[131] L. Feng, L. Zhou, A. Gupta, *et al.*, "Solving generalized vehicle routing problem with occasional drivers via evolutionary multitasking," *IEEE transactions on cybernetics*, vol. 51, no. 6, pp. 3171–3184, 2019.

[132] M. Gong, Z. Tang, H. Li, and J. Zhang, "Evolutionary multitasking with dynamic resource allocating strategy," *IEEE Transactions on Evolutionary Computation*, vol. 23, no. 5, pp. 858–869, 2019.

[133] W. Xia and L. Shen, "Joint resource allocation using evolutionary algorithms in heterogeneous mobile cloud computing networks," *China Communications*, vol. 15, no. 8, pp. 189–204, 2018.

[134] P. Korrai, E. Lagunas, S. K. Sharma, S. Chatzinotas, A. Bandi, and B. Ottersten, "A ran resource slicing mechanism for multiplexing of embb and urllc services in ofdma based 5g wireless networks," *IEEE Access*, vol. 8, pp. 45 674–45 688, 2020.

[135] S. Mondal and M. Ruffini, "Fairness guaranteed and auction-based x-haul and cloud resource allocation in multi-tenant o-rans," *arXiv preprint arXiv:2301.00597*, 2023.

[136] A. Feiten, R. Mathar, and M. Reyer, "Rate and power allocation for multiuser ofdm: An effective heuristic verified by branch-and-bound," *IEEE Transactions on Wireless Communications*, vol. 7, no. 1, pp. 60–64, 2008.

[137] B. Sahoo, C.-H. Yao, and H.-Y. Wei, "Millimeter-wave multi-hop wireless backhauling for 5g cellular networks," in *2017 IEEE 85th Vehicular Technology Conference (VTC Spring)*, IEEE, 2017, pp. 1–5.

[138] A. Yazar and H. Arslan, "A flexibility metric and optimization methods for mixed numerologies in 5g and beyond," *IEEE Access*, vol. 6, pp. 3755–3764, 2018.

[139] A. González, S. Kuhlmorgen, A. Festag, and G. Fettweis, "Resource allocation for block-based multi-carrier systems considering qos requirements," in *GLOBECOM 2017-2017 IEEE Global Communications Conference*, IEEE, 2017, pp. 1–7.

[140] Y. LeCun, Y. Bengio, and G. Hinton, "Deep learning," *nature*, vol. 521, no. 7553, pp. 436–444, 2015.

[141] Y. Zhang, D. S. Park, W. Han, *et al.*, "Bigssl: Exploring the frontier of large-scale semi-supervised learning for automatic speech recognition," *IEEE Journal of Selected Topics in Signal Processing*, vol. 16, no. 6, pp. 1519–1532, 2022.

[142] A. Karpathy, G. Toderici, S. Shetty, T. Leung, R. Sukthankar, and L. Fei-Fei, "Large-scale video classification with convolutional neural networks," in *Proceedings of the IEEE conference on Computer Vision and Pattern Recognition*, 2014, pp. 1725–1732.

[143] H. Ye, G. Y. Li, and B.-H. F. Juang, "Deep reinforcement learning based resource allocation for v2v communications," *IEEE Transactions on Vehicular Technology*, vol. 68, no. 4, pp. 3163–3173, 2019.

[144] V. Mnih, K. Kavukcuoglu, D. Silver, *et al.*, "Human-level control through deep reinforcement learning," *nature*, vol. 518, no. 7540, pp. 529–533, 2015.

[145] D. Silver, J. Schrittwieser, K. Simonyan, *et al.*, "Mastering the game of go without human knowledge," *nature*, vol. 550, no. 7676, pp. 354–359, 2017.

[146] N. Zhao, Y.-C. Liang, D. Niyato, Y. Pei, M. Wu, and Y. Jiang, "Deep reinforcement learning for user association and resource allocation in heterogeneous cellular networks," *IEEE Transactions on Wireless Communications*, vol. 18, no. 11, pp. 5141–5152, 2019.

[147] A. Moubayed and A. Shami, "Softwarization, virtualization, & machine learning for intelligent & effective v2x communications," *arXiv preprint arXiv:2006.04595*, 2020.

[148] Matlab, *Reinforcement Learning Onramp (Overview of Reinforcement Learning)*, online, accessed 04/04/23, https://matlabacademy.mathworks.com/details/reinforcement-learning-onramp/reinforcementlearning, 2023.

[149] A. Gündoğan, H. M. Gürsu, V. Pauli, and W. Kellerer, "Distributed resource allocation with multi-agent deep reinforcement learning for 5g-v2v communication," in *Proceedings of the Twenty-First International Symposium on Theory, Algorithmic Foundations, and Protocol Design for Mobile Networks and Mobile Computing*, 2020, pp. 357–362.

[150] J. Gao, M. R. Khandaker, F. Tariq, K.-K. Wong, and R. T. Khan, "Deep neural network based resource allocation for v2x communications," in *2019 IEEE 90th Vehicular Technology Conference (VTC2019-Fall)*, IEEE, 2019, pp. 1–5.

[151] M. Chen, J. Chen, X. Chen, S. Zhang, and S. Xu, "A deep learning based resource allocation scheme in vehicular communication systems," in *2019 IEEE*

Wireless Communications and Networking Conference (WCNC), IEEE, 2019, pp. 1–6.

[152] E. Ghadimi, F. D. Calabrese, G. Peters, and P. Soldati, "A reinforcement learning approach to power control and rate adaptation in cellular networks," in *2017 IEEE International Conference on Communications (ICC)*, IEEE, 2017, pp. 1–7.

[153] F. Meng, P. Chen, L. Wu, and J. Cheng, "Power allocation in multi-user cellular networks: Deep reinforcement learning approaches," *IEEE Transactions on Wireless Communications*, vol. 19, no. 10, pp. 6255–6267, 2020.

[154] A. Asadi, S. Müller, G. H. Sim, A. Klein, and M. Hollick, "Fml: Fast machine learning for 5g mmwave vehicular communications," in *IEEE INFOCOM 2018-IEEE Conference on Computer Communications*, IEEE, 2018, pp. 1961–1969.

[155] T. Şahin, R. Khalili, M. Boban, and A. Wolisz, "Reinforcement learning scheduler for vehicle-to-vehicle communications outside coverage," in *2018 IEEE Vehicular Networking Conference (VNC)*, IEEE, 2018, pp. 1–8.

[156] T. Fu, C. Wang, and N. Cheng, "Deep-learning-based joint optimization of renewable energy storage and routing in vehicular energy network," *IEEE Internet of Things Journal*, vol. 7, no. 7, pp. 6229–6241, 2020.

[157] F. Bahlke, O. D. Ramos-Cantor, S. Henneberger, and M. Pesavento, "Optimized cell planning for network slicing in heterogeneous wireless communication networks," *IEEE Communications Letters*, vol. 22, no. 8, pp. 1676–1679, 2018.

[158] R.-J. Wang, C.-H. Wang, G.-S. Lee, D.-N. Yang, W.-T. Chen, and J.-P. Sheu, "Resource allocation in 5g with noma-based mixed numerology systems," in *GLOBECOM 2020-2020 IEEE Global Communications Conference*, IEEE, 2020, pp. 1–6.

[159] X. Cheng, R. Zayani, H. Shaiek, and D. Roviras, "Analysis and cancellation of mixed-numerologies interference for massive mimo-ofdm ul," *IEEE Wireless Communications Letters*, vol. 9, no. 4, pp. 470–474, 2019.

[160] G. Naik, B. Choudhury, and J.-M. Park, "Ieee 802.11 bd & 5g nr v2x: Evolution of radio access technologies for v2x communications," *IEEE access*, vol. 7, pp. 70 169–70 184, 2019.

[161] M. U. Khan, A. Garcıéa-Armada, and J. Escudero-Garzás, "Service-based network dimensioning for 5g networks assisted by real data," *IEEE Access*, vol. 8, pp. 129 193–129 212, 2020.

[162] S. Sun, T. S. Rappaport, S. Rangan, *et al.*, "Propagation path loss models for 5g urban micro-and macro-cellular scenarios," in *2016 IEEE 83rd Vehicular Technology Conference (VTC Spring)*, IEEE, 2016, pp. 1–6.

[163] 3. G. P. Project, "Radio frequency (rf) requirements for lte pico node b (release 13)," 3GPP, Tech. Rep. document TR 36.931 V13.0.0, 2016.

[164] M. R. Akdeniz, Y. Liu, M. K. Samimi, *et al.*, "Millimeter wave channel modeling and cellular capacity evaluation," *IEEE journal on selected areas in communications*, vol. 32, no. 6, pp. 1164–1179, 2014.

[165] L. Marijanović, S. Schwarz, and M. Rupp, "Optimal resource allocation with flexible numerology," in *2018 IEEE International Conference on Communication Systems (ICCS)*, IEEE, 2018, pp. 136–141.

[166] F. Vatalaro and A. Forcella, "Doppler spectrum in mobile-to-mobile communications in the presence of three-dimensional multipath scattering," *IEEE Transactions on Vehicular Technology*, vol. 46, no. 1, pp. 213–219, 1997.

[167] AIMMS, *AIMMS Modeling Guide - Integer Programming Tricks*, online, accessed 29/11/22, https://download.aimms.com/aimms/download/manuals/AIMMS3OM-IntegerProgrammingTricks.pdf, 2022.

[168] ETSI, "Base station (bs) radio transmission and reception (3gpp ts 38.104 version 15.3.0 release 15)," ETSI, Tech. Rep. document TS 138 104 V15.3.0 (2018-10), 2018.

[169] 3. G. P. Project, "Technical specification: 5g nr- user equipment (ue) radio transmission and reception, version 15.3.0 release 15," 3GPP, Tech. Rep. document TS 38.874, 2018.

[170] B. Xu, Y. Chen, M. Elkashlan, T. Zhang, and K.-K. Wong, "User association in massive mimo and mmwave enabled hetnets powered by renewable energy," in *2016 IEEE Wireless Communications and Networking Conference*, IEEE, 2016, pp. 1–6.

[171] Kalvelagen, Erwin, *Piecewise linear functions in MIP models*, online, accessed 08/18/21, http://yetanothermathprogrammingconsultant.blogspot.com/2015/ 10 /piecewise-linear-functions-in-mip-models.html, 2015.

[172] AMPL, *WHY AMPL?* online, accessed 08/18/21, https://ampl.com/, 2021.

[173] M. Series, "Minimum requirements related to technical performance for imt-2020 radio interface (s)," *Report*, pp. 2410–, 2017.

[174] ——, "Guidelines for evaluation of radio interface technologies for imt-2020," *Report ITU-R M. 2412-0, Tech. Rep.*, 2017.

[175] T. S. Rappaport, *Wireless communications: Principles and practice, 2/E*. Pearson Education India, 2010.

[176] P. Winzer, R. Ryf, S. Randel, I. Kaminow, T. Li, and A. Willner, "Spatial multiplexing using multiple-input multiple-output signal processing," *Optical Fiber Telecommunications VIB*, 2013.

[177] L. H. Koopmans, *The spectral analysis of time series*. Elsevier, 1995.

[178] Y. Bengio, Y. LeCun, *et al.*, "Scaling learning algorithms towards ai," *Large-scale kernel machines*, vol. 34, no. 5, pp. 1–41, 2007.

[179] H. John, "Holland. genetic algorithms," *Scientific american*, vol. 267, no. 1, pp. 44–50, 1992.

[180] M. Srinivas and L. M. Patnaik, "Genetic algorithms: A survey," *computer*, vol. 27, no. 6, pp. 17–26, 1994.

[181] J. J. Grefenstette, "Optimization of control parameters for genetic algorithms," *IEEE Transactions on systems, man, and cybernetics*, vol. 16, no. 1, pp. 122–128, 1986.

[182] M. Srinivas and L. M. Patnaik, "Adaptive probabilities of crossover and mutation in genetic algorithms," *IEEE Transactions on Systems, Man, and Cybernetics*, vol. 24, no. 4, pp. 656–667, 1994.

[183] N. Sharma and A. Madhukumar, "Genetic algorithm aided proportional fair resource allocation in multicast ofdm systems," *IEEE Transactions on Broadcasting*, vol. 61, no. 1, pp. 16–29, 2015.

[184] Matlab, *Deep Learning or Machine Learning: Choosing the Best Approach*, online, accessed 18/06/20, https://explore.mathworks.com/machine-learning-vs-deep-earning/chapter-1-129M-100NU.html, 2020.

[185] M. Chen, U. Challita, W. Saad, C. Yin, and M. Debbah, "Machine learning for wireless networks with artificial intelligence: A tutorial on neural networks," *arXiv preprint arXiv:1710.02913*, vol. 9, 2017.

[186] K. Arulkumaran, M. P. Deisenroth, M. Brundage, and A. A. Bharath, "Deep reinforcement learning: A brief survey," *IEEE Signal Processing Magazine*, vol. 34, no. 6, pp. 26–38, 2017.

[187] Simplilearn - Online Certification Training Course Provider, *Machine Learning Steps: A Complete Guide!* online, accessed 16/02/23, https://www.simplilearn.com/tutorials/machine-learning-tutorial/machine-learning-steps, 2023.

[188] H. Ye, L. Liang, G. Y. Li, J. Kim, L. Lu, and M. Wu, "Machine learning for vehicular networks: Recent advances and application examples," *ieee vehicular technology magazine*, vol. 13, no. 2, pp. 94–101, 2018.

[189] X. Dong, D. Thanou, L. Toni, M. Bronstein, and P. Frossard, "Graph signal processing for machine learning: A review and new perspectives," *IEEE Signal processing magazine*, vol. 37, no. 6, pp. 117–127, 2020.

[190] B. Mahesh, "Machine learning algorithms-a review," *International Journal of Science and Research (IJSR).[Internet]*, vol. 9, pp. 381–386, 2020.

[191] Matlab, *What Is Reinforcement Learning?* online, accessed 05/01/23, https://uk.mathworks.com/discovery/reinforcement-learning.html, 2023.

[192] I. H. Sarker, "Machine learning: Algorithms, real-world applications and research directions," *SN computer science*, vol. 2, no. 3, p. 160, 2021.

[193] C. Szegedy, W. Liu, Y. Jia, *et al.*, "Going deeper with convolutions," in *Proceedings of the IEEE conference on computer vision and pattern recognition*, 2015, pp. 1–9.

[194] C. Szegedy, V. Vanhoucke, S. Ioffe, J. Shlens, and Z. Wojna, "Rethinking the inception architecture for computer vision," in *Proceedings of the IEEE conference on computer vision and pattern recognition*, 2016, pp. 2818–2826.

[195] Z. Ghahramani, "Unsupervised learning," *Advanced Lectures on Machine Learning: ML Summer Schools 2003, Canberra, Australia, February 2-14, 2003, Tübingen, Germany, August 4-16, 2003, Revised Lectures*, pp. 72–112, 2004.

[196] T. Berg-Kirkpatrick, A. Bouchard-Côté, J. DeNero, and D. Klein, "Painless unsupervised learning with features," in *Human Language Technologies: The*

2010 Annual Conference of the North American Chapter of the Association for Computational Linguistics, 2010, pp. 582–590.

[197] S. Hussein, P. Kandel, C. W. Bolan, M. B. Wallace, and U. Bagci, "Lung and pancreatic tumor characterization in the deep learning era: Novel supervised and unsupervised learning approaches," *IEEE transactions on medical imaging*, vol. 38, no. 8, pp. 1777–1787, 2019.

[198] C. Godard, O. Mac Aodha, and G. J. Brostow, "Unsupervised monocular depth estimation with left-right consistency," in *Proceedings of the IEEE conference on computer vision and pattern recognition*, 2017, pp. 270–279.

[199] M. Guillaumin, J. Verbeek, and C. Schmid, "Multimodal semi-supervised learning for image classification," in *2010 IEEE Computer society conference on computer vision and pattern recognition*, IEEE, 2010, pp. 902–909.

[200] V. François-Lavet, P. Henderson, R. Islam, M. G. Bellemare, J. Pineau, *et al.*, "An introduction to deep reinforcement learning," *Foundations and Trends® in Machine Learning*, vol. 11, no. 3-4, pp. 219–354, 2018.

[201] P. E. Utgoff and D. J. Stracuzzi, "Many-layered learning," *Neural computation*, vol. 14, no. 10, pp. 2497–2529, 2002.

[202] S. Levine, C. Finn, T. Darrell, and P. Abbeel, "End-to-end training of deep visuomotor policies," *The Journal of Machine Learning Research*, vol. 17, no. 1, pp. 1334–1373, 2016.

[203] OpenAI, *Introducing ChatGPT*, online, accessed 04/04/23, https://openai.com/blog/chatgpt, 2023.

[204] S. S. Biswas, "Potential use of chat gpt in global warming," *Annals of Biomedical Engineering*, pp. 1–2, 2023.

[205] ——, "Role of chat gpt in public health," *Annals of Biomedical Engineering*, pp. 1–2, 2023.

[206] M. Sallam, *Chatgpt utility in health care education, research, and practice: Systematic review on the promising perspectives and valid concerns. healthcare 2023, 11, 887*, 2023.

[207] L. Bottou, O. Chapelle, D. DeCoste, and J. Weston, "Scaling learning algorithms toward ai," 2007.

[208] F. Tang, Y. Kawamoto, N. Kato, and J. Liu, "Future intelligent and secure vehicular network toward 6g: Machine-learning approaches," *Proceedings of the IEEE*, vol. 108, no. 2, pp. 292–307, 2019.

[209] J. Starmer, *Neural networks pt. 3: Relu in action!!!* Online video, [Accessed 18/02/23], 2020. [Online]. Available: `https://www.youtube.com/watch?v=68BZ5f7P94E&ab_channel=StatQuestwithJoshStarmer`.

Appendix A

Appendix Chapter